Work Order No. 582-15-54264-010
Contract # 582-15-50417
Project #FY15-52

Final Report
Three-Dimensional Performance Comparison of CAMx and CMAQ Using the 2013 DISCOVER-AQ Field Study Data Base

PREPARED UNDER A CONTRACT FROM THE
TEXAS COMMISSION ON ENVIRONMENTAL QUALITY

The preparation of this report was financed through a contract from the State of Texas through the Texas Commission on Environmental Quality. The content, findings, opinions and conclusions are the work of the author(s) and do not necessarily represent findings, opinions or conclusions of the TCEQ.

Prepared for:
Jim Smith
Texas Commission on Environmental Quality
121 Park 35 Circle MC 164
Austin, TX 78753

Prepared by:
Uarporn Nopmongcol, Zhen Liu,
Jeremiah Johnson, DJ Rassmusen,
Andrew Wentland and Greg Yarwood
Ramboll Environ
773 San Marin Drive, Suite 2115
Novato, California, 94998

August 2015

06-35854J1-3

RAMBOLL ENVIRON

CONTENTS

EXECUTIVE SUMMARY 1
Base Case Simulations 1
Model Performance Evaluation 2
Sensitivity Simulations 3
Conclusions 3
Recommendations 4
1.0 INTRODUCTION 5
2.0 MODELING INPUT PREPARATION 6
2.1 Modeling Domains 6
2.2 Meteorological Inputs 9
2.2.1 WRF Model Configuration 9
2.2.2 WRF Model Performance Evaluation 10
2.3 Emissions Inputs 23
2.3.1 Anthropogenic Emissions 23
2.3.2 Natural Emissions 23
2.3.3 Emissions Merging 24
2.3.4 Emissions Summary 24
2.4 Lateral Boundary Conditions and other Ancillary Inputs 27
2.5 CMAQ Inputs Preparation 29
2.5.1 Emissions and Boundary Conditions 29
2.5.2 Ocean Mask File 29
3.0 CAMX AND CMAQ BASE CASE SIMULATION 30
3.1 CAMx and CMAQ Base Case Simulations 30
3.1.1 CAMx Model Configuration 30
3.1.2 CMAQ Model Configuration 31
3.2 CAMx and CMAQ 4 km Results 31
4.0 MODEL PERFORMANCE EVALUATION 34
4.1 Model Evaluation Methodology 34
4.2 Model Performance Evaluation against Surface Measurements 35
4.2.1 Evaluation of Ozone 37

4.2.2 Evaluation of Ozone Precursors 44
4.2.3 Evaluation of Fine Particulate Matter ($PM_{2.5}$) 55
4.3 Model Performance Evaluation against Aircraft Measurements 61
4.3.1 September 4 61
4.3.2 September 6 65
4.3.3 September 11 68
4.3.4 September 12 71
4.3.5 September 13 74
4.3.6 September 14 77
4.3.7 September 24 80
4.3.8 September 25 83
4.3.9 September 26 86
4.3.10 All flights 89
4.3.11 Summary of MPEs Against Aircraft Measurements 95

5.0 CAMX AND CMAQ SENSITIVITY TESTS 96
5.1 Sensitivity Simulations 96
5.1.1 Clear-Sky and Adjusted jNO_2 96
5.1.2 Introducing More Clouds 101
5.1.3 Vertical Diffusivity 103
5.1.4 Increasing Grid Model Resolution (1.33 km) 105
5.1.5 Emission Reduction 107
5.2 Summary of Sensitivity Analysis 110

6.0 CONCLUSIONS AND RECOMMENDATIONS FOR FUTURE WORK 115
6.1 Summary of Findings 115
6.1.1 Base Case 115
6.1.2 Sensitivity Tests 116
6.2 Conclusions 117
6.3 Recommendations 117

7.0 REFERENCES 118

APPENDICES
Appendix A. Spatial Plots Of Maximum Daily Average 8-Hour Ozone Concentrations
Appendix B. Model Performance Evaluation of the 36/12 km CAMx Simulation

Appendix C. Time Series of Observed and Predicted Ozone at TCEQ CAMS Sites in September 2013

Appendix D. C CAMx and CMAQ-estimated Average $PM_{2.5}$ Concentrations ($\mu g/m^3$) and their Components for Base Case

Appendix E. HYSPLIT Backward Trajectories

TABLES

Table 2-1. WRF and CAMx modeling domain extents. 8

Table 2-2. Summary of WRF configuration. 9

Table 2-3. Meteorological model performance statistics for the 4 and 1.33 km WRF domains over all CAMS monitors within the Houston-Galveston 1.33 km CAMx domain. 13

Table 2-4. Meteorological model performance statistics for the 4 and 1.33 km WRF domains over all ds472.0 monitors within the Houston-Galveston 1.33 km CAMx domain. 14

Table 2-5. Meteorological model performance statistics for the 4 and 1 .33 km WRF domains over all CAMS and ds472.0 monitors within the Houston-Galveston 1.33 km CAMx domain. 17

Table 2-6. WRF Performance Benchmarks. 21

Table 2-7. Typical weekday (Wednesday) emissions by source category for the TCEQ 4km domain. 25

Table 2-8. Maximum concentration limits for ozone precursors applied to the 36 km boundary condition grid cells across the Gulf of Mexico, Caribbean Sea, and Atlantic Ocean south of Cape Hatteras. 28

Table 3-1. Model Configurations Options for CAMx model. 30

Table 3-2. Model Configuration Options for the CMAQ Model. 31

Table 4-1. Definition of performance metrics for photochemical modeling. 34

Table 4-2. 1-hour ozone model performance statistics of CAMx and CMAQ Base Case for the 4 km domain over all CAMS monitors within the HGBPA 4 km CAMx domain. 42

Table 4-3. 1-hour $PM_{2.5}$ model performance statistics of CAMx and CMAQ Base Case for the 4 km domain over all CAMS monitors within the HGBPA 4 km CAMx domain. 59

FIGURES

Figure 2-1. 36 km/12km (red/dark blue) WRF and CAMx (black/light blue) modeling domains. 6

Figure 2-2. A) 4 km/1.33km (red/dark blue) WRF and CAMx (black/light blue) modeling domains. DISCOVER-AQ flight paths. B) Zoom in of HGBPA region. 7

Figure 2-3. CAMx/CMAQ vertical layer structure. 8

Figure 2-4. Time series of hourly solar radiation for observations (blue) and WRF 4 km (red) and 1.33 km (green) simulations at the Galveston 99th Street CAMS monitor for September 1-30, 2013. 17

Figure 2-5. Time series of hourly 2-m temperature, 10-meter wind speed and 10-meter wind direction for observations (blue) and WRF 4 km (red) and 1.33 km (green) simulations at the William P. Hobby airport (KHOU) for September 1-30, 2013. 18

Figure 2-6. Time series of hourly 2-m temperature, 10-meter wind speed and 10-meter wind direction for observations (blue) and WRF 4 km (red) and 1.33 km (green) simulations at the Galveston airport (KGLS) for September 1-30, 2013. 19

Figure 2-7. Soccer plots across all HG ds472.0 airports (13 sites) for temperature (top left), humidity (top right), wind speed (middle left), wind direction (middle right) and wind speed/wind direction (bottom) for the WRF 4 km results (red) and WRF 1.33 km results (green). Daily statistics are shown as circles and monthly statistics are shown as diamonds. Simple terrain benchmarks are marked with a black dashed line and complex terrain benchmarks are marked with a red dashed line. 22

Figure 2-8. Typical weekday (September 18) anthropogenic NOx, VOC, SO_2, and $PM_{2.5}$ emissions (short tons per day). 26

Figure 2-9. Typical weekday (September 18) natural NOx, VOC, SO_2, and $PM_{2.5}$ emissions (short tons per day). 27

Figure 3-1. Maps of September average daily maximum 8-hour ozone in the 4 km domain from CAMx (left), CMAQ (middle) and the differences between CAMx and CMAQ results (right). 32

Figure 3-2. Time series of observed (black) and predicted (CAMx/CMAQ; red/blue) ozone at Galveston (top) and Clinton (bottom) TCEQ CAMS sites in September 2013. 33

Figure 4-1. Locations of TCEQ CAMS monitoring sites used in the model performance evaluation (zoom-in map shown in the bottom). 36

Figure 4-2. Scatter plots of CAMx/CMAQ predicted and observed hourly ozone concentrations for TCEQ CAMS sites in Houston and nearby vicinity. 38

Figure 4-3. Time series of observed (black) and predicted (CAMx/CMAQ; red/blue) ozone at Galveston (top) and Clinton (bottom) TCEQ CAMS sites in September 2013. 41

Figure 4-4. Scatter plots of CAMx/CMAQ predicted and observed hourly NO (left) and NO_2 (right) concentrations for TCEQ CAMS sites in Houston and nearby vicinity. 44

Figure 4-5. Time series of observed (black) and predicted (CAMx/CMAQ; red/blue) NO concentrations at TCEQ CAMS sites in September 2013. 45

Figure 4-6. Time series of observed (black) and predicted (CAMx/CMAQ; red/blue) NO_2 concentrations at TCEQ CAMS sites in September 2013. 46

Figure 4-7. Scatter plots of CAMx/CMAQ predicted and observed hourly isoprene (top left), acetylene (top right), benzene (bottom left), and toluene (bottom right) concentrations for TCEQ CAMS sites in Houston and nearby vicinity. 48

Figure 4-8. Time series of observed (black) and predicted (CAMx/CMAQ; red/blue) isoprene concentrations at TCEQ CAMS sites in September 2013. 49

Figure 4-9. Time series of observed (black) and predicted (CAMx/CMAQ; red/blue) acetylene concentrations at TCEQ CAMS sites in September 2013. 50

Figure 4-10. Time series of observed (black) and predicted (CAMx/CMAQ; red/blue) benzene concentrations at TCEQ CAMS sites in September 2013. 51

Figure 4-11. Time series of observed (black) and predicted (CAMx/CMAQ; red/blue) toluene concentrations at TCEQ CAMS sites in September 2013....52

Figure 4-12. Scatter plots of CAMx/CMAQ predicted and observed hourly carbon monoxide concentrations for TCEQ CAMS sites in Houston and nearby vicinity. 53

Figure 4-13. Time series of observed (black) and predicted (CAMx/CMAQ; red/blue) carbon monoxide concentrations at TCEQ CAMS sites in September 2013. 54

Figure 4-14. Scatter plots of CAMx/CMAQ predicted and observed hourly $PM_{2.5}$ concentrations for TCEQ CAMS sites in Houston and nearby vicinity. 56

Figure 4-15. Time series of observed (black) and predicted (CAMx/CMAQ; red/blue) $PM_{2.5}$ concentrations at TCEQ CAMS sites in September 2013. 58

Figure 4-16. Observed $PM_{2.5}$ speciation at Conroe site [source: Sheesley and Usenko, 2015]....60

Figure 4-17. Predicted $PM_{2.5}$ speciation at Conroe site in September 2013 60

Figure 4-18. Flight paths of P3-B aircraft during the DISCOVER-AQ 2013 field study 61

Figure 4-19. Vertical profiles measured by P3-B aircraft compared to CAMx/CMAQ estimated on September 4, 2013....64

Figure 4-20. Vertical profiles measured by P3-B aircraft compared to CAMx/CMAQ estimated on September 6, 2013....67

Figure 4-21. Vertical profiles measured by P3-B aircraft compared to CAMx/CMAQ estimated on September 11, 2013....70

Figure 4-22. Vertical profiles measured by P3-B aircraft compared to CAMx/CMAQ estimated on September 12, 2013....73

Figure 4-23. Vertical profiles measured by P3-B aircraft compared to CAMx/CMAQ estimated on September 13, 2013....76

Figure 4-24. Vertical profiles measured by P3-B aircraft compared to CAMx/CMAQ estimated on September 14, 2013....79

Figure 4-25. Vertical profiles measured by P3-B aircraft compared to CAMx/CMAQ estimated on September 24, 2013....82

Figure 5-1. Clear-sky (top) and cloud-adjusted (bottom) jNO_2 predictions at surface by CAMx and CMAQ on September 4, 2013. 97

Figure 5-2. Clear-sky (top) and adjusted (bottom) jNO_2 predictions at 750 m. by CAMx and CMAQ on September 4, 2013. 98

Figure 5-3. JNO_2 Vertical profiles measured by P3-B aircraft compared to CAMx and CMAQ simulations with clear-sky/adjusted photolysis rates. 100

Figure 5-4. Ozone vertical profiles measured by P3-B aircraft compared to CAMx and CMAQ simulations with clear-sky/adjusted photolysis rates. 101

Figure 5-5. Vertical profiles measured by P3-B aircraft compared to CAMx base case and morstrat simulations. 103

Figure 5-6. Vertical profiles measured by P3-B aircraft compared to CAMx base case and CAMx with CMAQ_Kv simulations. 105

Figure 5-7. Vertical profiles measured by P3-B aircraft compared to CAMx base case and CAMx 1.33-km simulations. 107

Figure 5-8. CAMx and CMAQ ozone responses to 20% NOx and VOC emission reductions on September 5, 2013....108

Figure 5-9. CAMx and CMAQ ozone responses to 20% NOx and VOC emission reductions on September 15, 2013....109

Figure 5-10. CAMx and CMAQ ozone responses to 20% NOx and VOC emission reductions on September 25, 2013....110

Figure 5-11. Comparison of ozone model performance across all CAMS sites within the 1.33 km domain during September 2013 period....111

Figure 5-12. Time series of observed (black) and predicted (color) ozone concentrations (ppb) at Clinton in September 2013. 112

Figure 5-13. Time series of observed (black) and predicted (color) ozone concentrations (ppb) at Galveston in September 2013.....113

Figure 5-14. CAMx and CMAQ ozone responses to 20% NOx and VOC emission reductions based on monthly average MDA8 ozone.....114

EXECUTIVE SUMMARY

The Comprehensive Air quality Model with Extensions (CAMx) and the Community Multi-scale Air Quality model, (CMAQ) are the two photochemical air quality models most often used for State Implementation Plan (SIP) modeling. The Texas Commission on Environmental Quality (TCEQ) uses CAMx for Ozone SIP modeling. Although the two models are functionally equivalent in many respects, there are also numerous differences between their internal workings, and each has its own relative strengths. The purpose of this project is to perform a comprehensive comparison between CAMx and CMAQ. The results of this comparison help understand the relative strengths and weaknesses of the two systems and point towards potential improvements to TCEQ's modeling capabilities.

The NASA Deriving Information on Surface Conditions from COlumn and VERtically resolved observations – Air Quality (DISCOVER-AQ) project conducted extensive sampling of surface and aloft chemical and meteorological data during September of 2013 in and around Houston, providing a rare opportunity to perform a three-dimensional, multi-species model evaluation. Applying these models to the DISCOVER-AQ study period also adds to understanding of ozone formation in the Houston area.

Ramboll Environ prepared CAMx and CMAQ modelling inputs the September 2013 modeling period. Meteorological fields were developed using the WRF model. WRF surface performance was assessed through performance statistics and graphical model-observation comparisons for winds, temperature and solar radiation. The WRF model performance evaluation in the 4 km and 1.33 km suggest that both domains have acceptable performance, mostly meeting performance benchmarks.

We prepared CAMx-ready emissions for the 36/12/4 km domains and documented 4 km domain-wide emissions. Anthropogenic emissions were provided by TCEQ and biogenic emissions were derived using the MEGAN model. We used the CAMx2CMAQ program to convert the CAMx-formatted initial/boundary condition and emission inputs to CMAQ input format and visualized the CAMx and CMAQ input files to ensure correct conversion.

Base Case Simulations

CAMx and CMAQ predictions of maximum daily average 8-hour ozone in September 2013 are similar in spatial patterns and magnitude. The predicted average MDA8 ozone concentrations differ by less than 5 ppb across the HGBPA area. CMAQ-predicted MDA8 ozone tends to be lower around the area northeast of the Galveston Bay including Beaumont. The results in the Houston area are mixed with a tendency of higher CMAQ predictions for ozone maxima. CAMx predictions are generally lower than CMAQ along the coast (e.g., in Galveston) and in the Gulf.

Predicted time series of $PM_{2.5}$ concentrations by CAMx and CMAQ are comparable at inland sites. Both models predicted that OA and other PM are top two major constituents in $PM_{2.5}$. CAMx predictions tend to be higher than CMAQ near the coastline on average by 3-4 ug/m^3 due

to higher nitrate (PNO_3) and sea-salt sodium (Na). This discrepancy can be explained by a different methodology used to estimate and allocate sea-salt emissions.

Model Performance Evaluation

CAMx and CMAQ show similar model performance against surface measurements at TCEQ CAMS sites and P3-B aircraft measurements during DISCOVER-AQ study for all gaseous species examined:

- Ozone: Both models over predicted surface ozone across the HGBPA area. Large ozone bias is seen during the first half of September when observed ozone is generally lower than 40 ppb. Better performance is seen on high observed ozone days (i.e., September 24-27). Compared to aircraft measurements, ozone is generally over predicted near surface (< 300 m) but under predicated above 2000 m. The models under predict ozone at all heights on September 25. This day was influenced by a frontal passage and a re-circulation of pollution due to afternoon sea-breeze. The downward mixing due to the frontal passage was replicated well by the models but the re-circulation was not captured by WRF meteorology.
- Photolysis rate of NO_2 (jNO_2): Both models consistently over predicted jNO_2. The over prediction is expected due to under estimated clouds. Good jNO_2 performance is seen on clear-sky days. However, good performance of jNO_2 does not necessary yield good ozone performance.
- NOx: NO is under estimated while NO_2 is over estimated. Over estimation of NO_2 may indicate an inventory bias.
- VOC: Both models tend to over predict VOC. Isoprene performance is mixed with the models' tendency to overestimate 75-percentile concentrations but reasonably replicate lower concentrations. CMAQ tends to overestimate morning peaks with values often higher than CAMx by a factor of 2). We expect that the landuse Kv patch in CAMx introduces more night-time mixing which reduces isoprene buildup from lower planetary boundary layer. Formaldehyde performance is quite good. Acetaldehyde is over predicted under 2000 m with near-ground concentrations over predicted by ~50%. Predicted acetaldehyde vertical profiles are more similar to those of formaldehyde. In addition, high acetaldehyde events coincide with high formaldehyde and NOx events implying the same emitting sources. At surface, the models biased high on toluene but low on xylene and benzene suggesting a possible issue with VOC speciation profiles and/or overstated on-road mobile emissions. Both models do not capture potential emission events as they are not described in the emissions inventory.
- $PM_{2.5}$: EC is largely overestimated mostly likely due to overstated emissions. Sulphate, ammonium, and WSOC are underestimated. Under-prediction of sulphate may be related to under-prediction of clouds. Since sulphate dominates inorganic component in summer, ammonium performance follows that of sulphate. CMAQ-estimated secondary PMs are all lower than CAMx. With the primary PM being overstated and the secondary

PM being underestimated, it is less meaningful to examine $PM_{2.5}$ mass performance due to compensation effects among PM species.

Sensitivity Simulations

Five sensitivity simulations were conducted to examine various aspects of photochemical modeling including photochemistry, vertical transport, grid resolution, and emission inputs. The first four simulations show very similar diurnal profiles and the differences lie on ozone peak concentrations. More stratiform cloudiness helps reduce the day-time peak concentration up to 20 ppb on some days, but the simulation is still largely biased high. The model performance of the CAMx 1.33 km simulation shows slight improvement. CMAQ Base Case shows slightly lower NMB than CAMx simulations which maybe attributable to lower predicted jNO_2.

Predicted ozone in the HGBPA area is mostly insensitive to changes in photolysis rates and vertical diffusivity suggesting that local production is not the main contributor of high ozone bias. Modeled ozone shows persistent overestimates that are caused by other processes which are currently not well understood.

CAMx and CMAQ models show comparable ozone responses to 20% NOx and VOC emission reductions. On days with high predicted ozone concentrations in Houston (> 60 ppb), the emission reductions lower the MDA8 ozone up to 4% (3-4 ppb). Slightly larger ozone reductions are seen downwind in the west of Houston. Ozone disbenefit is seen close to Lake Charles, LA, suggesting that the area has a different NOx/VOC-sensitivity regime than in Houston. Ozone disbenefit in the Houston area occurs on days with low predicted ozone concentrations.

Conclusions

Modeling inputs are most critical in any photochemical modeling exercise. When using the same inputs and chemistry mechanism, CAMx and CMAQ show very comparable model performance despite some differences in modeling processes (e.g., nighttime mixing, photolysis rates).

The cause of high ozone bias is unresolved. While high ozone events, such as those on September 24-26, are related to frontal passages and re-circulation of sea-breeze, ozone predictions on other September days are likely influenced by continental transport or background ozone. Most days in September 2013 HGBPA area was influenced by easterly winds bringing air parcels from Louisiana and up-wind locations. Based on the back-trajectory analysis, the models could reasonably replicate the easterly wind direction with some exceptions. The tendency of the CAMx model to overestimate ozone in the south eastern US could partly attribute to the high ozone bias in the HGBPA area given the easterly wind directions. This is supported by the examination of ozone at an upwind and a downwind monitor which suggests reasonable predictions of local ozone production. Other possible explanations are too low marine boundary layers simulated by the models or missing removal processes.

Recommendations

- Accurate meteorological data is critical for accurate ozone prediction in the Houston area. Biases in the WRF model's simulation of clouds, wind direction, and wind speed introduce bias into the ozone prediction. Improvements to the WRF model treatment of clouds and sea-breeze re-circulation will enable the photochemical models to better estimate local production of ozone.
- Large discrepancy of the clear-sky jNO_2 estimated by CAMx and CMAQ should be further investigated. We also recommend a sensitivity test that approximates an upper-bound of cloud and aerosol adjustment in the Houston area.
- Despite a plume-in-grid feature in CAMx, CMAQ predicted higher peak NO_2 concentrations. Further examination on elevated source processes such as plume-rise treatment is recommended.
- CAMx and CMAQ overestimate several VOC at CAMS sites and along flight tracks. This likely indicates a bias in emissions inventory especially from those HRVOC sources that contribute to aldehydes. We recommend additional tests of different HRVOC sensitivity emissions in the Houston area.
- Beaumont monitors have the worst performance with modeled mean values more than doubling observational values. Since NOx emissions from refineries dominate mobile sources in this area, it may indicate a point source inventory bias.
- Future ozone modeling exercises for the Houston area should include halogen chemistry and explore other possible removal processes specific to the coastal conditions.

1.0 INTRODUCTION

The Comprehensive Air quality Model with Extensions (CAMx) and the Community Multi-scale Air Quality model, (CMAQ) are the two photochemical air quality models most often used for State Implementation Plan (SIP) modeling. CMAQ is developed by the U.S. Environmental Protection Agency (EPA) while CAMx is developed by Ramboll Environ. The Texas Commission on Environmental Quality (TCEQ) uses CAMx for Ozone SIP modeling. Although the two models are functionally equivalent in many respects, there are also numerous differences between their internal workings, and each has its own relative strengths. Using both models to simulate a common time period can help to elucidate these relative strengths, and can eventually lead to improvements in both systems.

The NASA Deriving Information on Surface Conditions from COlumn and VERtically resolved observations – Air Quality (DISCOVER-AQ) project conducted extensive sampling of surface and aloft chemical and meteorological data during September of 2013 in and around Houston, providing a rare opportunity to perform a three-dimensional, multi-species model evaluation. In addition to providing insight into the models themselves, running CAMx and CMAQ side-by-side for this period enhance understanding of the land-sea-bay wind patterns and their interaction with the complex mix of emission sources in the Houston area.

The purpose of this project is to perform a comprehensive comparison between CAMx and CMAQ. The results of this comparison help understand the relative strengths and weaknesses of the two systems and point towards potential improvements to TCEQ's modeling capabilities. Applying these models to the DISCOVER-AQ study period also adds to understanding of ozone formation in the Houston area.

This document provides the final report for the TCEQ Project #FY15-52 "Three-dimensional performance comparison of CAMx and CMAQ using the 2013 DISCOVER-AQ field study data base". Meteorological modeling and preparation of other model inputs are described in Section 2 of this report. A comparison of CAMx and CMAQ Base Case simulations is presented in Section 3. The model results were evaluated against surface and aircraft measurements as discussed in Section 4. Sensitivity simulations were performed to investigate model responses to various parameters as described in Section 5. Conclusions and recommendations are presented in Section 6.

2.0 MODELING INPUT PREPARATION

This section documents model input preparation, including meteorology generated using the Weather Research and Forecasting (WRF) model, emissions of ozone and particulate matter (PM) precursors, and lateral boundary conditions from global model outputs, specific to the selected period.

2.1 Modeling Domains

The WRF and CAMx/CMAQ modeling grids are shown in Figure 2-1 and Figure 2-2, and the dimensions of grids are given in Table 2-1. The layer structure is defined with 28 layers from the surface to 15 km and a surface layer depth of 34m (Figure 2-3). The outer 36 km grid covers the continental US (CONUS) and is the same grid that EPA and many States use for regional air quality modeling. The nested 12 km grid covers Texas and a substantial area that would typically be upwind of Texas during an ozone episode including adjacent States and the western Gulf of Mexico. The 4 km grid covers Houston-Galveston-Brazoria-Beaumont-Port Arthur (HGBPA) areas. The 1.33km grid encompasses the DISCOVER-AQ flight paths in Houston-Galveston areas (HG) during September 2013.

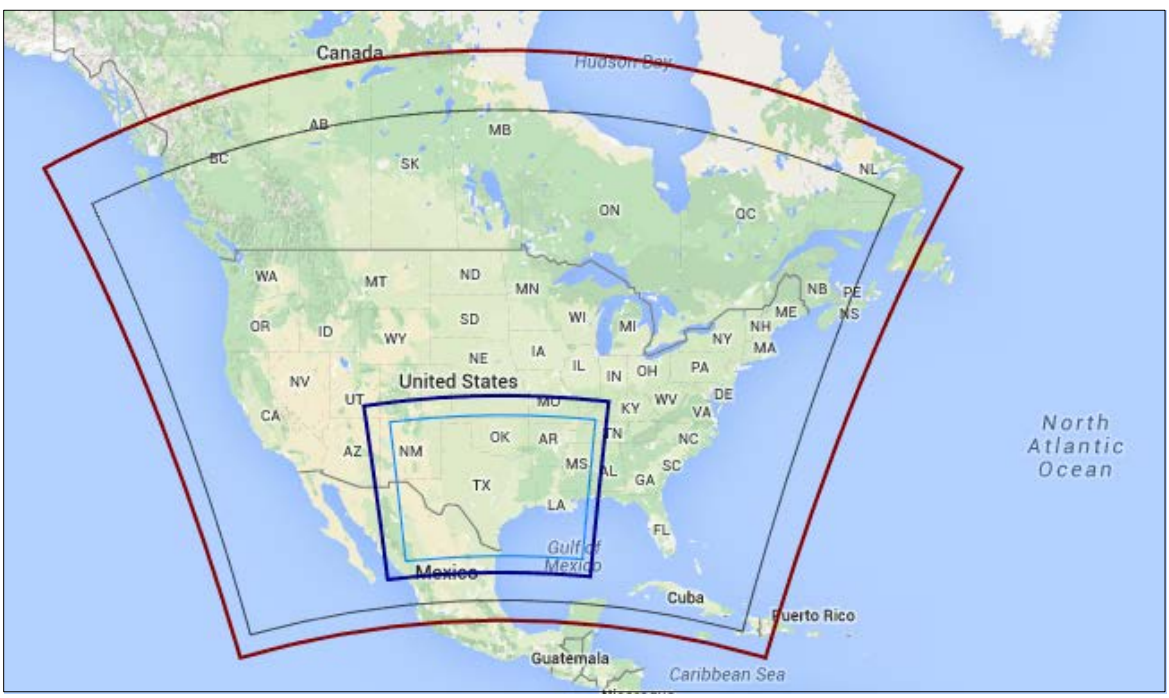

Figure 2-1. 36 km/12km (red/dark blue) WRF and CAMx (black/light blue) modeling domains[1].

[1] Figure from http://www.tceq.texas.gov/airquality/airmod/rider8/modeling/domain

A)

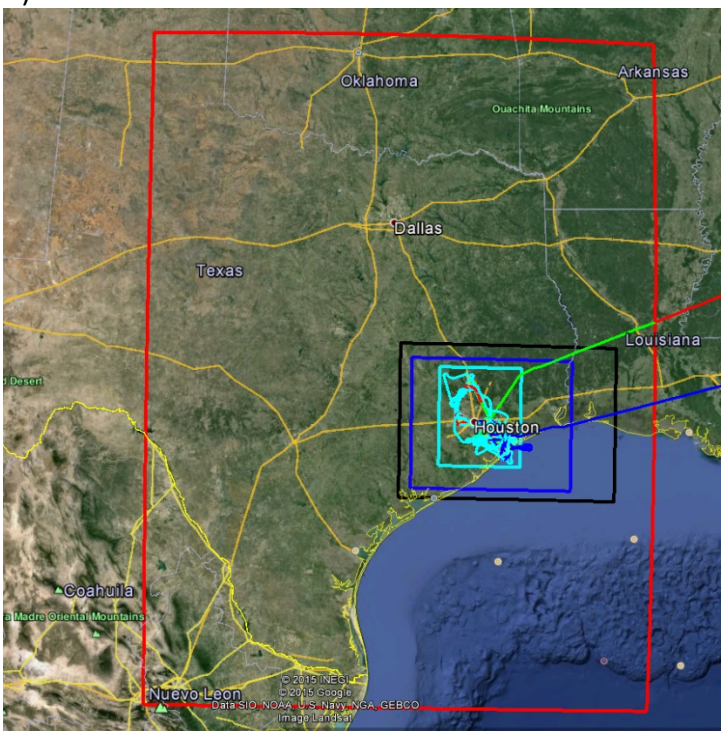

B)

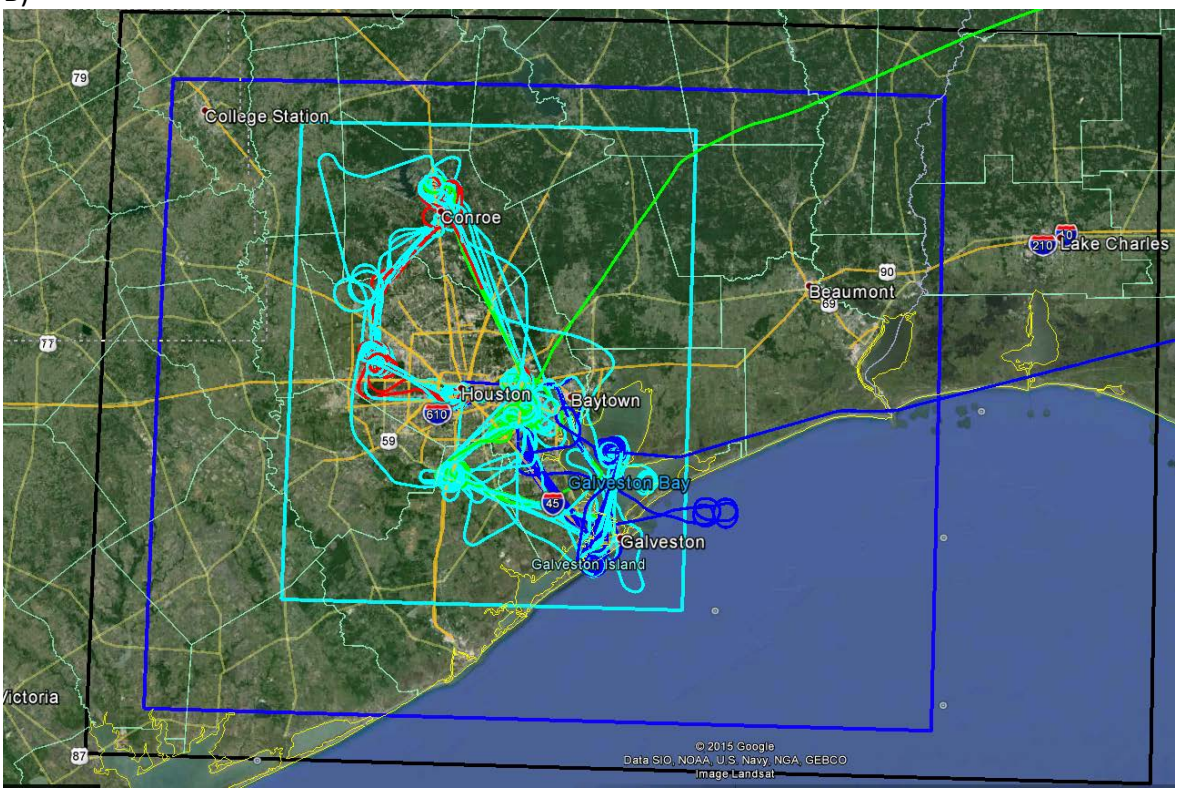

Figure 2-2. A) 4 km/1.33km (red/dark blue) WRF and CAMx (black/light blue) modeling domains. DISCOVER-AQ flight paths. B) Zoom in of HGBPA region.

Table 2-1. WRF and CAMx modeling domain extents.

Domain	Grid Size (number of grid cells)		
	East-West	North-South	Layers
WRF			
North America 36km	162	128	43
Texas 12km	174	138	43
Texas 4km	216	288	43
HG 1.33km	204	165	43
CAMx			
RPO 36km	148	112	28
Texas 12km	149	110	28
HGBPA 4km	92	65	28
HG 1.33km	104	125	28

Vertical Layer Structure

Corresponding WRF Layer	Layer Top (m AGL)	CAMx Layer	Layer Center (m AGL)	Thickness (m)
38	15179.1	28	13637.9	3082.5
36	12096.6	27	10631.6	2930.0
32	9166.6	26	8063.8	2205.7
29	6960.9	25	6398.4	1125.0
27	5835.9	24	5367.0	937.9
25	4898.0	23	4502.2	791.6
23	4106.4	22	3739.9	733.0
21	3373.5	21	3199.9	347.2
20	3026.3	20	2858.3	335.9
19	2690.4	19	2528.3	324.3
18	2366.1	18	2234.7	262.8
17	2103.3	17	1975.2	256.2
16	1847.2	16	1722.2	249.9
15	1597.3	15	1475.3	243.9
14	1353.4	14	1281.6	143.6
13	1209.8	13	1139.0	141.6
12	1068.2	12	998.3	139.7
11	928.5	11	859.5	137.8
10	790.6	10	745.2	90.9
9	699.7	9	654.7	90.1
8	609.7	8	565.0	89.3
7	520.3	7	476.1	88.5
6	431.8	6	387.9	87.8
5	344.0	5	300.5	87.1
4	256.9	4	213.8	86.3
3	170.6	3	127.8	85.6
2	85.0	2	59.4	51.0
1	33.9	1	17.0	33.9

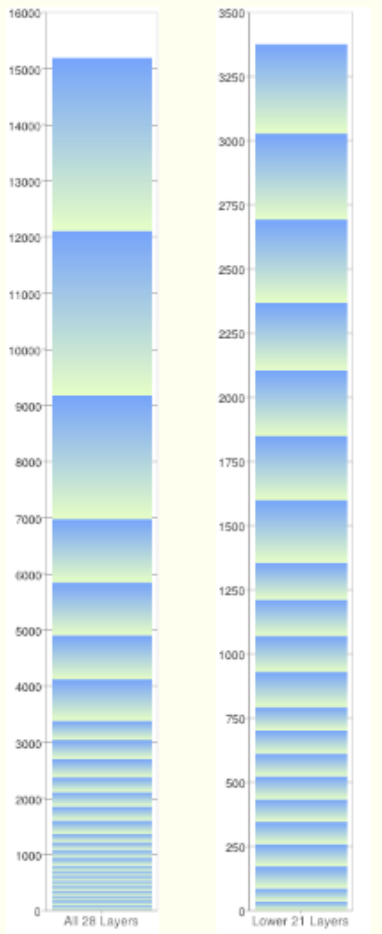

AGL - Above Ground Level.

Figure 2-3. CAMx/CMAQ vertical layer structure. [2]

[2] TCEQ figure from http://www.tceq.texas.gov/airquality/airmod/rider8/modeling/domain.

2.2 Meteorological Inputs

We developed CAMx meteorological inputs for this application using the latest version of the Weather Research Forecast (WRF; Skamarock et al., 2008) meteorological model (Version 3.6.1 released August 14, 2014) available at the time.

2.2.1 WRF Model Configuration

The WRF model was run for the September 2013 period in a configuration developed for a previous Texas modeling application. We provide a summary of the WRF model configuration in Table 2-2. The model was run as a series of independent 5-day simulations starting from Aug 15, 2013, in order to provide CAMx with meteorological inputs for a 2-week spinup period.

Table 2-2. Summary of WRF configuration.

WRF version	3.6.1
Horizontal Resolution	36/12/4/1.333 km
Microphysics	WSM6
Longwave Radiation	RRTMG
Shortwave Radiation	RRTMG
Surface Layer Physics	MM5 similarity
LSM	Noah
PBL scheme	Yonsei University (YSU)
Cumulus parameterization	36/12 km: Kain-Fritsch 4/1.333 km: none
Boundary and Initial Conditions Data Source	12 km NAM analysis
Analysis Nudging Coefficients (s^{-1})	36/12 km: 3-D 4/1.33 km: None
Winds	$3x10^{-4}$
Temperature	$3x10^{-4}$ (above BL only)
Water Vapor Mixing Ratio	$3x10^{-4}$ (above BL only)
Observation Nudging Coefficients (s^{-1})	36/12/4/1.33 km: None
Winds	None
Temperature	None
Water Vapor Mixing Ratio	None
Miscellaneous Notes	Using KF-RRTMG interaction which feeds back sub-grid cloud information to radiation scheme (36/12 km only)

Ramboll Environ applied several changes to the raw WRF meteorological fields before ingesting into CAMx. First, we applied the YSU Kv methodology within WRFCAMx in order to promote consistency between the WRF and CAMx models. Next, we enhanced sub-grid cloudiness for all domains using a diagnosis of thermodynamic properties similar to that used by the CMAQ model. Finally, we applied patches to the vertical diffusivity fields in order to enhance nighttime mixing in urban areas (commonly called “Kv100”) and mixing below convective clouds (Kv cloud patch).

2.2.2 WRF Model Performance Evaluation

The purpose of the WRF model performance evaluation is to determine if meteorological performance in the HG area is acceptable for air quality modeling and to determine if 1.33 km performance is better than 4 km performance.

In general, complex land use/land cover patterns present a significant challenge to wind predictions in WRF. Land and sea/bay breezes, which are frequent in the HGBPA region, further complicate these predictions. Because Gulf air is in general much cleaner than continental air, pollutant concentrations in HGBPA are greatly influenced by land/sea breeze circulations. Errors in the strength or timing of these circulations in WRF can lead to significant ozone biases in the photochemical model.

Clouds pose another significant challenge to WRF and are some of the most difficult meteorological phenomena to accurately simulate. As noted by Dolwick (2006) and Voulgarakis et al. (2009a), their widely varying spatial and temporal scales are often ill-suited to Eulerian modeling applications, especially at scales addressed by photochemical modeling. Although WRF can adequately characterize large-scale cloud patterns associated with well-resolved weather systems, these models must apply complex moisture and energy balance parameterizations to account for the bulk characteristics of cloud patterns at sub-grid scales. The simulation of cloud influences at these smaller scales, which range from scattered fair-weather cumulus to deep convective cells, is fraught with uncertainty and is often the source of poor performance in replicating cloud fields as well as associated temperature, wind, and turbulence (mixing) structures. Errors and uncertainties in cloud fields can translate to large errors and uncertainties in the photochemical models (Emery et al., 2010). Previous Texas modeling efforts show that coastal regions such as HGB and BPA tend to have poor solar radiation performance (indicating inaccurate characterization of clouds) relative to inland areas.

In this section, we evaluate wind speed, wind direction, solar radiation and 2-meter temperature statistics at CAMS sites within the HG 1.33 km domain. We also evaluate statistical performance at ds427.0 sites (commercial and municipal airports) for the same meteorological parameters (excluding solar radiation, as that is not measured at ds472.0 sites) within the same area and compare with the performance at CAMS sites. Finally, we present "soccer plots" of daily and monthly statistics at ds472.0 sites in order to place the meteorological performance in context of similar model exercises.

2.2.2.1 Statistics

The statistical metrics computed for CAMS monitoring locations are:

- Normalized Mean Bias (NMB)

$$NMB = \frac{\sum_{i=1}^{N}(P_i - O_i)}{\sum_{i=1}^{N} O_i}$$

where P_i and O_i are the predicted and observed values (O_i,P_i) in a data pair and N is the number of observed/modeled data pairs.

- Normalized Mean Error (NME)

$$NME = \frac{\sum_{i=1}^{N} |P_i - O_i|}{\sum_{i=1}^{N} O_i}$$

- Root Mean Squared Error (RMSE)

$$RMSE = \sqrt{\frac{\sum_{i=1}^{N} (P_i - O_i)^2}{N}}$$

2.2.2.2 Analysis of Model Performance in the HG Region

Table 2-3 presents meteorological performance statistics for the WRF 4 and 1.33 km domains across all CAMS sites within the CAMx HG 1.33 km modeling domain for 2-meter temperature, wind speed, wind direction and solar radiation. Note that the model performance statistics are computed for all hours (day and night), except for solar radiation.

Both WRF domains demonstrated considerable skill in predicting temperatures across the HG region. The normalized mean bias and error were around ±1 % and 3 %, respectively. It should be noted however, that with NME almost three times larger than NMB for September 2013 (and larger NME:NMB ratios exist on some days), it is likely that the very low biases are the result of mid-day over-predictions "cancelling out" overnight low under-predictions. The differences between the 4 km and 1.33 km WRF statistics are nearly identical (maximum daily NMB and NME of ±0.2 %) throughout the month.

Wind direction performance shows respectable biases (4 km NMB of 0.5 % and 1.33 km NMB of 5 %) over the entire month, but several individual days show NMB greater than 20 % (4 km: 4 days; 1.33 km: 5 days). September NME is near 30 % for both domains (4 km NME: 34 %; 1.33 km NME: 31 %), which is consistent with previous modeling efforts conducted in the region (Johnson et al., 2015). Each WRF domain's wind direction NME exceeds 50 % on 3 individual September days. Most days show some improvement in NME and RMSE from the increased resolution of the 1.33 km domain, though it is generally small.

Wind speed performance is not as good as wind direction at CAMS sites. September NMB for both domains is 31 % and NME is over 50 % for both domains (4 km: 57 %; 1.33 km: 51 %). As with the wind direction statistics, we observe small improvements in NME and RMSE on most days from the increased resolution of the 1.33 km domain. Examination of the daily statistics suggests that while most days display positive NMB (wind speeds over-predicted by WRF), NME is generally much larger, which indicates that the model is also under-predicting wind speeds compared to CAMS observations. As noted in Johnson et al. (2013), the WRF predicted winds during the afternoon hours were frequently lighter than the observed winds on some days with

poor model performance. Thus, the wind speed over-prediction bias from the model performance statistics is likely due to over-prediction of nocturnal winds. This has also been found in a WRF modeling study conducted by NOAA for TCEQ (Lee et al., 2012). In addition, recent WRF model performance efforts conducted by Ramboll Environ for a Northeast Texas June 2006 ozone episode show that inappropriate monitor siting at the Longview and possibly Karnack CAMS sites may play a role in inflating wind speed over-predictions under certain wind direction regimes. We examine model performance at ds472.0 (commercial and municipal airports) sites later in this section.

Solar radiation performance statistics indicate a slight over-prediction bias in September. While the WRF NMB for September is under 10 % (4 km: 7 %; 1.33 km: 6 %), there are several individual days where NMB is ±40 % or greater. In addition, the NME for both WRF domains is near 50 % and RMSE is around 160 W M^{-2}, indicating that clouds are not being predicted at the right time or location in the HG region. As noted earlier, previous Texas modeling studies suggest that solar radiation performance tends to be worse near coastal regions like BPA and HGB.

We note that the solar radiation values we are utilizing for this evaluation are adjusted for the presence of sub-grid cloudiness within WRFCAMx. First, WRFCAMx uses a cloud optical depth (COD) blending technique (DelGenio et al., 1996; Voulgarakis et al., 2009b) to add sub-grid and resolved clouds in each grid cell column. Then solar radiation in each grid cell column is attenuated for the adjusted COD using a technique developed by Chang et al. (1987). While this approach is not completely consistent with CAMx (which uses a streamlined version of the Tropospheric UltraViolet (TUV) radiative transfer model to attenuate photolysis rates), it is preferable to using the raw solar radiation fields from WRF which are unaltered by sub-grid clouds.

We present meteorological performance statistics for the WRF 4 and 1.33 km domains across all ds472.0 sites within the CAMx HG 1.33 km modeling domain for 2-meter temperature, wind speed and wind direction in Table 2-4. A comparison of the September 2013 statistics for CAMS versus ds472.0 sites is given in Table 2-5.

We note that 2-meter temperature statistics at airport sites are very similar to the values found at CAMS sites in Table 2-3 and performance is nearly identical for the two WRF domains. Wind direction performance in terms of NME is improved at airport sites (NME of around 28 %; improvement of 3-5 % over CAMS). RMSE performance for wind direction is also improved at airport sites (RMSE is below 50 degrees for both WRF domains; improvement of 5-6 degrees over CAMS). Wind speed bias improves significantly at airport sites (NMB drops from 31 % for CAMS to under 3 % for ds472.0 sites). NME is also improved over CAMS sites, with NME for WRF 4 km and 1.33 km domains dropping by around 5 % for both domains. RMSE for wind speeds also improves at airport sites, but only by 0.2 mph for both domains.

The statistics comparison shown in Table 2-5 (September 2013 monthly average statistics computed over all CAMS and ds472.0 sites) may suggest a difference in how the ds472.0

monitors are sited with respect to the CAMS monitors. This finding would agree with previous work that analysed siting issues for Northeast Texas monitors, but a thorough analysis of the CAMS monitors and their surroundings would need to be conducted to make a final determination. We note that the spatial distribution of airport sites is not the same as CAMS and the monitoring network is not as dense. So there may be alternative explanations for the different performance statistics for the two monitoring networks.

Table 2-3. Meteorological model performance statistics for the 4 and 1.33 km WRF domains over all CAMS monitors within the Houston-Galveston 1.33 km CAMx domain.

		Temperature						Wind Speed						Wind Direction						Solar Radiation					
		NMB (%)		NME (%)		RMSE (degrees F)		NMB (%)		NME (%)		RMSE (mph)		NMB (%)		NME (%)		RMSE (degrees)		NMB (%)		NME (%)		RMSE (W/m2)	
Site	Date	4km	1.33km	4km	1.33km	4km	1.33km	4km	1.33km	4km	1.33km	4km	1.33km	4km	1.33km	4km	1.33km	4km	1.33km	4km	1.33km	4km	1.33km	4km	1.33km
CAMS	**All**	**1.2**	**1.2**	**3.2**	**3.2**	**3.3**	**3.3**	**31.2**	**31.3**	**57.1**	**50.7**	**4.1**	**3.5**	**-0.2**	**5.1**	**33.6**	**30.7**	**53.2**	**49.8**	**7.0**	**5.9**	**48.6**	**48.3**	**158.2**	**158.5**
CAMS	20130901	0.7	0.7	2.2	2.3	2.3	2.4	15.5	8.1	46.7	35.7	3.5	2.6	-7.2	-0.1	22.7	14.6	56.3	44.0	11.6	12.0	33.0	31.6	151.2	141.1
CAMS	20130902	0.7	0.8	2.8	2.9	3.3	3.4	21.9	3.4	54.6	43.9	3.6	2.9	-12.0	-0.8	32.3	20.3	79.4	58.9	23.0	26.7	33.8	35.1	150.3	157.8
CAMS	20130903	-0.4	-0.4	2.7	2.8	3.1	3.2	3.2	-0.1	47.0	48.0	2.9	3.0	-10.5	-4.6	33.3	32.5	86.0	86.5	-30.7	-32.7	41.3	42.7	187.5	196.8
CAMS	20130904	1.7	1.7	3.6	3.7	3.7	3.8	74.1	77.9	80.6	85.1	4.3	4.4	3.9	-0.1	49.1	52.1	99.8	106.7	35.0	34.1	54.1	54.2	192.2	193.5
CAMS	20130905	1.6	1.7	2.8	2.9	3.1	3.2	39.9	30.4	56.2	43.1	3.6	2.8	-8.0	-6.5	36.3	33.8	55.7	54.4	16.7	13.2	39.6	35.6	162.0	147.8
CAMS	20130906	2.6	2.7	3.1	3.2	3.3	3.4	38.3	47.3	51.7	52.3	3.5	3.3	-9.3	13.6	26.2	27.6	45.1	50.5	39.5	41.1	65.4	63.7	217.5	214.8
CAMS	20130907	6.3	6.4	6.7	6.8	7.0	7.0	47.5	51.1	68.8	63.1	4.0	3.4	4.0	15.1	47.6	45.3	68.7	65.2	82.8	79.6	93.7	88.2	267.0	255.3
CAMS	20130908	4.6	4.6	4.7	4.8	4.5	4.6	43.8	72.4	59.6	74.6	3.7	4.4	-9.0	4.2	42.9	32.2	61.7	46.9	30.3	27.2	44.9	46.9	174.9	181.0
CAMS	20130909	1.9	1.9	2.8	2.9	3.0	3.0	7.5	18.2	49.2	36.0	4.2	3.2	0.4	-0.2	22.8	20.2	38.9	34.5	-15.4	-12.4	43.1	42.6	160.6	166.2
CAMS	20130910	1.2	1.3	2.6	2.7	2.8	2.9	31.2	27.2	51.7	37.8	4.4	3.1	7.4	4.7	22.3	21.9	40.0	39.4	36.3	35.4	45.6	45.0	147.1	142.8
CAMS	20130911	0.8	0.9	2.1	2.1	2.2	2.2	24.1	35.8	45.3	42.2	3.4	3.1	0.9	2.7	27.3	25.2	34.4	32.5	9.7	7.2	40.2	40.6	167.0	169.0
CAMS	20130912	1.0	1.1	2.4	2.4	2.6	2.6	38.4	36.9	49.4	46.8	3.5	3.3	-7.1	-2.0	30.8	29.3	47.0	45.8	5.6	4.6	22.5	23.1	114.3	121.1
CAMS	20130913	0.6	0.7	2.4	2.5	2.6	2.7	79.8	64.1	85.0	67.8	5.1	4.1	-4.9	4.7	22.8	23.4	43.6	44.1	14.3	16.4	21.8	21.8	96.5	97.2
CAMS	20130914	1.8	1.8	2.9	2.9	3.2	3.2	48.6	24.1	61.7	44.9	4.2	3.1	-2.4	-0.4	27.4	28.1	37.2	37.2	30.2	26.0	40.1	36.3	156.1	144.8
CAMS	20130915	0.4	0.4	2.0	2.1	2.3	2.3	25.3	39.8	45.5	46.1	4.0	3.8	-11.6	-6.0	22.0	20.7	25.7	24.3	2.9	4.2	37.2	37.9	134.4	136.2
CAMS	20130916	1.7	1.8	2.7	2.7	3.3	3.3	55.2	47.5	79.7	53.7	6.4	4.0	-2.1	-0.3	23.7	22.3	31.2	29.2	-35.1	-34.9	52.3	49.9	157.7	152.5
CAMS	20130917	0.8	0.9	2.5	2.5	2.6	2.6	45.4	48.9	59.2	56.4	4.9	4.3	-20.9	-11.7	28.8	25.0	35.8	32.1	-38.7	-44.2	45.3	48.4	196.1	210.6
CAMS	20130918	1.7	1.8	2.7	2.8	2.8	2.9	14.8	25.9	44.6	41.7	3.9	3.5	-1.7	2.5	27.3	30.0	41.1	44.8	-48.5	-51.9	53.3	54.7	201.2	203.3
CAMS	20130919	3.1	3.1	3.7	3.7	4.3	4.3	12.1	28.5	46.9	41.7	4.3	3.6	-12.0	-9.3	24.3	21.3	33.8	29.1	-10.4	0.6	72.4	70.3	206.8	197.0
CAMS	20130920	3.4	3.5	3.9	4.0	3.9	4.0	55.0	37.1	75.7	60.7	6.2	4.9	-4.4	-6.2	24.5	22.3	53.4	47.3	13.1	13.8	82.0	76.9	106.9	101.9
CAMS	20130921	4.1	4.1	4.5	4.5	3.8	3.8	63.3	40.2	66.3	47.6	6.4	4.6	47.6	29.7	57.2	39.9	36.2	28.6	11.3	2.9	57.3	53.5	80.2	83.8
CAMS	20130922	0.3	0.3	2.8	2.8	2.7	2.7	26.9	42.8	40.7	48.8	3.6	4.1	7.1	31.0	43.7	44.3	22.9	22.6	-11.1	-10.3	37.7	37.2	156.6	154.2
CAMS	20130923	-1.6	-1.6	3.2	3.2	3.2	3.2	-14.6	30.6	44.6	42.6	3.3	3.0	23.9	42.3	58.4	51.7	44.3	38.8	-53.5	-54.7	55.7	56.2	204.2	206.6
CAMS	20130924	-2.4	-2.4	3.7	3.7	3.9	4.0	31.0	38.3	54.1	50.9	3.4	3.0	23.2	40.6	46.4	47.9	56.2	56.5	22.7	23.8	31.6	31.9	117.7	118.4
CAMS	20130925	0.3	0.3	3.4	3.6	3.5	3.6	72.5	60.4	89.2	81.0	3.8	3.5	-6.6	-7.7	42.9	30.4	104.1	82.0	8.9	9.2	19.4	20.9	79.9	87.1
CAMS	20130926	-0.7	-0.5	3.5	3.6	3.5	3.6	-7.3	-19.8	54.5	49.0	3.8	3.4	1.5	9.9	34.4	33.1	75.4	69.6	9.2	9.5	21.5	21.2	91.5	90.7
CAMS	20130927	-2.6	-2.5	3.6	3.4	3.6	3.6	-8.4	-21.3	38.1	34.8	3.9	3.6	3.6	21.1	18.4	29.3	37.3	56.7	69.2	66.3	74.9	74.3	209.2	207.2
CAMS	20130928	-0.3	-0.1	2.9	2.9	3.0	2.9	-6.5	-0.1	37.6	29.7	3.8	3.1	-1.0	-6.2	16.9	12.9	30.9	24.1	48.5	40.9	89.4	90.9	199.9	199.4
CAMS	20130929	1.1	1.2	3.4	3.5	3.3	3.4	32.6	27.3	63.2	59.7	4.1	4.0	-1.6	-5.8	53.8	49.4	87.3	82.9	-32.9	-36.1	51.3	54.9	110.9	114.4
CAMS	20130930	1.1	1.2	2.5	2.5	2.6	2.6	26.1	16.1	65.4	55.1	3.6	3.2	4.2	0.0	41.3	35.1	85.7	77.9	-34.9	-40.3	57.8	61.0	149.6	162.0

Table 2-4. Meteorological model performance statistics for the 4 and 1.33 km WRF domains over all ds472.0 monitors within the Houston-Galveston 1.33 km CAMx domain.

		Temperature						Wind Speed						Wind Direction					
		NMB (%)		NME (%)		RMSE (degrees F)		NMB (%)		NME (%)		RMSE (mph)		NMB (%)		NME (%)		RMSE (degrees)	
Site	Date	4km	1.33km	4km	1.33km	4km	1.33km	4km	1.33km	4km	1.33km	4km	1.33km	4km	1.33km	4km	1.33km	4km	1.33km
ds472.0	**All**	**0.9**	**0.9**	**3.1**	**3.2**	**3.3**	**3.3**	**2.4**	**2.3**	**39.7**	**34.4**	**3.9**	**3.3**	**-0.9**	**1.5**	**28.4**	**26.8**	**47.3**	**45.2**
ds472.0	20130901	1.0	1.0	2.0	1.9	2.1	2.1	-6.3	-11.9	40.9	32.3	3.7	2.8	-2.0	-1.7	19.1	14.9	45.2	40.9
ds472.0	20130902	0.3	0.3	2.1	2.1	2.7	2.7	-5.4	-23.1	42.3	41.3	3.9	4.0	-15.8	-0.7	30.1	19.8	73.2	57.0
ds472.0	20130903	-0.3	-0.3	2.6	2.6	2.9	2.9	-16.8	-18.9	40.0	43.0	3.2	3.4	-9.3	-10.7	31.0	29.7	79.9	80.2
ds472.0	20130904	1.1	1.2	3.2	3.2	3.5	3.5	28.1	29.9	46.1	49.7	3.7	3.8	-12.8	-12.9	49.8	51.5	95.1	99.7
ds472.0	20130905	1.5	1.5	2.9	3.0	3.2	3.3	3.4	2.6	30.1	30.1	3.1	3.3	-9.5	-7.6	26.0	24.9	37.2	35.7
ds472.0	20130906	1.9	1.8	2.9	2.8	3.2	3.2	-3.0	5.5	30.2	28.9	3.2	3.0	-1.0	7.1	20.8	25.4	29.9	36.8
ds472.0	20130907	5.8	5.8	6.2	6.1	6.9	6.9	1.3	6.4	42.0	33.6	3.7	3.1	0.6	5.0	36.5	36.1	48.7	49.2
ds472.0	20130908	4.3	4.3	4.4	4.5	4.2	4.2	8.2	31.0	34.1	42.4	3.1	3.8	-19.8	-9.9	32.1	26.4	51.5	43.7
ds472.0	20130909	2.0	2.0	2.8	2.8	3.0	3.0	-16.4	-4.4	36.9	27.6	4.3	3.3	2.6	-3.7	20.8	19.5	32.4	32.0
ds472.0	20130910	1.3	1.2	3.0	3.1	3.3	3.3	7.2	6.8	37.3	27.2	4.0	2.9	3.9	1.5	17.7	17.1	24.8	23.7
ds472.0	20130911	0.7	0.7	2.3	2.4	2.5	2.5	-0.8	8.4	32.0	24.0	3.1	2.4	-3.4	-4.2	22.0	19.3	25.5	23.3
ds472.0	20130912	0.4	0.5	2.3	2.3	2.4	2.4	10.1	13.1	31.6	30.1	3.1	3.0	-12.0	-6.5	24.5	24.9	33.8	34.7
ds472.0	20130913	-0.1	-0.1	2.6	2.7	2.7	2.8	32.3	26.4	46.8	40.8	4.1	3.6	-6.0	3.0	21.5	23.3	37.9	42.2
ds472.0	20130914	0.8	0.8	2.3	2.3	2.5	2.6	16.8	-2.8	36.6	28.3	3.5	2.7	-3.7	-5.7	23.0	22.7	31.7	31.8
ds472.0	20130915	0.6	0.6	2.3	2.4	2.5	2.6	7.5	19.4	35.8	31.1	3.8	3.3	-6.8	-4.9	20.7	20.3	25.1	25.5
ds472.0	20130916	1.3	1.3	2.9	2.9	3.2	3.2	38.3	22.9	57.1	34.2	5.5	3.3	-0.9	-1.6	24.5	24.5	31.2	29.9
ds472.0	20130917	0.7	0.7	2.7	2.7	2.8	2.8	19.5	11.6	37.1	37.7	4.1	4.0	-17.6	-11.3	24.5	22.5	32.4	30.6
ds472.0	20130918	1.6	1.6	3.4	3.5	3.6	3.7	-5.5	3.9	32.3	31.7	3.6	3.5	-6.6	-3.3	22.8	27.2	30.6	43.0
ds472.0	20130919	3.6	3.6	4.1	4.1	4.6	4.6	-3.8	9.0	37.0	30.3	4.0	3.3	-10.1	-10.6	24.6	22.5	34.1	31.6
ds472.0	20130920	3.1	3.1	3.6	3.7	3.6	3.6	24.5	7.4	50.5	37.9	5.1	4.1	-4.8	-1.2	27.2	22.4	61.2	53.1
ds472.0	20130921	2.9	3.0	3.6	3.6	3.2	3.2	24.2	1.7	34.3	23.8	4.6	3.2	31.0	17.4	32.5	20.6	38.5	26.4
ds472.0	20130922	-0.7	-0.6	3.0	3.0	2.8	2.9	-3.9	4.2	33.5	27.7	3.8	3.1	26.4	34.0	33.5	39.1	26.5	29.8
ds472.0	20130923	-2.6	-2.5	4.0	4.0	4.0	4.0	-31.2	2.4	46.5	27.4	4.2	2.4	28.2	40.2	52.1	48.3	46.7	39.9
ds472.0	20130924	-3.0	-3.0	4.5	4.5	4.5	4.5	-7.2	-2.0	34.5	28.5	3.3	2.7	13.8	22.0	22.0	23.7	54.9	55.4
ds472.0	20130925	0.2	0.2	3.4	3.4	3.5	3.5	21.7	15.3	47.1	47.2	3.2	3.2	0.8	5.3	36.9	29.2	96.6	80.6
ds472.0	20130926	-0.5	-0.6	2.9	3.0	3.0	3.1	-29.2	-36.2	50.6	49.0	4.5	4.5	-3.5	10.3	30.8	31.5	63.8	58.9
ds472.0	20130927	-2.5	-2.6	3.5	3.6	3.4	3.4	-19.4	-30.0	38.0	35.6	4.6	4.3	3.9	9.3	14.7	17.8	25.0	29.5
ds472.0	20130928	-0.1	-0.1	3.0	3.0	3.1	3.1	-19.9	-9.6	38.2	26.0	4.2	2.9	-2.2	-9.2	17.0	15.6	28.8	26.1
ds472.0	20130929	1.2	1.2	3.3	3.3	3.5	3.5	5.7	-0.6	45.9	40.0	3.9	3.5	3.5	-2.5	52.1	50.2	92.9	89.5
ds472.0	20130930	1.0	1.0	2.4	2.4	2.4	2.4	-8.7	-18.1	46.0	44.2	3.5	3.4	5.1	-1.4	40.2	34.1	84.7	76.6

As noted earlier, the solar radiation statistics indicated that WRF lacked skill in predicting clouds at the right time or location in the HG region. In order to examine solar radiation performance more closely, we present hourly solar radiation time series for the observations (blue), WRF 4 km domain (red) and WRF 1.33 km domain (green) for September 1-30, 2013 at the Galveston 99th Street CAMS monitor in Figure 2-4. These solar radiation values are attenuated for the presence of sub-grid cloudiness within WRFCAMx, in the same manner as used for the statistics calculations.

First, we examine the first half of September, where WRF predicts mostly clear skies during the midday hours (smooth peak with maximum near 900 W/m^2). This contrasts with the observations, which suggest scattered to mostly cloudy conditions over Galveston during this time period. This positive solar radiation bias is especially large from September 7-10. Next, we inspect the second half of September, where we observe that WRF under-predicts solar radiation (over-predicts cloudiness) for September 16-17, and 22-23. WRF also shows some significant solar radiation positive biases during this period on September 27-28. For the most part, the solar radiation predictions for the two WRF domains are very similar. One exception occurs on September 19, where the 1.33 km simulation generates much less cloudiness over Galveston in the early to mid-afternoon hours than the 4 km simulation. However, both WRF

results show considerable bias (in opposite directions), so one simulation is not preferable over the other.

We present hourly time series for September 1-30, 2013 at William P. Hobby (KHOU; Figure 2-5) and Galveston (KGLS; Figure 2-6) airports for 2-m temperature (top), wind speed (middle) and wind direction (bottom). We chose airport sites in order to assure that siting issues do not impact our analysis. The KGLS and KHOU airports are selected in order to evaluate a coastal site and a site close to the Houston urban core, respectively.

From the temperature time series at KHOU, we see respectable performance through the first 10 days of September. One exception occurs in the mid-afternoon of September 2, where WRF fails to accurately predict thunderstorm activity in the area, which leads to a large positive temperature bias. In fact, temperature observations at KHOU indicate a 16 °F temperature decrease from 16:00 to 17:00 CST. Another exception occurs on September 4, where WRF over-predicts the midday peak temperature by roughly 4 °F. KHOU observations suggest extensive cloud cover on this day, so it is likely that WRF did not generate enough clouds on this day. WRF performance deteriorates over the next ten days (September 11-20), with significant under-predictions of midday peak temperatures on September 12-13 and 15-17. During these days, it is likely that WRF is over-predicting the amount of cloud cover, leading to reduced peak temperatures. Starting in the afternoon of September 19 and continuing through September 21, KHOU experiences periods of rainfall interspersed with periods of mostly cloudy or overcast conditions, resulting in lower daytime temperatures. It appears that WRF is not characterizing this event properly, as the peak temperature on September 19 is shifted by a few hours and the temperature bias at 13:00 CST on September 20 is around 9 °F. For September 22-30, the midday temperature peaks are replicated fairly well by WRF. However, significant early morning low temperatures are biased low frequently throughout the period. As noted previously, there are no significant differences in 2-m temperatures between the two WRF domains, as indicated by the KHOU performance statistics shown on the plot.

The wind speed and wind direction time series plots for KHOU show that the WRF 1.33 km performs slightly better than the 4 km domain as indicated by the KHOU site's performance statistics for NMB, NME and RMSE shown in the top right corner of each chart. In general, WRF tends to under-predict wind speeds during the day while over-predicting nocturnal wind speeds. This behavior explains the low wind speed biases (positive biases are averaged together with negative biases) and the large difference between bias and error statistics. The WRF wind direction biases appear to be in the same direction for most of the time, but the 1.33 km results have a slightly lower bias. This phenomenon could be the result of enhanced characterization of the complex variation of HG land use types available at 1.33 km resolution.

We note that the temperature statistics for KGLS (top of Figure 2-6) show similar performance as for KHOU, but with a small positive bias for September (1.2 %) compared to the small negative bias (-0.6 %) found at KHOU. Galveston's marine influence is obvious from the temperature time series, with observed temperatures mostly ranging from about 80 to 90 °F throughout the first 3 weeks of September. During this time period, WRF shows significant

midday peak temperature over-predictions on September 4, and 7-8. On all three of these days, KGLS shows periods of rain and/or thunderstorms with considerable clouds, so it is likely that WRF did not simulate these conditions properly. The solar radiation time series at the Galveston 99th Street CAMS monitor showed that WRF over-predicted clouds on September 16 and 17, and this enhanced cloudiness likely caused midday peak temperatures to be under-predicted on these days. On most days from September 14-23, WRF tends to over-predict early morning low temperatures. This may suggest a lack of nighttime radiational cooling resulting from nocturnal cloudiness in WRF. From September 23-30, midday peak temperatures are mostly under-predicted by WRF. Because WRF both under- and over-predicts solar radiation at the Galveston 99th Street monitor during this time period, it is unclear what is causing these negative temperature biases and more investigation would be required to understand this feature.

As with KHOU, wind speed performance at KGLS is slightly better for the WRF 1.33 km results. While the 4 km nocturnal wind speeds tend to be consistently under-predicted, the 1.33 km results tend to match the observations better by over-predicting the nocturnal wind speeds to a lesser degree. During a period of offshore flow from September 21-25, both the WRF 4 and 1.33 km results show wind speed under-predictions, but the 1.33 km biases are smaller in magnitude.

Table 2-5. Meteorological model performance statistics for the 4 and 1 .33 km WRF domains over all CAMS and ds472.0 monitors within the Houston-Galveston 1.33 km CAMx domain.

		Temperature						Wind Speed (cutoff 1 mph)						Wind Direction					
		NMB (%)		NME (%)		RMSE (degrees F)		NMB (%)		NME (%)		RMSE (mph)		NMB (%)		NME (%)		RMSE (degrees)	
Site	Date	4km	1.33km	4km	1.33km	4km	1.33km	4km	1.33km	4km	1.33km	4km	1.33km	4km	1.33km	4km	1.33km	4km	1.33km
CAMS	All	1.2	1.2	3.2	3.2	3.3	3.3	31.2	31.3	57.1	50.7	4.1	3.5	-0.2	5.1	33.6	30.7	53.2	49.8
ds472.0	All	0.9	0.9	3.1	3.2	3.3	3.3	2.4	2.3	39.7	34.4	3.9	3.3	-0.9	1.5	28.4	26.8	47.3	45.2

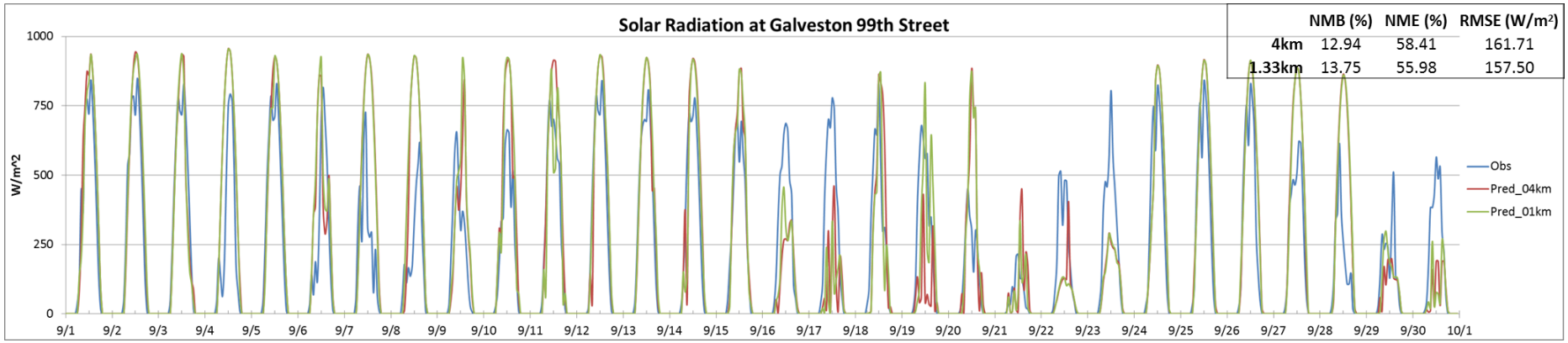

Figure 2-4. Time series of hourly solar radiation for observations (blue) and WRF 4 km (red) and 1.33 km (green) simulations at the Galveston 99th Street CAMS monitor for September 1-30, 2013.

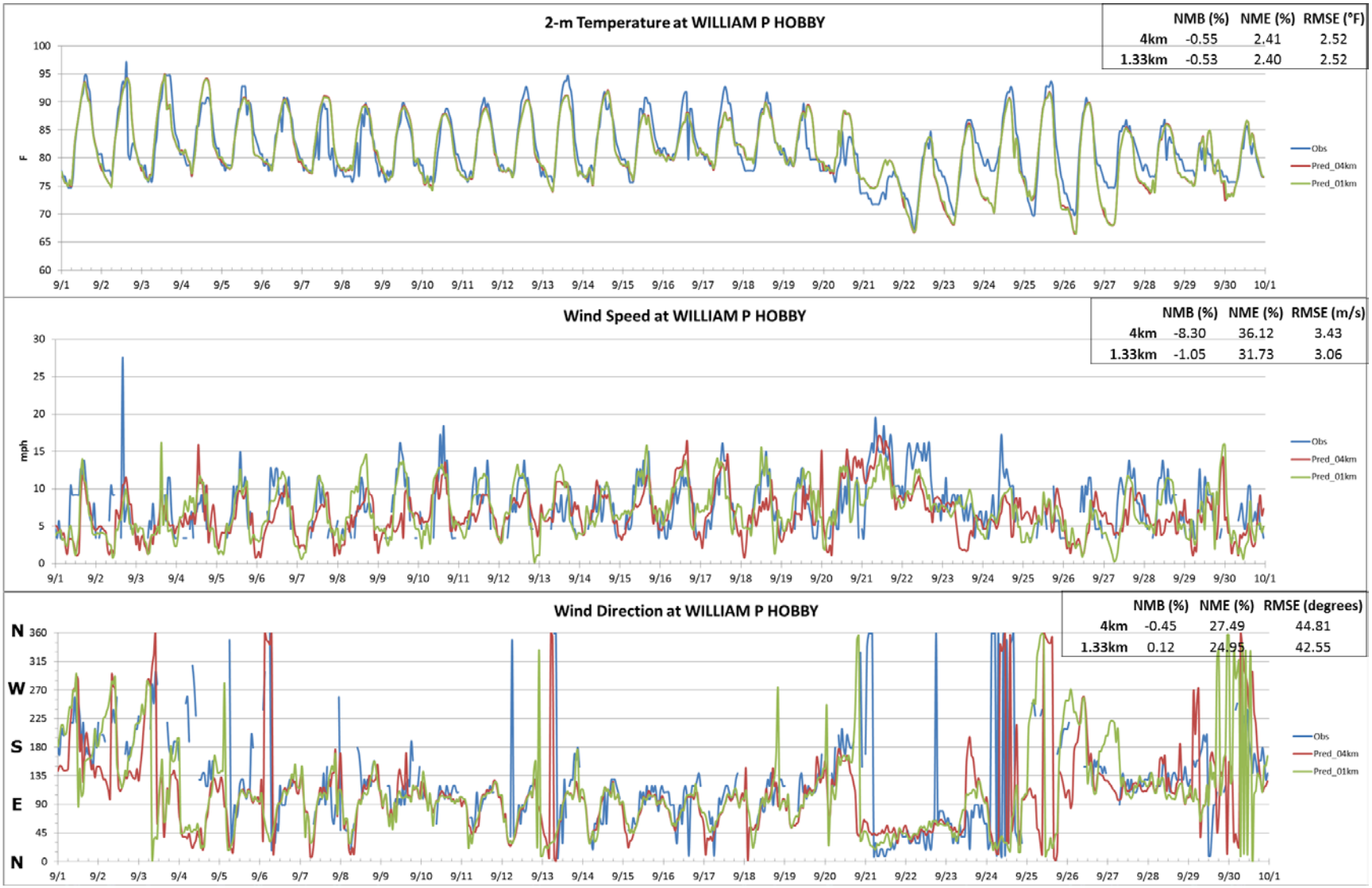

Figure 2-5. Time series of hourly 2-m temperature, 10-meter wind speed and 10-meter wind direction for observations (blue) and WRF 4 km (red) and 1.33 km (green) simulations at the William P. Hobby airport (KHOU) for September 1-30, 2013.

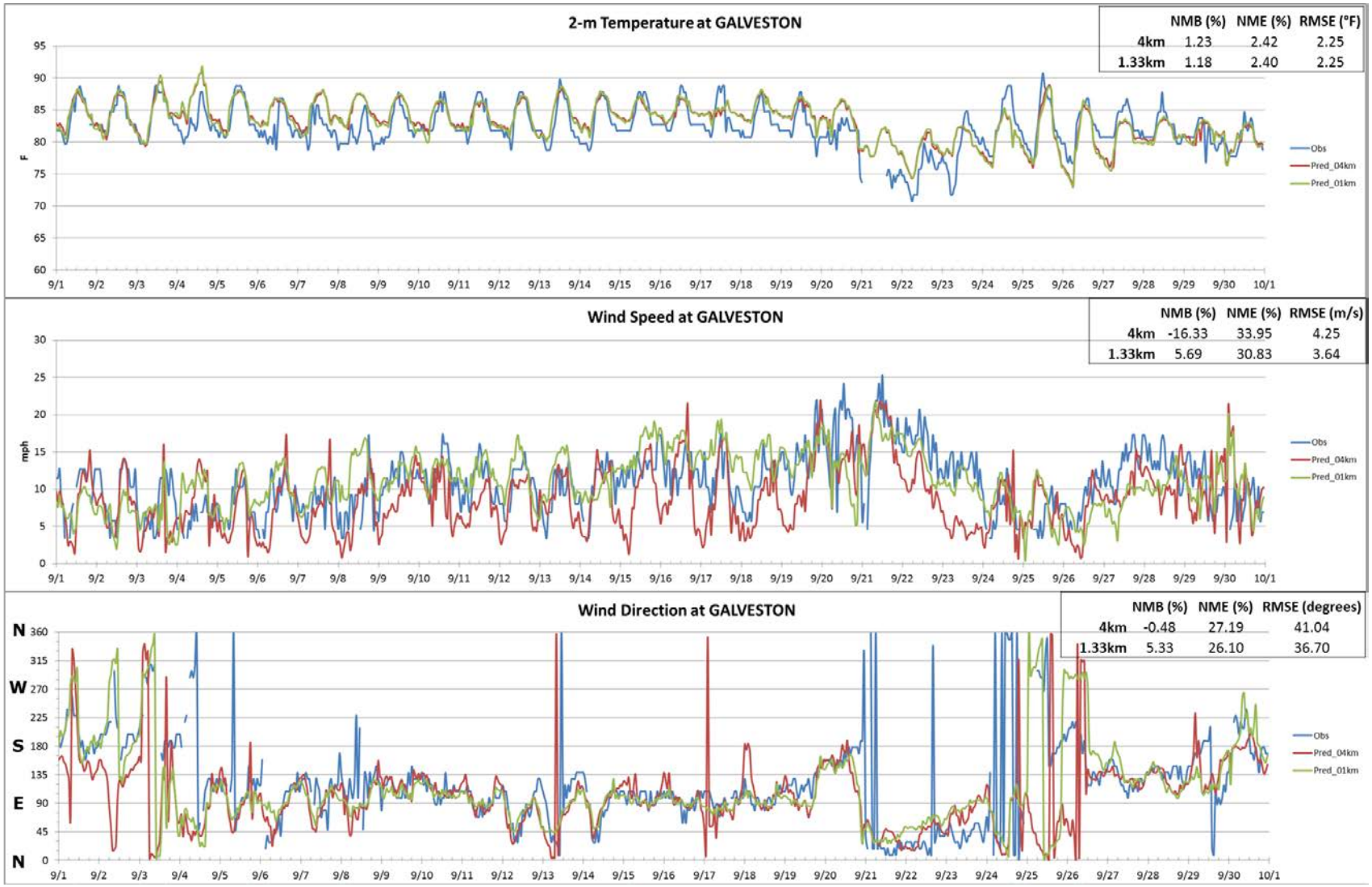

Figure 2-6. Time series of hourly 2-m temperature, 10-meter wind speed and 10-meter wind direction for observations (blue) and WRF 4 km (red) and 1.33 km (green) simulations at the Galveston airport (KGLS) for September 1-30, 2013.

Emery et al. (2001) derived and proposed a set of daily performance benchmarks for typical meteorological model performance. These standards were based upon the evaluation of about 30 meteorological simulations (using a variety of regional meteorological models) since 1993 in support of air quality applications as reported by Tesche et al. (2001) and other studies. The purpose of these benchmarks was not to give a passing or failing grade to any one particular meteorological model application, but rather to put its results into the proper context of other models and meteorological data sets. Kemball-Cook et al., (2005) proposed model performance benchmarks for complex conditions. The determination to use simple or complex benchmarks will be made on a site-by-site basis depending on the presence of significant terrain or local circulations (e.g. Houston land/sea breeze). The benchmarks for each variable are shown in Table 2-6.

Soccer plots display the daily or monthly average bias (x-axis) versus the daily or monthly average error (y-axis). Along with the results are the simple (plotted as a black dashed line) and complex benchmark results (plotted as a red dashed line). It is desirable to have all the monthly values lay inside the benchmark figure (a "goal"). For these soccer plots, we perform the analysis with ds472.0 sites due to previous experience with the dataset and proper siting.

We present a set of soccer plots for the ds472.0 airports (13 sites) located within the HG 1.33 CAMx domain in Figure 2-7 for temperature (top left), humidity (top right), wind speed (middle left), wind direction (middle right) and wind speed/wind direction (bottom) for the WRF 4 km results (red) and WRF 1.33 km results (green). Daily statistics are shown as circles and monthly statistics are shown as diamonds. The first feature that stands out is the results from the WRF 4 km and 1.33 km domains are stacked very closely to each other, indicating that no significant difference exists in terms of daily/monthly performance statistics. For the remainder of this discussion, we treat the results of the two WRF domains as one.

For temperature, we note that all WRF model results daily average temperatures lie within the complex benchmark, with about half of the days within the simple terrain benchmark (bias: ±2 K; error: 0-2 K). The monthly average lies within the simple terrain benchmark.

The humidity soccer plot shows daily statistics are mostly within the complex benchmark (18 of 30 days), with another 4 days within are within or very near the simple benchmark. Note that because the complex terrain includes high elevation locations where less moisture is available, the humidity bias is more stringent for the complex benchmark (± 0.8 g/kg) than for the simple terrain benchmark (± 1.0 g/kg). Considering that HGBPA is a low lying coastal region, the simple terrain benchmark is more appropriate in this case. The humidity monthly average statistics are within the complex benchmark, with a bias of around -0.5 g/kg and error less than 2 g/kg.

For wind speed (middle left of Figure 2-7), all but one daily value lie within the complex terrain benchmark (bias ± 1.5 m/s; RMSE: 0-2.5 m/s) and the monthly average is completely within the simple terrain benchmark (bias ± 0.5 m/s; RMSE: 0-2.0 m/s). Note that the monthly average bias is near zero, but this is simply the effect of averaging days with positive bias and days with negative bias of similar magnitude. For wind direction (middle right of Figure 2-7), we note a

large spread in the daily statistics, with 17 of the 30 days within the complex terrain benchmark. Another 5 days lie within the complex terrain benchmark and outside of the simple goal. The monthly average lies just outside the simple terrain benchmark, with an error of around 40 degrees. As with the wind speed plot, the wind direction monthly average bias is near zero, but this is the result of averaging positive and negative biases. Finally, we examine the wind speed/wind direction plot (bottom of Figure 2-7). This plot shares the same y-axis as the wind direction plot (wind direction error) and uses the y-axis of the wind speed plot (wind speed RMSE) as its x-axis. This allows comparison of wind speed and wind direction on a single plot. We note that the wind direction errors do not appear to be correlated to wind speed errors: of all the daily averages that exceed the complex benchmark (55 degrees), the wind speed simple benchmark (RMSE: 0-2.0 m/s) is not exceeded.

Overall, the soccer plots for temperature and wind speed are respectable and reasonable for the HGBPA region. Humidity performance is also good for most days. Days with significant bias are likely due to mischaracterization of clouds and/or convection. As mentioned previously, the Houston sea breeze is a difficult phenomenon for WRF to capture and it involves large shifts in wind direction over a short period of time. If WRF misses timing of these shifts, large errors in wind direction can result.

Table 2-6. WRF Performance Benchmarks.

Parameter	Emery et al. (2001)	Kemball-Cook et al. (2005)
Conditions	Simple	Complex
Temperature Bias	≤ ±0.5 K	≤ ±2.0 K
Temperature Error	≤ 2.0 K	≤ 3.5 K
Humidity Bias	≤ ±1.0 g/kg	≤ ±0.8 g/kg
Humidity Error	≤ 2.0 g/kg	≤ 2.0 g/kg
Wind Speed Bias	≤ ±0.5 m/s	≤ ±1.5 m/s
Wind Speed RMSE	≤ 2.0 m/s	≤ 2.5 m/s
Wind Dir. Bias	≤ ±10 degrees	(not addressed)
Wind Dir. Error	≤ 30 degrees	≤ 55 degrees

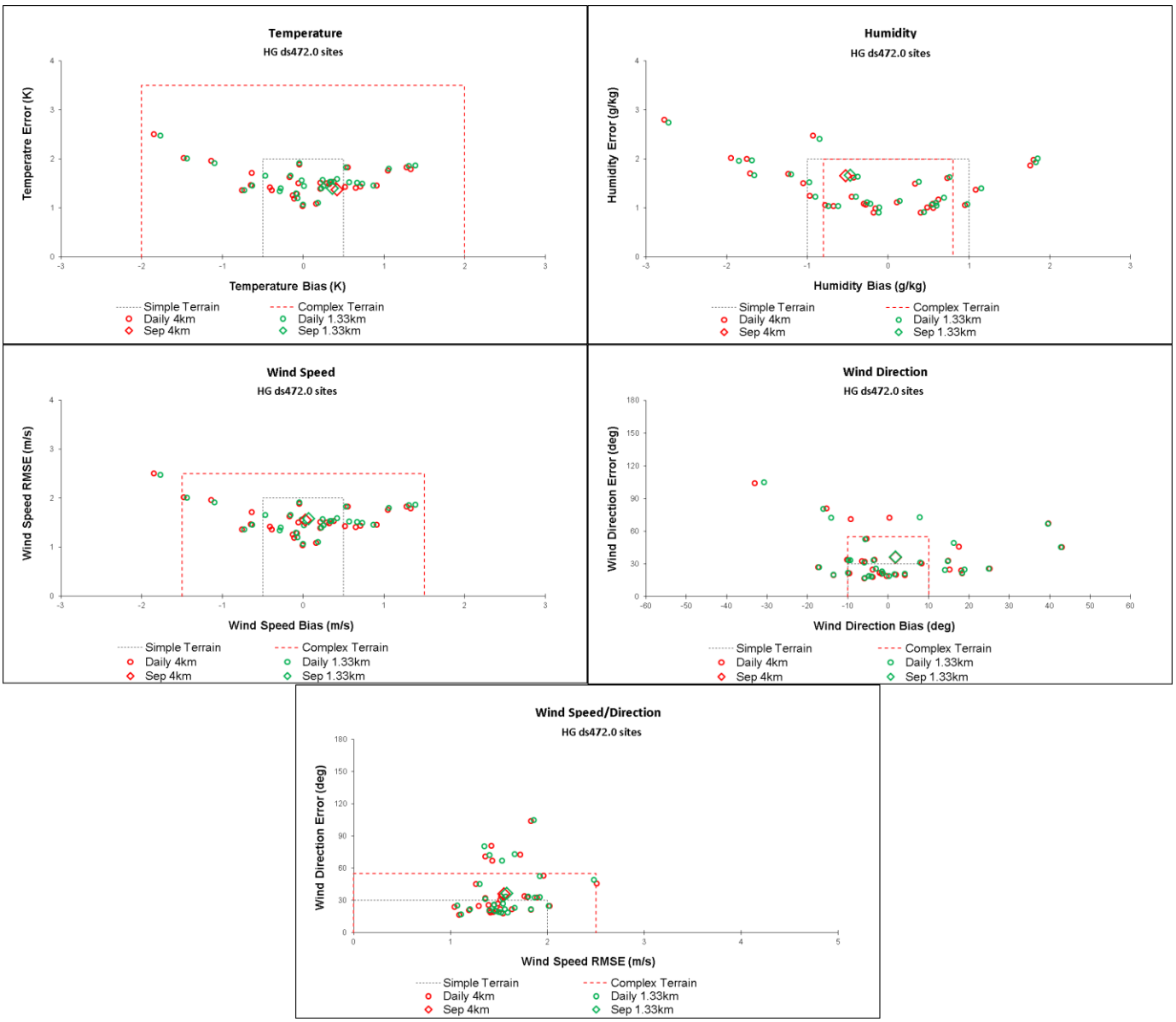

Figure 2-7. Soccer plots across all HG ds472.0 airports (13 sites) for temperature (top left), humidity (top right), wind speed (middle left), wind direction (middle right) and wind speed/wind direction (bottom) for the WRF 4 km results (red) and WRF 1.33 km results (green). Daily statistics are shown as circles and monthly statistics are shown as diamonds. Simple terrain benchmarks are marked with a black dashed line and complex terrain benchmarks are marked with a red dashed line.

2.2.2.3 Conclusion

We conclude from our meteorological model performance evaluation that both the WRF 4 and 1.33 km domains are suitable for use in photochemical modeling efforts. While the 1.33 km results show slightly better skill in predicting wind speed and direction, it is unlikely that these differences would translate to meaningful differences in pollutant concentrations. Evaluation of solar radiation performance suggests that WRF does not consistently generate clouds and/or convective activity in the right locations and times. No performance benchmarks currently exist for solar radiation, but this finding is consistent with other recent modeling efforts in the Houston-Galveston area (Johnson et al., 2015).

2.3 Emissions Inputs

2.3.1 Anthropogenic Emissions

Anthropogenic emissions were provided by TCEQ in CAMx-ready format for the 36/12/4 km domains compatible with Carbon bond 6 (CB6) mechanism. Elevated point source emissions include day-specific Continuous emissions monitoring (CEM) data made available by the Acid Rain Program for the September 2013 modeling period. Surface emissions including area, mobile, and low-point sources are from TCEQ's 2012 day-of-week specific emissions inventory[3]. TCEQ's anthropogenic emissions include PM precursors (e.g., sulphur dioxide and ammonia) and primary fine PM emissions. Emissions of coarse PM are not included.

2.3.2 Natural Emissions

The inventory of biogenic emissions was generated using the Model of Emissions of Gases and Aerosols from Nature (MEGAN) version 2.1 (Guenther et al., 2012), the same model used in TCEQ's SIP modeling. MEGAN driving variables include weather data, Leaf Area Index (LAI), plant functional type (PFT) cover and compound-specific emission factors (EF) that are based on plant species composition. TCEQ provided the LAI data for the 36/12/4 km domains. ArcGIS software was applied to generate MEGAN PFT/EF input files. The MEGAN model was applied using the daily meteorology (temperature and solar radiation) from the WRF model outputs to generate day-specific biogenic emissions for the 36/12/4 km domains. A recent modelling study suggested that the MEGAN biogenic emissions model may be generating excessive isoprene emissions (ENVIRON and ERG, 2013). To mitigate this issue, we reduced MEGAN isoprene by a factor of two following an improvement introduced in the Near Real-Time ozone modelling (Johnson et al., 2013).

Fire emissions were based on the Fire Inventory from NCAR (FINN) version 1 dataset, downloadable from http://bai.acd.ucar.edu/Data/fire/. The global dataset contains daily emissions for each satellite pixel, an area of approximately 1 km^2. Emission species include NO, NO_2, $PM_{2.5}$, CO, and NMOC. Fire points within 5 km of one another are assumed to be part of the same fire and assigned properties of a larger fire. The daily fire emissions were processed

[3] Downloaded from ftp://amdaftp.tceq.texas.gov/pub/TX/camx/basecase/bc12_12jun.reg3a.2012_wrf361_p2a_i2_a/input/ei/Components/ on April 14, 2015

for the September 2013 modelling period using an updated version of EPS3 version 3.20. EPS3 incorporates the Western Regional Air Partnership (WRAP) methodology to temporally and vertically allocate the fire emissions.

Emissions of sea-salt particles including sodium, chloride, and sulfate (SO_4), were estimated from the 2013 WRF hourly, gridded meteorology. The sea salt aerosol fluxes from both open oceans (Smith and Harrison 1998; Gong, 2003) and breaking waves in the surf zone (de Leeuw et al., 2000) are a function of wind speed at 10 meter height.

2.3.3 Emissions Merging

Anthropogenic and natural emissions were merged to provide day-specific emissions input to CAMx. CAMx treats anthropogenic toluene, xylene, and benzene as secondary organic aerosol precursors and requires that the emissions of these species are provided separately for gas-phase and aerosol-phase chemistry. So before the merge, TCEQ anthropogenic emissions were updated with secondary aerosol precursors' emissions. To do this, we replicated anthropogenic emissions of TOL, XYL and BENZ model species for gas-phase chemistry and renamed them to TOLA, XYLA, and BNZA, respectively, for aerosol-phase chemistry. Surface anthropogenic and natural emissions were then merged for each simulation day for the TCEQ 36/12/4km domain (TX_36km, TX_12km, and TX_4km, respectively) using EPS3 MRGUAM program. Next, we windowed the TX_4km emissions to the HGBPA 4 km domain. For elevated sources, anthropogenic emissions were merged with FINN fire emissions using PTSMERGE program. All of the elevated point emissions files share the same stack list (i.e., the stack list of elevated point sources is the same every day).

Anthropogenic surface emissions for the 1.33 km HG domain were not readily available so they were disaggregated from the 4 km domain. Note that the point source emissions files contain stack locations and do not require any emissions disaggregation.

2.3.4 Emissions Summary

Table 2-7 shows a typical weekday emissions by pollutant by source category for the large TX_4km domain. Point (elevated and low-level) sources dominate nitrogen oxides (NOx), carbon monoxide (CO) and sulphur dioxide (SO_2) emissions while area sources dominate ammonia (NH3) and find particle ($PM_{2.5}$) emissions. Spatial distributions of anthropogenic and natural emissions are shown in Figure 2-8 and Figure 2-9, respectively.

Table 2-7. Typical weekday (Wednesday) emissions by source category for the TCEQ 4km domain.

Category	NOx	CO	VOC	SO_2	NH_3	$PM_{2.5}$
Anthropogenic						
Area	605	900	3,130	63	627	695
Nonroad	432	2,573	274	1	2	36
Offroad	180	137	15	10	0	7
Low-point	987	4,338	378	6	23	27
Elevated-point	1,053	1,053	136	1,659	10	122
Mexico	69	63	285	9	3	19
Natural						
Biogenics	258	1,865	18,100	-	-	-
Sea-salt	-	-	-	-	-	702
Fire	9	141	11	1	2	20
Total Anthropogenic	3,325	9,064	4,217	1,747	664	905
Total Anthro+Natural	3,593	11,069	22,328	1,749	666	1,628

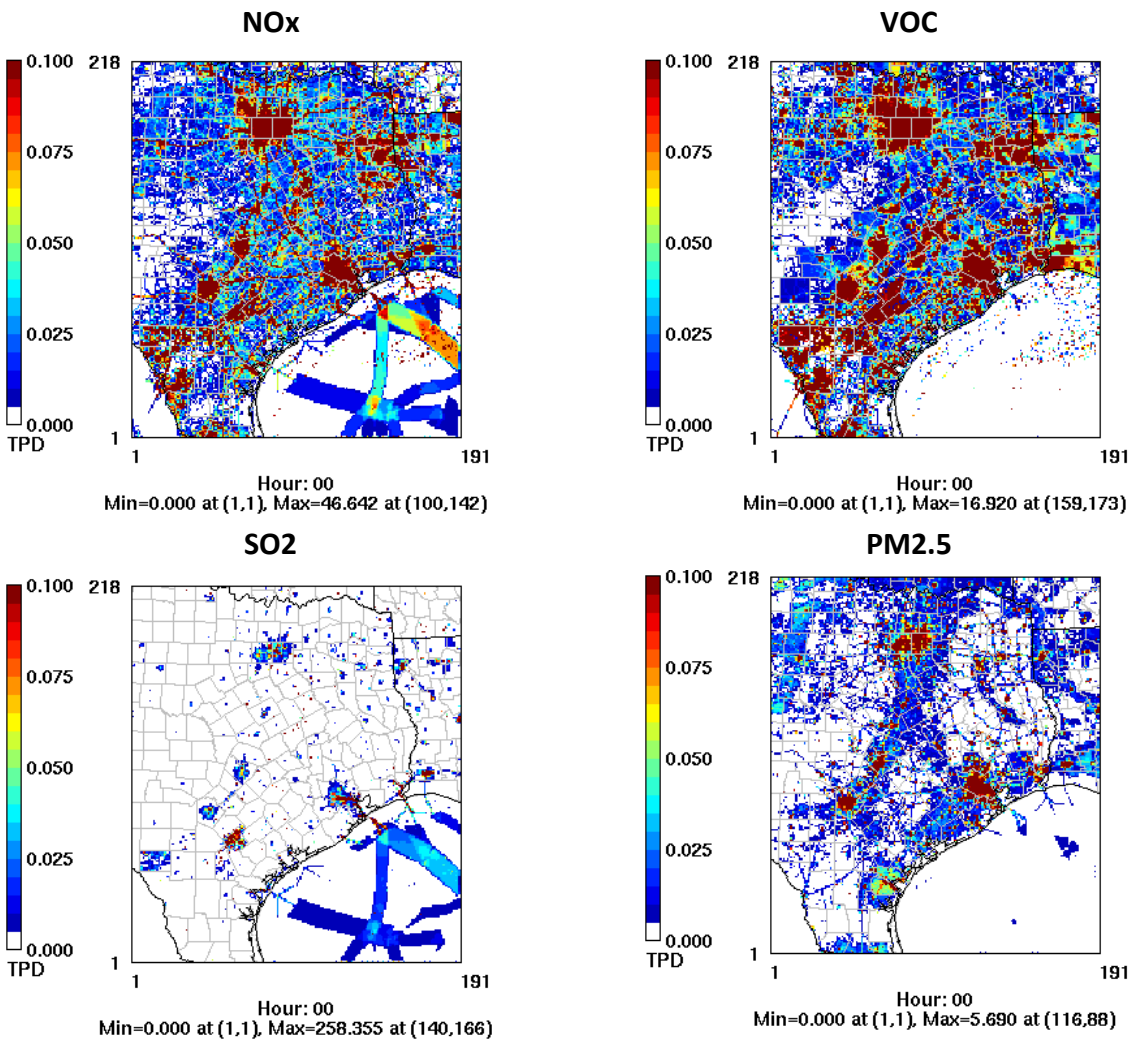

Figure 2-8. Typical weekday (September 18) anthropogenic NOx, VOC, SO_2, and $PM_{2.5}$ emissions (short tons per day).

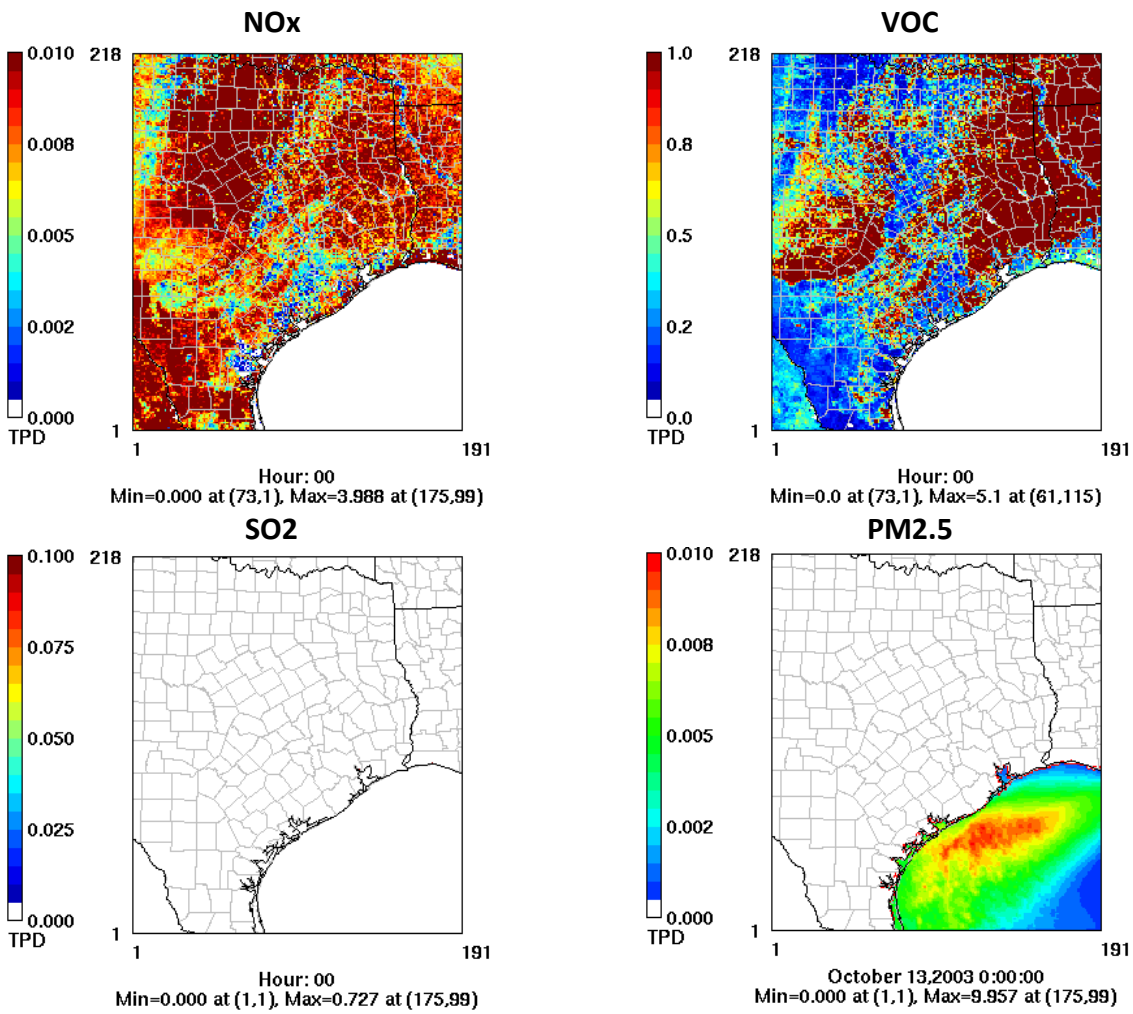

Figure 2-9. Typical weekday (September 18) natural NOx, VOC, SO_2, and $PM_{2.5}$ emissions (short tons per day).

2.4 Lateral Boundary Conditions and other Ancillary Inputs

Initial and boundary conditions (IC/BCs) for the 36 km domain were extracted from MOZART global model output for the year 2013[4] using the Mozart2CAMx version 3.0 software. The MOZART outputs are every 6-hour interval and are at 1.9x2.5 degree resolution with 56 vertical layers. We performed a flat 15 ppb ozone reduction over the Gulf of Mexico and Atlantic Ocean in order to deplete the ozone coming onshore. A flat 5 ppb ozone reduction was applied elsewhere. Caps of various ozone precursors are shown in Table 2-8.

[4] Available at http://www.acd.ucar.edu/wrf-chem/mozart.shtml

We also prepared the following inputs for CAMx:

- O3MAP: 2013 day-specific values from 1 degree Total Ozone Mapping Spectrometer (TOMS) satellite ozone column data
- Photolysis rates files generated using 2013 O3MAP
- Land use / land cover inputs generated using USGS 24-category dataset; monthly LAI data from MODIS satellite

Table 2-8. Maximum concentration limits for ozone precursors applied to the 36 km boundary condition grid cells across the Gulf of Mexico, Caribbean Sea, and Atlantic Ocean south of Cape Hatteras.

Species	Description	Max. Concentration (ppb)
NO2	Nitrogen dioxide	0.05
CO	Carbon monoxide	150.0
N2O5	Dinitrogen pentoxide	0.001
HNO3	Nitric acid	0.25
PNA	Peroxynitric acid	0.001
H2O2	Hydrogen peroxide	0.5
NTR	Organic nitrates	0.01
FORM	Formaldehyde	0.25
ALD2	Acetaldehyde	0.05
ALDX	Propionaldehyde and higher aldehydes	0.02
PAR	Paraffin carbon bond (C-C)	1.0
OLE	Terminal olefin carbon bond (R-C=C)	0.01
ETHA	Ethane	1.0
MEPX	Methylhydroperoxide	0.1
PAN	Peroxyacetyl Nitrate	0.01
PANX	C3 and higher peroxyacyl nitrate	0.001
INTR	Organic nitrates from ISO2 reaction with NO	0.001
ISOP	Isoprene	0.1
ISPD	Isoprene product (lumped methacrolein, methyl vinyl ketone, etc.)	0.1
TERP	Monoterpenes	0.05
ISP	Isoprene (SOA chemistry)	0.1
TRP	Monoterpenes (SOA chemistry)	0.05
TOL	Toluene and other monoalkyl aromatics	0.02
XYL	Xylene and other polyalkyl aromatics	0.01
SO2	Sulfur dioxide	0.1
PRPA	Propane	0.5
ACET	Acetone	0.25
KET	Ketone carbon bond (C=O)	0.05
BENZ	Benzene	0.1

2.5 CMAQ Inputs Preparation

2.5.1 Emissions and Boundary Conditions

CMAQ will be run over 4km HGBPA and 1.33 HG domains. We used CAMX2CMAQ program (developed by Ramboll Environ in project FY14-20) to convert the CAMx-formatted initial/boundary condition (for the 4 km domain) and emission inputs to CMAQ input format. CMAQ input files were visualized and compared to CAMx files to ensure correct conversion. The meteorological inputs were generated by processing the WRF meteorological model output using the CMAQ Meteorological-Chemistry Interface Program (MCIP). MCIP provides the complete set of meteorological data required by CMAQ. The vertical layer mapping of the 43 WRF layers to 28 CMAQ layers is similar to the WRF-CAMx mapping shown in Figure 2-3 except that the CMAQ top layer extends to match the WRF top layer (i.e., sigma of 0.00) as required by MCIP. The MCIP Version 4.2 (released December 2013) was used.

2.5.2 Ocean Mask File

CMAQ aerosol option AERO5 can compute sea salt emissions from both open ocean grid cells and surf zone grid cells. The Ocean file defines what fraction of each grid cell is on land, on the ocean, or on the surf zone where waves break against the shore. This file was created for the 4/1.33-km domains using the Spatial Allocator tool for the SMOKE emissions processor.

3.0 CAMX AND CMAQ BASE CASE SIMULATION

CAMx and CMAQ Base Case simulations were conducted for the DISCOVER-AQ study period during September of 2013. The focus area is in and around Houston. This section documents model setups and compares ozone predictions by two models.

3.1 CAMx and CMAQ Base Case Simulations

Ramboll ENVIRON used the 2013 photochemical modeling platform described in Section 2 of this project to simulate ozone and PM conditions during DISCOVER-AQ 2013 study using both CAMx and CMAQ models. CMAQ only supports one-way nesting grid, which means that the nested domains are run after the coarse domain and there is no feedback from the fine nests to the coarse domain. For consistency between the two models, CAMx was run first using two-way nested grid for the 36 km and 12 km domains. The CAMx 12 km results provided initial boundary conditions for the 4 km domain for both CAMx and CMAQ. Model performance evaluation and sensitivity analysis for the 36 and 12km domains are described in Appendix A.

3.1.1 CAMx Model Configuration

CAMx version 6.2 was chosen for this work since it was the most updated version at the time this work was initiated. The model configuration is shown in Table 3-1. We used the latest version of the Carbon Bond chemical mechanism implemented in CAMx, namely revision 2 of Carbon Bond 6 (CB6r2) which TCEQ is using. The CAMx model was first run using two-way nested grids for the 36 km and 12 km domains and a 15 day spin up period to limit the influence of initial concentrations. Then, the 4 km domain was run using one-way nested grid.

Table 3-1. Model Configurations Options for CAMx model.

Science Options	Configurations
Model Code	Version 6.2
Horizontal Grid Mesh	36/12/4 km
Vertical Grid Mesh	28 Layers
Initial Conditions	15 days full spin-up for 36/12 km; 5 days for 4 km
Boundary Conditions	Extracted from CAMx 12 km
Emissions Processing	Described in Section 2
Gas-Phase Chemistry	CB6r2
Aerosol Chemistry	ISORROPIA equilibrium and SOAP; CF scheme
Meteorological Processor	WRFCAMx v3.4
Horizontal Transport	Piecewise Parabolic Method (PPM scheme)
Horizontal Diffusion	K-theory
Vertical Advection Scheme	WRF
Vertical Eddy Diffusivity Scheme	K-theory
Vertical Diffusivity Corrections	Kv-patch depending on landuse category up to 100 m and to cloud tops
Deposition Scheme	Zhang

3.1.2 CMAQ Model Configuration

CMAQ version 5.0.2 was chosen for this study. This version includes AE5 scheme compatible with emission inputs available for this study. Later versions of CMAQ require emissions of additional PM components including trace metals and non-carbon organic mass (i.e., AE6 scheme) not included in the current inventory. For gaseous chemistry, CB6 mechanism is not available in any released versions of CMAQ so we implemented CB6r3 mechanism in CMAQ to be consistent with the CAMx model. Ramboll ENVIRON is already assisting EPA in implementing CB6 in CMAQ for future release. The CMAQ model configuration is shown in Table 3-2.

Table 3-2. Model Configuration Options for the CMAQ Model.

Science Options	Configurations
Model Code	CMAQ Version 5.0.2 plus updates by Ramboll ENVIRON
Horizontal Grid Mesh	4 km
Vertical Grid Mesh	28 Layers
Initial Conditions	5 days full spin-up ; converted from CAMx IC file
Boundary Conditions	Converted from CAMx BC files
Emissions Processing	Converted from CAMx emission files
Gas-Phase Chemistry	CB6r3
Aerosol Chemistry	AE5 (With Sea Salt Emissions)
Meteorological Processor	MCIP Version 4.2
Horizontal Transport	PPM
Horizontal Diffusion	K-theory spatially varying
Vertical Advection Scheme	WRF
Vertical Eddy Diffusivity Scheme	ACM2
Diffusivity Lower Limit	Kzmin = 0.01 to 1.0 m2/s (PURB option) (KZMIN set to true)
Deposition Scheme	M3dry

3.2 CAMx and CMAQ 4 km Results

CAMx and CMAQ predictions of monthly average maximum daily 8-hour (MDA8) ozone in September 2013 are comparable in spatial pattern and magnitude. The predicted average MDA8 ozone concentrations differ by less than 5 ppb across the H*ouston/Galveston/*Brazoria-Beaumont/Port Arthur (*HGBPA*) area (Figure 3-1). However, the differences of MDA8 ozone exceed 10 ppb on some days (Appendix A). CMAQ-predicted MDA8 ozone tends to be lower in the first quadrant of the 4 km domain which covers the area northeast of the Galveston Bay including Beaumont. The results in the Houston area are mixed with a tendency of higher CMAQ predictions for ozone maxima. The highest ozone difference occurs on September 4 in Houston where CMAQ predicted peak ozone exceeding 85 ppb, 15 ppb higher than CAMx value (not shown). CAMx predictions are generally lower than CMAQ along the coast (e.g., in Galveston) and in the Gulf.

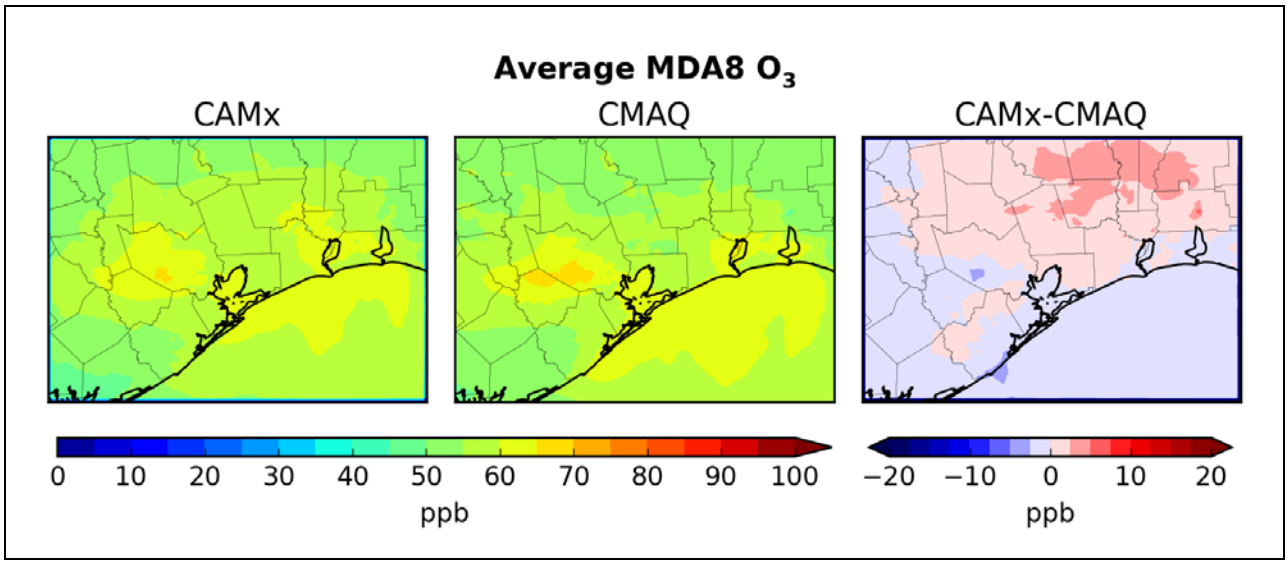

Figure 3-1. Maps of September average daily maximum 8-hour ozone in the 4 km domain from CAMx (left), CMAQ (middle) and the differences between CAMx and CMAQ results (right).

Time series at selected monitors also indicate similar ozone over predictions across the HGBPA area by both models. At Galveston and Clinton, the worst model performance is seen during September 1-9 period when observed ozone is generally lower than 40 ppb (Figure 3-2). Better performance is seen on high observed ozone days (i.e., Sep 25-27). Model performance evaluation covering both of these periods is discussed in detail in our Section 4.

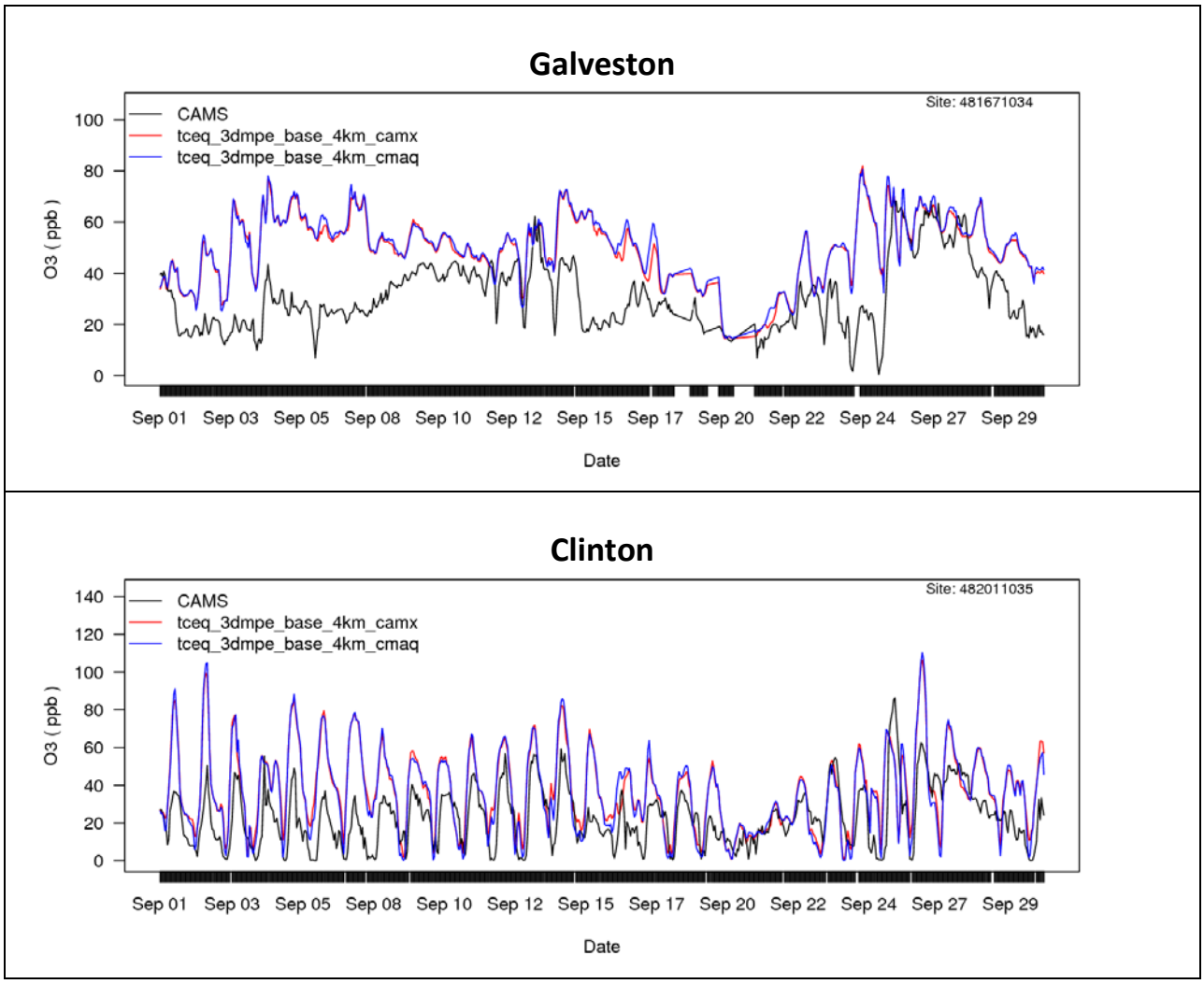

Figure 3-2. Time series of observed (black) and predicted (CAMx/CMAQ; red/blue) ozone at Galveston (top) and Clinton (bottom) TCEQ CAMS sites in September 2013.

4.0 MODEL PERFORMANCE EVALUATION

This section documents evaluation of CAMx and CMAQ model outputs against surface observations and aloft observations collected by the aircraft participating in the Discover-AQ project. Pollutants of interest are ozone, particulate matter (PM) and their precursors.

4.1 Model Evaluation Methodology

We carried out two types of model performance evaluation for this study. The first type of evaluation assesses CAMx and CMAQ model performance in simulating observed ground level ozone and other gaseous species measured at TCEQ CAMS sites in Houston and its vicinity during the September 2013. Pollutants evaluated against TCEQ CAMS data include ozone, isoprene, ethylene, toluene, formaldehyde, carbon monoxide, nitrogen oxide and nitrogen dioxide.

Similarly, we evaluated the CAMx and CMAQ model performance against aircraft measurements along the NASA's P-3 flight path. The flight paths were mapped to grid cells within the 4 km modeling domain. For the grid cells containing aircraft transects, we described in this report the model's performance in simulating measured concentrations of ozone and other gaseous species. In addition, we evaluated particulate PM including nitrate, sulphate, ammonium, and water-soluble organic carbon against aircraft measurements. Photolysis rate of NO_2 was also evaluated.

To quantify model performance, several statistical measures were calculated and evaluated. Table 4-1 lists the definitions of statistical performance measures that were used in model performance evaluation discussed below. The statistical measures selected were based on the recommendations outlined in the USEPA's Draft Modeling Guidance for Demonstrating Attainment of Air Quality Goals for ozone, $PM_{2.5}$, and Regional Haze (USEPA, 2014).

Table 4-1. Definition of performance metrics for photochemical modeling.

Metric	Definition[1]
Mean Bias (MB)	$\frac{1}{N}\sum_{i=1}^{N}(P_i - O_i)$
Mean Error (ME)	$\frac{1}{N}\sum_{i=1}^{N}\lvert P_i - O_i\rvert$
Root Mean Squared Error (RMSE)	$\sqrt{\frac{\sum_{i=1}^{N}(P_i - O_i)^2}{N}}$
Normalized Mean Bias (NMB) (-100% to +∞)	$\frac{\sum_{i=1}^{N}(P_i - O_i)}{\sum_{i=1}^{N}O_i}$
Normalized Mean Error (NME) (0% to +∞)	$\frac{\sum_{i=1}^{N}\lvert P_i - O_i\rvert}{\sum_{i=1}^{N}O_i}$

Metric	Definition[1]
Fractional Bias (FB) (-200% to +200%)	$\frac{2}{N}\sum_{i=1}^{N}\left(\frac{P_i - O_i}{P_i + O_i}\right)$
Fractional Error (FE) (0% to +200%)	$\frac{2}{N}\sum_{i=1}^{N}\left\lvert\frac{P_i - O_i}{P_i + O_i}\right\rvert$
Coefficient of Determination (r^2) (0 to 1)	$\left(\frac{\sum_{i=1}^{N}(P_i - \overline{P})(O_i - \overline{O})}{\sqrt{\sum_{i=1}^{N}(P_i - \overline{P})^2 \sum_{i=1}^{N}(O_i - \overline{O})^2}}\right)^2$

[1] P_i and O_i are prediction and observation at the *i*-th site, respectively; $\overline{P}$ and $\overline{O}$ are mean prediction and observation, respectively.

4.2 Model Performance Evaluation against Surface Measurements

Locations of TCEQ CAMS sites in Houston and its vicinity are shown in Figure 4-1.

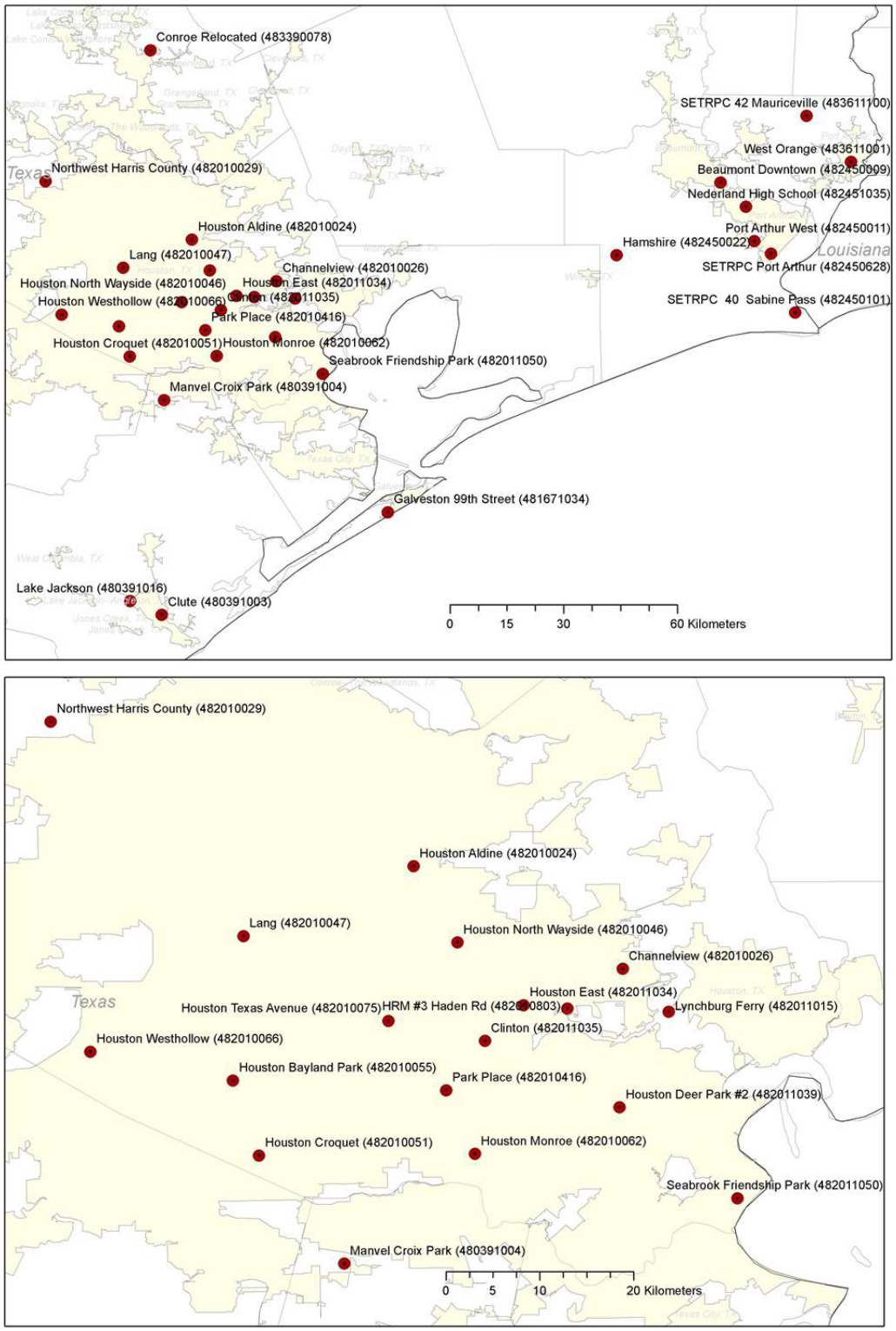

Figure 4-1. Locations of TCEQ CAMS monitoring sites used in the model performance evaluation (zoom-in map shown in the bottom).

4.2.1 Evaluation of Ozone

Figure 4-2 displays scatter plots of predicted and observed hourly ozone concentrations for the CAMx and CMAQ 4 km base case simulation. No threshold is applied in this plot. Overall, CAMx and CMAQ show similar ozone performance. The scatter plot shows some large over predictions by both models with the predictions centered above the 1:1 line of perfect agreement. NMB for CAMx and CMAQ are 67% and 62%, respectively, failing U.S. EPA's performance goal (≤±15%). NME for both models are comparable to NMB (CAMx/CMAQ: 72%/70%) confirming the models' tendency to over predict ozone. High ozone bias in the Houston area has been noted in previous modeling studies (Johnson et al., 2015; Kemball-Cook et al., 2015).

Table 4-2 displays the 2013 September ozone model performance statistics metrics for each individual monitoring site within the 1.33 km domain. The over prediction bias is largest at SETRPC Port Arthur, Houston North Wayside and Lake Jackson where NMB and NME are over 100%. The ozone performance is improved at urban sites but the overestimation is persistent particularly during the first half of September.

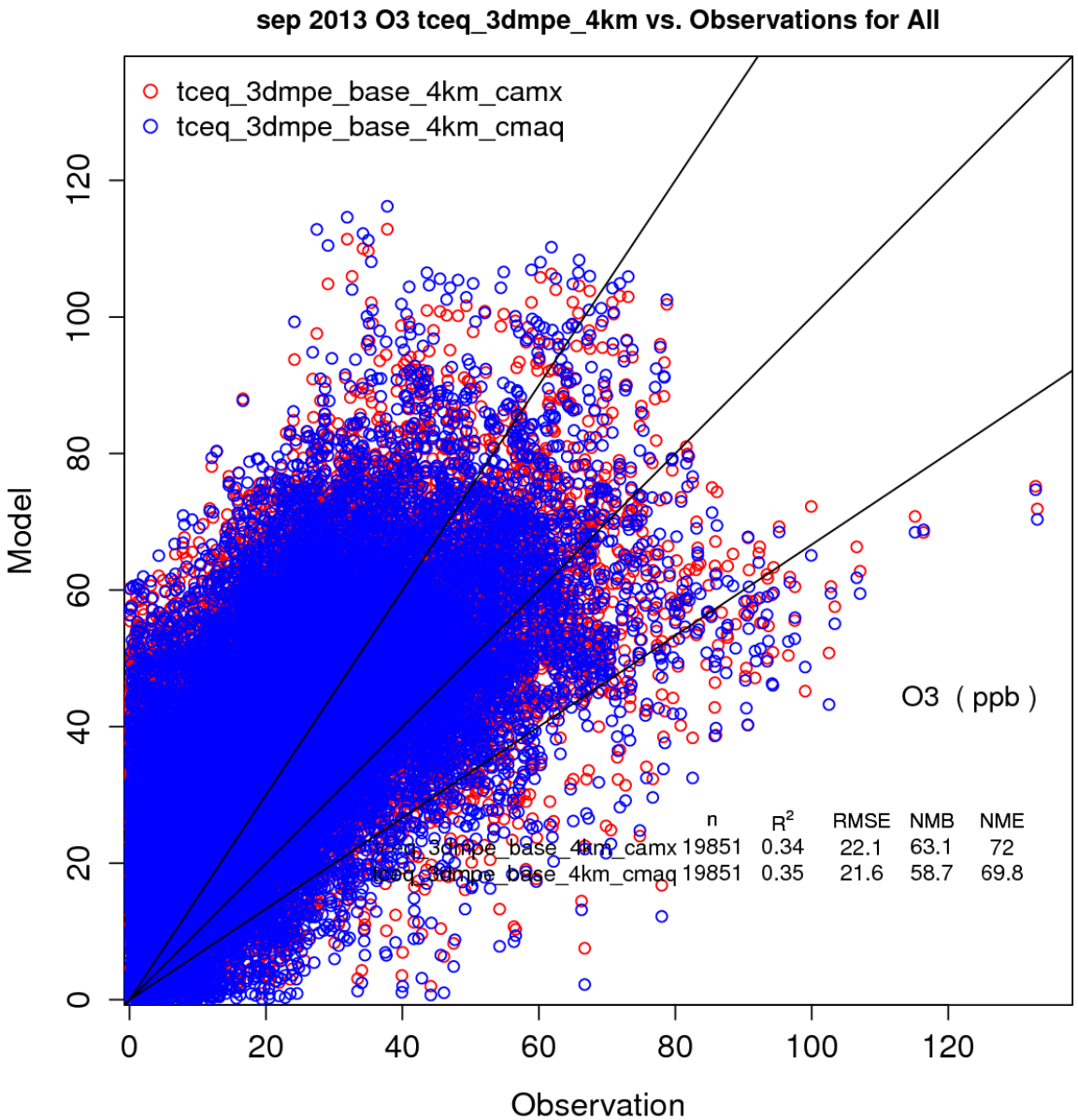

Figure 4-2. Scatter plots of CAMx/CMAQ predicted and observed hourly ozone concentrations for TCEQ CAMS sites in Houston and nearby vicinity.

The hourly ozone time series at TCEQ CAMS stations are shown in Figure 4-3 (see also Appendix C). The observed data show similar features among the CAMS sites analysed:

- September 1-10 were cloudy days resulting in low ozone concentrations (generally below 50 ppb) during this period

- Heavy rain before the first September frontal passage on September 21 lowered ozone level across the HGBPA area
- A second frontal boundary passed through Houston on September 25, coinciding with and contributing to the ozone exceedance event at several sites on that day (as well as September 26). The progression of the 21 and 25 passages has been documented elsewhere (Morris and Lefer, 2014)
- Daytime and nighttime ozone is less distinguishable at Galveston and Seabrook Friendship Park suggesting background ozone influences at these sites.

The diurnal cycle of September ozone shows that both CAMx and CMAQ generally reproduce well the daily modulation. Nighttime ozone is replicated better at urban monitors (e.g., Clinton, Houston North Wayside) than at monitors further away from the city. This may suggest that ozone titration by NOx at night is effective in both models. Conversely, on several days, daytime ozone is over estimated across all monitors by more than a factor 2. At non-urban monitors (such as Conroe, Mauriceville, Northwest Harris County), both models reproduce the daily modulation in ozone but with an offset due to a consistent high bias. Continental ozone transport is anticipated to cause high bias at these monitors.

The low (September 21-25) and high (September 24-26) ozone periods were also replicated well by the models. Poor ozone performance during September 1-10 could be partly related to insufficient clouds simulated by the WRF model. The lack of cloud could overstate solar attenuation which influences photochemistry (more discussion on photolysis prediction performance in Section 3. However, the examination of maximum daily average 8-hour (MDA8) ozone at upwind (e.g., La Porte Sylvan Beach) and downwind (Houston West hollow) site suggests that CAMx reasonably predicts local ozone production. The difference of MDA8 ozone between the upwind and downwind site during September 1-10 is about 8 ppb, not much higher than the observed value of 5 ppb.

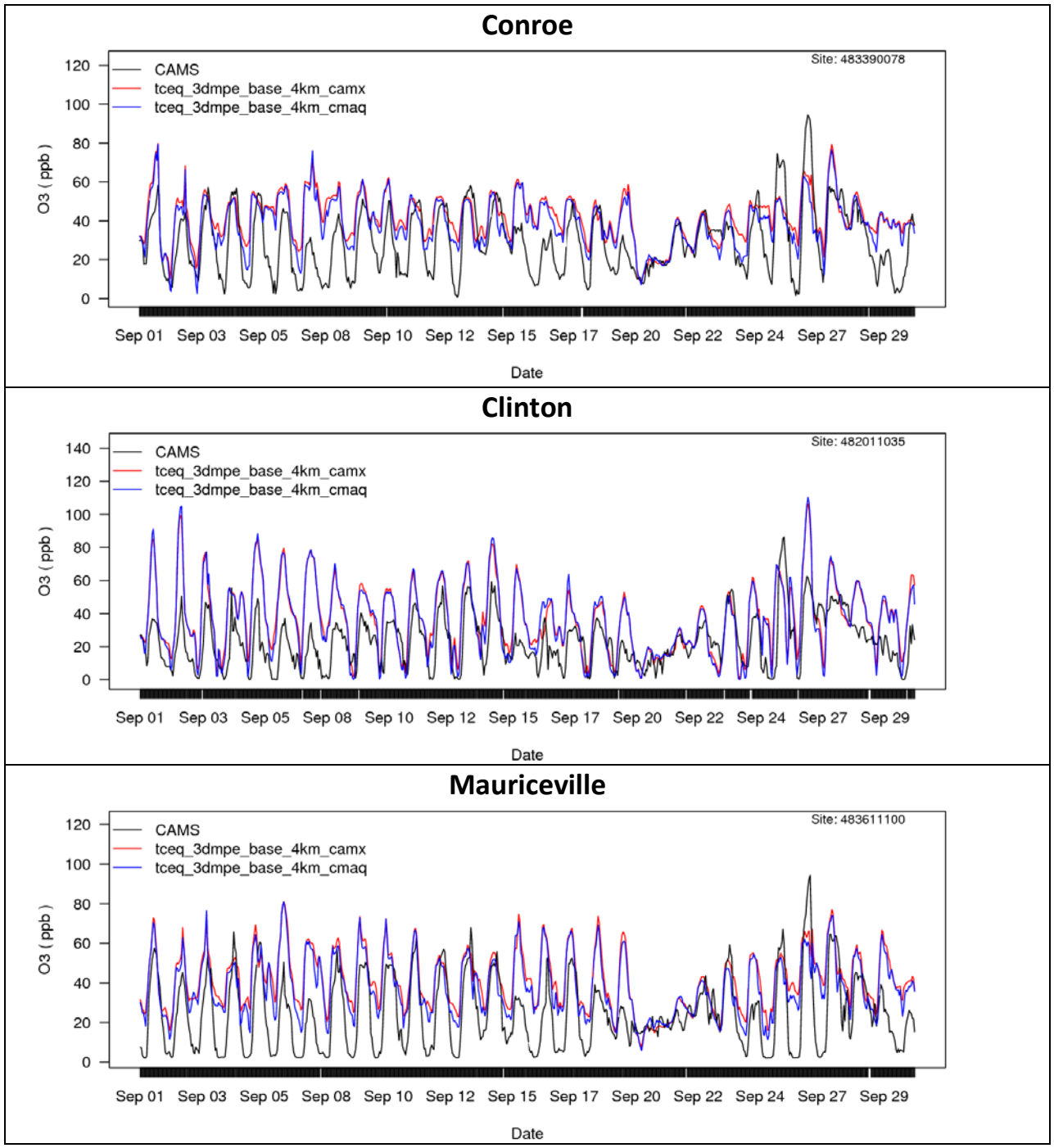
Conroe
Site: 483390078
CAMS
tceq_3dmpe_base_4km_camx
tceq_3dmpe_base_4km_cmaq
O3 (ppb)
Date
Clinton
Site: 482011035
CAMS
tceq_3dmpe_base_4km_camx
tceq_3dmpe_base_4km_cmaq
O3 (ppb)
Date
Mauriceville
Site: 483611100
CAMS
tceq_3dmpe_base_4km_camx
tceq_3dmpe_base_4km_cmaq
O3 (ppb)
Date
Sep 01 Sep 03 Sep 05 Sep 08 Sep 10 Sep 12 Sep 15 Sep 17 Sep 20 Sep 22 Sep 24 Sep 27 Sep 29

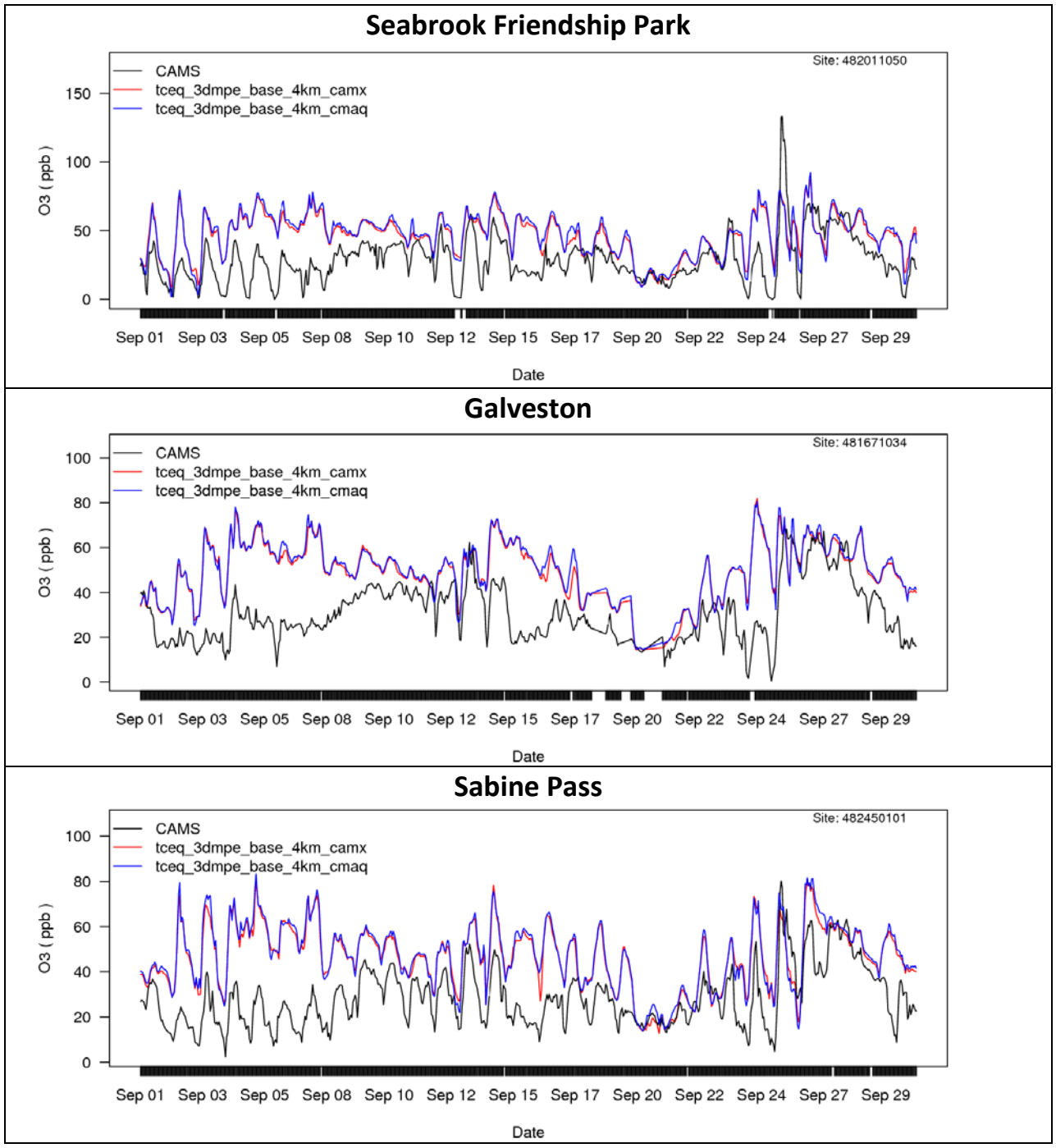

Figure 4-3. Time series of observed (black) and predicted (CAMx/CMAQ; red/blue) ozone at Galveston (top) and Clinton (bottom) TCEQ CAMS sites in September 2013.

Table 4-2. 1-hour ozone model performance statistics of CAMx and CMAQ Base Case for the 4 km domain over all CAMS monitors within the HGBPA 4 km CAMx domain.

Site ID	Site Name	#Obs	Mean			MB		ME		NMB (%)		NME (%)		FB		FE		R^2		RMSE	
			Obs	CAMx	CMAQ	CAMx	CMAQ	CAMx	CMAQ	CAMx	CMAQ	CAMx	CMAQ	CAMx	CMAQ	CAMx	CMAQ	CAMx	CMAQ	CAMx	CMAQ
480391004	Manvel Croix Park	703	24	41.9	40.0	17.4	15.6	19.3	18.0	71.2	63.7	79.0	73.6	62.8	56.1	69.2	66.6	0.33	0.36	23.1	21.8
480391016	Lake Jackson	680	21	42.6	42.0	21.4	20.8	22.0	21.4	100.9	98.1	103.9	101.1	73.8	73.2	77.0	76.2	0.18	0.23	25.8	25.1
481671034	Galveston 99th Street	666	31	49.5	50.3	18.6	19.4	19.2	20.0	60.3	62.7	62.2	64.6	49.4	50.8	50.7	52.1	0.19	0.19	23.2	23.9
482010024	Houston Aldine	706	23	39.6	37.5	16.9	14.8	19.3	17.6	74.4	65.4	85.0	77.8	67.6	61.0	75.6	71.9	0.37	0.39	22.9	21.5
482010026	Channelview	629	23	37.1	36.5	14.0	13.4	17.1	17.0	60.7	58.2	73.9	73.7	55.1	51.9	66.2	66.2	0.31	0.32	21.2	21.2
482010029	Northwest Harris County	643	25	40.9	38.6	15.8	13.5	18.2	16.9	63.0	53.7	72.6	67.4	63.3	57.0	68.9	66.6	0.36	0.37	21.9	20.6
482010046	Houston North Wayside	698	21	42.1	40.9	21.2	20.0	22.4	21.3	101.8	96.0	107.3	102.1	83.4	80.8	87.0	85.0	0.39	0.41	25.8	24.8
482010047	Lang	697	24	42.9	43.0	18.8	18.8	19.8	19.8	77.6	77.9	81.7	82.0	71.0	69.8	73.6	73.0	0.44	0.45	23.5	23.9
482010051	Houston Croquet	701	25	40.8	39.6	16.2	15.0	18.4	17.6	65.7	60.9	74.8	71.6	58.9	52.8	66.8	65.6	0.37	0.40	22.4	21.8
482010055	Houston Bayland Park	576	27	45.3	45.8	17.9	18.4	19.4	20.1	65.5	67.0	70.7	73.2	57.2	55.4	61.1	62.7	0.38	0.37	23.9	25.0
482010062	Houston Monroe	703	24	36.5	34.9	12.7	11.1	16.0	15.1	53.4	46.7	67.0	63.2	50.2	40.7	63.3	62.4	0.36	0.39	20.0	19.1
482010066	Houston Westhollow	700	27	38.2	37.8	11.7	11.2	15.4	15.6	43.8	42.1	58.0	58.6	38.3	30.4	53.3	55.5	0.36	0.39	19.8	20.1
482010075	Houston Texas Avenue	704	23	39.5	38.7	16.3	15.5	17.7	17.6	70.1	66.6	76.1	75.8	60.8	51.9	67.3	68.0	0.47	0.49	21.9	22.0
482010416	Park Place	697	25	38.8	38.1	13.8	13.1	16.4	16.5	55.2	52.2	65.5	65.8	51.8	42.0	62.5	64.4	0.46	0.47	20.6	20.8
482010803	HRM #3 Haden Rd	706	24	35.0	34.1	11.1	10.2	15.8	15.4	46.2	42.6	66.1	64.3	48.3	43.5	66.7	66.8	0.34	0.37	20.0	19.5
482011015	Lynchburg Ferry	695	25	36.4	36.4	11.8	11.8	15.8	16.0	48.0	48.0	64.1	65.1	43.5	41.1	59.8	60.1	0.31	0.32	19.9	20.2
482011034	Houston East	707	23	39.3	38.0	16.2	14.9	18.4	17.5	70.0	64.2	79.7	75.4	65.5	60.9	73.4	71.5	0.38	0.41	22.6	21.8
482011035	Clinton	698	23	37.2	36.3	14.2	13.4	17.5	17.4	62.0	58.3	76.3	75.9	51.7	44.6	68.6	69.6	0.37	0.38	21.8	21.9
482011039	Houston Deer Park #2	651	26	40.7	40.2	14.6	14.0	16.8	16.8	55.8	53.7	64.3	64.1	50.4	46.1	57.4	57.1	0.39	0.39	20.8	20.9
482011050	Seabrook Friendship Park	691	29	46.3	47.4	17.2	18.2	19.4	20.5	59.0	62.6	66.5	70.4	52.0	53.3	56.3	58.0	0.25	0.24	23.6	24.8
482450009	Beaumont Downtown	701	27	38.2	36.0	10.8	8.6	14.7	13.8	39.6	31.5	53.9	50.4	39.2	31.1	52.7	51.1	0.36	0.36	18.8	17.8
482450011	Port Arthur West	708	28	41.8	40.2	14.2	12.6	16.5	15.8	51.5	45.7	59.8	57.2	45.4	38.9	52.9	53.0	0.33	0.34	20.4	19.6
482450022	Hamshire	703	25	42.7	39.7	18.1	15.1	19.2	17.0	73.8	61.7	78.3	69.3	64.3	56.5	67.9	63.8	0.33	0.35	23.2	20.9
482450101	SETRPC 40 Sabine Pass	706	28	46.5	47.4	18.4	19.3	19.4	20.2	65.7	69.0	69.1	72.2	51.6	53.4	54.4	55.8	0.23	0.22	22.9	23.9
482450628	SETRPC Port Arthur	703	20	41.0	40.2	21.4	20.6	22.4	22.1	109.3	105.4	114.3	112.7	71.9	67.6	76.1	76.1	0.21	0.21	26.2	26.0

Site ID	Site Name	#Obs	Mean			MB		ME		NMB (%)		NME (%)		FB		FE		R^2		RMSE	
			Obs	CAMx	CMAQ	CAMx	CMAQ	CAMx	CMAQ	CAMx	CMAQ	CAMx	CMAQ	CAMx	CMAQ	CAMx	CMAQ	CAMx	CMAQ	CAMx	CMAQ
482451035	Nederland High School	562	29	43.8	42.6	14.8	13.7	17.1	16.3	51.3	47.4	59.1	56.5	50.0	46.2	55.8	53.9	0.37	0.38	20.9	20.3
483390078	Conroe Relocated	707	29	41.7	38.5	12.9	9.7	15.3	13.3	44.7	33.8	53.0	46.3	46.9	39.0	51.9	47.6	0.34	0.35	18.9	16.8
483611001	West Orange	700	25	38.2	36.0	13.1	10.8	15.4	14.4	52.0	43.1	61.4	57.1	50.4	44.0	59.7	58.2	0.37	0.38	19.2	17.8
483611100	SETRPC 42 Mauriceville	708	25	41.3	38.0	16.8	13.5	18.4	16.1	68.6	55.2	75.1	65.8	67.6	61.0	71.8	67.6	0.44	0.44	21.8	19.3

4.2.2 Evaluation of Ozone Precursors

4.2.2.1 Nitric oxide (NO) and nitrogen dioxide (NO_2)

The left panel in Figure 4-4 displays a scatter plot of the predicted and observed hourly NO concentrations across the selected CAMS sites. The predicted magnitude is considerably off during episodic events which are indicated by spikes in the time series (Figure 4-5). It would be expected that a grid model with 4 km grid resolution would underestimate narrow plumes of a primary emitted pollutants, like NO, since it would instantaneously disperse the pollutants across a 4 km grid. In addition, except for power plants, emissions are for average ozone season, not specific to September 2013 episode. CMAQ shows smaller NO performance bias (NMB = -55%) than CAMx (NMB = -68%), but has comparable error (NME = 85%). The effect of the poor NO model performance on ozone is unclear. However, good performing photochemical grid model applications for ozone frequently are performing poorly for NO.

In contrast to NO performance, NO_2 is over predicted across all monitors with NMB of 49% and 60% for CAMx and CMAQ, respectively (Figure 4-4, right). NME is lower in CAMx (81%) than CMAQ (91%). Time series at Houston Aldine shows that the models reproduce the diurnal pattern of NO_2 relatively well but largely overestimated afternoon peaks (Figure 4-6, top). At Clinton, the models overestimated both morning and afternoon peaks (Figure 4-6, bottom). Night-time NO_2 predictions agree with the observations. Beaumont monitors have the worst performance with NMB and NME larger than 100% and the modelled mean values more than doubling the observational mean values. Since NOx emissions from refineries dominate mobile sources in this area, it may indicate a point source inventory bias.

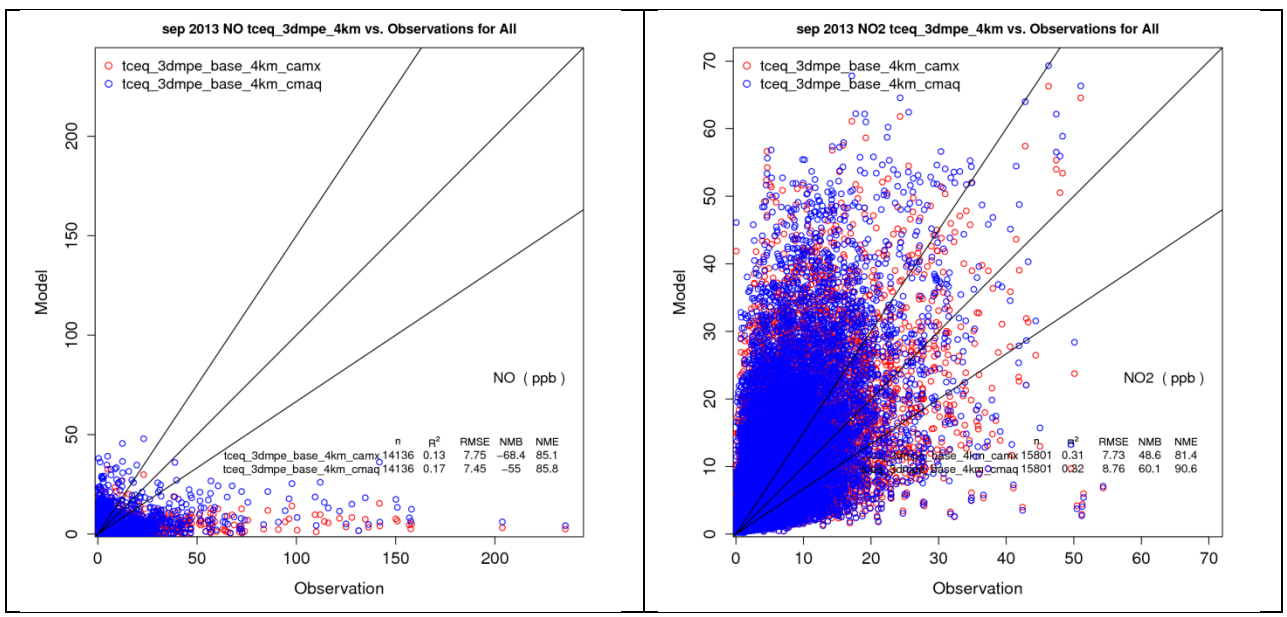

Figure 4-4. Scatter plots of CAMx/CMAQ predicted and observed hourly NO (left) and NO_2 (right) concentrations for TCEQ CAMS sites in Houston and nearby vicinity.

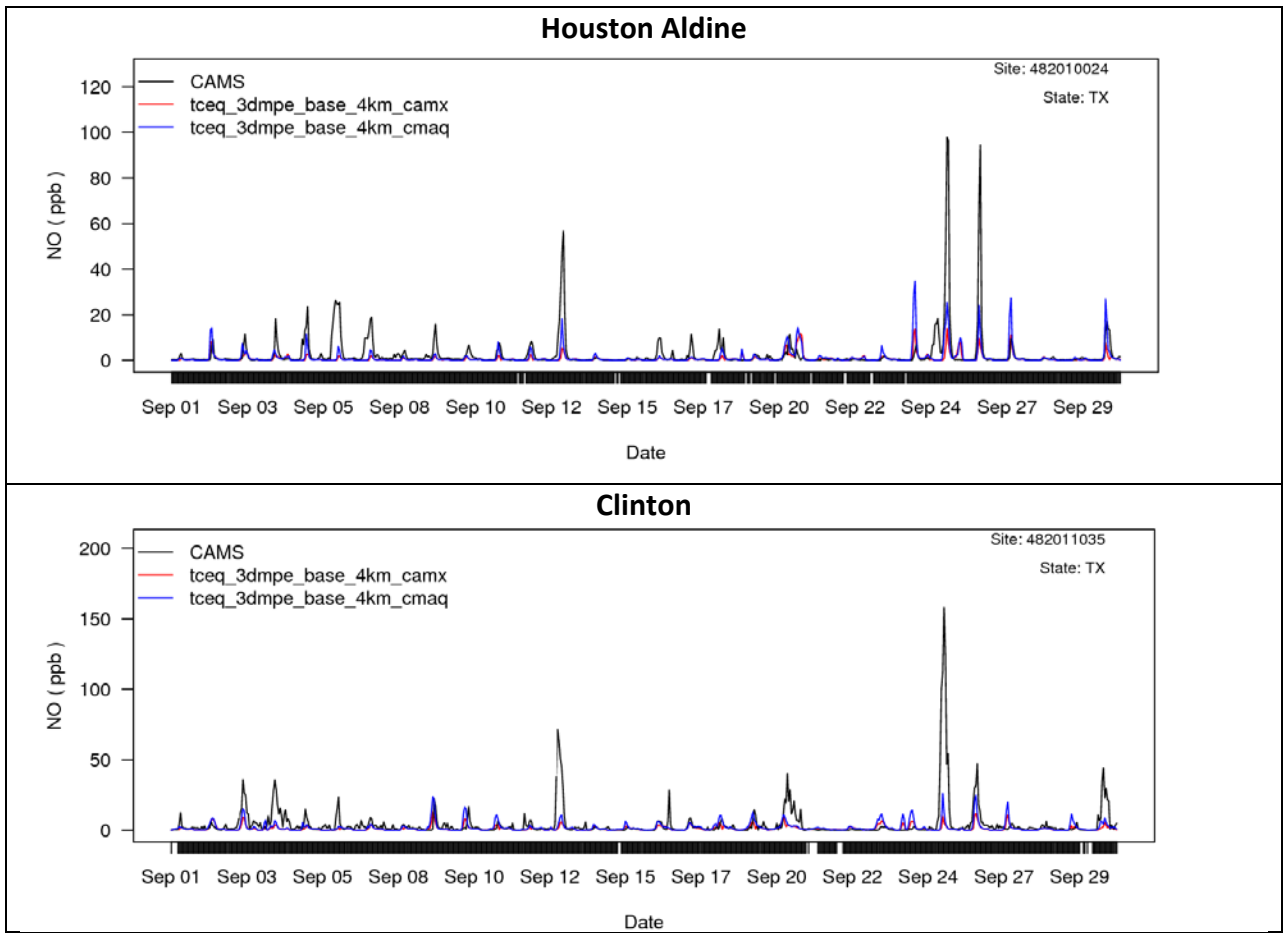

Figure 4-5. Time series of observed (black) and predicted (CAMx/CMAQ; red/blue) NO concentrations at TCEQ CAMS sites in September 2013.

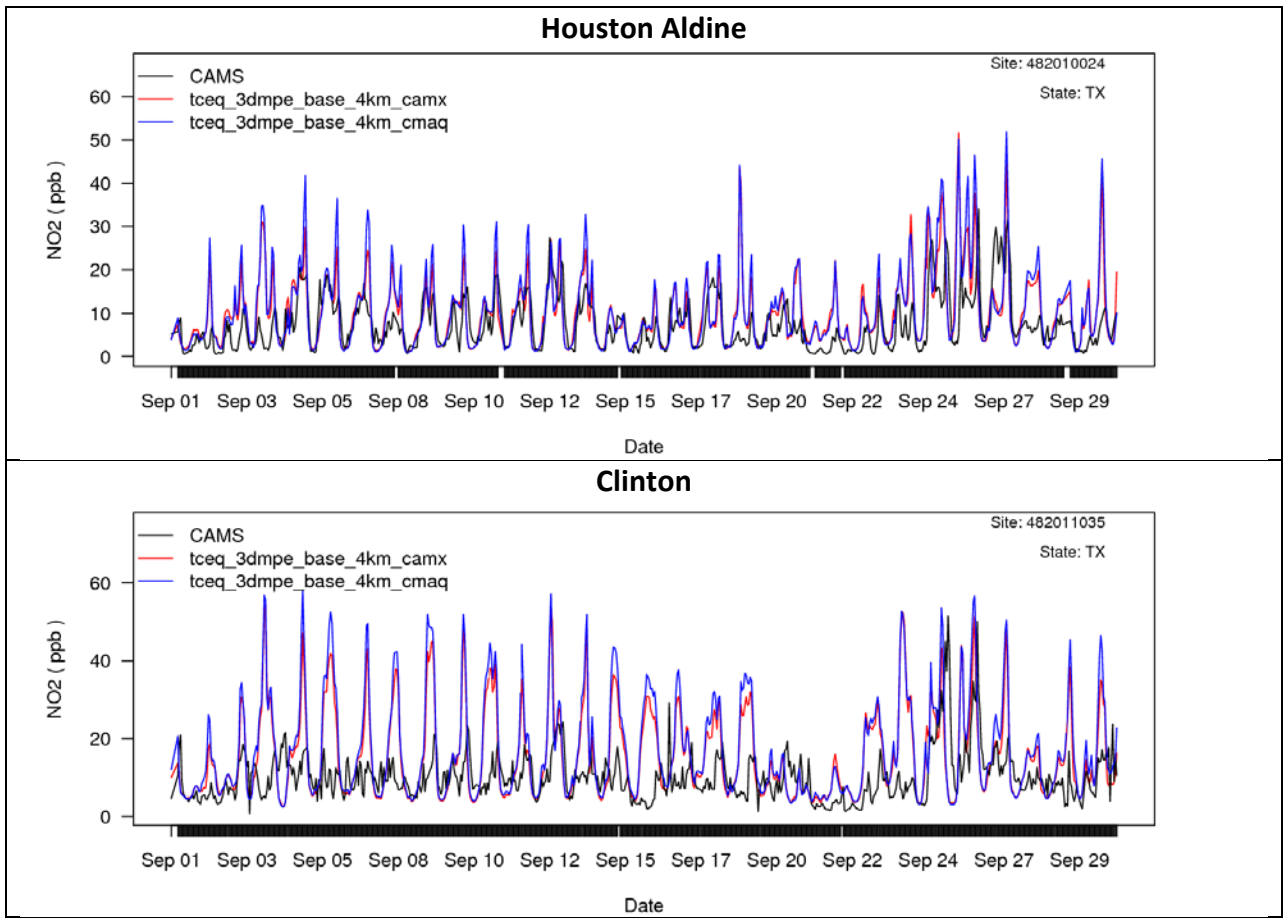

Figure 4-6. Time series of observed (black) and predicted (CAMx/CMAQ; red/blue) NO_2 concentrations at TCEQ CAMS sites in September 2013.

4.2.2.2 Isoprene, acetylene, benzene

Time series for isoprene (Figure 4-8) show morning and evening peaks for both models and observations, but these peaks are much stronger in the models and strongly influence model bias and error statistics. A scatter plot of the predicted and observed hourly isoprene concentrations across the selected CAMS sites (Figure 4-7) shows overestimation bias by CAMx (NMB=116%) and CMAQ (NMB=120%). NMB and NME are of almost the same magnitude which suggests that the overestimation bias is systematic. Both models over estimate day-time isoprene, but their diurnal profiles differ. CMAQ tends to overestimate morning peaks with values often higher than CAMx by a factor of 2 (Figure 4-8). We expect that the landuse Kv patch in CAMx introduces more night-time mixing which reduces isoprene buildup from lower planetary boundary layer. Even so, CAMx consistently overestimates both morning and afternoon peaks as seen in the previous finding (Kemball-Cook et al., 2015). Isoprene is mainly emitted by biogenic sources and further reduction of biogenic emissions may help improve the model performance. Kemball-Cook et al. (2015) suggested that latest revisions to emission factors in the MEGAN biogenic model reduced ozone predictions as large as 20 ppb in the

Houston-Galveston-Brazoria area. However, the ozone overestimation bias is still pronounced and is likely caused by other processes which are currently not well understood.

Slightly better performance is seen in acetylene. A scatter plot (Figure 4-9) shows an over-estimation bias by CAMx (NMB=45%) and CMAQ (NMB=62%). Although acetylene is strongly associated with vehicle emissions (Scheff et al., 1989), its observed weekday concentrations associated with heavy morning traffic are comparable to weekend values (Figure 4-10). Relatively high concentrations occur sporadically at any hours or days. The sites that have acetylene measurements available (i.e., Houston Deer Park, West Orange, Nederland High School, Northwest Harris County) may have weak traffic patterns.

Benzene and toluene are both biased high which could imply overstated aromatic emissions, although some concentration spikes, such as those seen for benzene on September 2 and 24-26 at Lynchburg Ferry site, are not well captured by the models. This could be due to sources that are not present in the model, emission events not included in the emission inputs, or misalignment of the modeled plume. Similar concentration spikes of toluene at Lynchburg Ferry occurred on different days indicating different emitting sources. CAMx performance is slightly better than CMAQ, but NMEs from both models are large, in the range of 99-123% (Figure 4-7, bottom). Lower bias predicted by CAMx implies more rigorous vertical mixing in the evening and early morning.

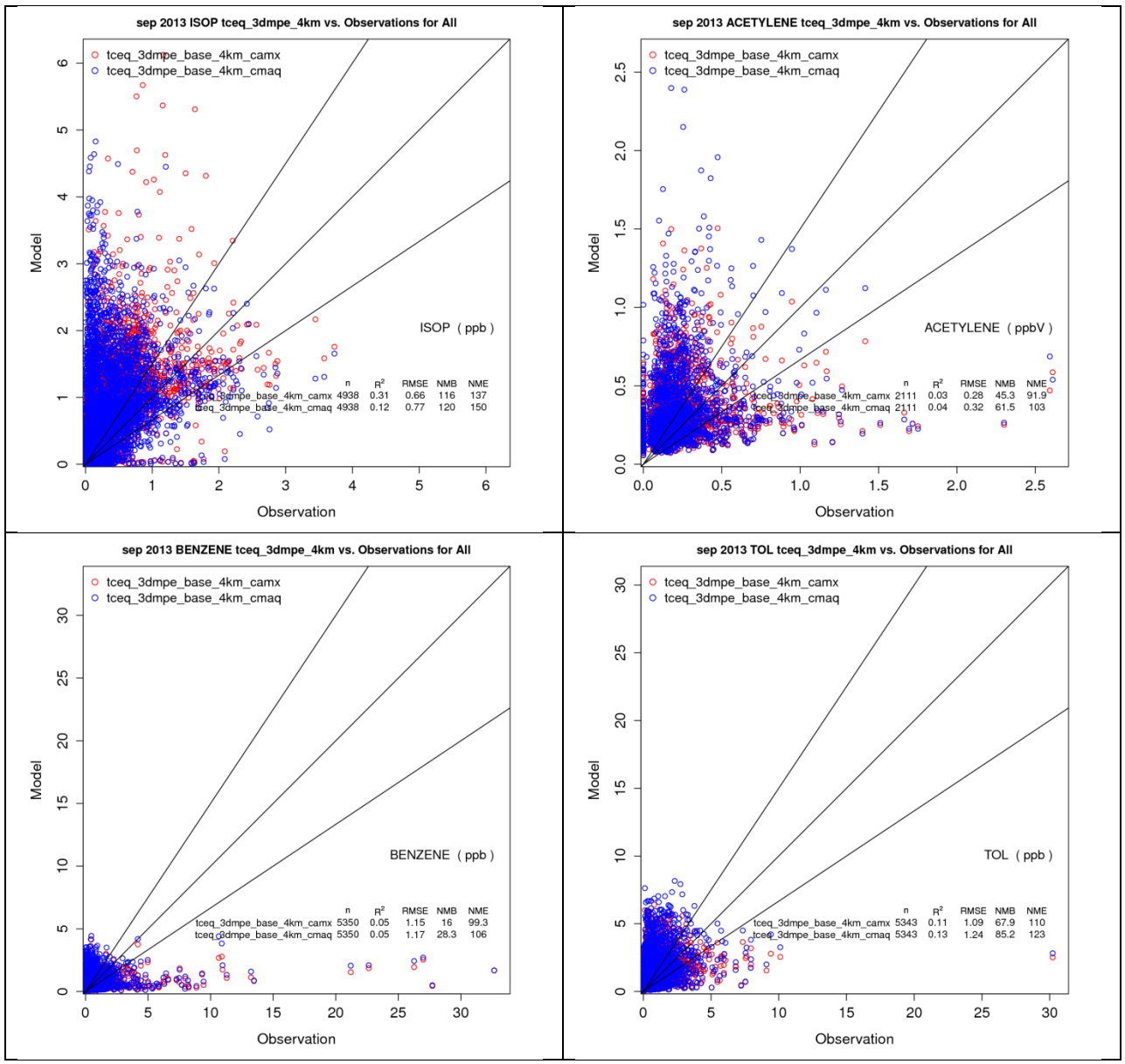

Figure 4-7. Scatter plots of CAMx/CMAQ predicted and observed hourly isoprene (top left), acetylene (top right), benzene (bottom left), and toluene (bottom right) concentrations for TCEQ CAMS sites in Houston and nearby vicinity.

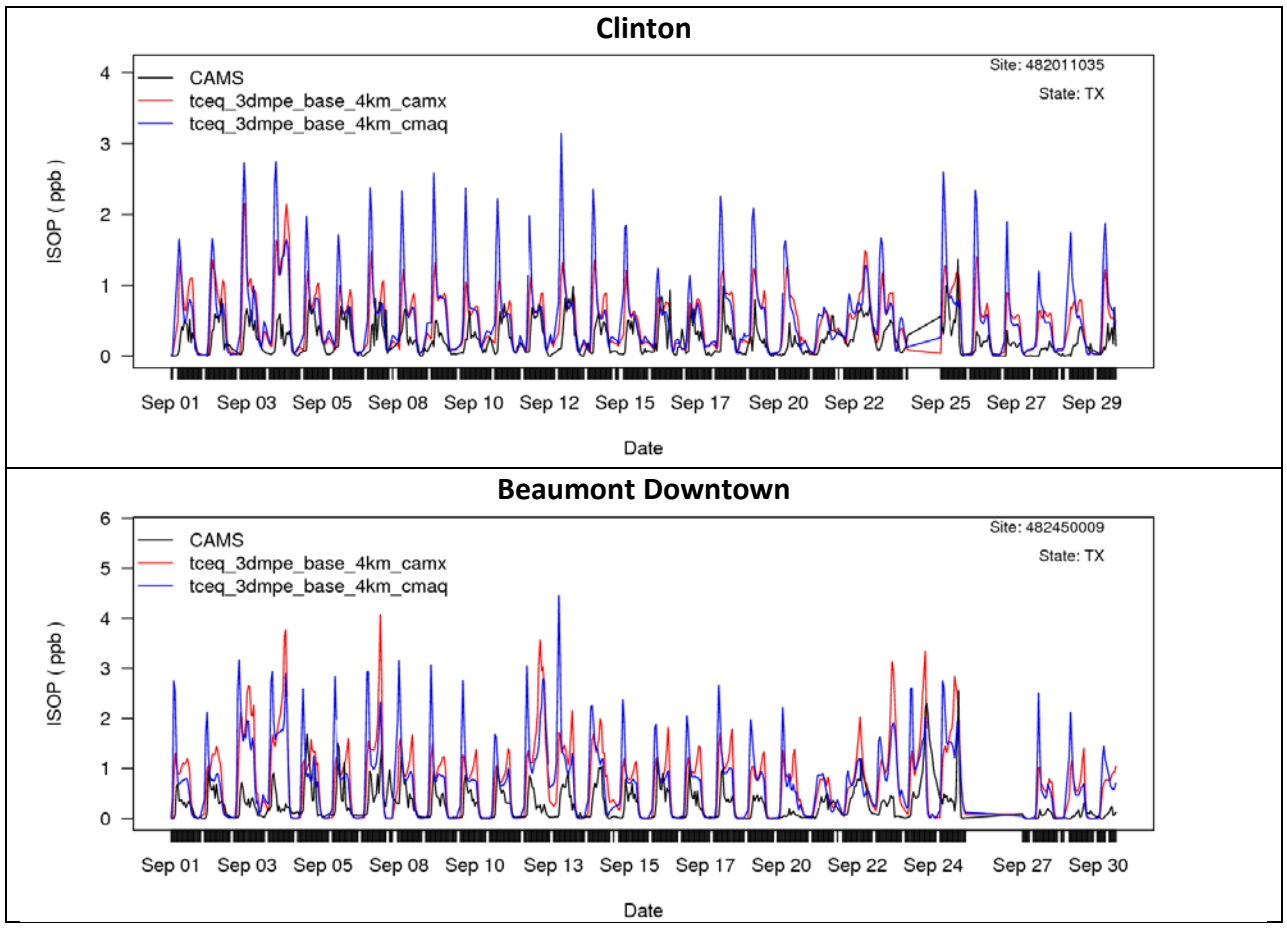

Figure 4-8. Time series of observed (black) and predicted (CAMx/CMAQ; red/blue) isoprene concentrations at TCEQ CAMS sites in September 2013.

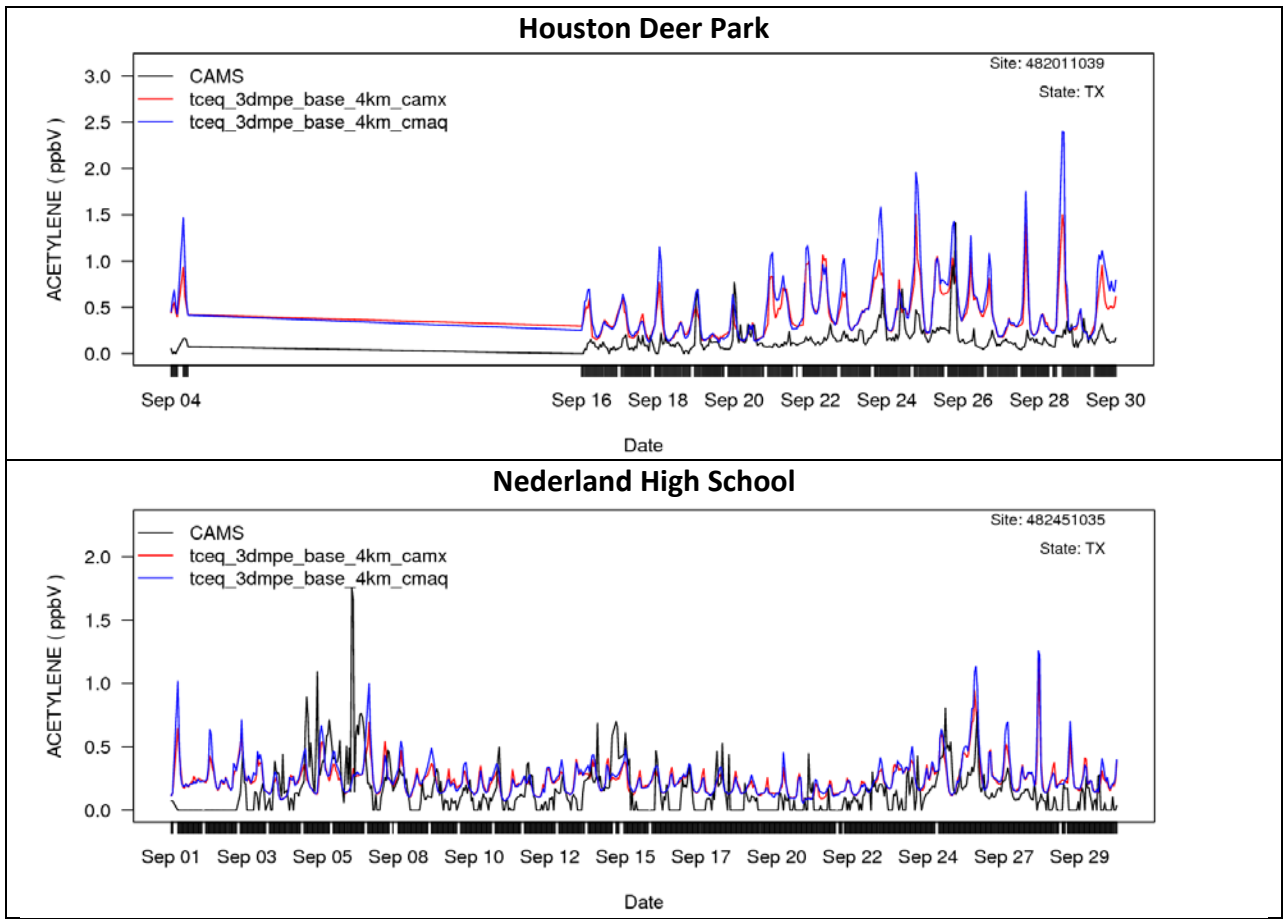

Figure 4-9. Time series of observed (black) and predicted (CAMx/CMAQ; red/blue) acetylene concentrations at TCEQ CAMS sites in September 2013.

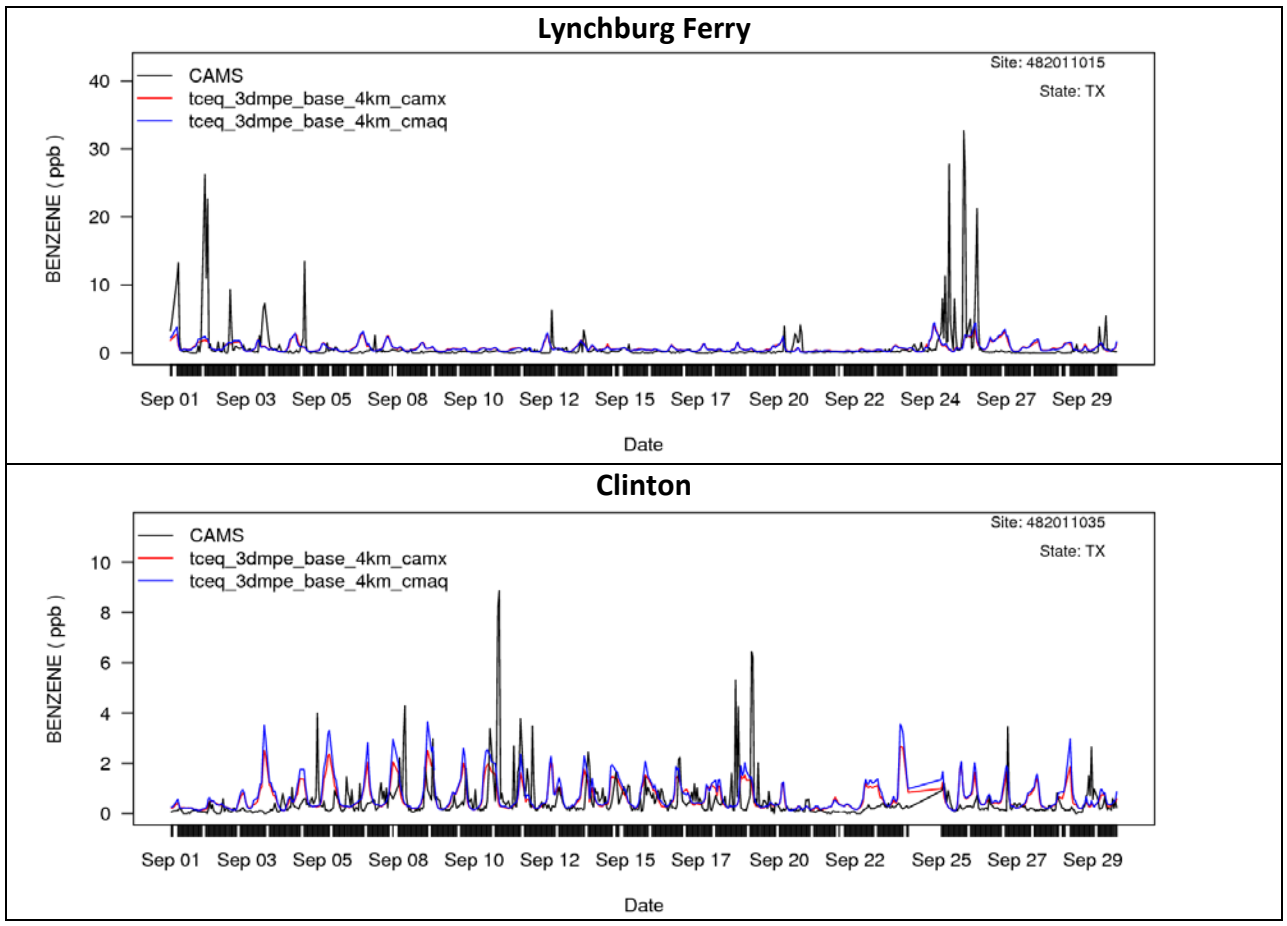

Figure 4-10. Time series of observed (black) and predicted (CAMx/CMAQ; red/blue) benzene concentrations at TCEQ CAMS sites in September 2013.

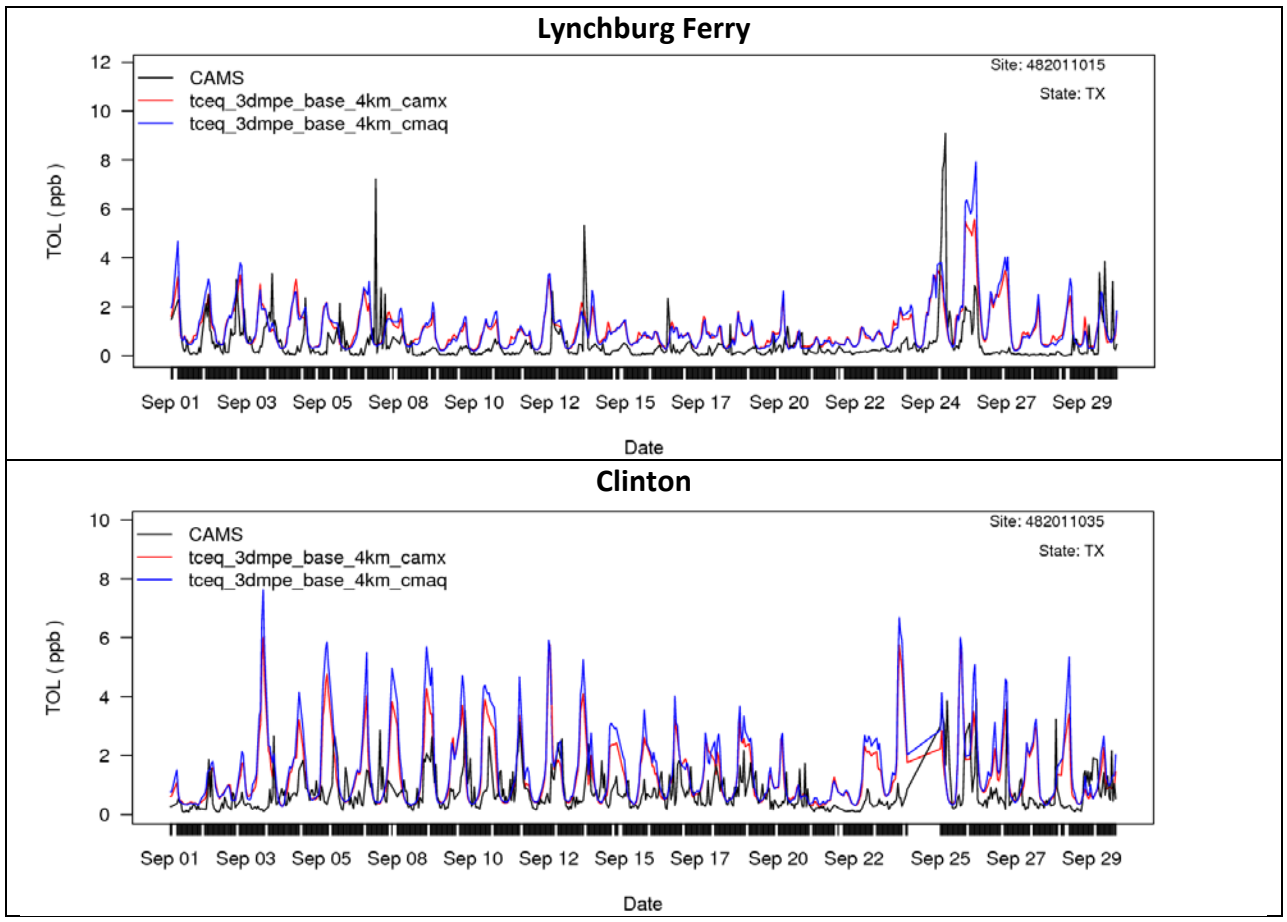

Figure 4-11. Time series of observed (black) and predicted (CAMx/CMAQ; red/blue) toluene concentrations at TCEQ CAMS sites in September 2013.

4.2.2.3 Carbon monoxide (CO)

Model performance for CO is quite good (Figure 4-12), for which both models have a slight high bias and reasonably good skill (NME of 34%). Episodic events of observed CO concentrations at Clinton and Houston Aldine (Figure 4-13) such as a peak on September 24 appear to correlate with NO concentrations (Figure 4-5, top and middle). High observed CO concentrations at Nederland High School correlate better with acetylene concentrations, suggesting influences from incomplete combustion sources.

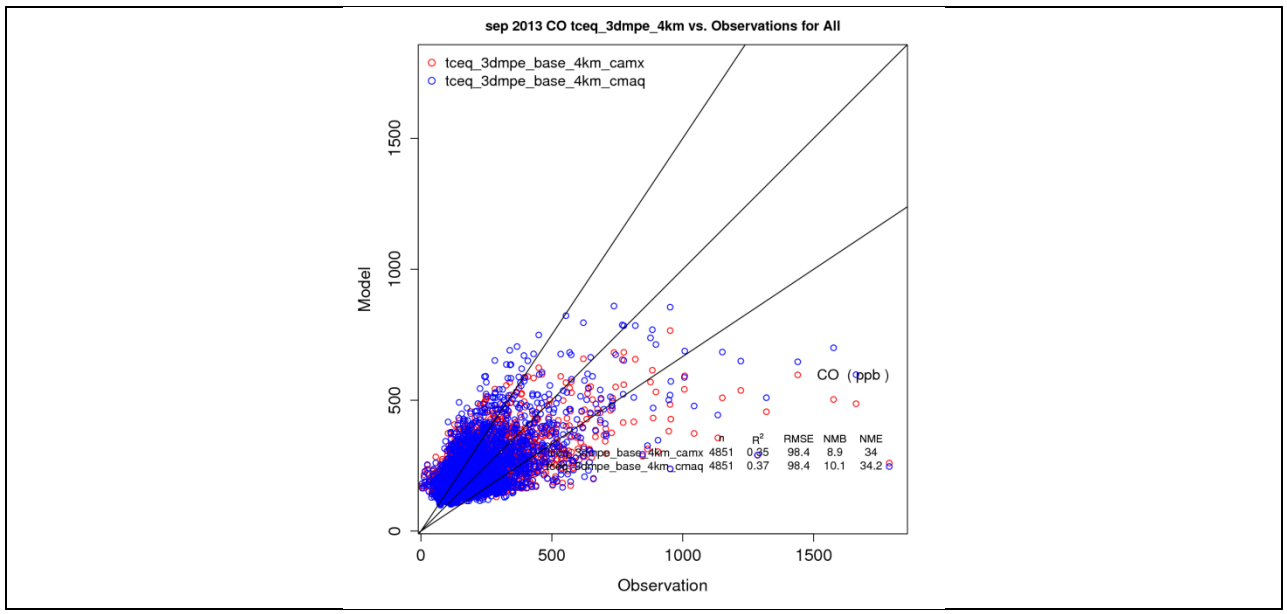

Figure 4-12. Scatter plots of CAMx/CMAQ predicted and observed hourly carbon monoxide concentrations for TCEQ CAMS sites in Houston and nearby vicinity.

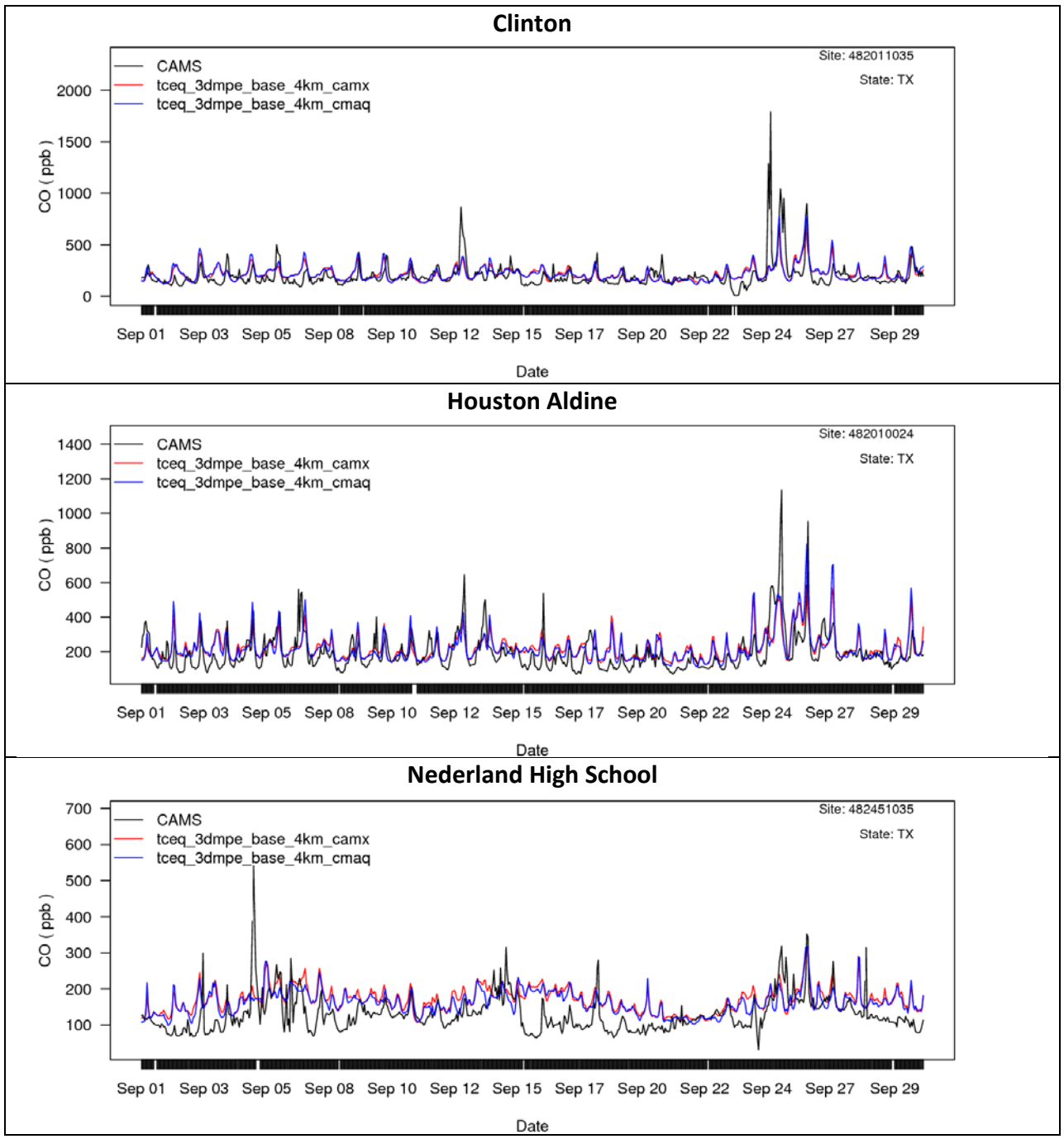

Figure 4-13. Time series of observed (black) and predicted (CAMx/CMAQ; red/blue) carbon monoxide concentrations at TCEQ CAMS sites in September 2013.

4.2.3 Evaluation of Fine Particulate Matter ($PM_{2.5}$)

PM model performance is examined for $PM_{2.5}$ mass using hourly observation data at CAMS sites. Model performance was evaluated with no threshold. The PM performance goals and criteria for bias (≤±30% and ≤±60%) and error (≤50% and ≤75%) have been used by the Regional Planning Organizations (RPOs) to assist in evaluating regional PM models. The FB and FE metrics indicate that CAMx overestimates the observed hourly $PM_{2.5}$ concentrations across the 4 km domain by 47% with 57% error achieving the PM performance criteria (Figure 4-14). CMAQ performance is better with FB of 30% and FE of 51%. Predicted high $PM_{2.5}$ on September 26 at Conroe and on September 12 at Mauriceville (Figure 4-15) are influenced by fire events as indicated by high CO and organic aerosols (OA) emissions during the same period. The observations at Conroe do not show this fire signature. The observed data at Mauriceville shows some fire signatures but the magnitude is three times lower than the predicted values. Modeling fire events remains a challenge at fine grid resolution.

Sahara dust that moves off from African coast can transport to southern Texas. This transport is simulated by Mozart and provided to CAMx via boundary conditions. A backward trajectory analysis suggested that high observed concentrations (> 20 ug/m3) on September 15 at multiple sites are associated with Sahara dust transport. Both models did not capture this event even though the predicted wind directions agree well with observations on this day. It appears that the influence of Sahara dust through boundary conditions, at least on September 15, is understated.

Figure 4-15 shows that predicted time series of $PM_{2.5}$ concentrations by CAMx and CMAQ are comparable at inland sites (such as Conroe, Clinton, and Mauriceville). CAMx predictions tend to be higher than CMAQ near the coastline by 3-4 ug/m^3 on average (Table 4-3) due to higher nitrate (PNO_3) and sea-salt sodium (Na) (see Appendix D). In coastal regions, significant emissions of sea salt originate from wave-breaking in the surf zone. CAMx (through off-line sea-salt processor) defines all grid cells along the coast lines as surf zone whereas CMAQ excludes bays and inlets. So sea salt emissions in the Galveston bay are lower in CMAQ than CAMx. Although CMAQ predicts lower $PM_{2.5}$ nitrate than CAMx, it estimates substantial coarse nitrate (k mode). The reasons are that CMAQ partly allocates sea salt particles into k mode and sodium nitrate ($NaNO_3$) is hygroscopic and can grow larger than 2.5 μm.

PM speciation measurements during DISCOVER-AQ were conducted at four sites in Houston by Baylor University (Sheesley and Usenko, 2015). Figure 4-16 shows that observed $PM_{2.5}$ at Conroe is dominated by OA (shown in Figure 4-16 as OC x 1.2), sulfate, and ammonium. Both models predicted that OA and other PM[5] are two major constituents across all sites (example is given in Figure 4-17). Elevated OA concentrations in Northern America are often related to fire events. Several sites are predicted to have elevated $PM_{2.5}$ concentrations on September 25-26 influenced by fires (e.g., high OC and other PM). However, the fire influences are not seen in the observations. EC and other PM concentrations are predicted slightly lower in CAMx. Since

[5] Other PM = total $PM_{2.5}$ mass – PSO_4 – PNO_3 – PNH_4 – NACL – PEC - POA

the two species are inert, the lower estimates suggest CAMx has more vertical mixing. Secondary aerosols (i.e., sulphate, nitrate, OA), however, are predicted higher in CAMx.

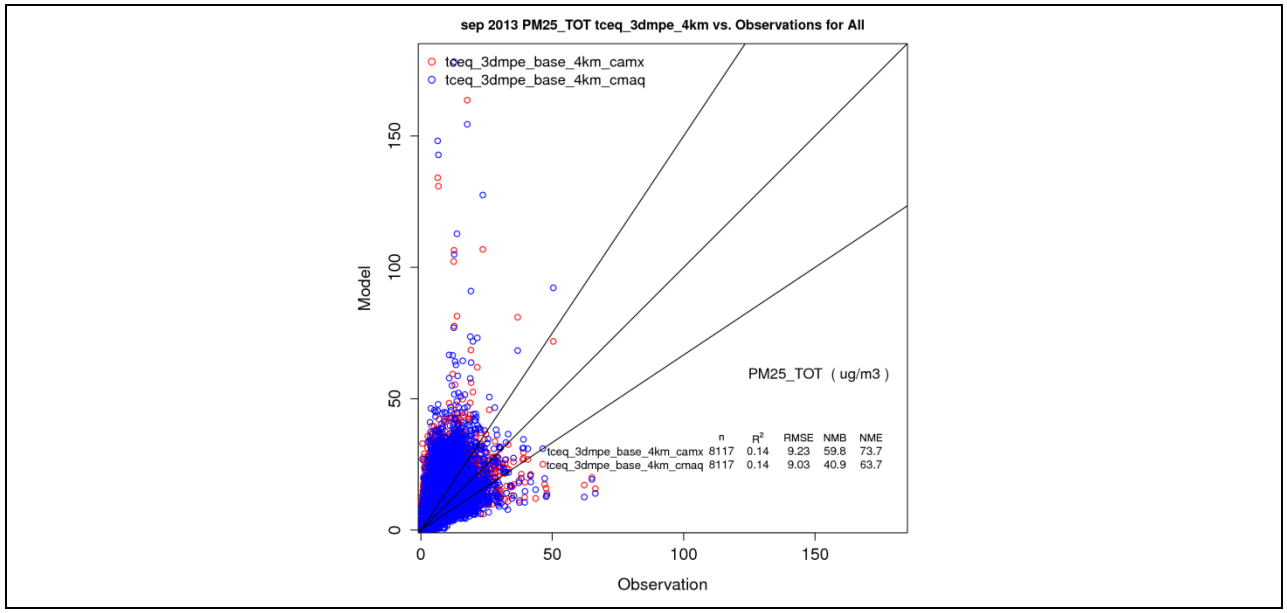

Figure 4-14. Scatter plots of CAMx/CMAQ predicted and observed hourly $PM_{2.5}$ concentrations for TCEQ CAMS sites in Houston and nearby vicinity.

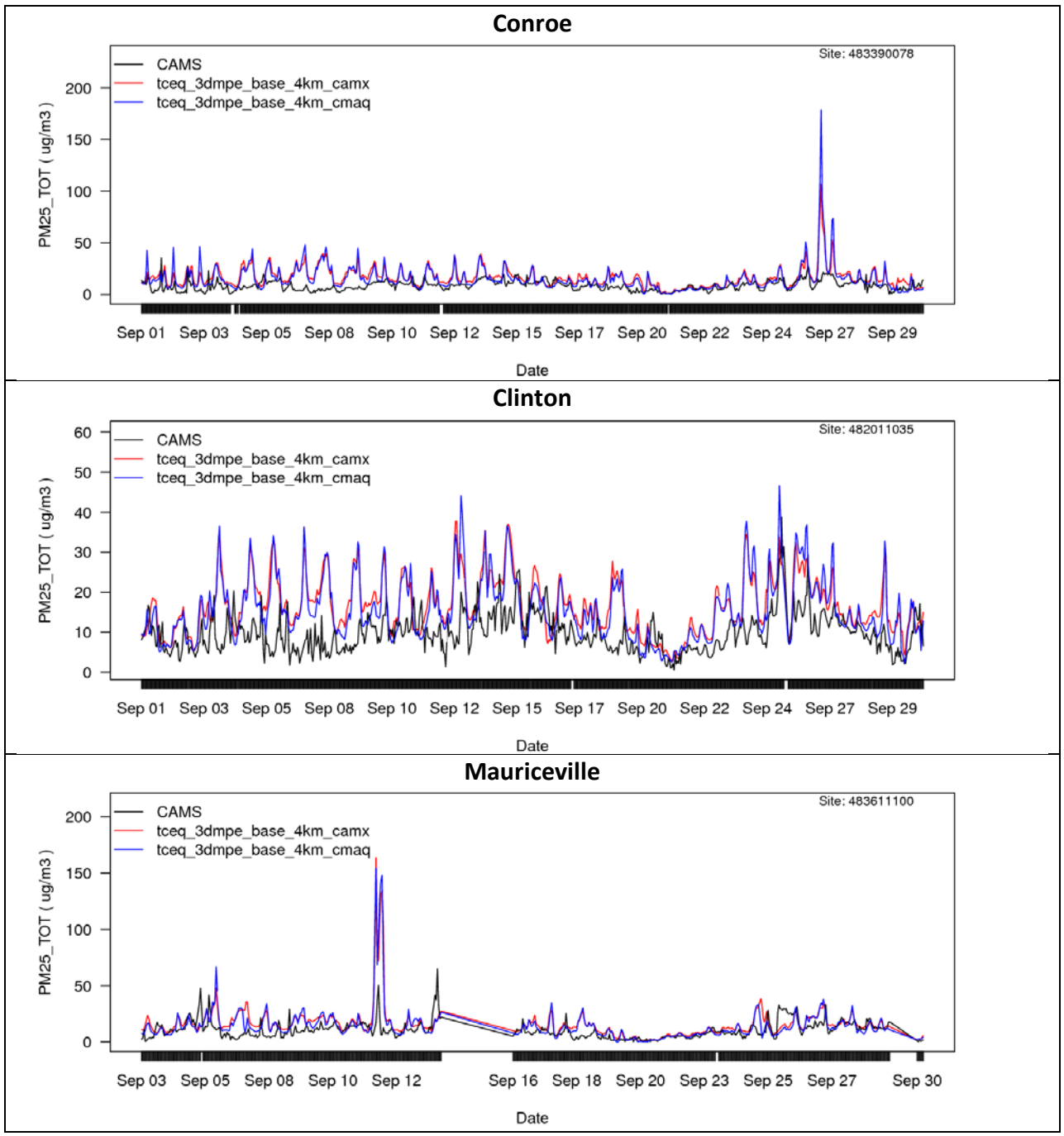
Conroe
Site: 483390078
CAMS
tceq_3dmpe_base_4km_camx
tceq_3dmpe_base_4km_cmaq
PM25_TOT (ug/m3)
0
50
100
150
200
Sep 01
Sep 03
Sep 05
Sep 08
Sep 10
Sep 12
Sep 15
Sep 17
Sep 20
Sep 22
Sep 24
Sep 27
Sep 29
Date
Clinton
Site: 482011035
CAMS
tceq_3dmpe_base_4km_camx
tceq_3dmpe_base_4km_cmaq
PM25_TOT (ug/m3)
0
10
20
30
40
50
60
Sep 01
Sep 03
Sep 05
Sep 08
Sep 10
Sep 12
Sep 15
Sep 17
Sep 20
Sep 22
Sep 24
Sep 27
Sep 29
Date
Mauriceville
Site: 483611100
CAMS
tceq_3dmpe_base_4km_camx
tceq_3dmpe_base_4km_cmaq
PM25_TOT (ug/m3)
0
50
100
150
200
Sep 03
Sep 05
Sep 08
Sep 10
Sep 12
Sep 16
Sep 18
Sep 20
Sep 23
Sep 25
Sep 27
Sep 30
Date

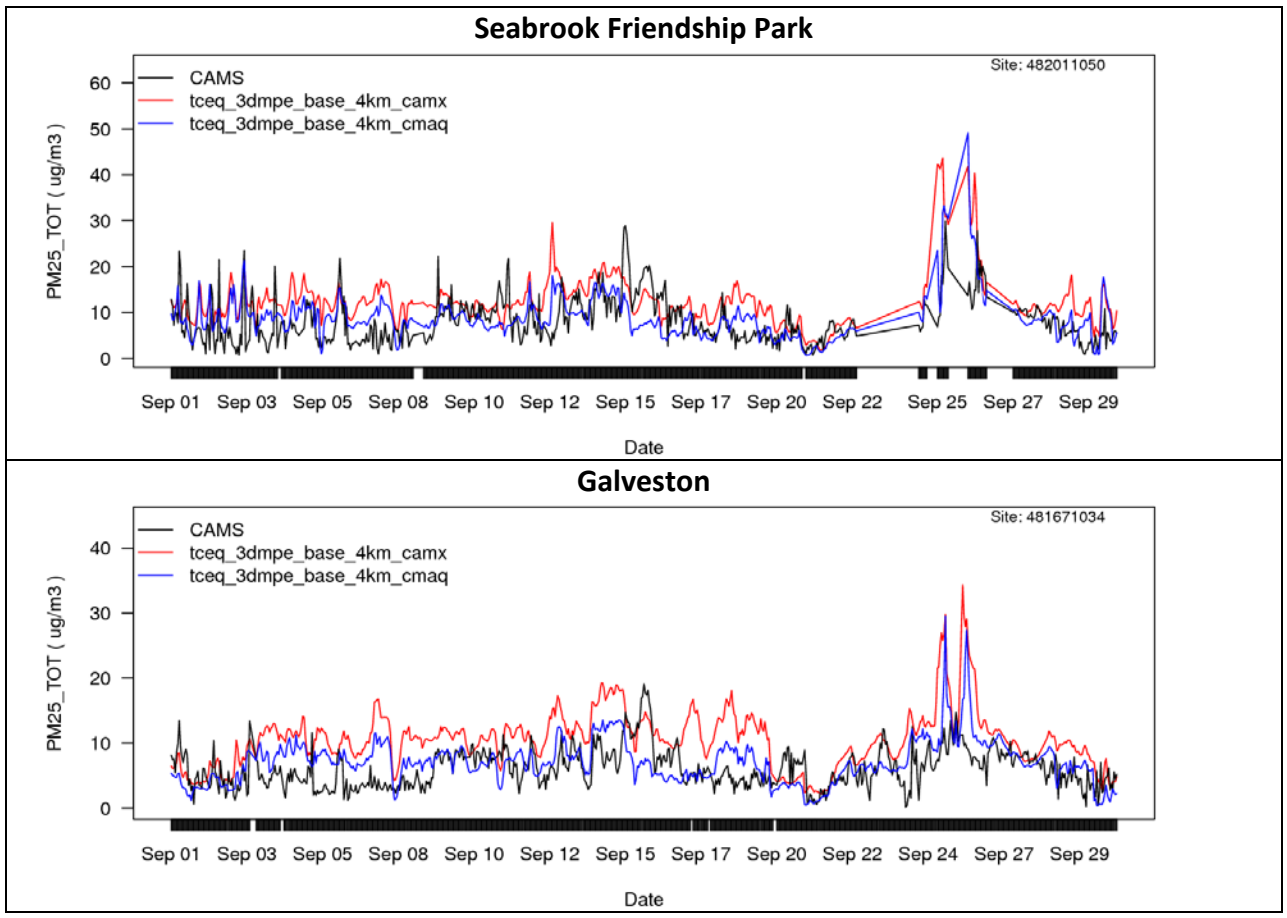

Figure 4-15. Time series of observed (black) and predicted (CAMx/CMAQ; red/blue) $PM_{2.5}$ concentrations at TCEQ CAMS sites in September 2013.

Table 4-3. 1-hour $PM_{2.5}$ model performance statistics of CAMx and CMAQ Base Case for the 4 km domain over all CAMS monitors within the HGBPA 4 km CAMx domain.

Site ID	Site Name	#Obs	Mean			MB		ME		NMB (%)		NME (%)		FB		FE		R^2		RMSE	
			OBS	CAMx	CMAQ	CAMx	CMAQ	CAMx	CMAQ	CAMx	CMAQ	CAMx	CMAQ	CAMx	CMAQ	CAMx	CMAQ	CAMx	CMAQ	CAMx	CMAQ
481671034	Galveston 99th Street	703	6.1	10.5	7.1	4.5	1.0	5.0	2.9	73.5	16.9	82.7	48.4	53.8	15.0	61.5	47.0	0.11	0.108	6.3	3.8
482010024	Houston Aldine	706	9.6	15.3	14.1	5.6	4.5	6.7	6.2	58.5	46.6	69.8	64.0	45.3	32.8	54.2	50.1	0.207	0.21	8.6	8.8
482010058	Baytown	711	9.2	17.5	14.8	8.3	5.7	9.2	7.2	90.4	61.6	100.6	78.4	63.6	46.9	70.4	59.2	0.081	0.096	11.4	9.9
482010416	Park Place	710	9.7	14.9	14.2	5.2	4.6	6.0	5.8	54.0	47.1	62.3	59.9	43.1	33.3	49.6	46.1	0.226	0.245	7.7	8.1
482011034	Houston East	710	9.6	15.1	14.2	5.5	4.6	6.6	6.0	57.5	47.8	68.2	62.8	46.6	37.7	54.5	50.2	0.17	0.199	8.2	8.1
482011035	Clinton	708	9.8	16.7	15.7	6.9	6.0	7.7	7.0	70.8	61.2	78.9	72.2	51.7	43.7	57.7	52.9	0.115	0.157	9.8	9.4
482011039	Houston Deer Park #2	608	10.1	15.1	13.2	4.9	3.1	6.4	5.6	48.8	30.5	63.0	55.4	42.4	25.7	53.1	48.8	0.166	0.183	8.1	7.5
482011050	Seabrook Friendship Park	616	8.1	12.4	8.8	4.3	0.7	5.6	3.9	52.6	8.4	68.8	47.9	47.3	11.6	58.3	48.4	0.144	0.181	7.2	5.3
482450021	Port Arthur Memorial School	663	8.4	11.9	10.6	3.5	2.2	5.2	4.7	41.2	25.7	62.0	55.9	38.1	24.1	53.5	51.0	0.145	0.132	6.8	6.6
482450022	Hamshire	710	9.0	11.5	9.9	2.5	0.9	5.0	4.4	27.8	10.2	55.8	49.2	30.0	13.0	51.6	48.3	0.144	0.155	7.0	6.6
483390078	Conroe Relocated	705	8.5	16.4	15.2	7.9	6.7	8.6	7.9	92.5	78.1	100.2	92.6	60.8	45.8	66.6	60.6	0.125	0.107	11.9	13.6
483611100	SETRPC 42 Mauriceville	567	10.6	16.0	14.6	5.4	4.0	7.9	7.4	51.0	37.4	74.0	69.9	40.4	24.8	55.1	52.5	0.074	0.074	14.7	15.2
	All site	8117	9.0	14.4	12.7	5.41	3.69	6.66	5.76	59.8	40.9	73.7	63.7	47.1	29.9	57.3	51.3	0.137	0.144	9.23	9.03

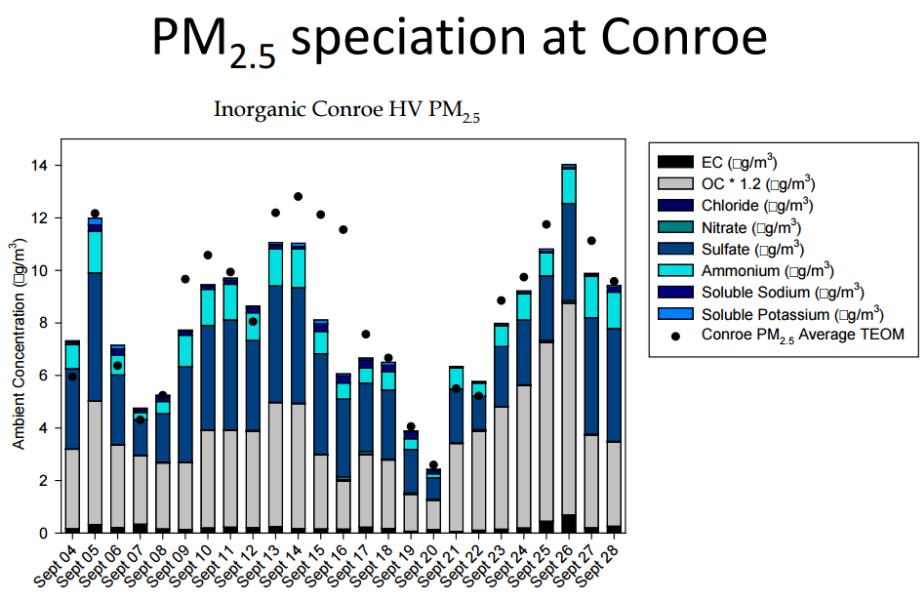

Figure 4-16. Observed $PM_{2.5}$ speciation at Conroe site [source: Sheesley and Usenko, 2015]

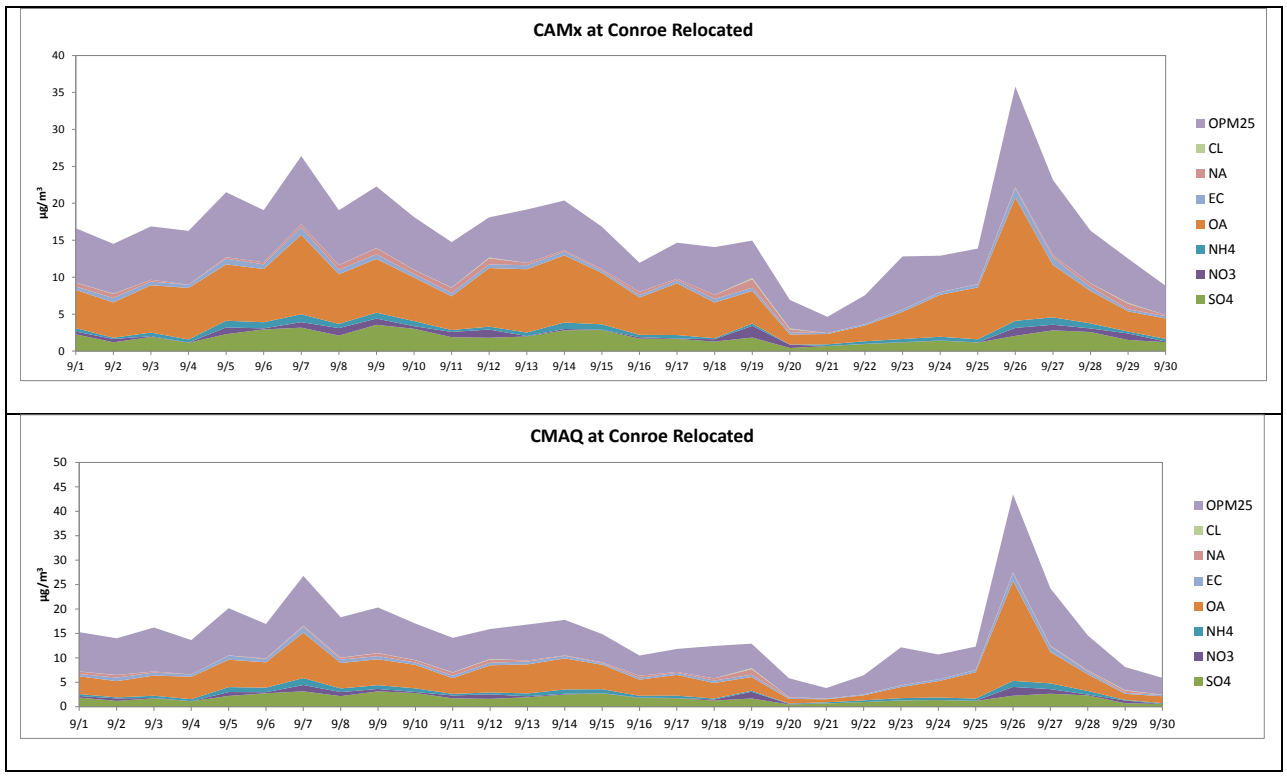

Figure 4-17. Predicted $PM_{2.5}$ speciation at Conroe site in September 2013

4.3 Model Performance Evaluation against Aircraft Measurements

The National Aeronautics and Space Administration (NASA) P-3B aircraft made available a suite of In situ aerosol and trace gas measurements over Houston during the DISCOVER-AQ 2013 field study (Figure 4-18). These aircraft measurement data are available from the DISCOVER-AQ website http://www-air.larc.nasa.gov/missions/discover-aq/discover-aq.html. This section presents model performance of CAMx and CMAQ for each of the nine days (September 4, 6, 11-14, 24-26) that the P-3B aircraft flew spirals in the Houston metropolitan area. In addition to gaseous pollutants, we evaluate radiation flux and nitrogen dioxide photolysis rate (jNO_2) and particulate PM including nitrate, sulphate, ammonium, and water-soluble organic carbon. Back trajectories with three types of meteorology data: 1) Eta Data Assimilation System (EDAS, 40 km), 2) North American Meso (NAM, 12 km) and 3) WRFCAMx (this study, 12 km) are also presented.

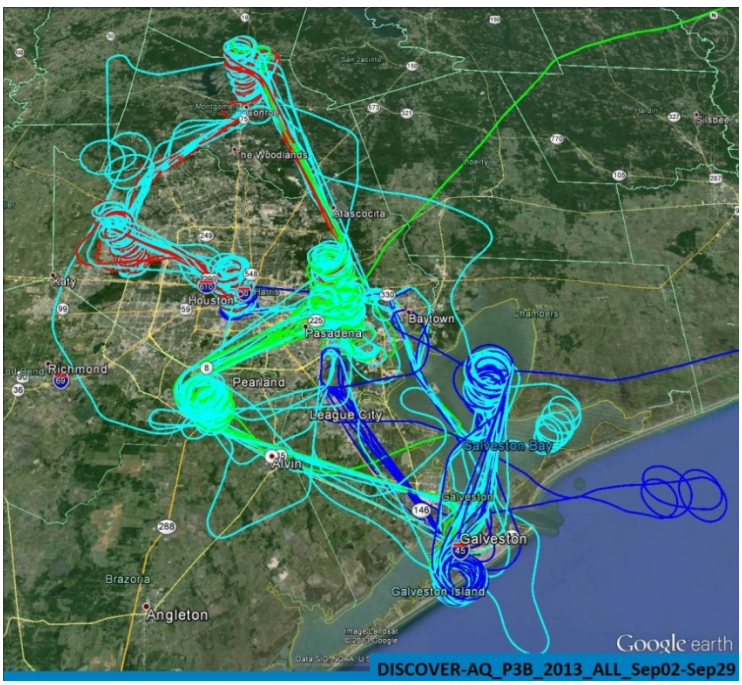

Figure 4-18. Flight paths of P3-B aircraft during the DISCOVER-AQ 2013 field study[6]

4.3.1 September 4

There was thunderstorm activity in the morning along the coastal region and over Galveston Bay which dissipated by midday. Winds were very light today, leading to an ill-defined transport pattern. The HGB maximum 8-hour ozone concentration is 62 ppb.

Ozone performance is similar between CAMx and CMAQ despite higher predicted jNO_2 above 500 m in CAMx (Figure 4-19). Both models overestimate observed ozone under 50 ppb that are below an altitude of about 1000 m, but underestimate ozone aloft. Lower vertical gradients of

[6] Source: http://www-air.larc.nasa.gov/missions/discover-aq/discover-aq.html

predicted ozone profiles indicate overstated vertical mixing. Modeled jNO_2 is biased high (NMB = 35% and 24% for CAMx and CMAQ, respectively) which is attributable to under representation of cloud predicted by WRF on this day (Appendix E). At fine scales (<10 km), WRF can generally resolve and generate small-scale clouds, so the diagnostic option in WRFCAMx is not applied. For this simulation, however, we diagnosed sub-grid clouds at 4 km to help improve cloud representation particularly along the coast. CMAQ applies similar diagnostic parameterization regardless of a grid resolution. Lower jNO_2 in CMAQ could imply more diagnosed sub-grid cloud or lower UV-scattering aerosols compared to CAMx.

The over-prediction of ozone could be due to inaccurate transport of lower air parcels. The EDAS and NAM back trajectories indicate transport from the Gulf at 500 m which brings relatively clean air onshore. However, WRF suggests continental transport by north-easterly winds which would bring more influences of anthropogenic pollution (Appendix E).

CAMx and CMAQ predicted vertical profiles of other gaseous species are comparable. NOx and reactive nitrogen compounds (NOy)[7] are under predicted especially at below 1000 m. The models tend to over predict isoprene above 50 percentile concentrations but reasonably replicate 25-percentile concentrations. Observed isoprene is depleted by an altitude of 1500 m, whereas the models predicted non-zero concentrations up to 2500 m. Predicted formaldehyde and NOy also have a sharp gradient at 2500 m but this was not observed.

[7] include NOx, nitric acid (HNO3), nitrous acid (HONO), peroxyl acetyl nitrate (PAN), methyl peroxyl acetyl nitrate (MPAN), peroxyl propionyl nitrate (PPN), and particulate nitrates

Ozone

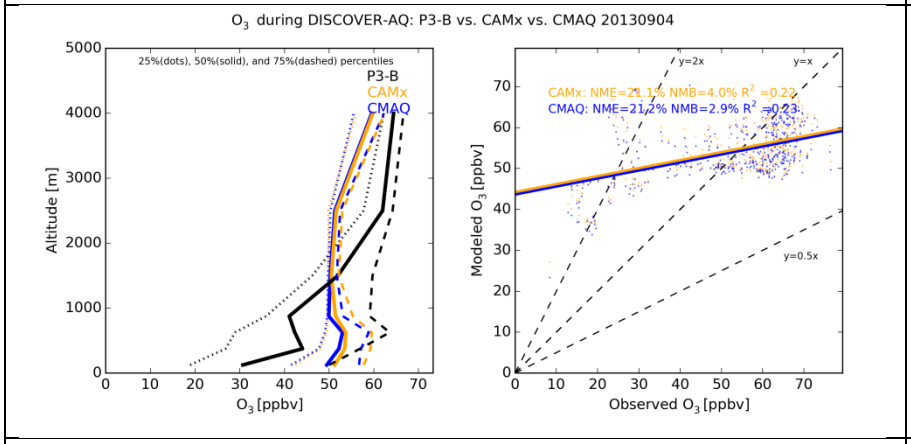

NOx

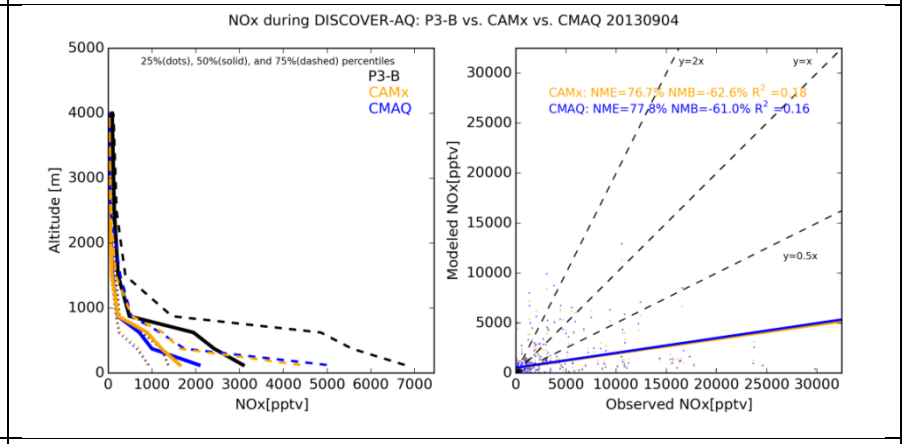

jNO2

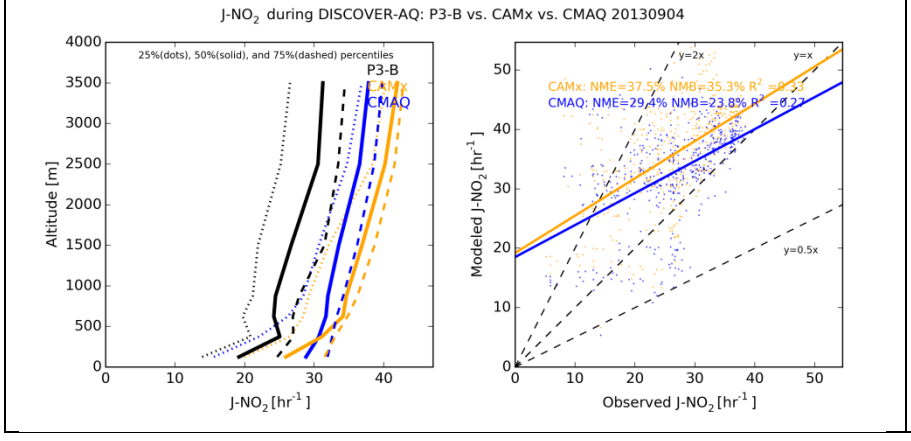

NOy

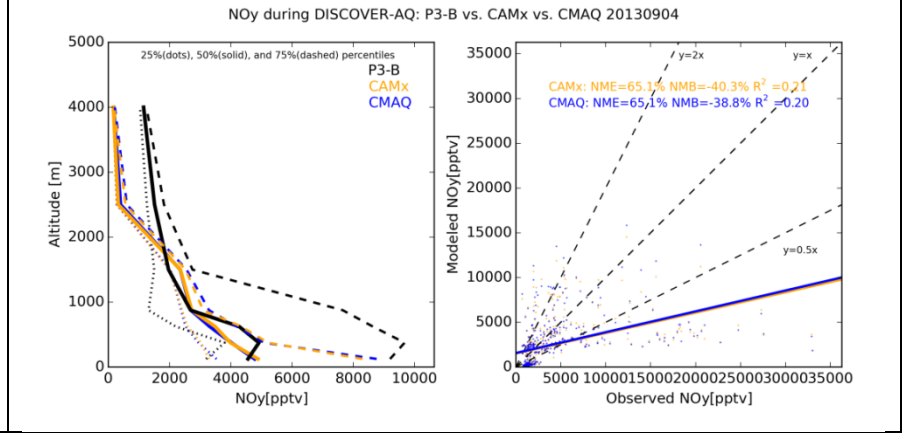

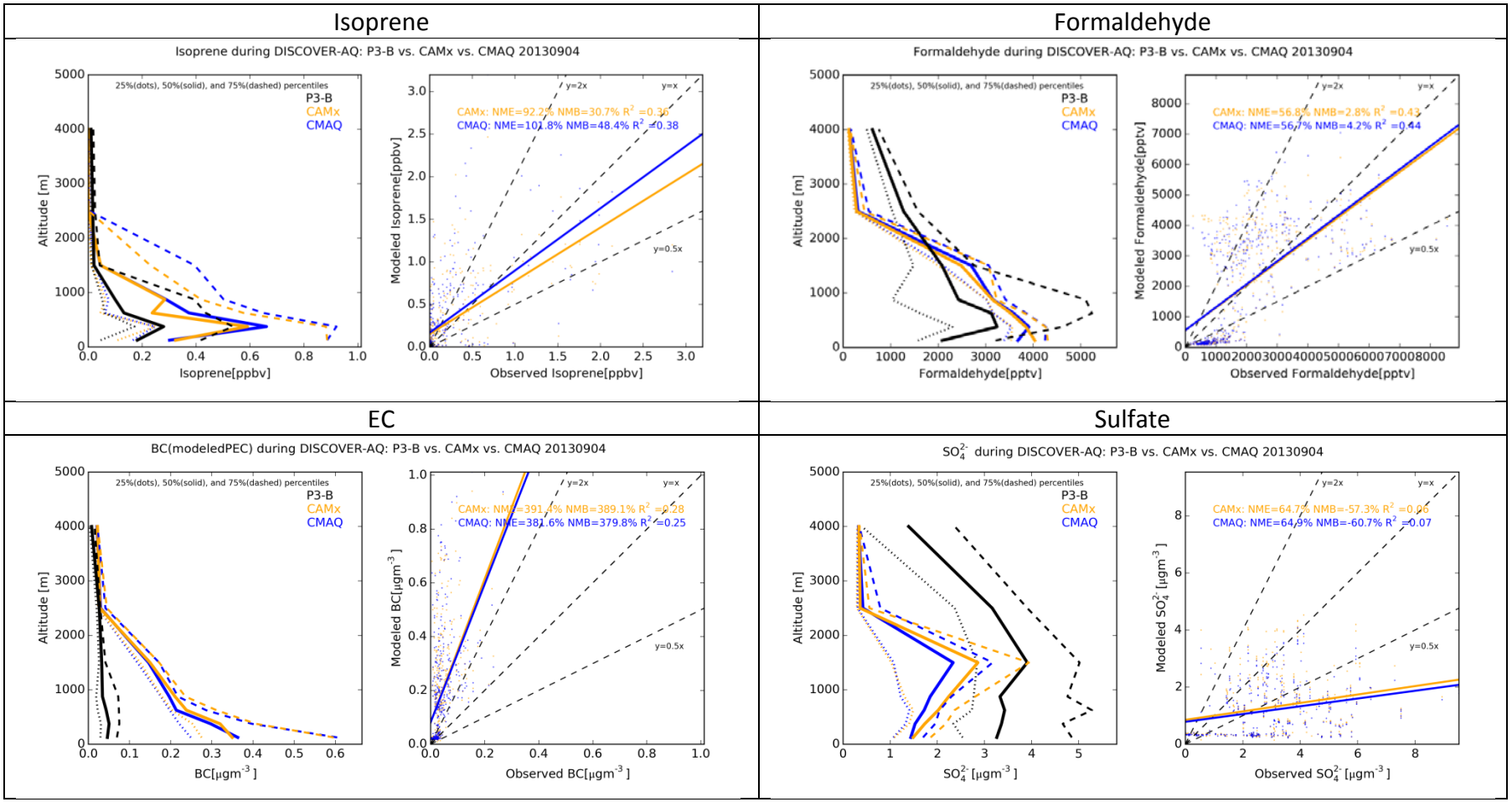

Figure 4-19. Vertical profiles measured by P3-B aircraft compared to CAMx/CMAQ estimated on September 4, 2013.

4.3.2 September 6

There was thunderstorm activity throughout the Houston area. The HGB maximum 8-hour ozone concentration is only 45 ppb. HYSPLIT back trajectories suggest transport from southern Louisiana.

Figure 4-20 compares vertical profiles measured by P3-B aircraft and model predictions on September 6. CAMx and CMAQ over predicted near-ground ozone by about 25 ppb. Similar to September 4 MPEs, modeled jNO_2 is biased high which is attributable to under representation of cloud predicted by WRF on this day (Appendix E). Although CAMx predicted higher aloft jNO_2 than CMAQ, predicted ozone vertical profiles by the two models are very similar. NOx model performance is reasonable near surface but is biased low at 300-1000 m high. CAMX performance for NOx and NOy are slightly better than CMAQ near surface. Isoprene performance is good albeit tendency of overestimation near surface (R^2 = 0.68 for CAMx; 0.63 for CMAQ). Good model performance is seen in formaldehyde (R^2 = 0.72 for CAMx; 0.74 for CMAQ) particularly the 75 percentile concentrations.

Ozone

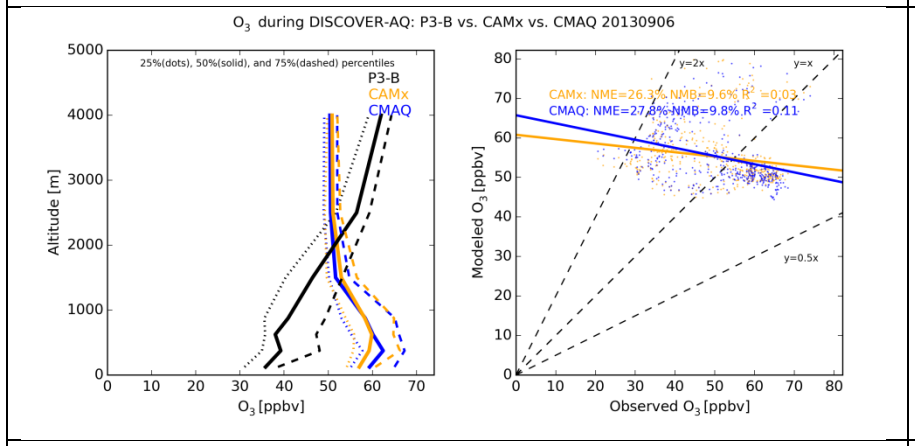

NOx

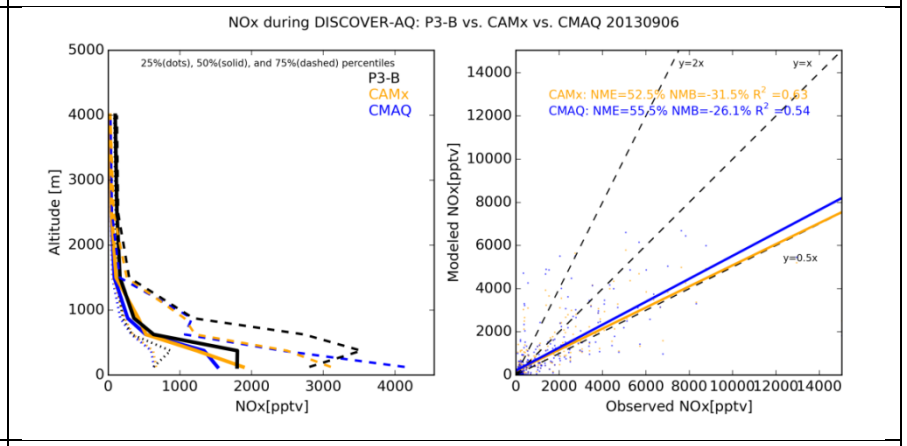

jNO_2

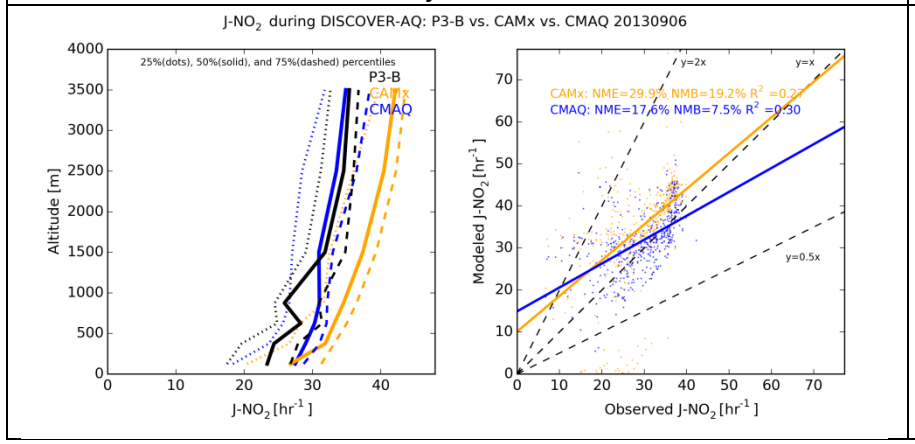

NOy

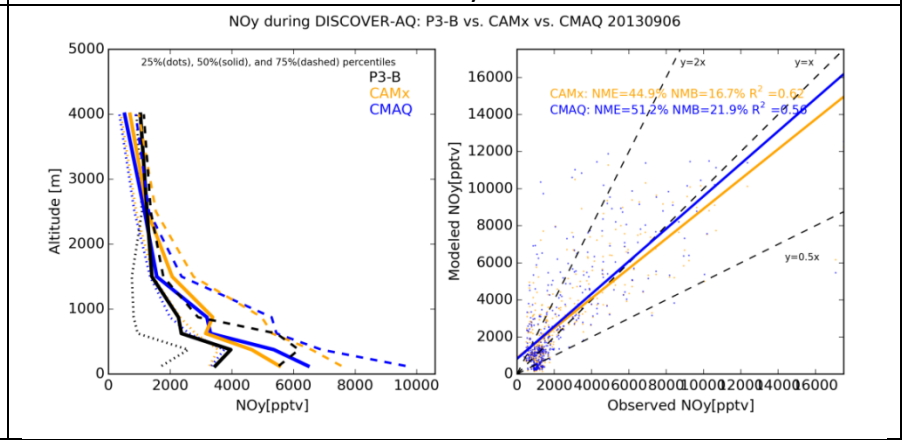

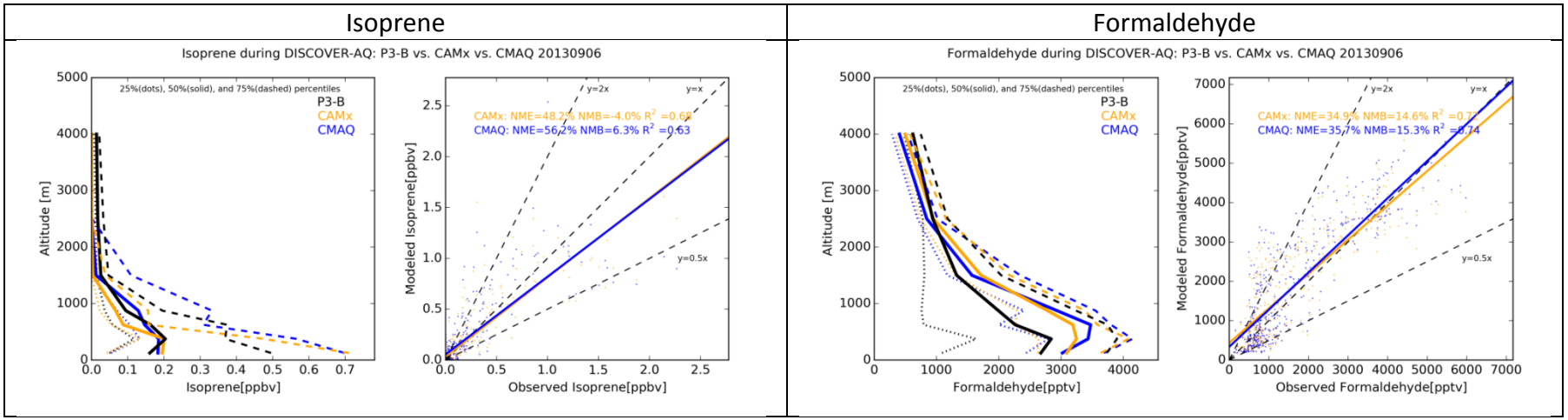

Figure 4-20. Vertical profiles measured by P3-B aircraft compared to CAMx/CMAQ estimated on September 6, 2013.

4.3.3 September 11

Scattered cirrus clouds were present. The HGB maximum 8-hour ozone concentration is only 51 ppb. HYSPLIT back trajectories suggest transport from southern Louisiana and the Gulf of Mexico.

Figure 4-21 compares vertical profiles measured by P3-B aircraft and model predictions on September 11. Model performance is fairly good below 500 m. for all gaseous species except isoprene. CAMx and CMAQ ozone vertical profiles suggest well mixing above 1000 m. while the observations indicate tilt vertical gradient. Similar to previous days, the models over predict jNO_2 throughout the vertical heights with CAMx estimates consistently higher than CMAQ estimates. Both models replicate the mixed layer near the surface fairly well showing peak concentrations of formaldehyde and isoprene at about 500 m.

Ozone

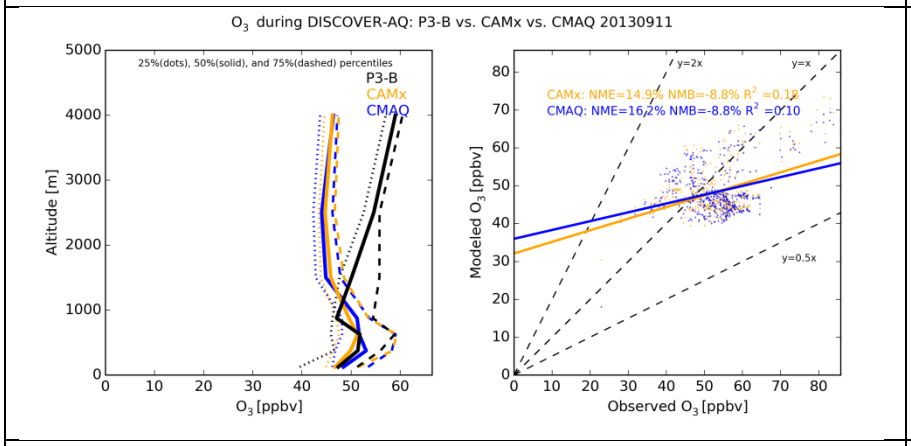

NOx

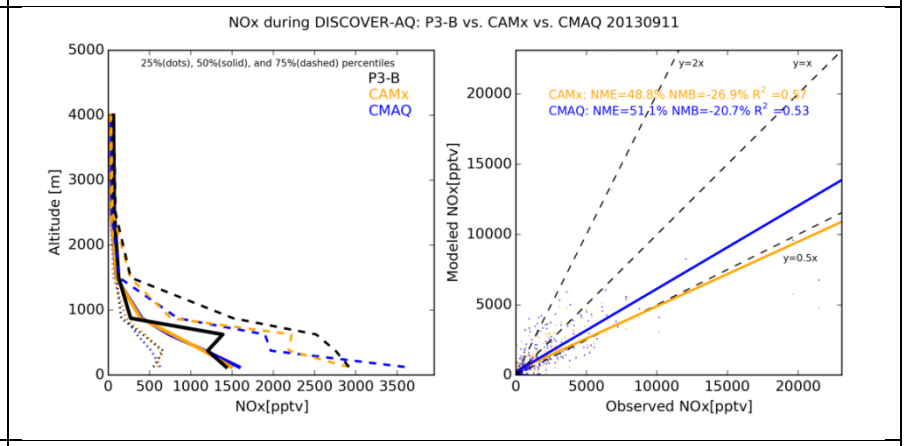

jNO_2

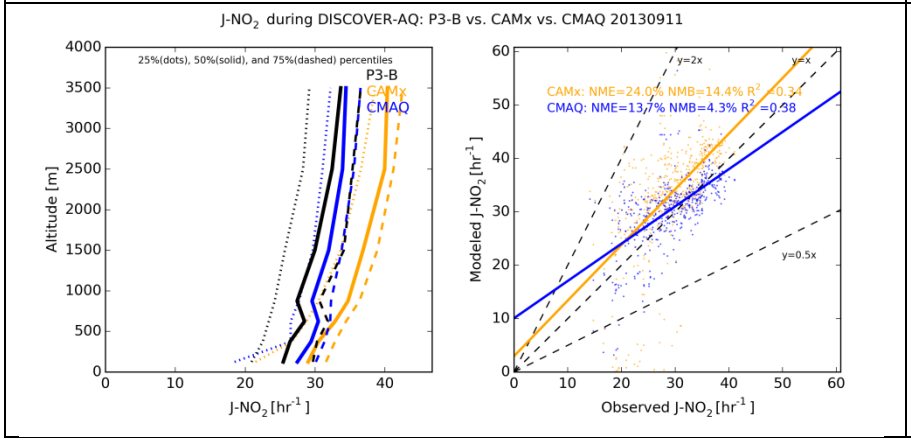

NOy

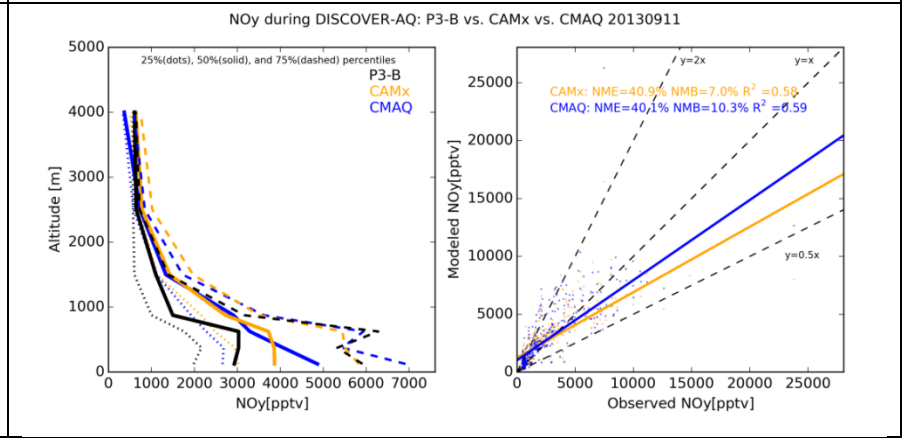

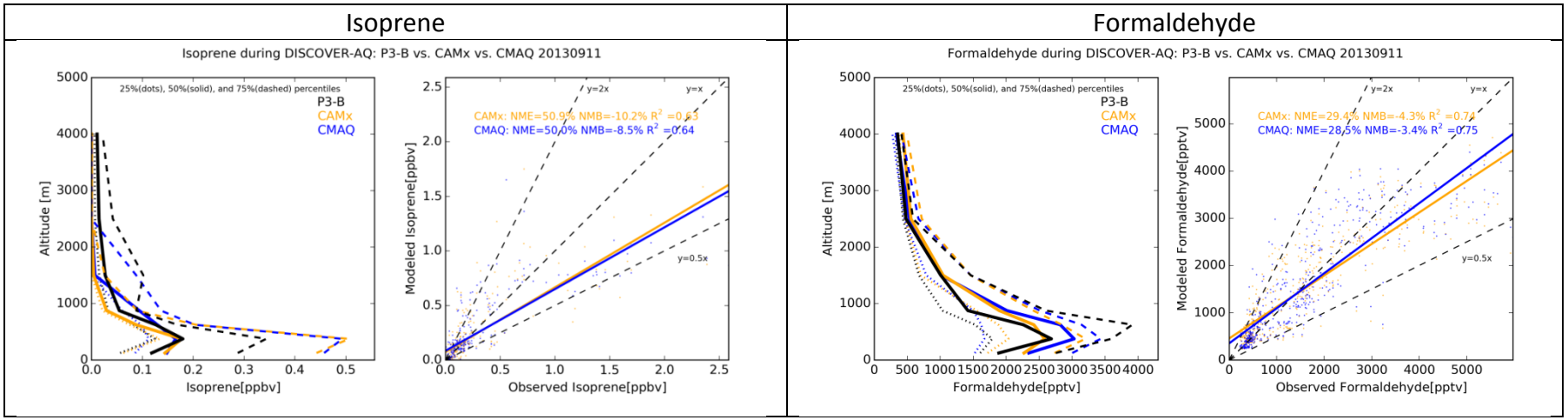

Figure 4-21. Vertical profiles measured by P3-B aircraft compared to CAMx/CMAQ estimated on September 11, 2013.

4.3.4 September 12

This was a relatively cloud-free day. The HGB maximum 8-hour ozone concentration is 66 ppb. HYSPLIT back trajectories suggest transport from southern Louisiana and the Gulf of Mexico.

Figure 4-22 compares vertical profiles measured by P3-B aircraft and model predictions on September 12. Even on a relatively clear day, modelled jNO_2 is still biased high. CAMx and CMAQ over predicted the 25- and 50-percentile ozone near surface by about 10 ppb, but replicated the 75-percentile observed ozone well. Near-surface NOx plumes are not captured by the models, but overall NOx performance is fairly good. Isoprene performance is good albeit tendency of overestimation near surface (R^2 = 0.76 for CAMx; 0.66 for CMAQ).

Ozone

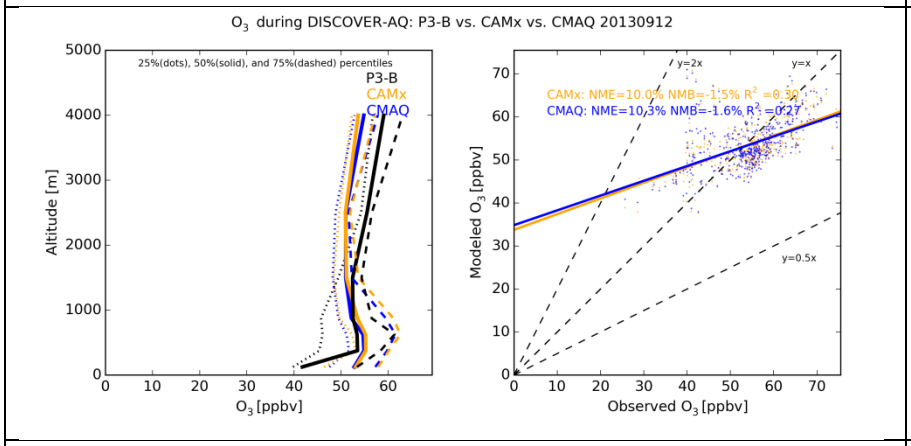

NOx

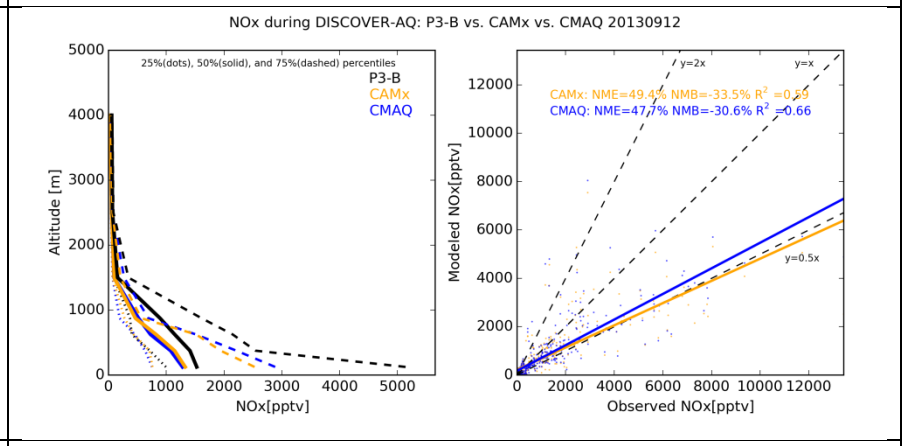

jNO_2

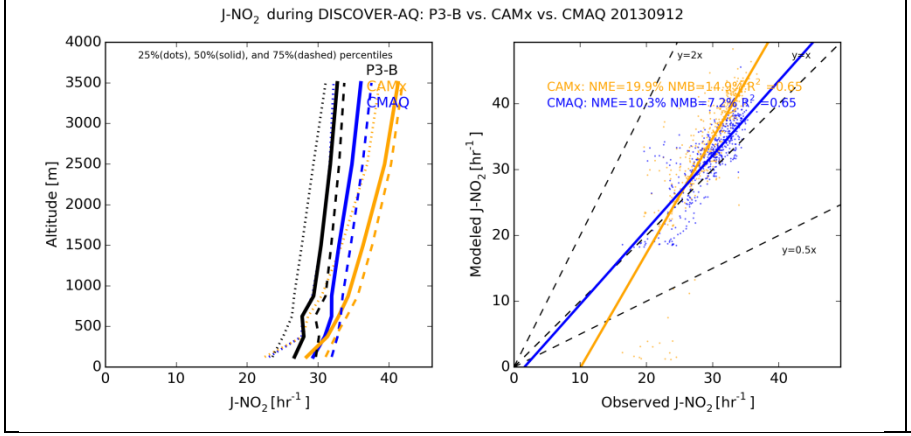

NOy

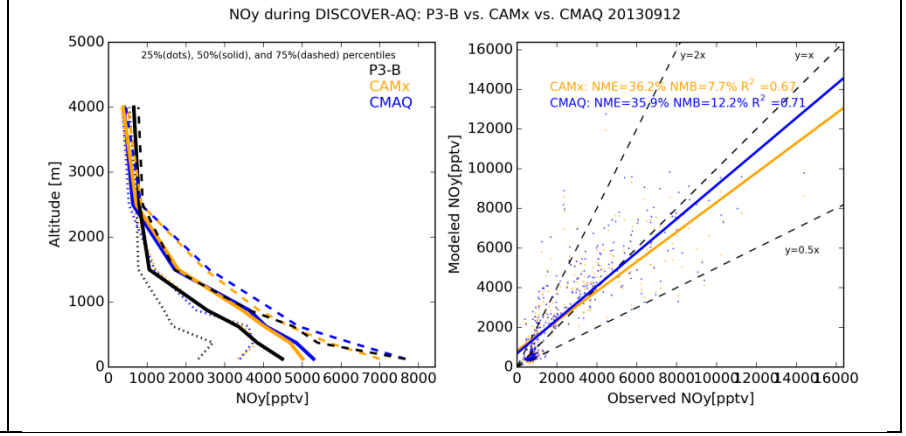

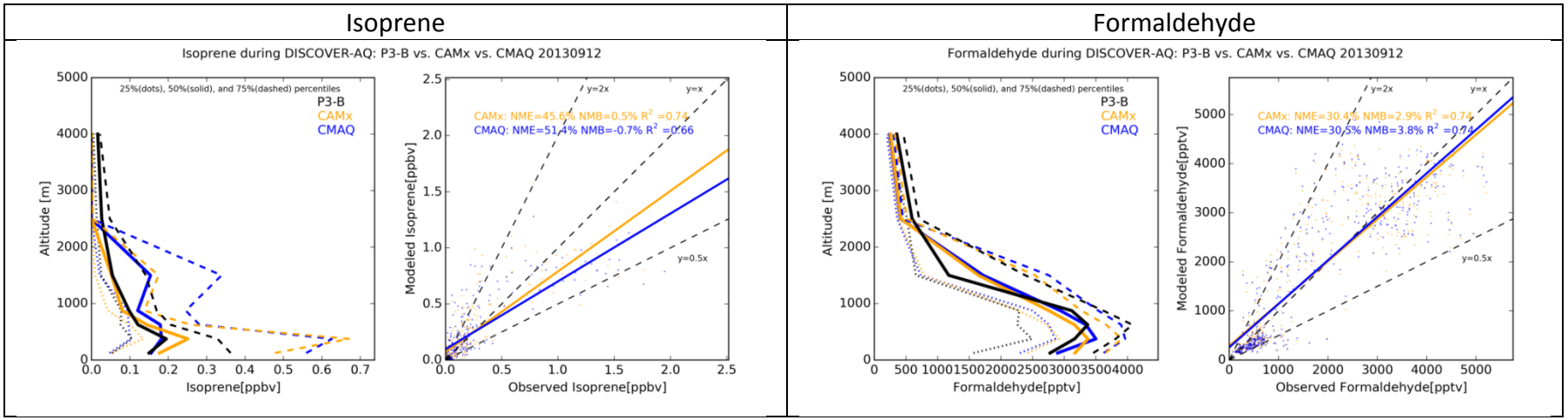

Figure 4-22. Vertical profiles measured by P3-B aircraft compared to CAMx/CMAQ estimated on September 12, 2013.

4.3.5 September 13

Typical fair weather condition was present. The HGB maximum 8-hour ozone concentration is 66 ppb. The EDAS back trajectory indicates a mild recirculation of air mass at 500 m in Houston which enhances surface ozone concentrations. The under estimation of ozone shown in Figure 4-23 could be related to the absence of this circulation predicted by WRF. Again, jNO_2 performance shows no correlation to ozone performance. Model performance of other gaseous species are similar to those on September 12.

Ozone

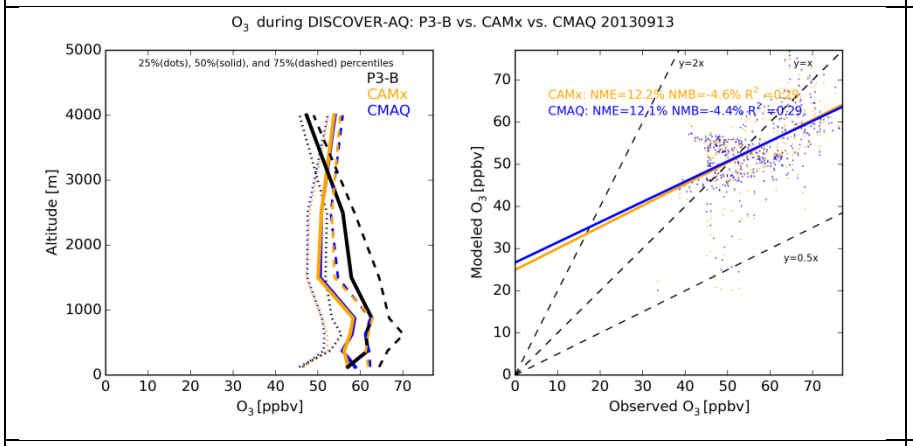

NOx

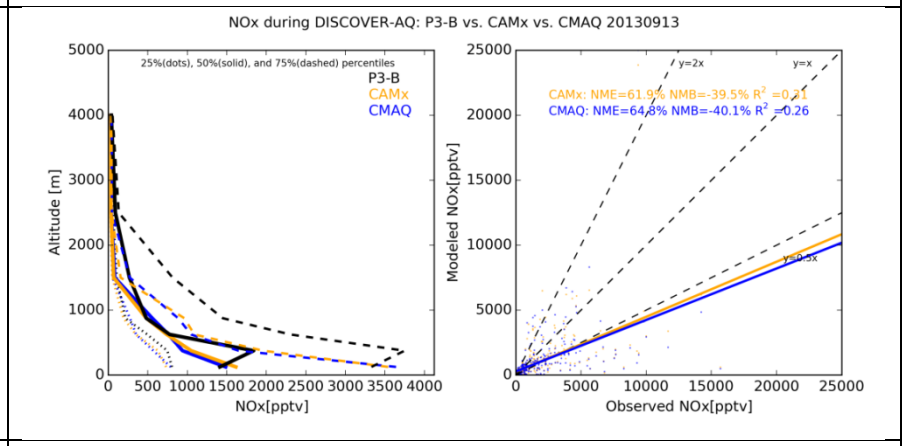

jNO_2

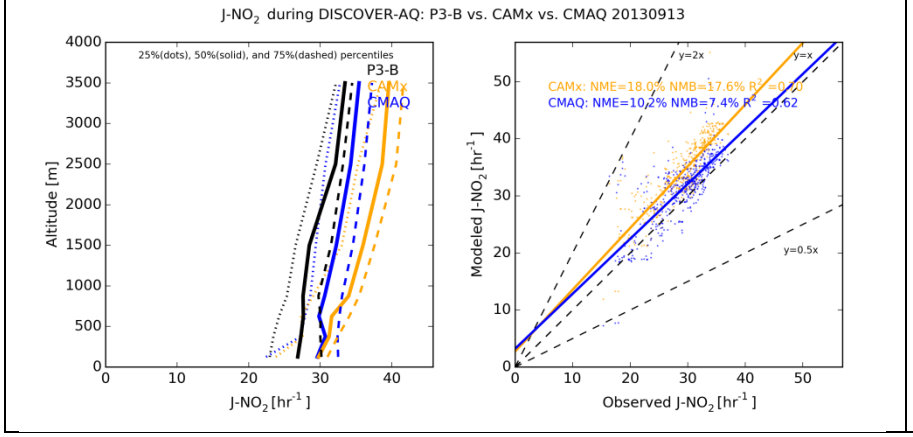

NOy

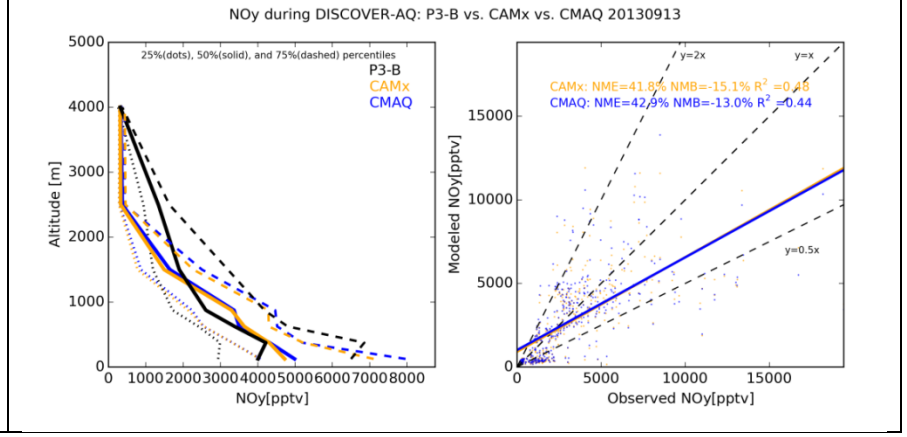

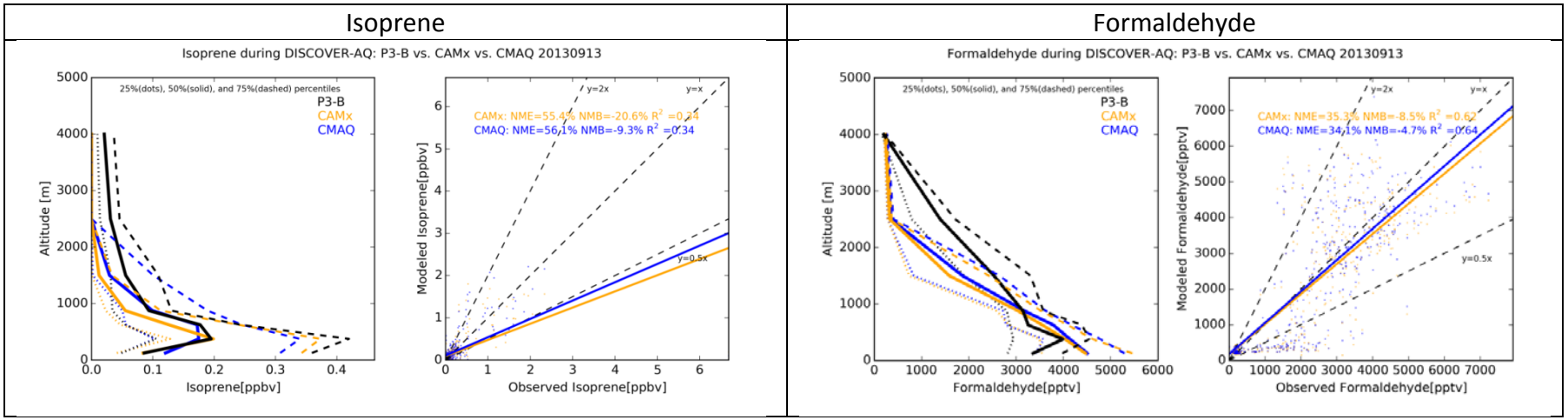

Figure 4-23. Vertical profiles measured by P3-B aircraft compared to CAMx/CMAQ estimated on September 13, 2013.

4.3.6 September 14

Intermittent clouds and afternoon pop-up showers were present. The HGB maximum 8-hour ozone centration is 64 ppb. The EDAS and NAM back trajectories indicate transport from the Gulf at 500 m which brings relatively clean air onshore. However, WRF suggests continental transport by north-easterly winds which would bring more influences of anthropogenic pollution.

CAMx and CMAQ over predicted ozone near surface by about 15 ppb, but under predicted ozone above 1000 m. The discrepancy of aloft ozone worsens with altitude. NOx is under predicted but NOy is over predicted throughout the vertical heights. Isoprene performance is fairly good. CMAQ can better capture the elevated isoprene plumes at 1000 m.

Ozone

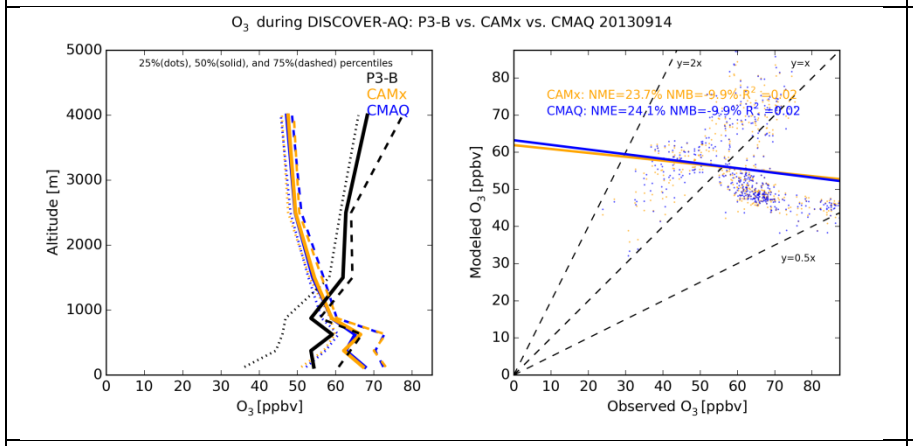

NOx

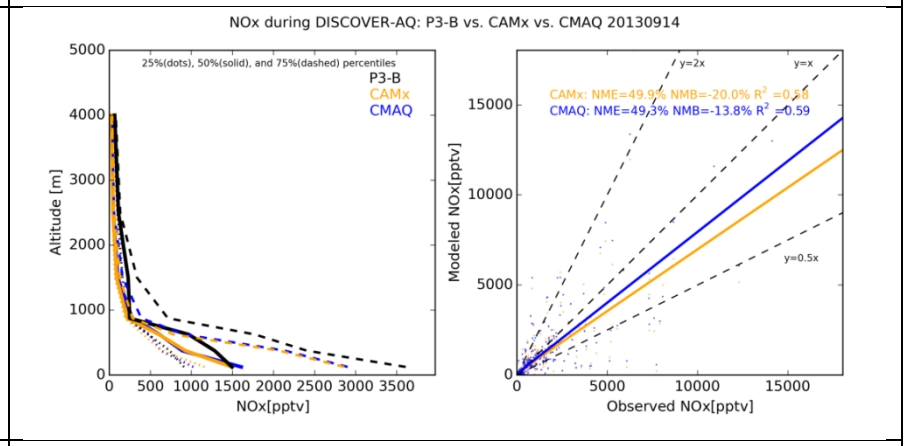

jNO2

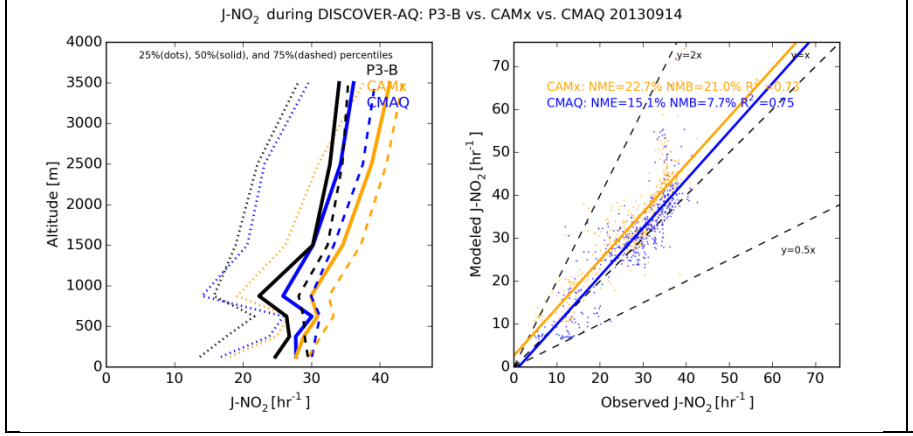

NOy

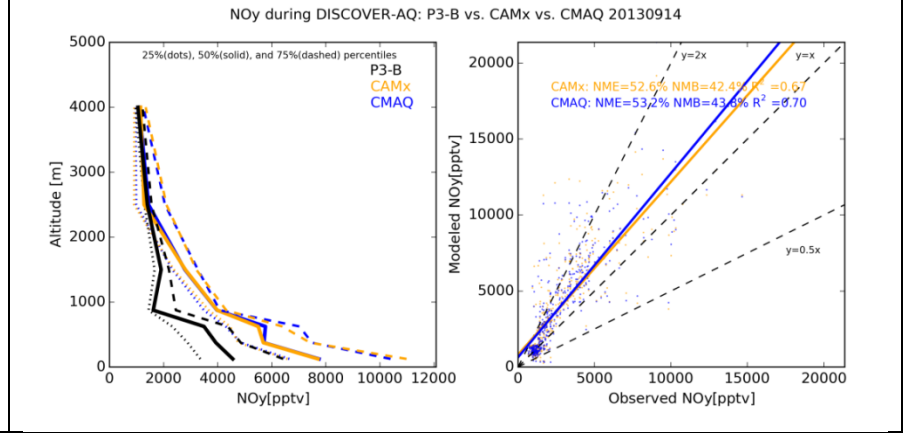

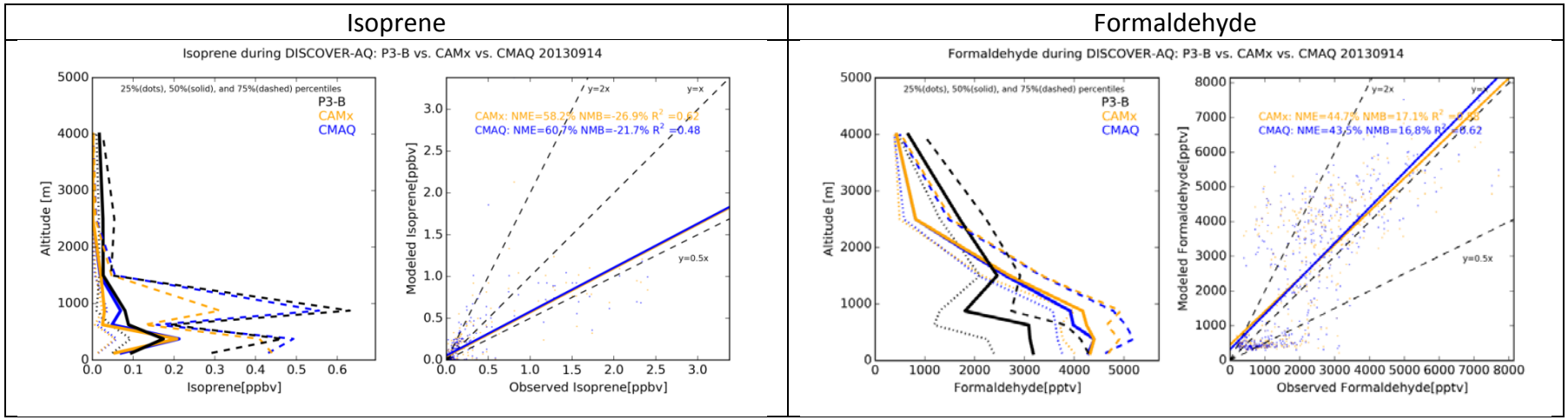

Figure 4-24. Vertical profiles measured by P3-B aircraft compared to CAMx/CMAQ estimated on September 14, 2013.

4.3.7 September 24

This day is three days after the first frontal passage on September 21. Previous study has shown that cold frontal passages are associated with pollution events during the August – October ozone season in Houston. We see the strong tilt of ozone profile suggesting weak impacts from the first passage. The HGB maximum 8-hour ozone centration is only 51 ppb. Clouds and cumulus formed during the late morning hours. The EDAS and NAM back trajectories indicate transport of air mass at 1500 m from the Gulf which then circulated north of the Galveston bay before moving to the Houston city. However, WRF suggests transport of air mass at 1500 m from Dallas area.

CAMx and CMAQ models predicted small vertical gradients of ozone with values ~60 ppb below 800 m. but large gradients between 800-1500 m. Low ozone (< 40 ppb) was predicted from 1500 to 2500 m. In contrast, the observations suggest a stable layer below 800 m. with 75-percentile values increasing from 40 to 60 ppb and staying above 50 ppb through 5000 m. The models perform well for isoprene and formaldehyde with R^2 values more than 0.6. NOx under 500 m. is over predicted. Near-surface 75-percentile NOy concentrations are over predicted by a factor of two.

Ozone

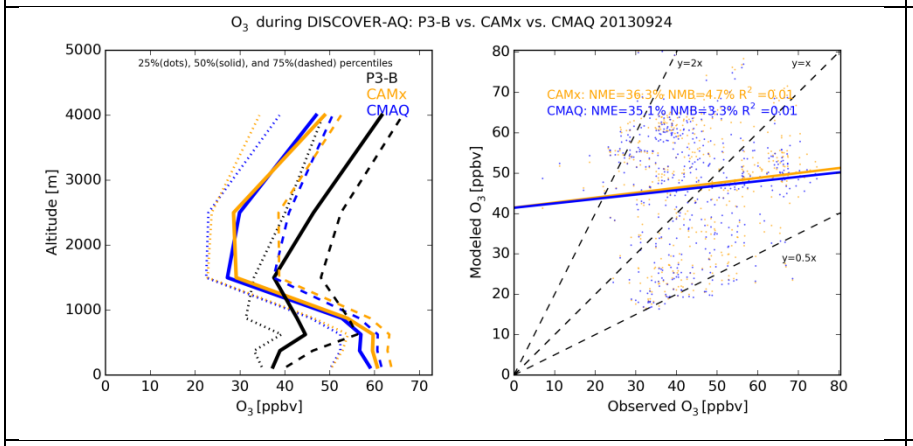

NOx

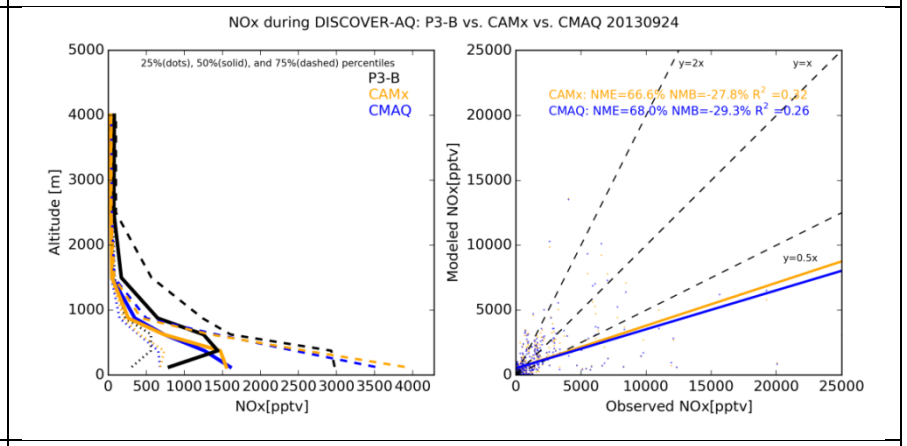

jNO_2

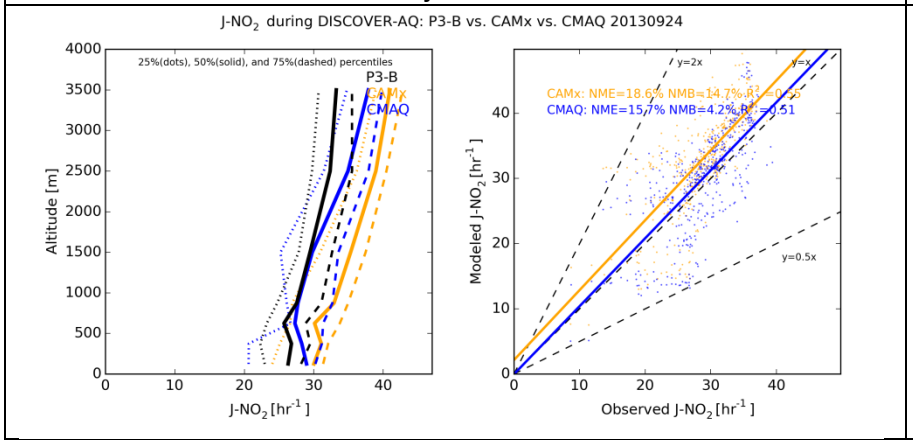

NOy

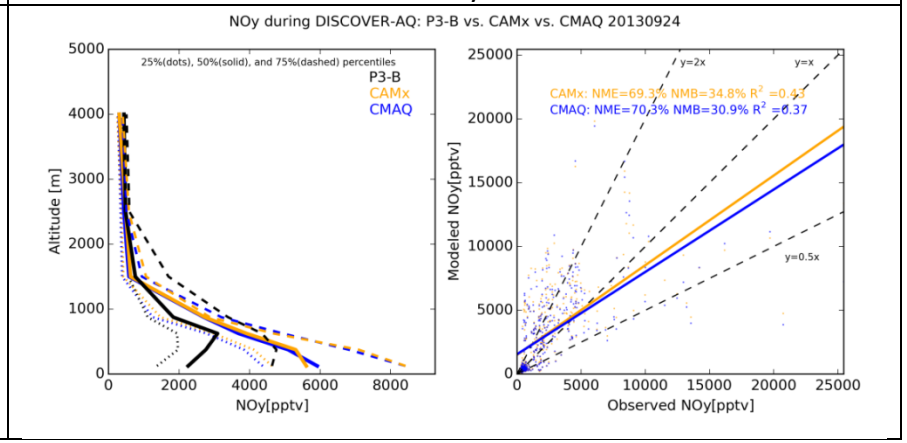

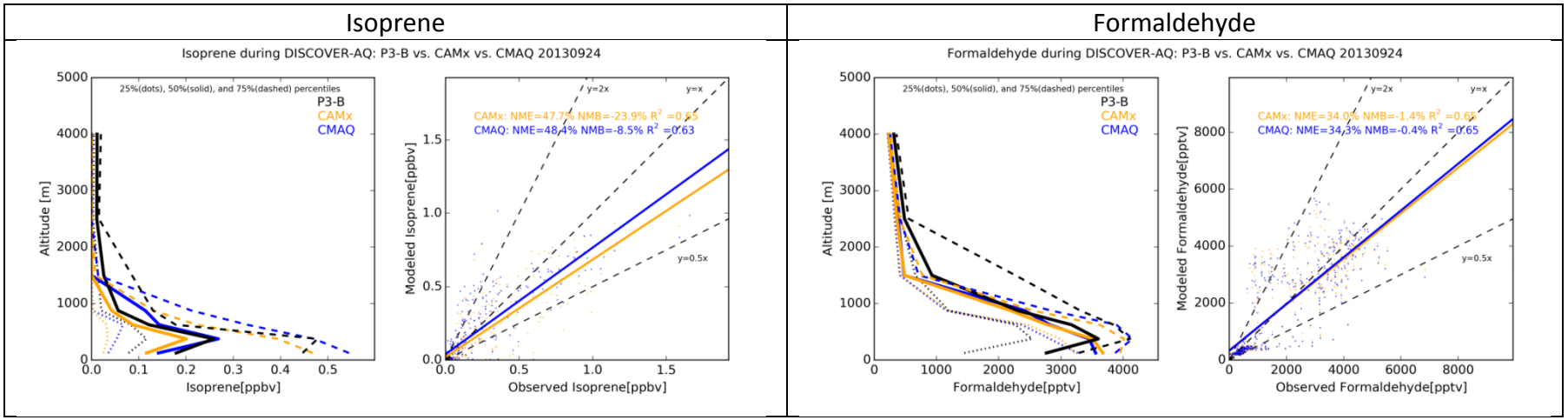

Figure 4-25. Vertical profiles measured by P3-B aircraft compared to CAMx/CMAQ estimated on September 24, 2013.

4.3.8 September 25

The secondary frontal boundary passed through Houston, four days after the first one on September 21. The HGB maximum 8-hour ozone centration is 124 ppb, highest in the month.

In additional to the frontal passage, severe pollution days in Houston often relate to offshore flow in the morning and onshore flow in the late afternoon due to the sea breeze. The pollution plume can be re-circulated, entrained, and catalysed to produce intense ozone events. This feature occurred on September 25 based on an observed shift in RH and ozone concentrations at Smith Point as a result of offshore flow in the morning and onshore flow in the late afternoon (Morris and Lefer, 2014).

Predicted ozone profiles are less tilted than other days. It appears that the models could replicate well the mix-down of ozone aloft to the surface due to the frontal passage. However, the models largely under estimated ozone throughout the 5000 m altitude, particularly near the surface. The low bias could be partially attributable to inability of WRF to accurately simulate sea-breeze in the area. Our back trajectories indicate northerly winds with some circulations within the Houston area, but the re-circulation of onshore flow is not evident. The wind direction performance discussed in Section 2.2.2 also shows poor performance during this period.

The models perform well for formaldehyde with R^2 values of about 0.6. High observed formaldehyde concentrations (>15 ppb) indicate that the aircraft likely passed through a region of high formaldehyde precursors such as reactive olefins. The same air parcel appears to have high NOx concentrations. These high concentrations were observed over Galveston Bay under northerly winds suggesting the emitting sources near Baytown. The models did not capture the high events. NOx under 2500 m. is under predicted. Based on 50-percentile concentration, NOy performance is quite good. However, near-surface 75-percentile NOy concentrations are under predicted by a factor of 1.5.

Ozone

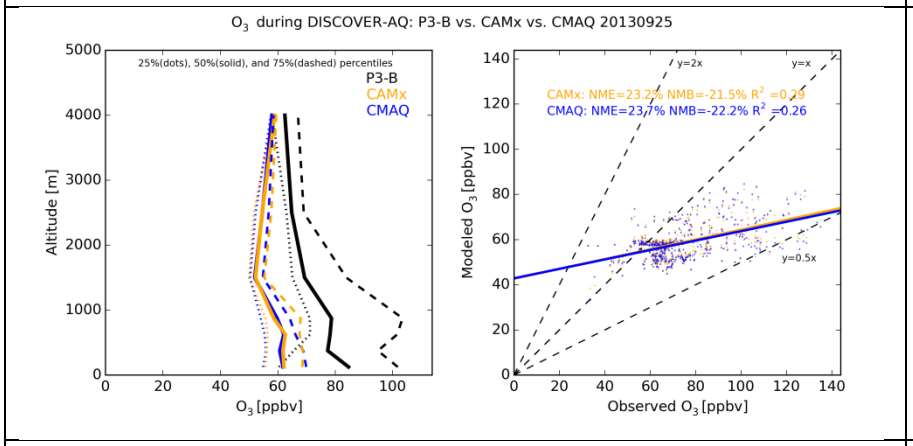

NOx

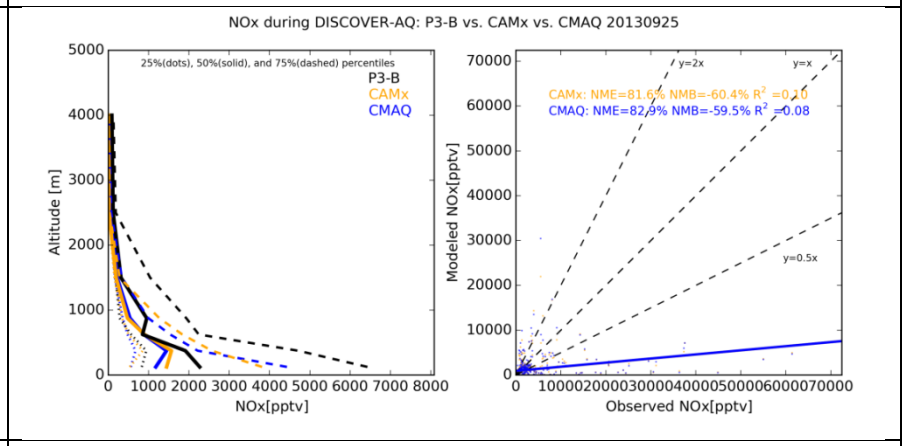

jNO_2

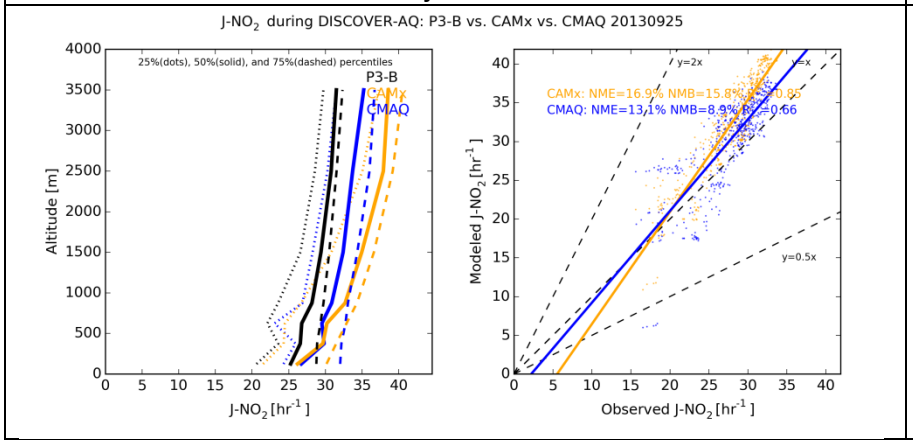

NOy

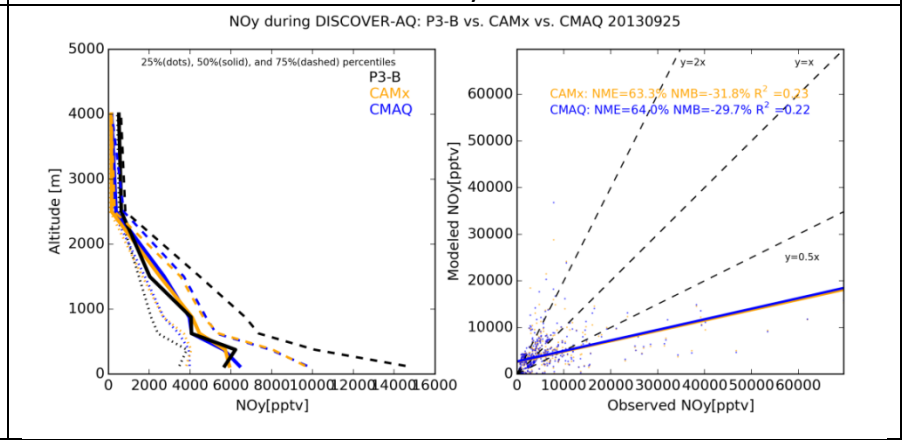

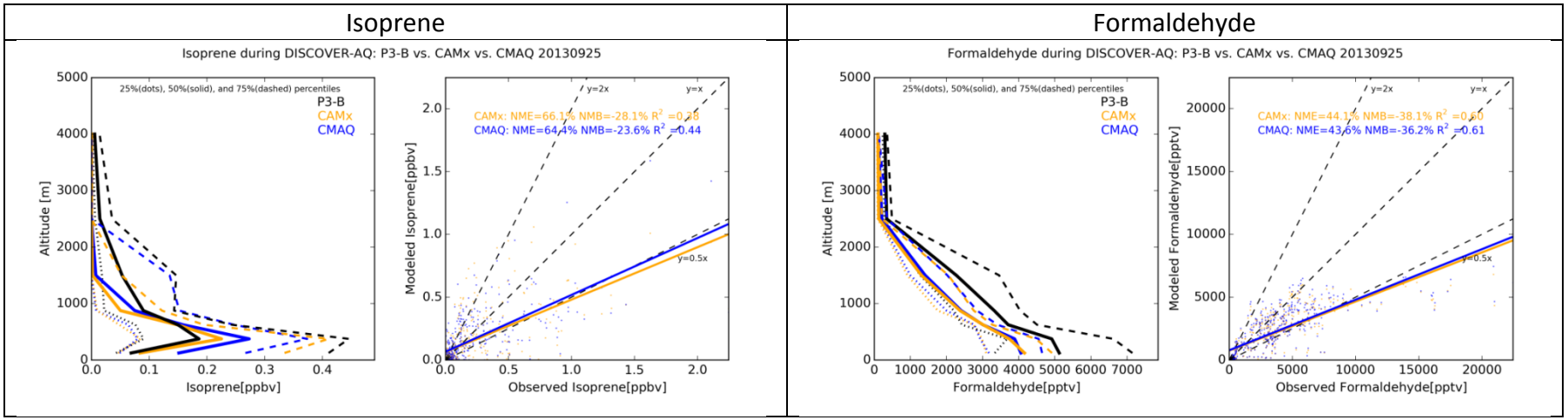

Figure 4-26. Vertical profiles measured by P3-B aircraft compared to CAMx/CMAQ estimated on September 25, 2013.

4.3.9 September 26

This was the second day after the September 25 front passage. The HGB maximum 8-hour ozone centration remained high at 89 ppb. The EDAS and NAM back trajectories indicate a re-circulation of onshore flow. WRF also suggests a re-circulation at 500 m.

Predicted ozone agrees well with observations near surface with the 50- and 75-percentile concentrations of about 80 ppb. The ozone performance worsens with altitude above 1500 m. Vertical profiles based on the 50-percentile values of observed ozone, NOx, NOy and formaldehyde all suggest at least two mixed layers below 1000 m. CAMx and CMAQ models only capture one of these layers. The models tend to under estimate removal processes near surface so the predictions are biased high.

Ozone

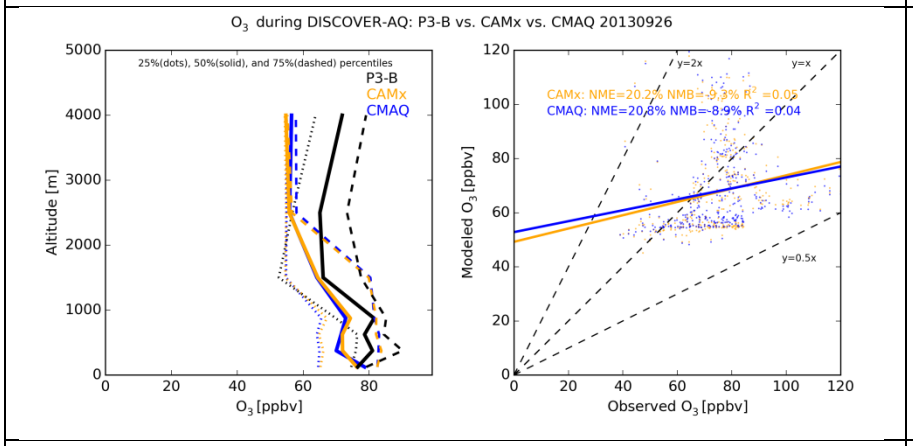

NOx

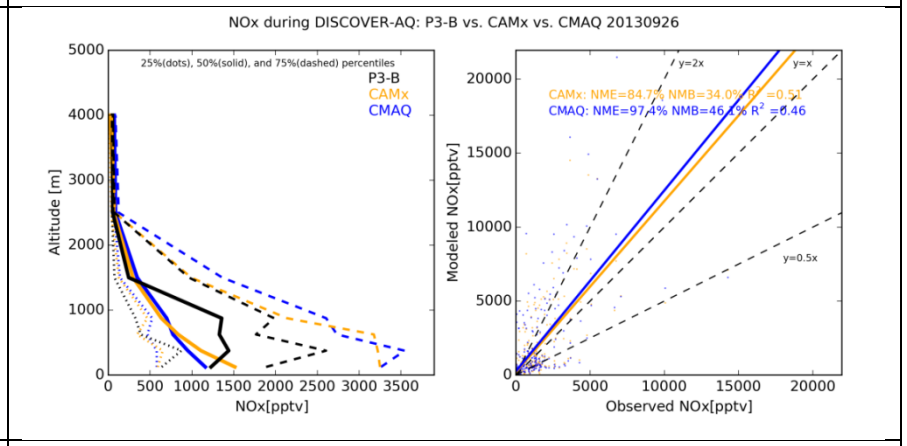

jNO_2

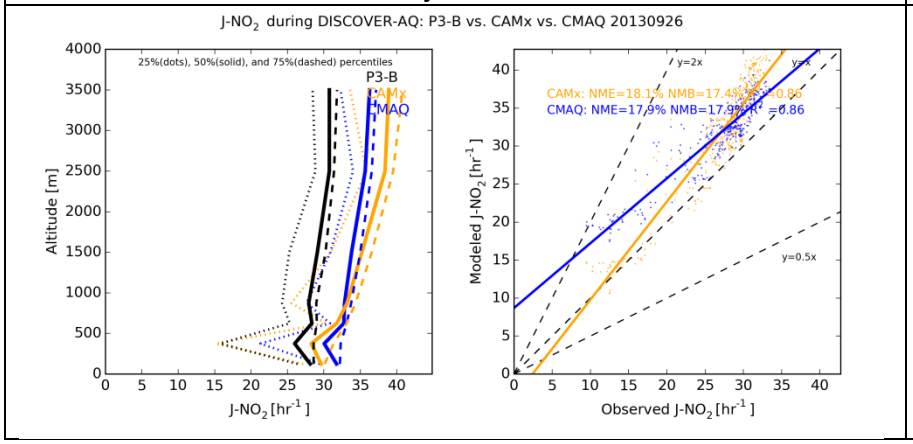

NOy

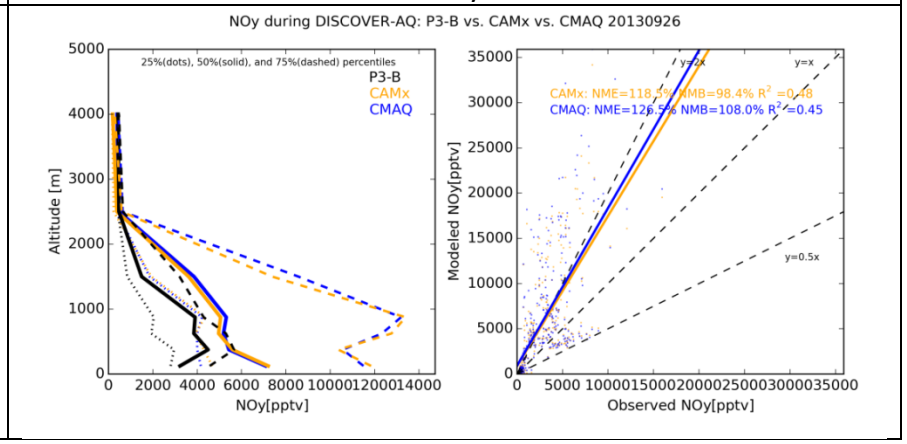

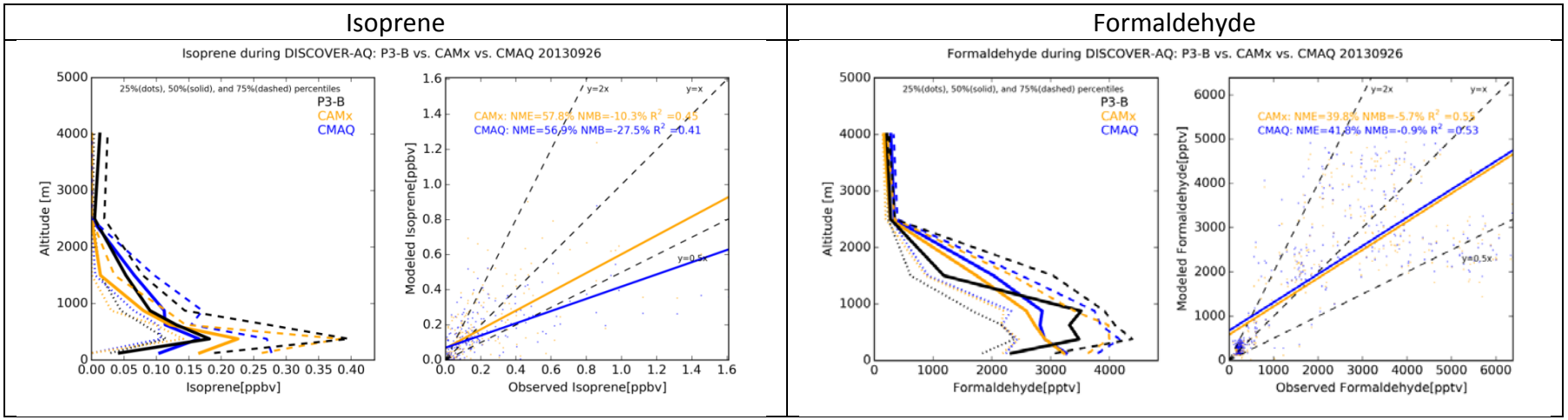

Figure 4-27. Vertical profiles measured by P3-B aircraft compared to CAMx/CMAQ estimated on September 26, 2013.

4.3.10 All flights

Overall, CAMx and CMAQ show similar model performance for gaseous species (Figure 4-28). Isoprene performance is mixed. The first half of September both models tend to overestimate 75-percentile concentrations but reasonably replicate lower concentrations. During the high ozone period after the front passages on September 21 and 25, the 75-percentile isoprene is under-predicted.

Formaldehyde performance is generally good. The reasons are that formaldehyde is low in free troposphere and higher when isoprene is present, and CB6r2 performs well in predicting formaldehyde production from isoprene (Kemball-Cook et al., 2015). There are cases where formaldehyde is evidently under predicted including September 14, 25, and 26 during possible emission events. Observed formaldehyde plumes on September 14 and 26 near Channelview are also high in acetaldehyde and toluene. Another formaldehyde plume observed near Conroe on September 26 has high acetaldehyde but low toluene concentrations. On September 25, the high observations were collected over the Galveston Bay under northerly winds suggesting the emitting sources near Baytown that also contribute to high acetaldehyde and toluene concentrations.

Both models overestimate acetaldehyde below 2000 m. in altitude. Kemball-Cook et al., (2015) reported that the overestimates of acetaldehyde against aircraft measurements during June-July 2013 were consistent with isoprene overestimates, indicating a bias in the chemical mechanism in which too much acetaldehyde is produced from reactions of isoprene. In this study, predicted acetaldehyde vertical profiles are more similar to those of formaldehyde. High acetaldehyde events coincide with high formaldehyde and NOx events implying the same emitting sources (e.g., flares).

Toluene has large over-prediction bias on all days, while xylene and benzene are consistently under predicted. This may suggest an issue with aromatic VOC speciation profiles used in emissions processing. Since acetylene is over predicted in the Houston area, the overestimation of toluene could also be related to overstated on-road mobile emissions. High observed toluene concentrations, possibly due to emission events, coincide with high concentrations of other aromatic VOCs such as benzene and C8/C9-alkyl benzenes. The emissions inventory did not capture any reported events.

Model performance for CO is quite good, for which both models have a slight high bias and reasonably good skill (NME of 23-24%).

Both models show poor model performance for EC and water-soluble organic carbon (WSOC[8]). Near surface EC concentrations are over predicted by at least a factor of five. Since EC in the

[8] WSOC is typically considered as secondary organic carbons and is mapped to
CAMx species: SOA1/2 + SOA2/2.0 + SOA3/1.6 + SOA4/1.6 + SOA5/1.4 + SOA6/1.4 + SOA7/2.1 + SOAH/2.0 + SOPA/2.1 + SOPB/2.1

atmosphere is inert and is due solely to direct aerosol emissions from sources, such large overestimation bias serves as a strong evidence of overstated EC emissions in the inventory. In contrast, WSOC is largely under predicted. CAMx predictions are about a factor of two higher than CMAQ, but the 75-percentile concentrations are at least a factor of three too low. Predicted WSOC shows less variability than the observed values through 5000 m. Because WSOC is produced from condensation of the low vapor pressure products of atmospheric (i.e., secondary formation, not directly emitted as primary aerosol), the cause of under prediction is unclear due to complexity of processes involved. Nonetheless, the CAMx model predictions appear to broadly agree with surface observations reported by Sheesley and Usenko (2015). CAMx-predicted WSOC is in the range of 2-3 $\mu g/m^3$ and WSOC/OC ratio is in the range of 40-60%. WSOC estimates by CMAQ are lower and the WSOC/OC ratio is in the range of 20-40%.

Elevated secondary $PM_{2.5}$ concentrations are typically associated with either summer sulphate episodes, when there is lots of photochemical activity to convert the SO_2 to sulphate. Because sulphate is a stronger acid than nitrate, ammonia will preferentially bond with sulphate over nitric acid. This appears to be the case during September 2013 period when observed sulphate is much higher than nitrate. Observed near-surface nitrate is generally lower than 0.3 $\mu g/m^3$ (except on September 25), while sulphate is higher than 2 $\mu g/m^3$. On most days, the models predicted sulphate below 1500 m fairly well with scatter along the 1:1 line. The models tend to under predict concentrations above 1500 m which are generally lower than 2 $\mu g/m^3$. CAMx sulphate estimates are slightly higher than CMAQ values. With sulphate being under estimated it is not surprising that ammonium (NH_4) is also under estimated with similar scatters.

Both models under estimated particulate chloride (Cl-) which is likely due to the omission of Cl-containing anthropogenic emissions. Na is predominantly from sea salt and both models appear to overstate sea salt emissions. As discussed previously, CAMx sea-salt emissions tend to be higher than CMAQ due to a different definition of surf zone and size distribution.

CMAQ species: (AXYL1J+AXYL2J+AXYL3J)/2.0 +(ATOL1J+ATOL2J+ATOL3J)/2.0 +(ABNZ1J+ABNZ2J+ABNZ3J)/2.0 +(AISO1J+AISO2J)/1.6 +AISO3J/2.7 +(ATRP1J+ATRP2J)/1.4 +ASQTJ/2.1 +0.64*AALKJ +AORGCJ/2.0 +(AOLGBJ+AOLGAJ)/2.1

Isoprene

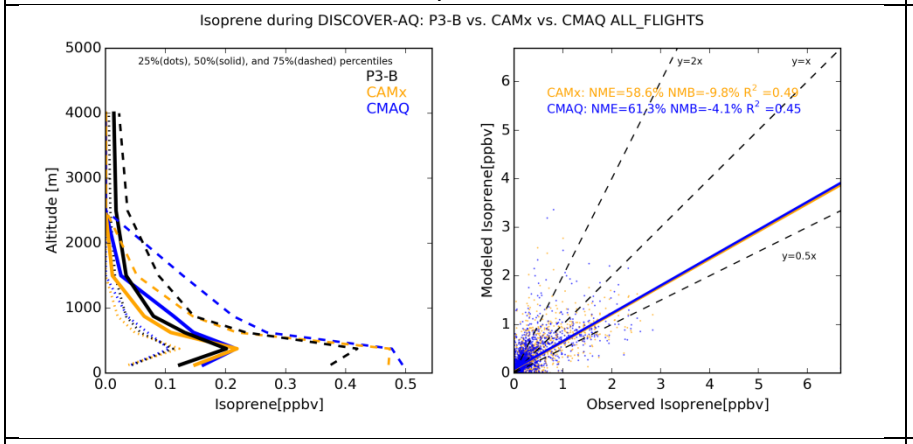

Acetaldehyde

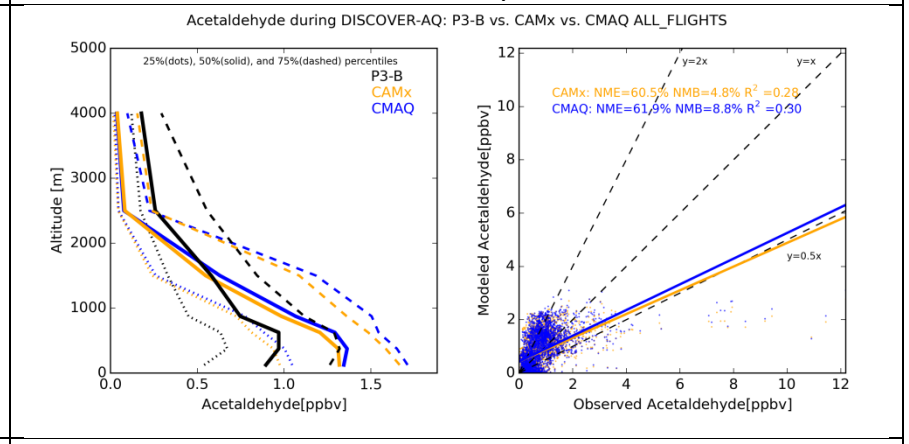

Formaldehyde

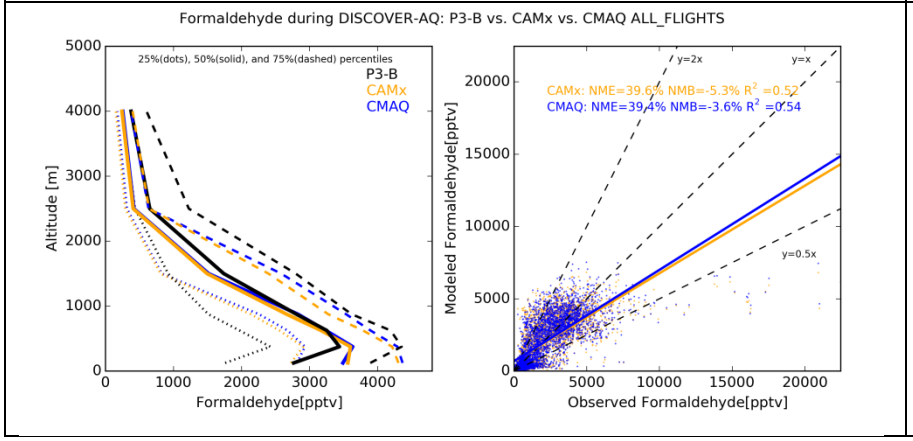

Toluene

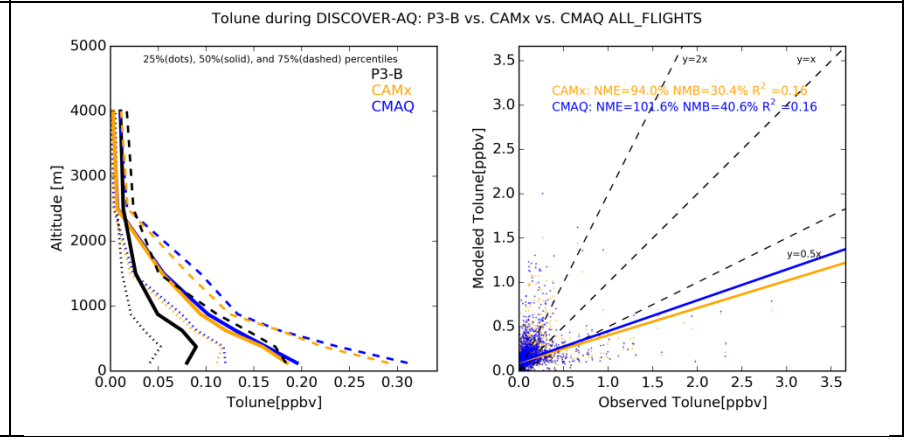

Benzene

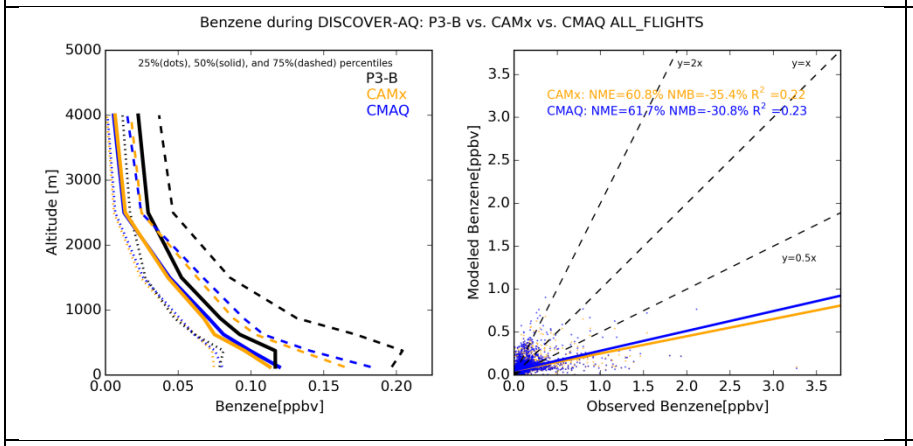

Xylene

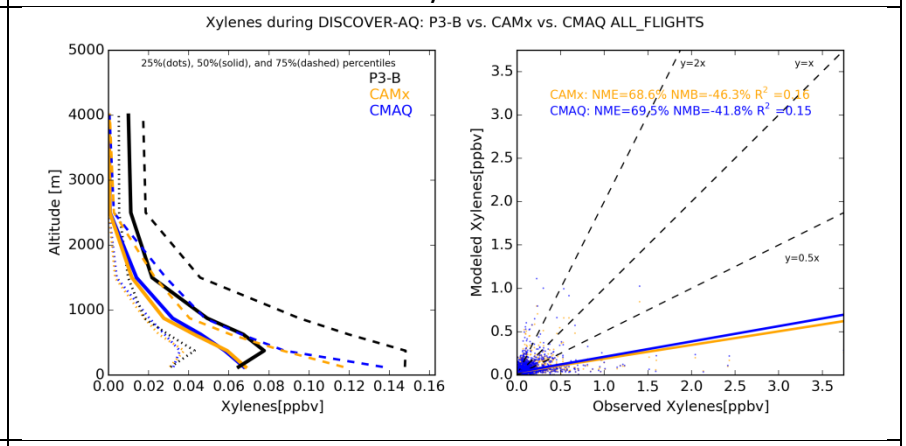

Carbon monoxide

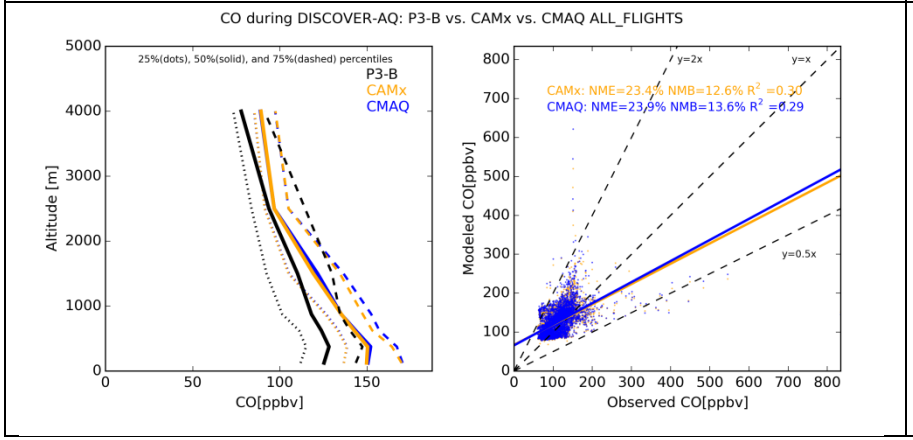

EC

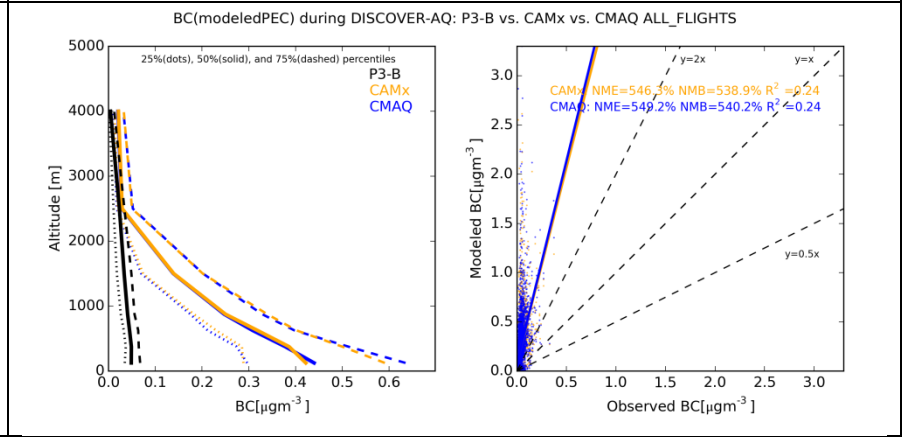

Water-soluble OC

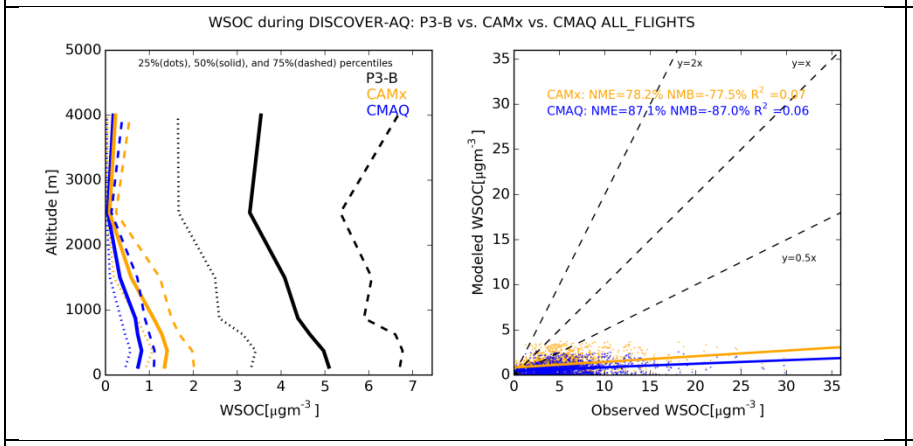

Sulfate

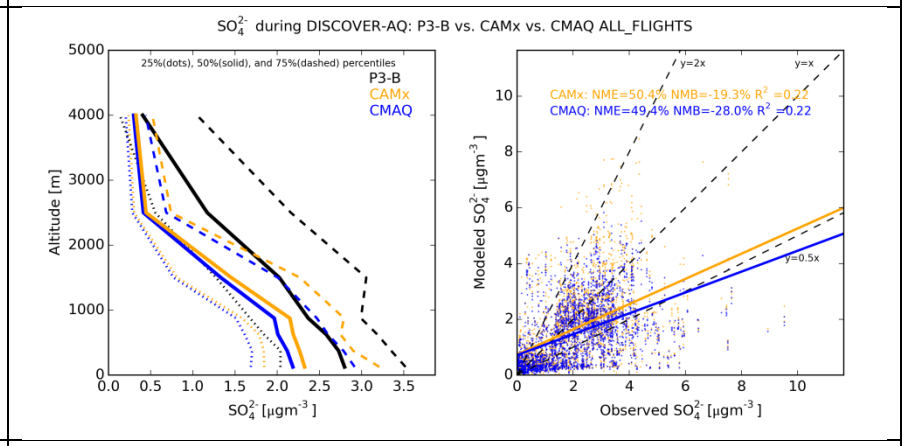

Nitrate

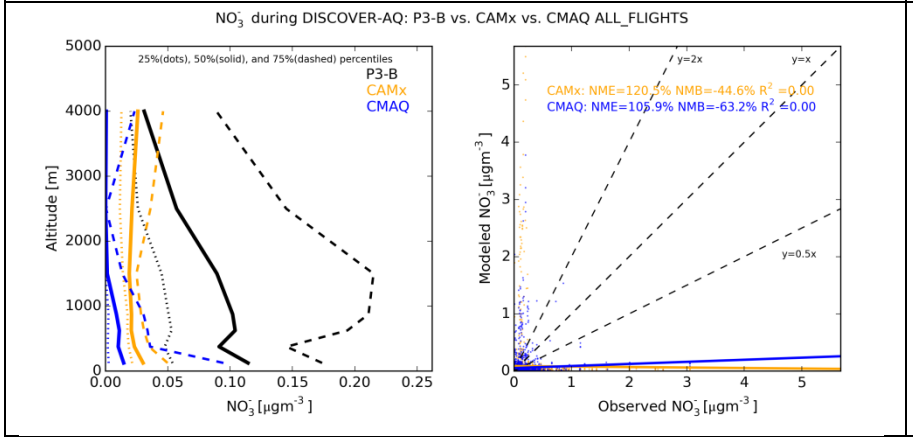

Ammonium

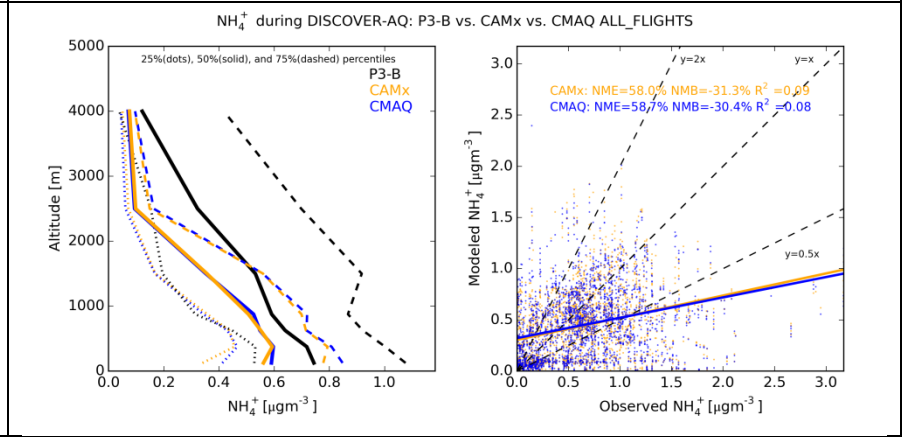

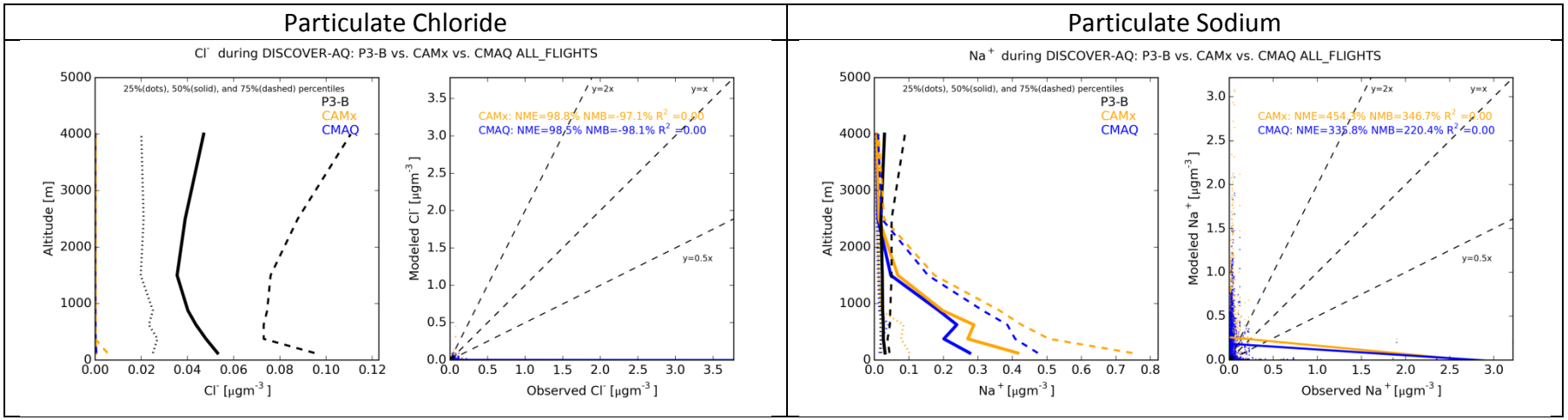

Figure 4-28. Vertical profiles measured by P3-B aircraft compared to CAMx/CMAQ estimated during DISCOVER-AQ September 2013 period.

4.3.11 Summary of MPEs Against Aircraft Measurements

CAMx and CMAQ show similar model performance for all gaseous species examined. Ozone is generally over predicted near surface (< 300 m) but under predicated above 2000 m. The models under predict ozone at all heights on September 25. This day was influenced by a frontal passage and a re-circulation of pollution due to afternoon sea-breeze. The downward mixing due to the frontal passage was replicated well by the models but the re-circulation was not captured by WRF meteorology.

Both models consistently over predicted jNO_2. The over prediction is expected due to under estimated clouds. Lower jNO_2 above 300 m. by CMAQ may suggest that it diagnoses more sub-grid clouds at 4 km resolution than CAMx. Good jNO_2 performance is seen on clear-sky days (September 12, 25, and 26). However, good performance of jNO_2 does not necessary yield good ozone performance. Despite lower jNO_2 in CMAQ, the 50-percentile ozone estimates by the two models only differ by a few ppb. While high ozone events, such as those on September 24-26, are related to frontal passages and re-circulation of sea-breeze, ozone predictions on other September days are likely influenced by continental transport or background ozone.

The models under predicted 75-percentile NOx between 300-1500 m except on September 26.

Isoprene performance is mixed with the first half of September having a tendency for the models to overestimate 75-percentile concentrations and to underestimate during high ozone period (September 25-26). Formaldehyde performance is quite good. Acetaldehyde is over predicted under 2000 m with near-ground concentrations over predicted by ~50%. Predicted acetaldehyde vertical profiles are more similar to those of formaldehyde. High acetaldehyde events coincide with high formaldehyde and NOx events implying the same emitting sources. The models biased high on toluene but low on xylene and benzene suggesting a possible issue with VOC speciation profiles and/or overstated on-road mobile emissions. Both models do not capture potential emission events as they are not described in the emissions inventory.

Large bias of EC suggests overstated EC emissions in the inventory. CAMx predictions of WSOC are about a factor of two higher than CMAQ, but the 75-percentile concentrations are at least a factor of three too low. Nitrate concentrations in the Houston area during the September period is small. On most days, the models predicted sulphate below 1500 m well. The under estimation of sulphate above 1500 m may be related to under predicted availability of clouds. With sulphate being under estimated it is not surprising that ammonium is also under estimated.

5.0 CAMX AND CMAQ SENSITIVITY TESTS

Based on the results of the Base Case simulation and the performance evaluation described in Section 4, we conducted additional modeling runs to assess the response of both models to changes to the respective physics options. The goal of these runs is to determine whether changing options allows the models to better replicate the observations, with particular emphasis on vertical concentration gradients and aloft measurements.

5.1 Sensitivity Simulations

Five sensitivity simulations were conducted to examine various aspects of photochemical modeling including photochemistry, vertical transport, grid resolution, and emission inputs. Photochemistry is strongly influenced by the presence of clouds, which can both attenuate and enhance the actinic flux of ultraviolet (UV) and visible radiation responsible for photolysis. Cloud impacts on photolysis depend on many factors, including height, depth and fractional sky cover; water content; and water phase (i.e., liquid droplets or ice crystals). The first two sensitivity tests examine the effects of cloud on photolysis rates and ozone concentrations. The third sensitivity test enhances vertical mixing in the planetary boundary layer (PBL) by increasing vertical diffusion coefficient (Kv). The fourth test uses finer model grid resolution (1.33 km) and compares to 4 km resolution. The last test examines model responses to NOx and VOC emission reductions.

5.1.1 Clear-Sky and Adjusted jNO_2

The method for calculating photolysis rates is slightly different between the two models. CAMx uses the TUV radiative transfer and photolysis model to obtain a multi-dimensional lookup table of clear-sky photolysis rates. Then, CAMx internally adjusts clear-sky rates for the presence of clouds and aerosols using a fast in-line version of TUV. CMAQ in-line photolysis does not use a lookup table, but uses an internal photolysis model (Fast-J) to compute photolysis rates for the local cloud, aerosol, albedo, and meteorological profiles. For both models we turned off the cloud adjustment to obtain clear-sky photolysis rates.

Figure 5-1 shows that CMAQ jNO_2 at surface is consistently higher than CAMx with or without cloud adjustment. At higher altitude (e.g., 750 m. as shown in Figure 5-2), CMAQ jNO_2 at surface is consistently lower than CAMx with or without cloud adjustment. Lower jNO_2 in CMAQ may explain slightly lower ozone predictions (< 5 ppb) compared to CAMx. Vertical profiles of jNO_2 (Figure 5-3) show that below 500 m. altitude CAMx jNO_2 has a sharper vertical gradient than CMAQ jNO_2. This could reflect default altitude bins specified in the lookup table (i.e., starting at 0-150 m.) which could be changed.

Due to limited clouds predicted by WRF, even when both models diagnose sub-grid clouds, the adjusted jNO_2 is comparable to clear-sky jNO_2. Figure 5-3 (middle; bottom) and Figure 5-4 confirm that the effect of clouds to jNO_2 and ozone is minimal throughout 3500 m vertical profile. On September 4, the cloud adjustment actually increases reflection of ultra violet (UV) aloft enhancing jNO_2 above low-level clouds. CMAQ appears to be slightly more responsive to the cloud adjustment than CAMx.

Perhaps the most important finding from this test is that the clear-sky difference of jNO_2 is larger between the two models than that due to the effect of cloud. The discrepancy of clear-sky jNO_2 values between the two models should be further investigated.

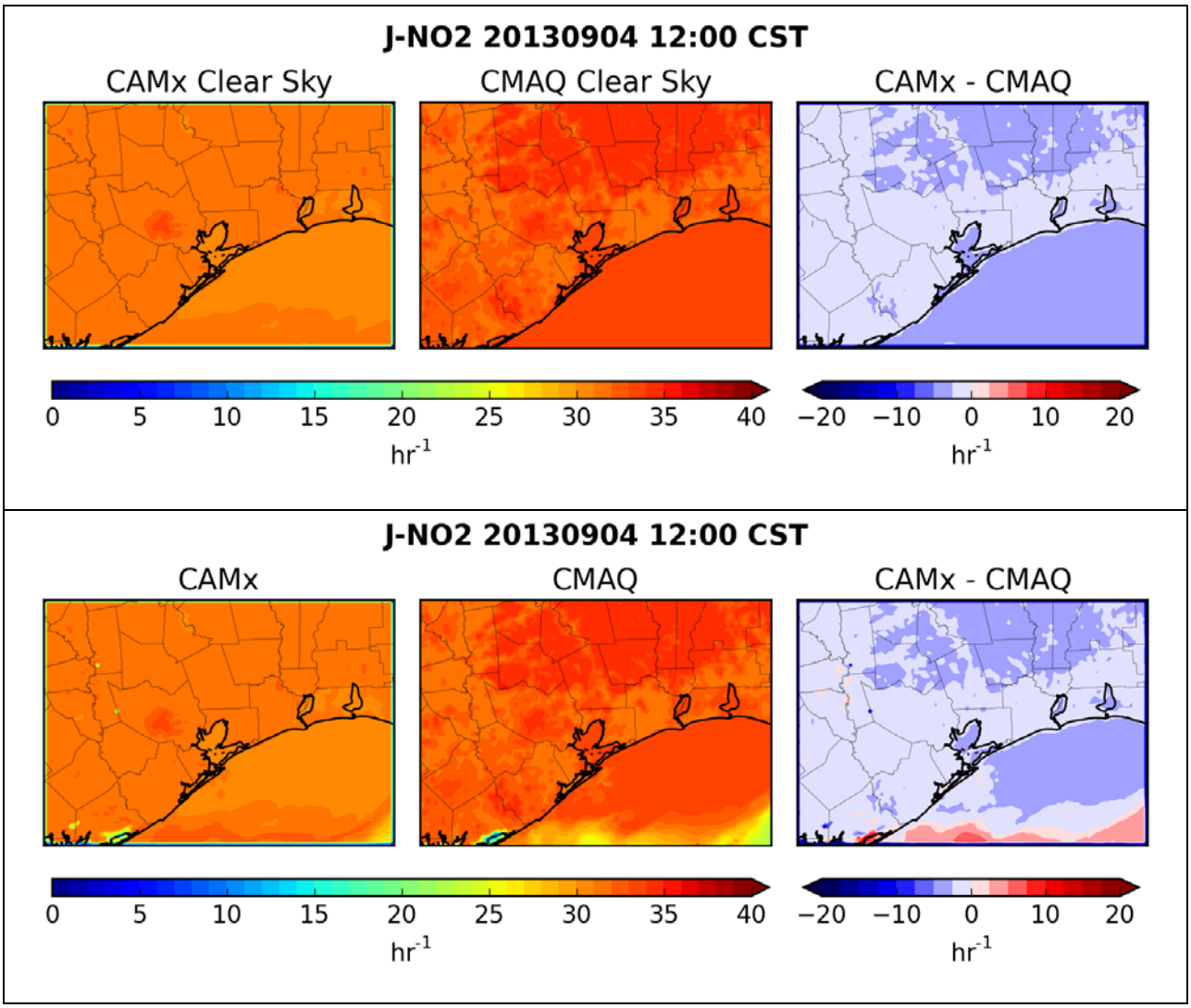

Figure 5-1. Clear-sky (top) and cloud-adjusted (bottom) jNO_2 predictions at surface by CAMx and CMAQ on September 4, 2013.

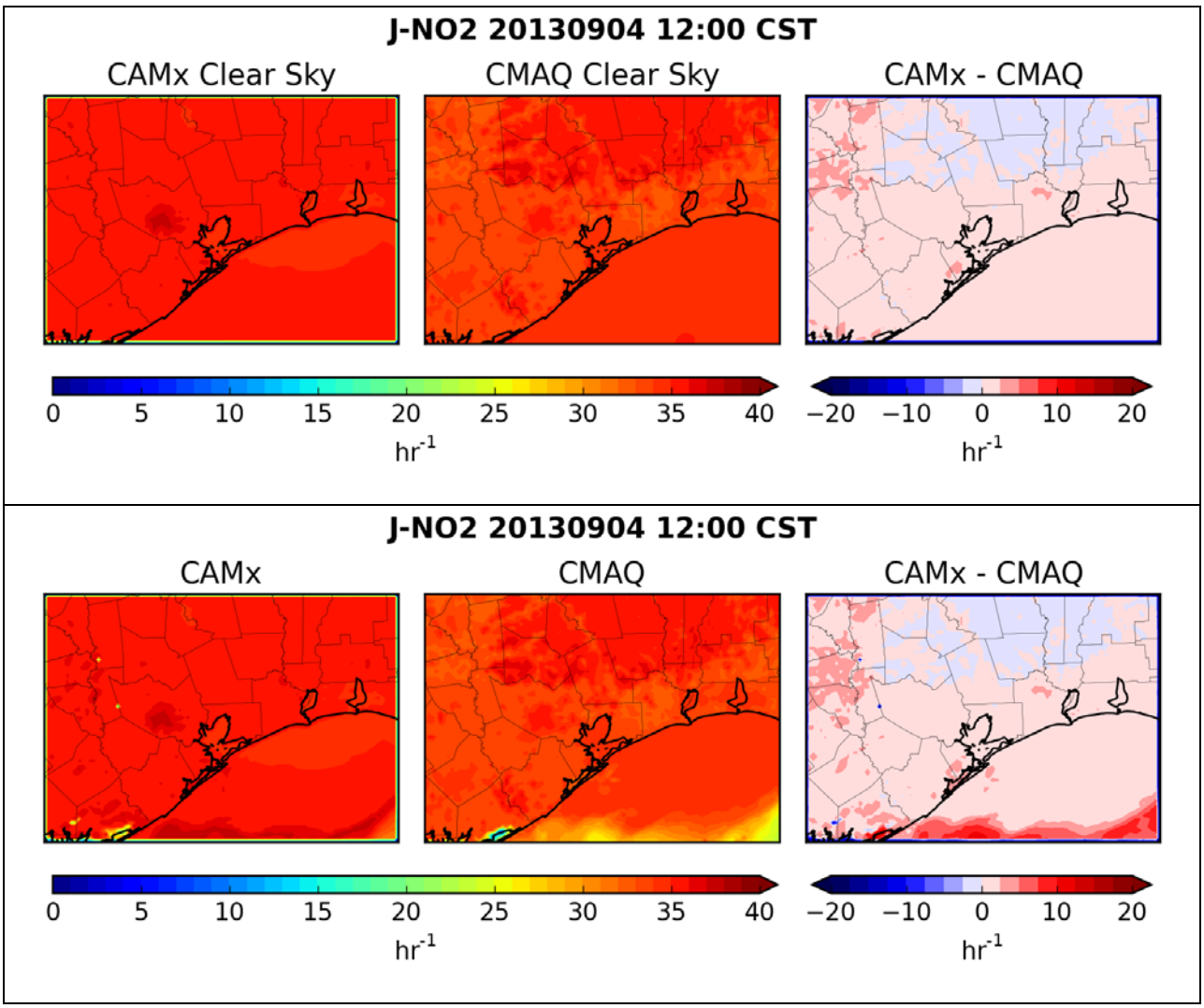

Figure 5-2. Clear-sky (top) and adjusted (bottom) jNO_2 predictions at 750 m. by CAMx and CMAQ on September 4, 2013.

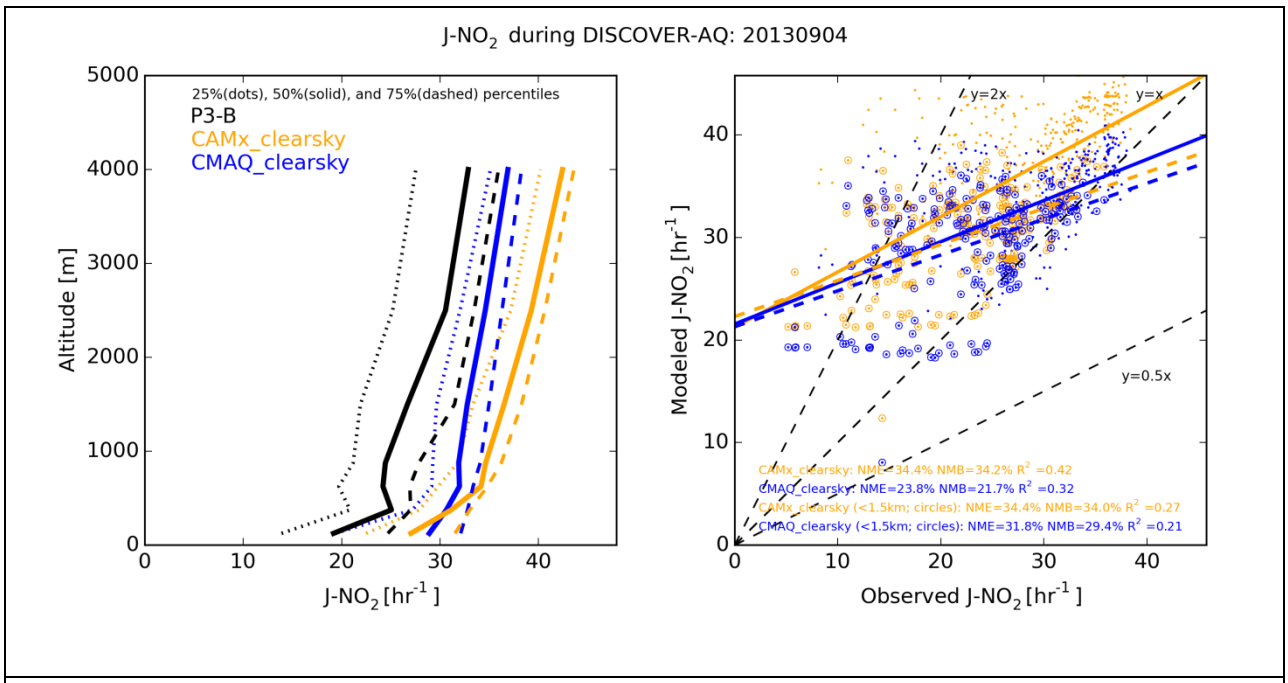
J-NO2 during DISCOVER-AQ: 20130904
25%(dots), 50%(solid), and 75%(dashed) percentiles
P3-B
CAMx_clearsky
CMAQ_clearsky
Altitude [m]
J-NO2 [hr-1]
y=2x
y=x
y=0.5x
Modeled J-NO2 [hr-1]
Observed J-NO2 [hr-1]
CAMx_clearsky: NME=34.4% NMB=34.2% R2 =0.42
CMAQ_clearsky: NME=23.8% NMB=21.7% R2 =0.32
CAMx_clearsky (<1.5km; circles): NME=34.4% NMB=34.0% R2 =0.27
CMAQ_clearsky (<1.5km; circles): NME=31.8% NMB=29.4% R2 =0.21

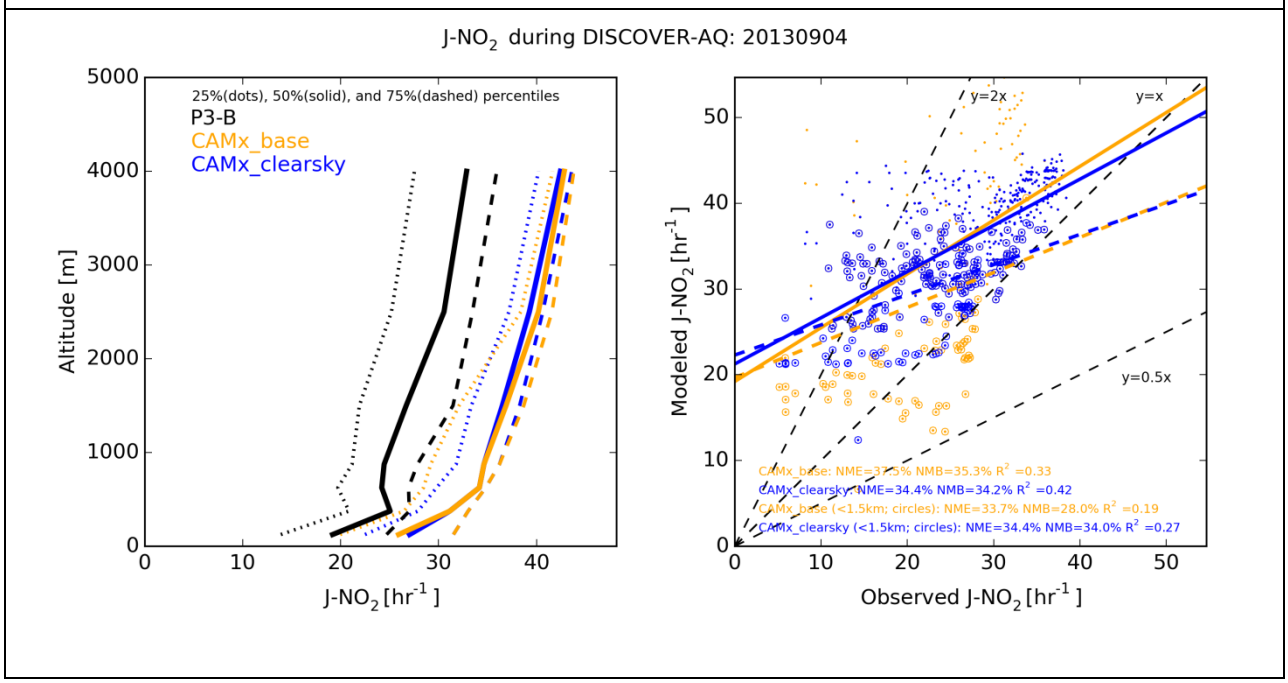
J-NO2 during DISCOVER-AQ: 20130904
25%(dots), 50%(solid), and 75%(dashed) percentiles
P3-B
CAMx_base
CAMx_clearsky
Altitude [m]
J-NO2 [hr-1]
y=2x
y=x
y=0.5x
Modeled J-NO2 [hr-1]
Observed J-NO2 [hr-1]
CAMx_base: NME=37.3% NMB=35.3% R2 =0.33
CAMx_clearsky: NME=34.4% NMB=34.2% R2 =0.42
CAMx_base (<1.5km; circles): NME=33.7% NMB=28.0% R2 =0.19
CAMx_clearsky (<1.5km; circles): NME=34.4% NMB=34.0% R2 =0.27

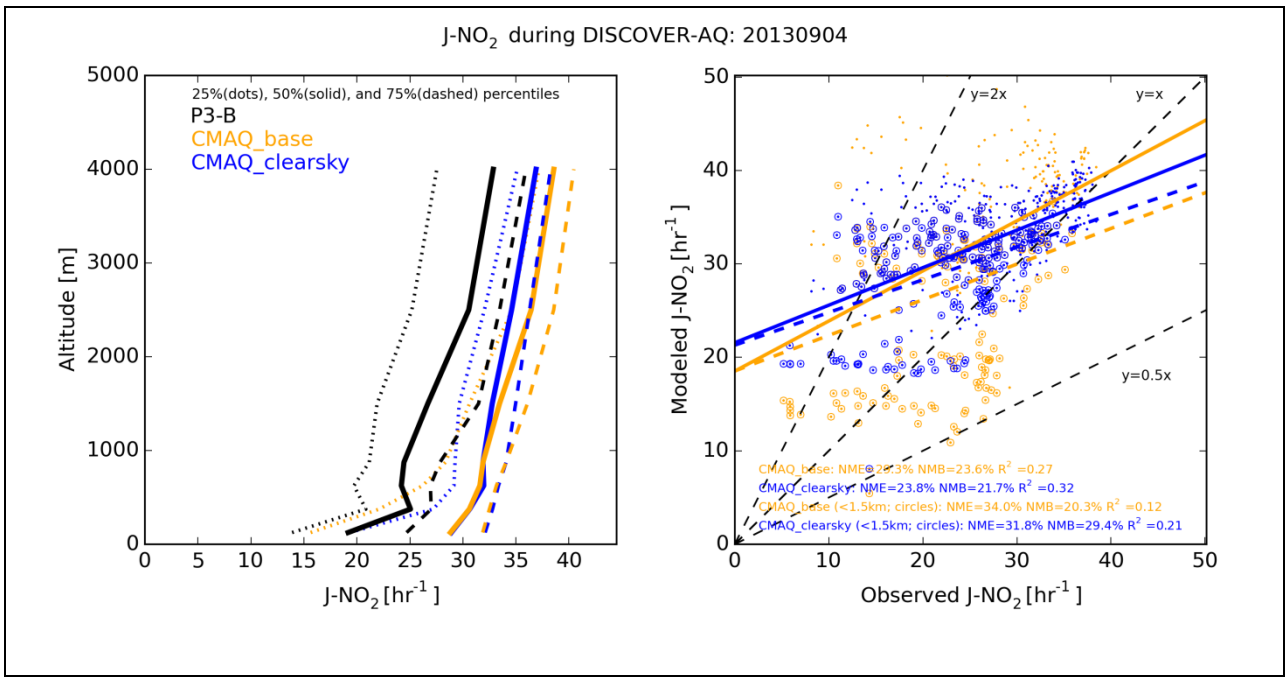

Figure 5-3. JNO_2 Vertical profiles measured by P3-B aircraft compared to CAMx and CMAQ simulations with clear-sky/adjusted photolysis rates.

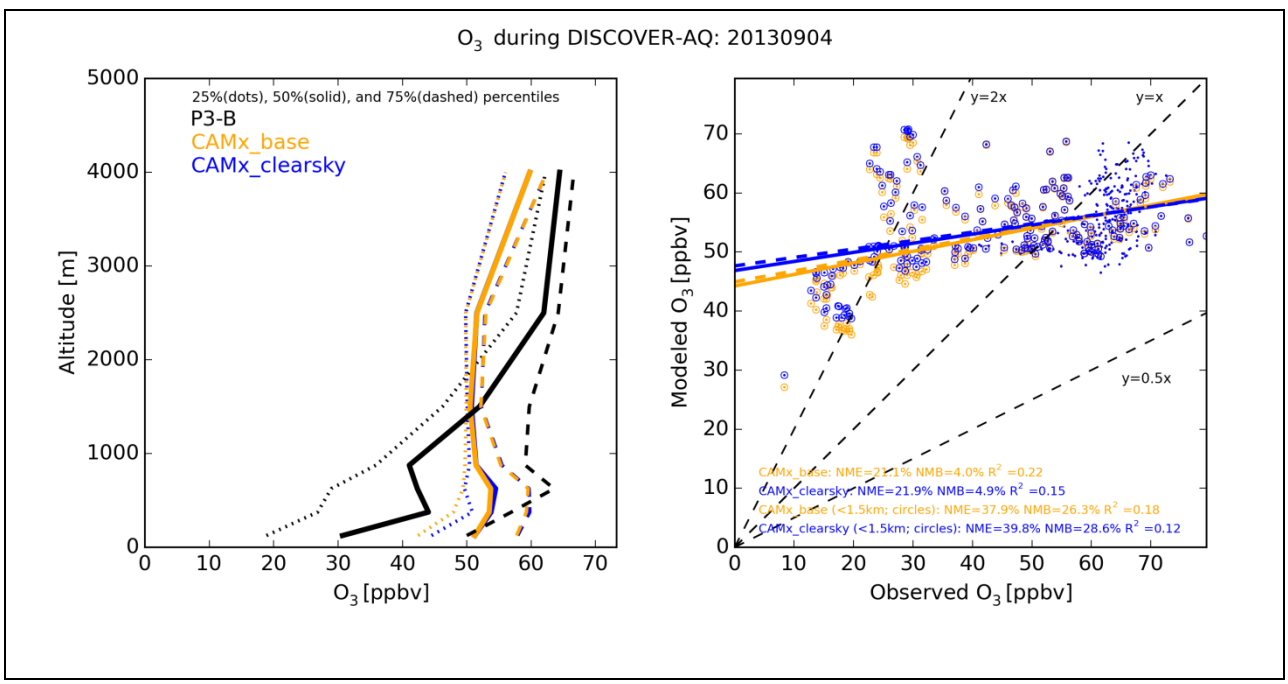

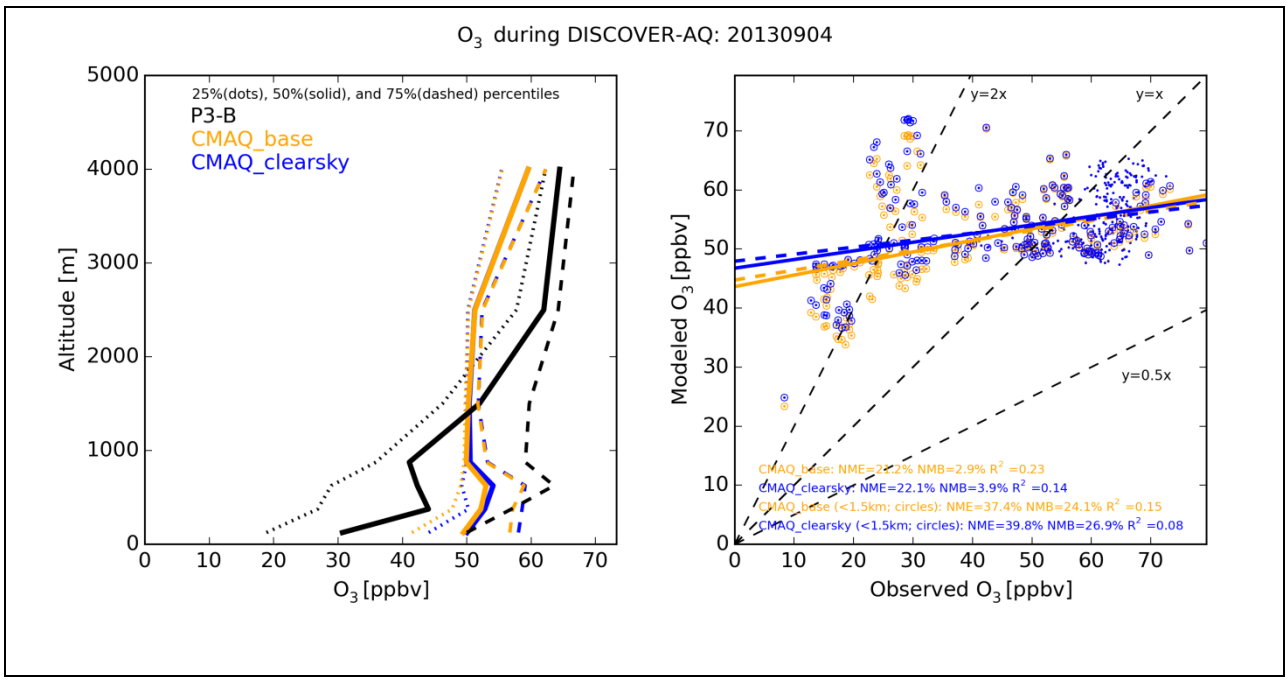

Figure 5-4. Ozone vertical profiles measured by P3-B aircraft compared to CAMx and CMAQ simulations with clear-sky/adjusted photolysis rates.

5.1.2 Introducing More Clouds

A CAMx sensitivity case was run in which the diagnosis of sub-grid stratiform cloudiness was altered to dramatically increase the amount non-convective boundary layer cloudiness. The standard algorithm is based on the approach used in MCIP. It specifies a vertical profile of critical relative humidity (RHc). Clouds are diagnosed for any layers with relative humidity above RHc, and then the cloud fraction and liquid water contents are set according to the amount of excess humidity. The sensitivity test modified 3 controlling factors: (1) the usual constant 98% RHc applied in the boundary layer was changed to a linear slope from 98% at the surface to a minimum of 50% at 2 km; (2) the cloud cover calculated from excess humidity was increased from a maximum of 34% to a maximum of 100%; and (3) the cloud water content of diagnosed clouds was doubled.

The effect of enhanced clouds is evident in both sulphate and jNO_2 profiles (shown in Figure 5-5 as CAMx_morstrat). More clouds at low levels increase reflection of UV aloft enhancing jNO_2 above those clouds. More sulphate is formed below 2000 m. but the model performance switches from under-prediction to over-prediction, implying that the addition of cloud was overdone. Impact to ozone performance is small with near surface concentrations decreasing only by a few ppb. The results suggest that while jNO_2 is sensitive to cloud availability, ozone appears less responsive to the cloud adjustment.

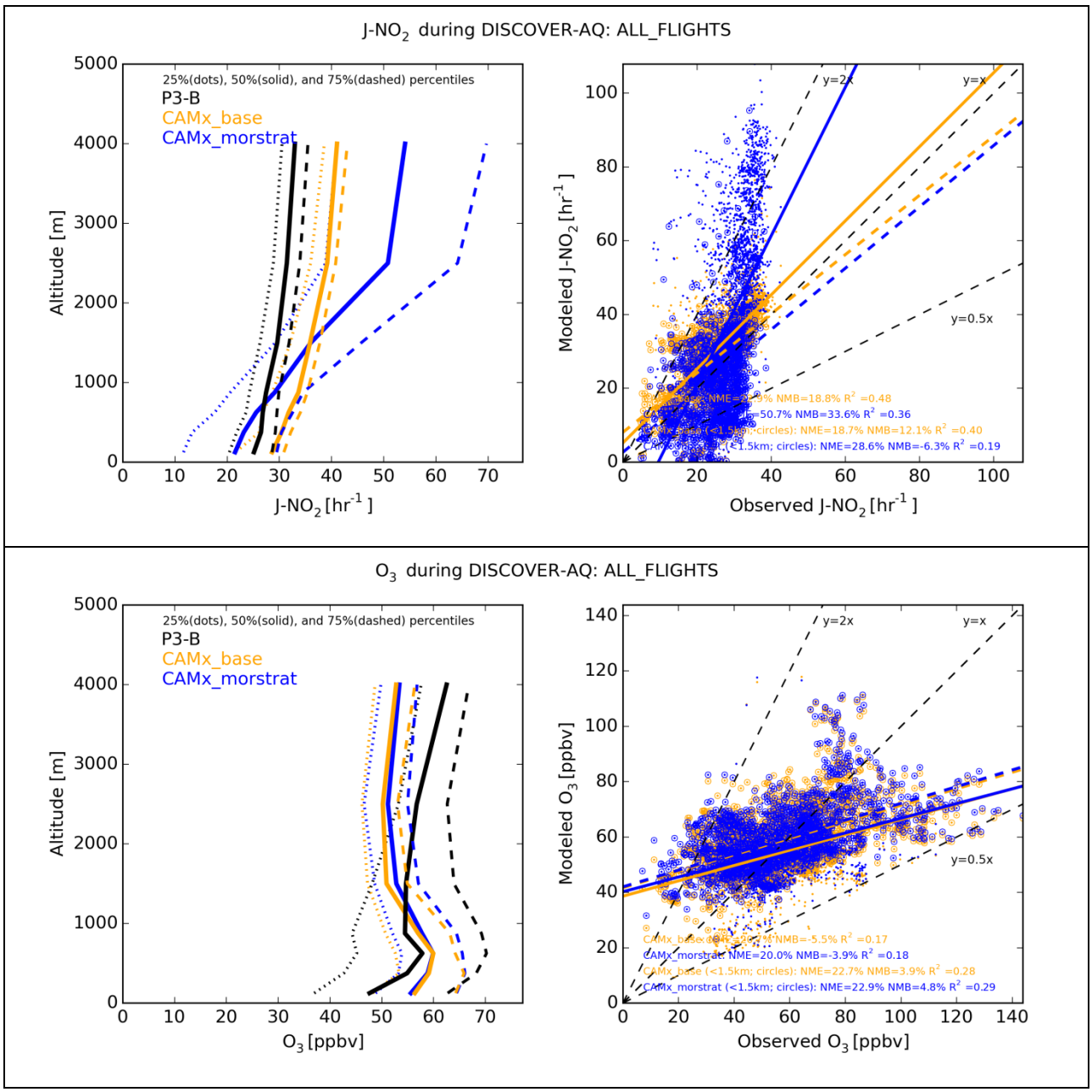
J-NO2 during DISCOVER-AQ: ALL_FLIGHTS
25%(dots), 50%(solid), and 75%(dashed) percentiles
P3-B
CAMx_base
CAMx_morstrat
Altitude [m]
J-NO2 [hr-1]
Modeled J-NO2 [hr-1]
Observed J-NO2 [hr-1]
y=2x
y=x
y=0.5x
NMB=18.8% R2 =0.48
NME=50.7% NMB=33.6% R2 =0.36
NME=18.7% NMB=12.1% R2 =0.40
NME=28.6% NMB=-6.3% R2 =0.19
O3 during DISCOVER-AQ: ALL_FLIGHTS
25%(dots), 50%(solid), and 75%(dashed) percentiles
P3-B
CAMx_base
CAMx_morstrat
Altitude [m]
O3 [ppbv]
Modeled O3 [ppbv]
Observed O3 [ppbv]
y=2x
y=x
y=0.5x
NMB=-5.5% R2 =0.17
NME=20.0% NMB=-3.9% R2 =0.18
CAMx_base (<1.5km; circles): NME=22.7% NMB=3.9% R2 =0.28
CAMx_morstrat (<1.5km; circles): NME=22.9% NMB=4.8% R2 =0.29

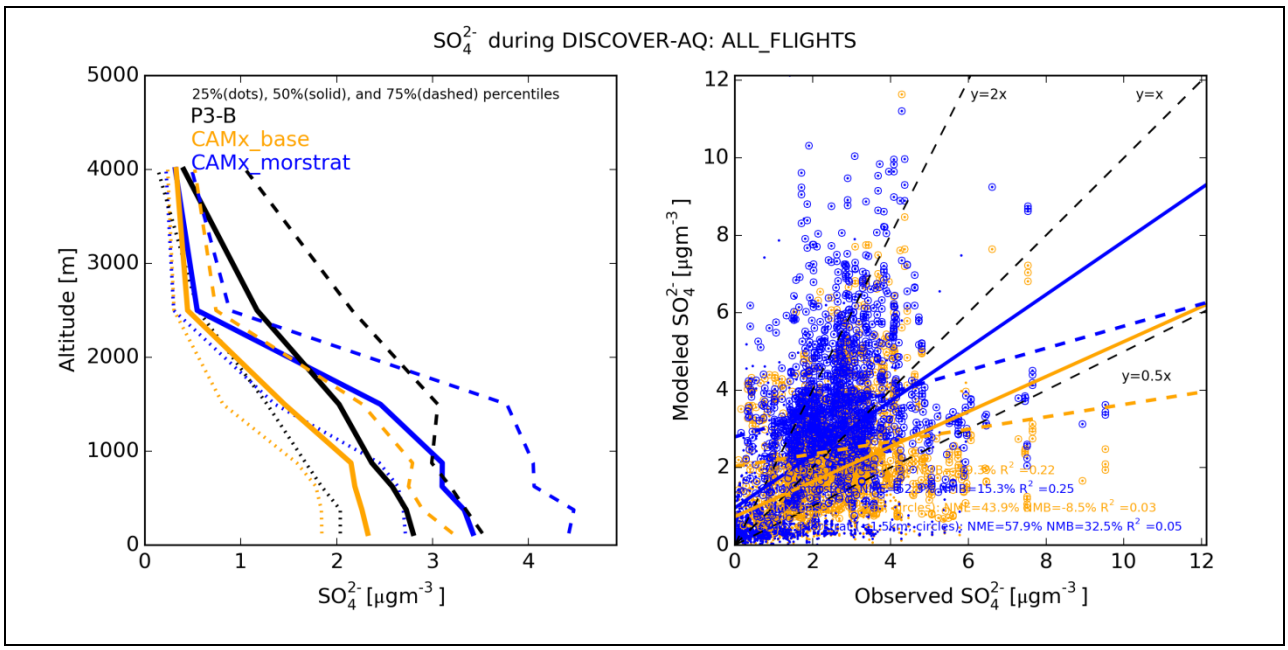

Figure 5-5. Vertical profiles measured by P3-B aircraft compared to CAMx base case and morstrat simulations.

5.1.3 Vertical Diffusivity

Several options are available to derive vertical diffusivity (Kv) fields from WRF output using the WRFCAMx meteorological pre-processor. This study utilized the Yonsei University (YSU) planetary boundary layer (PBL) scheme in WRF. WRF can be run with a PBL scheme that does not output turbulent kinetic energy (TKE), as is the case with the YSU scheme. In this case, WRFCAMx diagnoses Kv fields from wind, temperature, surface and PBL parameters using one of the following diagnoses: OB70 (O'Brien, 1970), CMAQ or YSU. A previous TCEQ modeling study (ENVIRON, 2011) showed that OB70 typically generated the lowest daytime Kv's and highest ozone and NOx. This same study showed that the CMAQ Kv scheme typically generated the highest vertical diffusivities and lowest surface ozone and NOx. The YSU Kv methodology resulted in daytime Kv's in between the OB70 and CMAQ bounds. In the Base Case simulation, we selected the YSU Kv methodology in WRFCAMx. For this sensitivity test, we ran CAMx with CMAQ Kv's.

Because the YSU and CMAQ schemes tend to show rapidly decreasing vertical diffusivities at night, the OB70 Kv patch is applied to help enhance nighttime mixing in urban areas. Another Kv patch is applied to maintain elevated diffusivities in vertical grid columns where afternoon deep cloud development cools the surface and suppresses or collapses WRF boundary layer depths (ENVIRON, 2012).

Predicted ozone is not sensitive to a different Kv scheme (Figure 5-6). More mixing introduced by CMAQ Kv's lowers ozone concentrations by a few ppb but the effect is limited below 800 m. The reduction is more evident for species that have near-ground sources such as NO_2 and EC.

The reduction of EC concentration is not sufficient to address the model's over-prediction which is likely due to overstated EC emissions. The Kv effect is reversed above 800 m. as surface air is mixed upward.

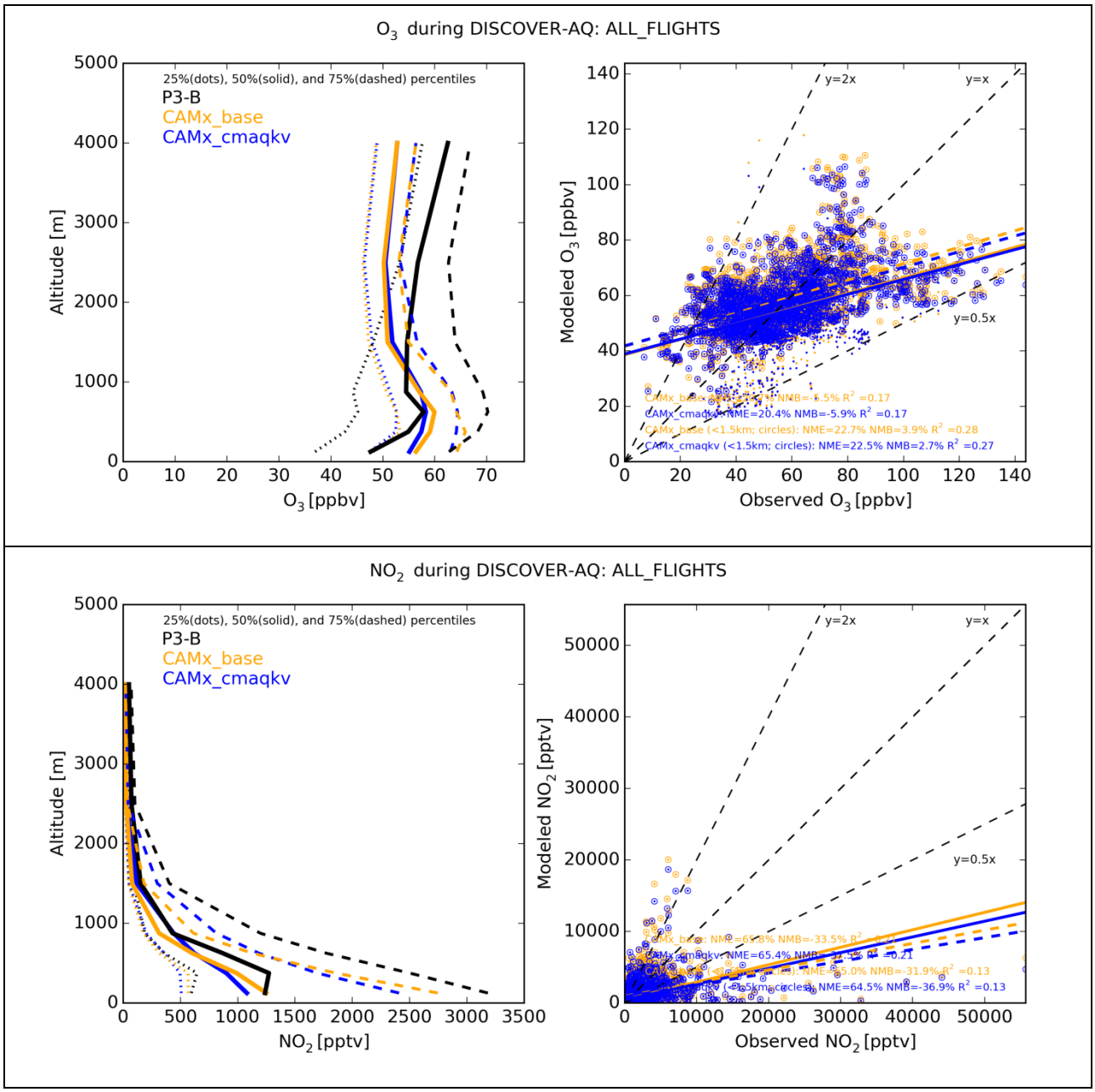

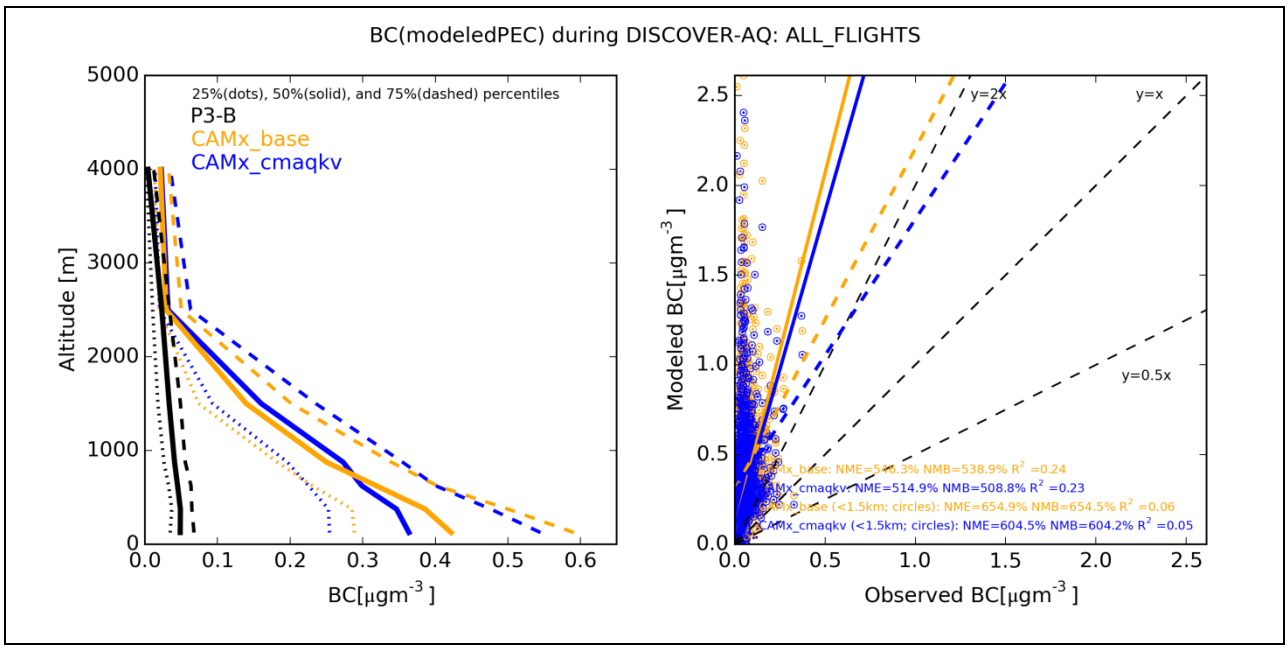

Figure 5-6. Vertical profiles measured by P3-B aircraft compared to CAMx base case and CAMx with CMAQ_Kv simulations.

5.1.4 Increasing Grid Model Resolution (1.33 km)

The point source inventory in the HGBPA area includes hundreds of petrochemical sources. The 4 km grid resolution cannot resolve the sharp concentration gradients and may introduce artificial dilution of stack emissions. We conducted a CAMx sensitivity test that aims to improve treatment of these elevated sources by increasing the grid resolution from 4 km to 1.33 km.

Figure 5-7 compares the CAMx 4 km and 1.33 km simulations. Except for pollutants that are fairly under estimated in the Base Case, such as sulphate, the model performance of the 1.33 km simulation shows no improvement. Ozone vertical profiles generally hold similar shapes but the concentrations increase through 2500 m.

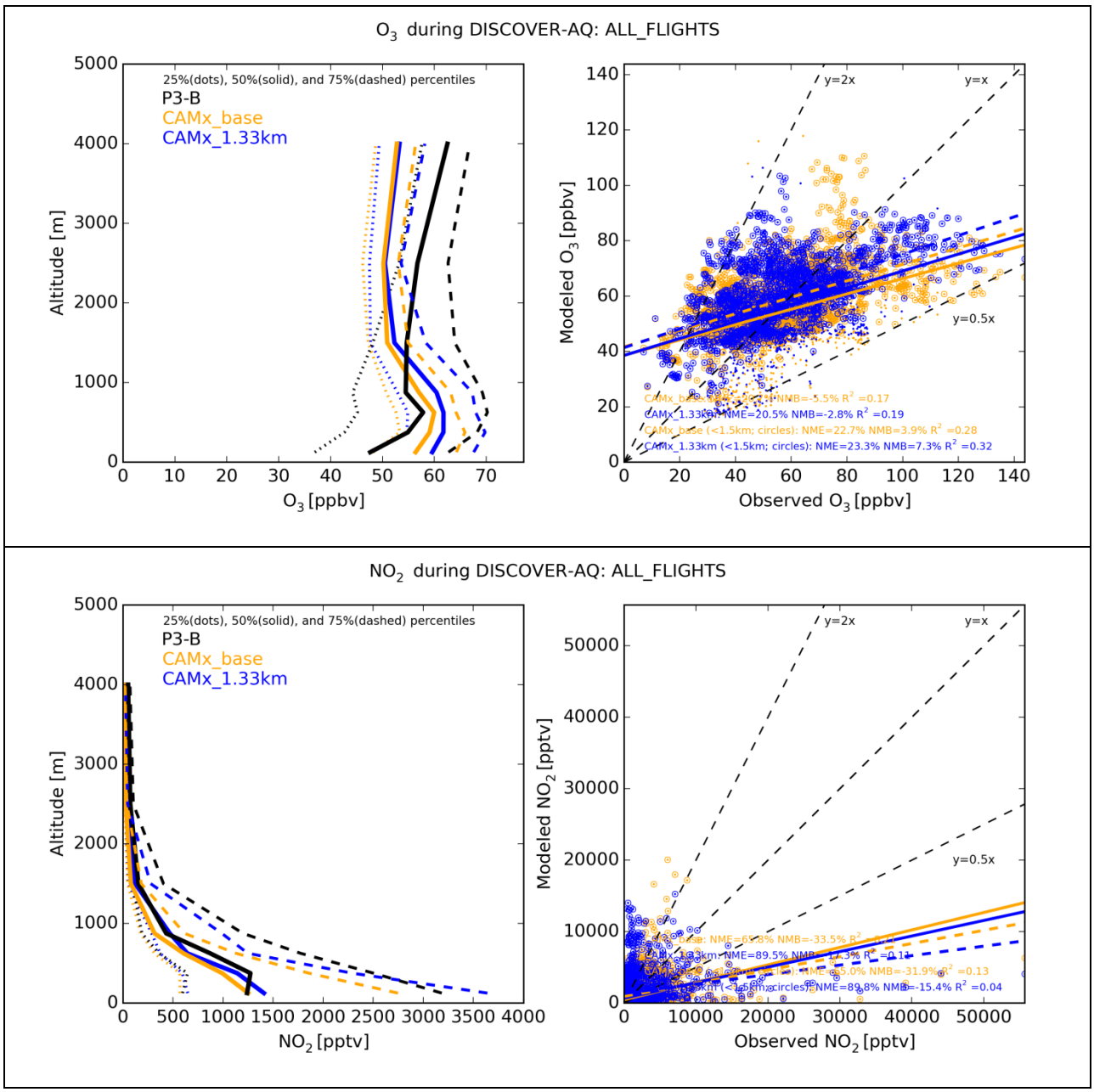
O3 during DISCOVER-AQ: ALL_FLIGHTS
25%(dots), 50%(solid), and 75%(dashed) percentiles
P3-B
CAMx_base
CAMx_1.33km
Altitude [m]
O3 [ppbv]
y=2x
y=x
y=0.5x
Modeled O3 [ppbv]
Observed O3 [ppbv]
CAMx_1.33km: NME=20.5% NMB=-2.8% R2 =0.19
CAMx_base (<1.5km; circles): NME=22.7% NMB=3.9% R2 =0.28
CAMx_1.33km (<1.5km; circles): NME=23.3% NMB=7.3% R2 =0.32
NO2 during DISCOVER-AQ: ALL_FLIGHTS
25%(dots), 50%(solid), and 75%(dashed) percentiles
P3-B
CAMx_base
CAMx_1.33km
Altitude [m]
NO2 [pptv]
y=2x
y=x
y=0.5x
Modeled NO2 [pptv]
Observed NO2 [pptv]

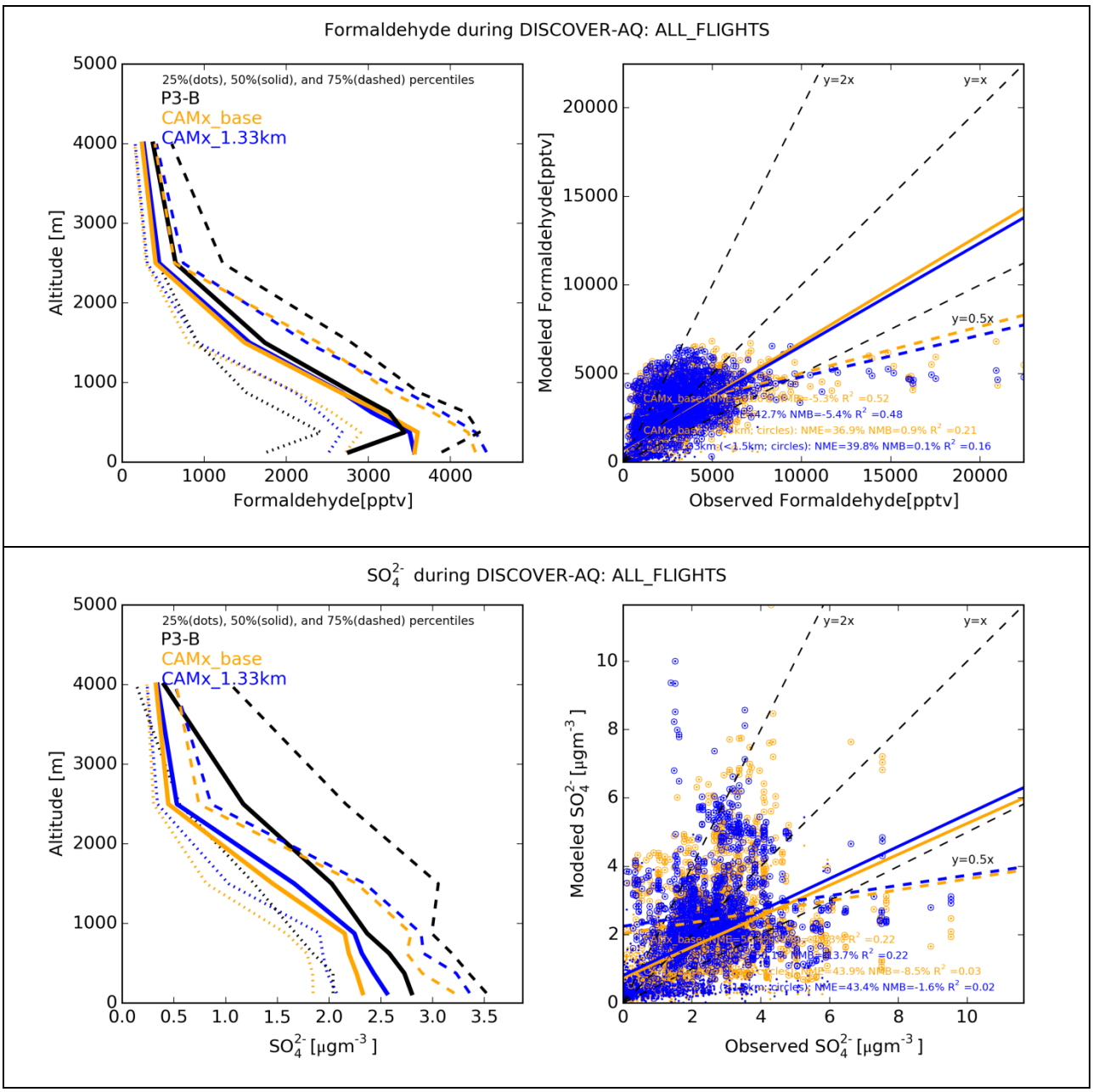

Figure 5-7. Vertical profiles measured by P3-B aircraft compared to CAMx base case and CAMx 1.33-km simulations.

5.1.5 Emission Reduction

We performed an analysis of the sensitivity of ozone concentrations to reductions in anthropogenic emissions of both nitrogen oxides (NOx) and volatile organic compounds (VOCs). The emissions are reduced by 20% across all anthropogenic sources. A 20 percent reduction is high enough to establish ozone response, yet low enough to be comparable to possible near-term emission changes.

CAMx and CMAQ models show comparable ozone responses to NOx and VOC emission reductions (Figure 5-8 to Figure 5-10). On days with high predicted ozone concentrations in the Houston metropolitan (> 60 ppb), the emission reductions lower the MDA8 ozone up to 4% (3-4 ppb). Slightly larger ozone reductions are seen downwind in the west of Houston. Ozone disbenefit is seen close to Lake Charles, LA, suggesting that the area has a different NOx/VOC-sensitivity regime than in Houston. Ozone disbenefit in the Houston area occurs on days with low predicted ozone concentrations.

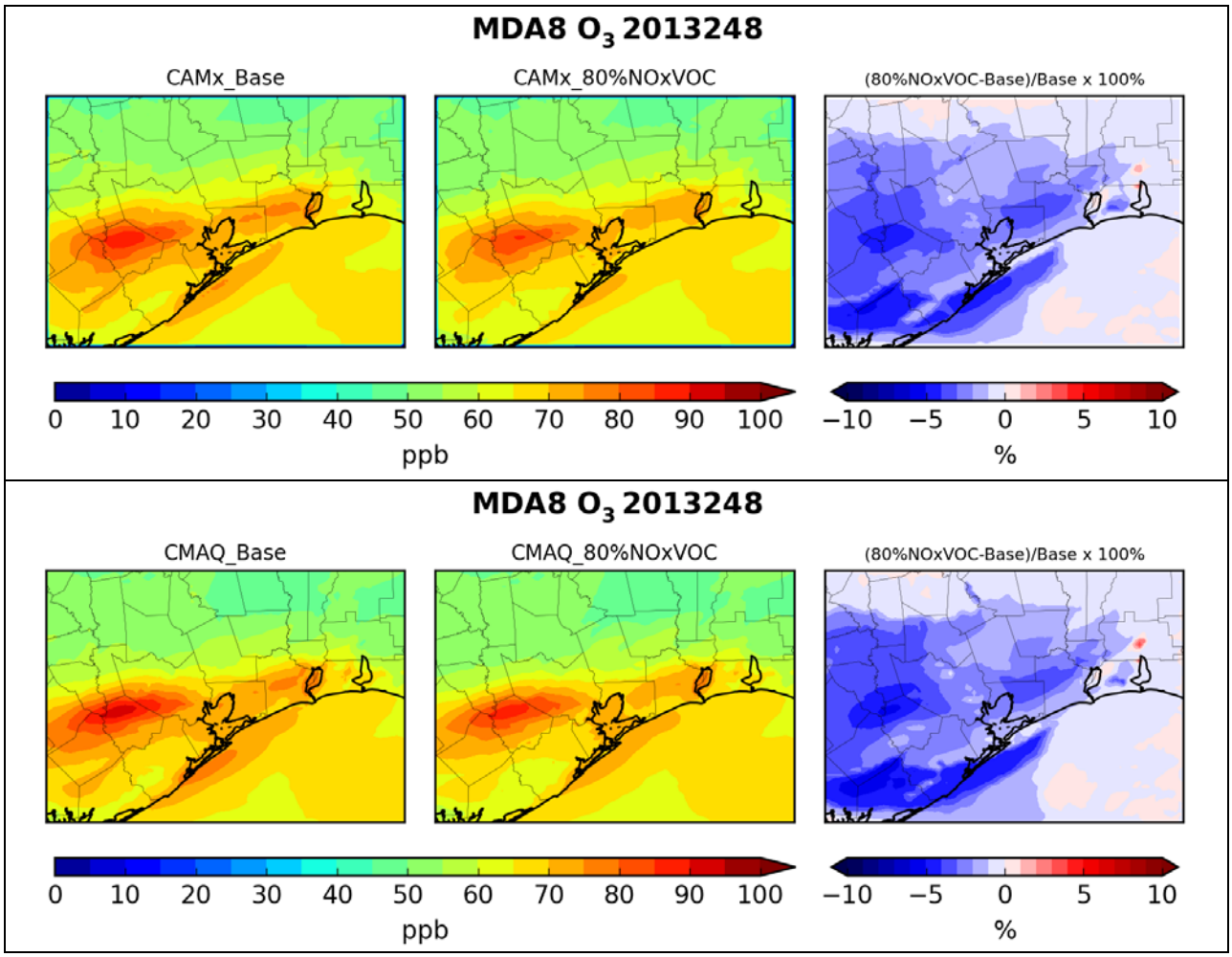

Figure 5-8. CAMx and CMAQ ozone responses to 20% NOx and VOC emission reductions on September 5, 2013.

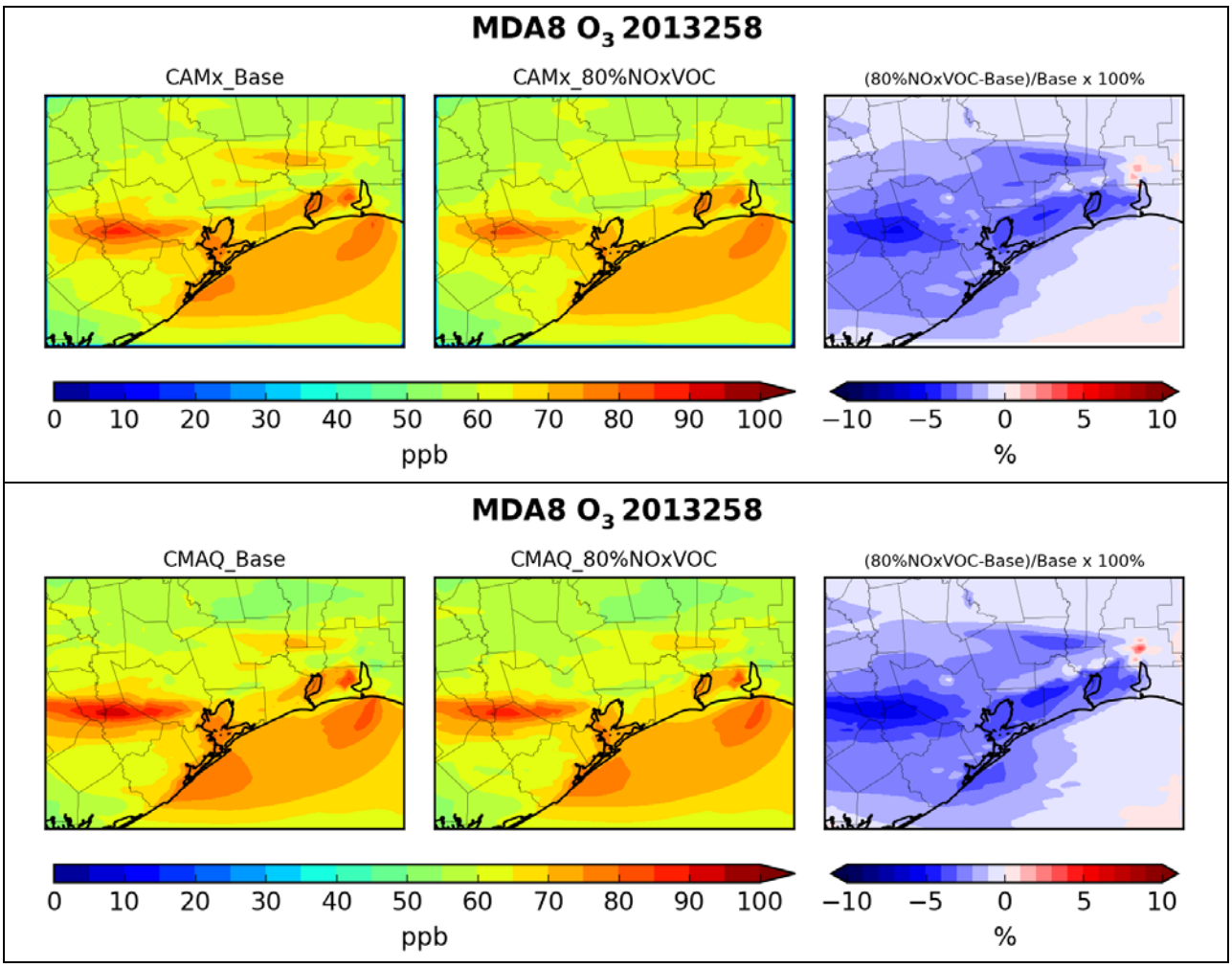

Figure 5-9. CAMx and CMAQ ozone responses to 20% NOx and VOC emission reductions on September 15, 2013.

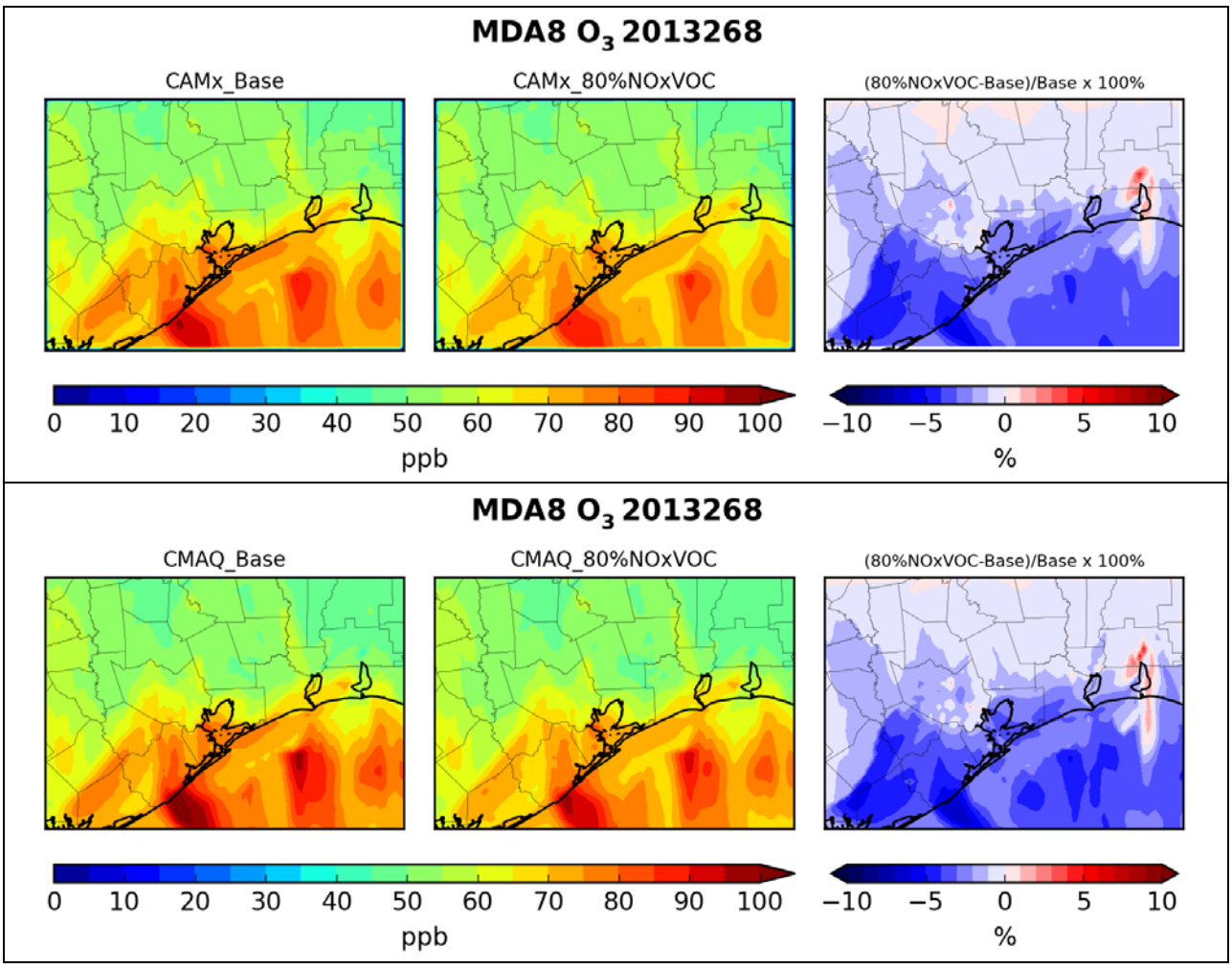

Figure 5-10. CAMx and CMAQ ozone responses to 20% NOx and VOC emission reductions on September 25, 2013.

5.2 Summary of Sensitivity Analysis

Four of the five sensitivity tests examine various aspects of photochemical modeling including photochemistry, vertical transport, and grid resolution. Ozone model performance in the Base Run and these sensitivity tests are comparable (Figure 5-11). As shown in Figure 5-12 and Figure 5-13, all simulations show very similar diurnal profiles and the differences lie on ozone peak concentrations. More stratiform cloudiness helps reduce the day-time peak concentration up to 20 ppb on some days, but the simulation is still largely biased high. The model performance of the CAMx 1.33 km simulation shows slight improvement. CMAQ Base Case shows slightly lower NMB than CAMx simulations which maybe attributable to lower predicted jNO_2.

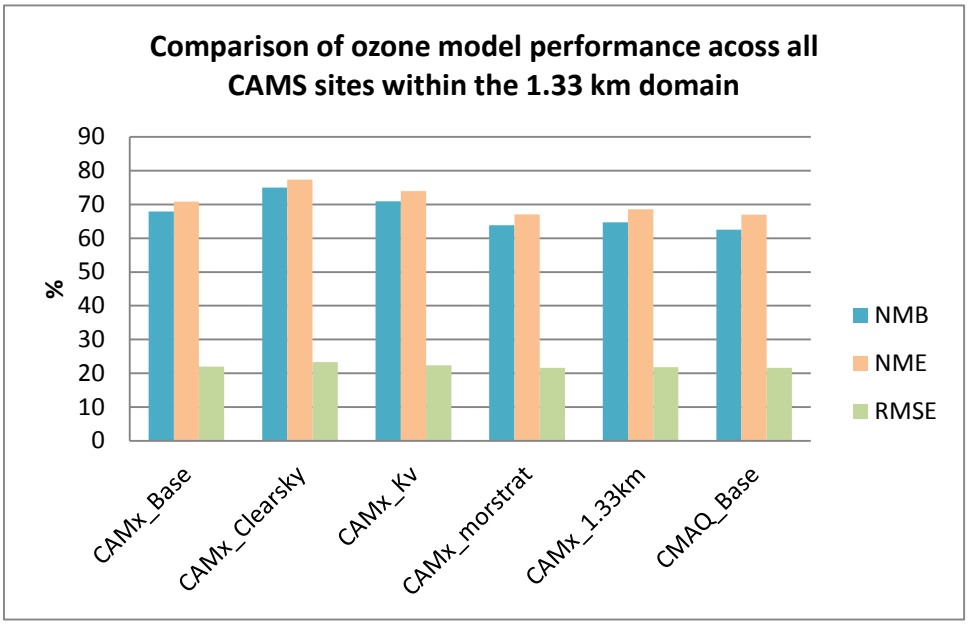

Figure 5-11. Comparison of ozone model performance across all CAMS sites within the 1.33 km domain during September 2013 period.

The clear-sky sensitivity suggests that the difference of jNO_2 is larger between the two models than that due to the effect of cloud. The discrepancy of clear-sky jNO_2 values between the two models should be further investigated. Nonetheless, predicted ozone in the HGBPA area is mostly insensitive to changes in photolysis rates and vertical diffusivity suggesting that local production is not the main contributor of high ozone bias. Modeled ozone shows persistent overestimates that are caused by other processes which are currently not well understood.

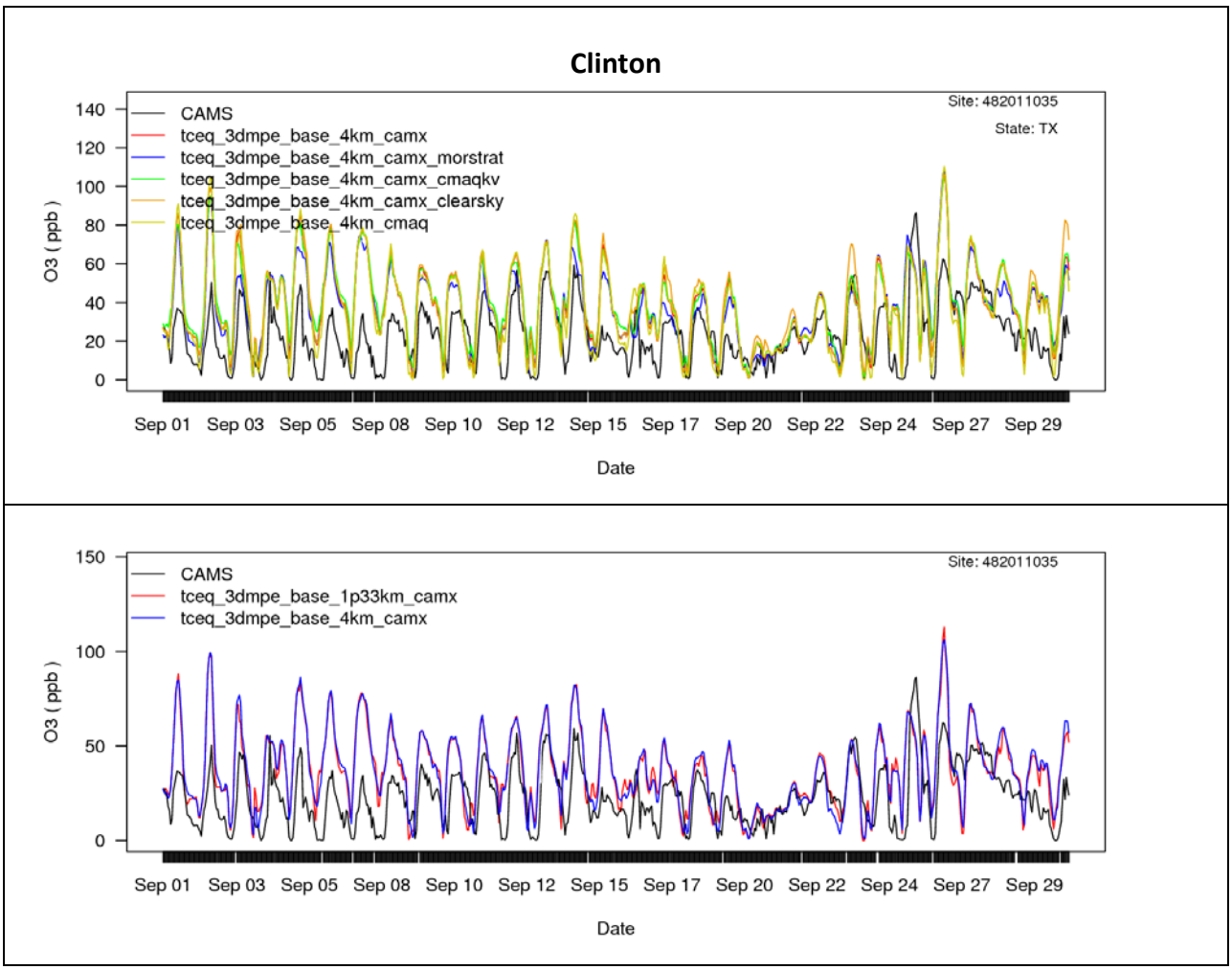

Figure 5-12. Time series of observed (black) and predicted (color) ozone concentrations (ppb) at Clinton in September 2013.

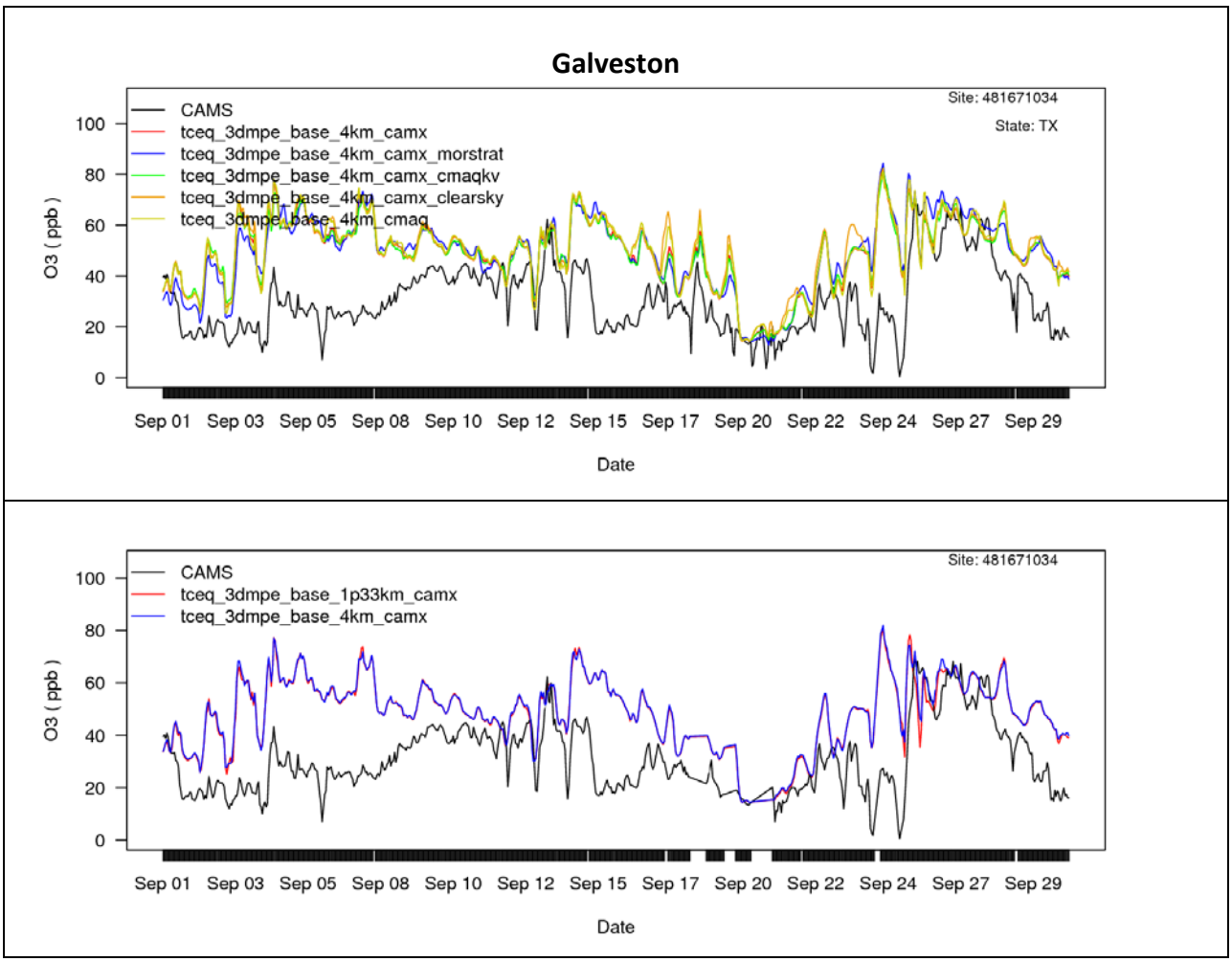

Figure 5-13. Time series of observed (black) and predicted (color) ozone concentrations (ppb) at Galveston in September 2013.

CAMx and CMAQ models show comparable ozone responses to the emission reductions. Reducing NOx and VOC anthropogenic emissions by 20% reduce monthly average MDA8 ozone in the Houston area by about 3% or 2 ppb (Figure 5-14). Ozone disbenefit is seen close to Lake Charles, LA, suggesting that the area has a different NOx/VOC-sensitive regime than in Houston.

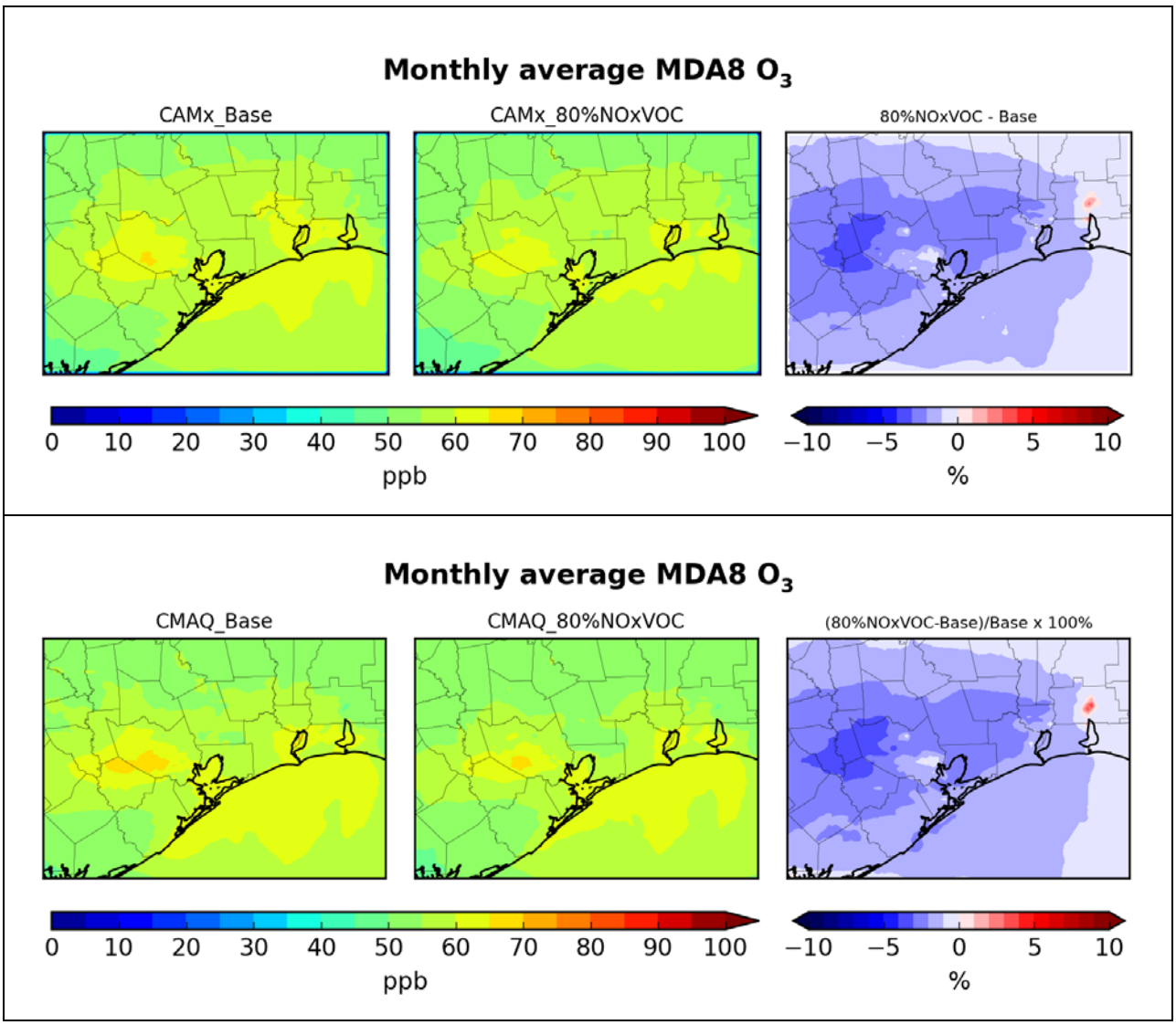

Figure 5-14. CAMx and CMAQ ozone responses to 20% NOx and VOC emission reductions based on monthly average MDA8 ozone.

6.0 CONCLUSIONS AND RECOMMENDATIONS FOR FUTURE WORK

6.1 Summary of Findings

6.1.1 Base Case

- CAMx and CMAQ predictions of maximum daily average 8-hour ozone in September 2013 are similar in spatial patterns and magnitude. The predicted average MDA8 ozone concentrations differ by less than 5 ppb across the HGBPA area. CMAQ-predicted MDA8 ozone tends to be lower around the area northeast of the Galveston Bay including Beaumont. The results in the Houston area are mixed with a tendency of higher CMAQ predictions for ozone maxima. CAMx predictions are generally lower than CMAQ along the coast (e.g., in Galveston) and in the Gulf.
- Predicted time series of $PM_{2.5}$ concentrations by CAMx and CMAQ are comparable at inland sites. Both models predicted that OA and other PM are top two major constituents in $PM_{2.5}$. CAMx predictions tend to be higher than CMAQ near the coastline on average by 3-4 ug/m^3 due to higher nitrate (PNO_3) and sea-salt sodium (Na). This discrepancy can be explained by a different methodology used to estimate and allocate sea-salt emissions.
- CAMx and CMAQ show similar model performance against surface measurements at TCEQ CAMS sites and P3-B aircraft measurements for all gaseous species examined.
    - <u>Ozone</u>: Both models over predicted surface ozone across the HGBPA area. Large ozone bias is seen during the first half of September when observed ozone is generally lower than 40 ppb. Better performance is seen on high observed ozone days (i.e., September 24-27). Compared to aircraft measurements, ozone is generally over predicted near surface (< 300 m) but under predicated above 2000 m. The models under predict ozone at all heights on September 25. This day was influenced by a frontal passage and a re-circulation of pollution due to afternoon sea-breeze. The downward mixing due to the frontal passage was replicated well by the models but the re-circulation was not captured by WRF meteorology.
    - <u>jNO_2</u>: Both models consistently over predicted jNO_2. The over prediction is expected due to under estimated clouds. Good jNO_2 performance is seen on clear-sky days (September 12, 25, and 26). However, good performance of jNO_2 does not necessary yield good ozone performance.
    - <u>NOx</u>: NO is under estimated while NO_2 is over estimated. Over estimation of NO_2 may indicate an inventory bias.
    - <u>VOC:</u> Both models tend to over predict VOC. Isoprene performance is mixed with the models' tendency to overestimate 75-percentile concentrations but reasonably replicate lower concentrations. CMAQ tends to overestimate morning peaks with values often higher than CAMx by a factor of 2). We expect that the landuse Kv patch in CAMx introduces more night-time mixing which reduces isoprene buildup from lower planetary boundary layer. Formaldehyde performance is quite good. Acetaldehyde is over predicted under 2000 m with near-ground concentrations over predicted by ~50%. Predicted acetaldehyde vertical profiles are more similar to

those of formaldehyde. In addition, high acetaldehyde events coincide with high formaldehyde and NOx events implying the same emitting sources. At surface, the models biased high on toluene but low on xylene and benzene suggesting a possible issue with VOC speciation profiles and/or overstated on-road mobile emissions. Both models do not capture potential emission events as they are not described in the emissions inventory.

- $PM_{2.5}$: EC is largely overestimated mostly likely due to overstated emissions. Sulphate, ammonium, and WSOC are underestimated. Nonetheless, CAMx estimates broadly agree with the WSOC and OC observations reported by Sheesley and Usenko (2015). The discrepancy between surface and aircraft measurements is unclear. Under-prediction of sulphate may be related to under-prediction of clouds. Since sulphate dominates inorganic component in summer, ammonium performance follows that of sulphate. CMAQ-estimated secondary PMs are all lower than CAMx. With the primary PM being overstated and the secondary PM being underestimated, it is less meaningful to examine $PM_{2.5}$ mass performance due to compensation effects among PM species.

6.1.2 Sensitivity Tests

- The initial CAMx 36/12 km simulation shows consistent high ozone bias at CASTNET sites, especially in the south eastern US. Sensitivity tests for the CAMx 36/12 km domains suggest that capping ozone from boundary conditions only slightly impact ozone performance. Reducing the transmission of solar radiation threshold helps reduce the over estimation of ozone during peak hours by 10-20 ppb near the coastal site, but worsens ozone performance further inland.
- Four of the five sensitivity tests examine various aspects of photochemical modeling including photochemistry, vertical transport, and grid resolution. All simulations show very similar diurnal profiles and the differences lie on ozone peak concentrations.
- Due to limited clouds predicted by WRF, even when both models diagnose sub-grid clouds, the adjusted jNO_2 is comparable to clear-sky jNO_2. CMAQ appears to be slightly more responsive to the cloud adjustment than CAMx.
- More stratiform cloudiness helps reduce the day-time peak concentration up to 20 ppb on some days, but the simulation is still largely biased high.
- The model performance of the CAMx 1.33 km simulation shows slight improvement.
- CAMx and CMAQ models show comparable ozone responses to 20% NOx and VOC emission reductions. On days with high predicted ozone concentrations in Houston (> 60 ppb), the emission reductions lower the MDA8 ozone up to 4% (3-4 ppb). Slightly larger ozone reductions are seen downwind in the west of Houston. Ozone disbenefit is seen close to Lake Charles, LA, suggesting that the area has a different NOx/VOC-sensitivity regime than in Houston. Ozone disbenefit in the Houston area occurs on days with low predicted ozone concentrations.

6.2 Conclusions

Below, we present conclusions drawn from the results of this study:

- Modeling inputs are most critical in any photochemical modeling exercise. When using the same inputs and similar chemistry mechanism (CB6r2 versus CB6r3), CAMx and CMAQ show very comparable model performance despite some differences in modeling processes (e.g., nighttime mixing, photolysis rates).
- The cause of high ozone bias is unresolved. While high ozone events, such as those on September 24-26, are related to frontal passages and re-circulation of sea-breeze, ozone predictions on other September days are likely influenced by continental transport or background ozone. Most days in September 2013 HGBPA area was influenced by easterly winds bringing air parcels from Louisiana and up-wind locations. Based on the back-trajectory analysis, the models could reasonably replicate the easterly wind direction with some exceptions. The tendency of the CAMx model to overestimate ozone in the south eastern US could partly attribute to the high ozone bias in the HGBPA area given the easterly wind directions. This is supported by the examination of ozone at an upwind and a downwind monitor which suggests reasonable predictions of local ozone production. Other possible explanations are too low marine boundary layers simulated by the models or missing removal processes.

6.3 Recommendations

- Accurate meteorological data is critical for accurate ozone prediction in the Houston area. Biases in the WRF model's simulation of clouds, wind direction, and wind speed introduce bias into the ozone prediction. Improvements to the WRF model treatment of clouds and sea-breeze re-circulation will enable the photochemical models to better estimate local production of ozone.
- Large discrepancy of the clear-sky jNO_2 estimated by CAMx and CMAQ should be further investigated. We also recommend a sensitivity test that approximates an upper-bound of cloud and aerosol adjustment in the Houston area.
- Despite a plume-in-grid feature in CAMx, CMAQ predicted higher peak NO_2 concentrations. Further examination on elevated source processes such as plume-rise treatment is recommended.
- CAMx and CMAQ overestimate several VOC at CAMS sites and along flight tracks. This likely indicates a bias in emissions inventory especially from those HRVOC sources that contribute to aldehydes. We recommend additional tests of different HRVOC sensitivity emissions in the Houston area.
- Beaumont monitors have the worst performance with modeled mean values more than doubling observational values. Since NOx emissions from refineries dominate mobile sources in this area, it may indicate a point source inventory bias.
- Future ozone modeling exercises for the Houston area should include halogen chemistry and explore other possible removal processes specific to the coastal conditions.

7.0 REFERENCES

Chang, J.S., R.A. Brost, I.S.A. Isaksen, S. Madronich, P. Middleton, W.R. Stockwell, and C.J, Walcek. 1987. A Three-dimensional Eulerian Acid Deposition Model: Physical Concepts and Formulation. *J. Geophys. Res.*, **92**, 14,681-14,700.

de Leeuw, G, Neele, F.P., Hill, M., Smith, M.H., and Vignati, E. 2000. Production of sea spray aerosol in the surf zone. J. Geophys. Res. V105, pp. 29,397-29,409.

Del Genio, A.D., M.S. Yao, W. Kovari, K.K.W. Lo. 1996. A prognostic cloud water parameterization for global climate models. *J. Climate*, **9**, 270-304.

Dolwick, P. 2006. "The Effects of Cloud Attenuation on Air Quality: A Comparison of Model Treatments." Presented at the 2006 Annual Conference of the American Meteorological Society.

Emery, C., E. Tai, and G. Yarwood. 2001. Enhanced Meteorological Modeling and Performance Evaluation for Two Texas Episodes. Prepared for the Texas Natural Resources Conservation Commission, by ENVIRON, International Corp, Novato, CA.

Emery, C., J. Jung, J. Johnson, G. Yarwood, S. Madronich, G.Grell. 2010. Improving the Characterization of Clouds and their Impact on Photolysis Rates within the CAMx Photochemical Grid Model. Prepared for the Texas Commission on Environmental Quality, Austin, TX. Prepared by ENVIRON International Corporation, Novato, CA (August 27, 2010).

ENVIRON. 2011. "Dallas-Fort Worth Modeling Support: Improving the Representation of Vertical Mixing Processes in CAMx, Final Report." Prepared for the Texas Commission on Environmental Quality, Austin, TX. WO 582-11-10365-FY11-02. August.

ENVIRON. 2012. "Dallas-Fort Worth Modeling Support: Improving Vertical Mixing, Plume-in-Grid, and Photolysis Rates in CAMx, Final Report." Prepared for the Texas Commission on Environmental Quality, Austin, TX. WO 582-11-10365-FY12-06. August.

ENVIRON and ERG. 2013. Technical Support Document: Photochemical Modeling for the Louisiana 8-Hour Ozone State Implementation Plan. Prepared for the Louisiana Department of Environmental Quality, Office of Environmental Services, Air Permits Division, Baton Rouge, LA. Prepared by ENVIRON International Corporation, Novato, CA and Eastern Research Group, Inc., Rancho Cordova, CA (in progress).

EPA. 2014. Draft Modeling Guidance for Demonstrating Attainment of Air Quality Goals for ozone, PM2.5, and Regional Haze, USEPA Office of Air Quality and Planning Standards, Research Triangle Park, NC, December.

Gong, S. L., 2003. A parameterization of sea-salt aerosol source function for sub- and super-micron particles. Global Biogeochemical Cycles 17: 1097-1104.

Guenther, A. B., X. Jiang, C. L. Heald, T. Sakulyanontvittaya, T. Duhl, L. K. Emmons, and X. Wang, 2012. The Model of Emissions of Gases and Aerosols from Nature version 2.1 (MEGAN2.1): an extended and updated framework for modeling biogenic emissions, Geosci. Model Dev., 5(6), 1471-1492.

Heather, S., K.R. Baker, S. Phillips. 2012. Compilation and interpretation of photochemical model performance statistics published between 2006 and 2012. Atmospheric Environment 61, 124-139.

Johnson, J., E. Tai, P. Karamchandani, G. Wilson, and G. Yarwood, 2013. TCEQ Ozone Forecasting System. Prepared for Mark Estes, TCEQ. November.

Johnson, J., G. Wilson, DJ Rasmussen, and G. Yarwood. 2015. Daily Near Real-Time Ozone Modeling for Texas. Prepared for Mark Estes, TCEQ. January.

Johnson, J., G., Wilson, DJ, Rasmussen, G. Yarwood. 2015. Daily Near Real-Time Ozone Modeling for Texas. WO 582-11-10365-FY14-16 Final Report, prepared for TCEQ. January.

Kemball-Cook, S.R., Y. Jia, R. C. Emery, R. Morris. 2005. "Alaska MM5 Modeling for the 2002 Annual Period to Support Visibility Modeling." Prepared for the Western Regional Air Partnership, Denver CO. September.

Kembell-Cook S., J., Jung, J., Johnson, L, Ziu, G. Yarwood. 2015. Improved Land Cover and Emission Factor Inputs for Estimating Biogenic Isoprene and Monoterpene Emissions for Texas Air Quality Simulations. Final report. Air Quality Research Program (AQRP) Project 14-016.

Lee, P., H.-C. Kim, and F. Ngan, 2012. Investigation of nocturnal surface wind bias by the Weather Research and Forecasting (WRF)/ Advanced Research WRF (ARW) meteorological model for the Second Texas Air Quality Study (TexAQS-II) in 2006. Report prepared for TCEQ by NOAA-ARL, Silver Spring, MD.

Morris G.A., B., Lefer. 2014. Ozonesonde launches from the University of Houston and Smith Point, Texas in support of DISCOVER AQ. Final Report. Air Quality Research Program (AQRP) Project 12-016

O'Brien, J. 1970. "A Note on the Vertical Structure of the Eddy Exchange Coefficient in the Planetary Boundary Layer." Journal of the Atmospheric Sciences, 27, 1213-1215.

Scheff P. A., Wadden R. A., Bates B. A., and Aronian P. F. 1989 Source Fingerprints for Receptor Modeling of Volatile Organics. Journal Air Pollution Control Association 39

Sheesley R.J, S., Usenko. 2015. DISCOVER-AQ Houston as a case study for understanding spatial and temporal trends in urban particulate matter. Presentation. Air Quality Research Program (AQRP) Project 14-029. [http://aqrp.ceer.utexas.edu/files/AQRP%20WS%2006-17-15/14-029%20Sheesley_aqrp_June_2015_v7_rjs.pdf]

Skamarock, W. C., J. B. Klemp, J. Dudhia, D. O. Gill, D. M. Barker, W. Wang, and J. G. Powers, 2008. A description of the Advanced Research WRF Version 3. NCAR Tech Notes-475+STR. http://www.mmm.ucar.edu/wrf/users/docs/arw_v3.pdf.

Smith, M.H., Harrison, N. M. 1998. The Sea Spray Generation Function. Journal of Aerosol Science 29(Suppl I): S189-S190.

Tesche, T.W., D.E. McNally, C.A. Emery, E. Tai. 2001. "Evaluation of the MM5 Model Over the Midwestern U.S. for Three Oxidant Episodes." Prepared for the Kansas City Ozone Technical Workgroup, by Alpine Geophysics, LLC, Ft. Wright, KY, and ENVIRON International Corp, Novato, CA.

Voulgarakis, A., O. Wild, N.H. Savage, , G.D. Carver, J.A. Pyle. 2009a. Clouds, photolysis and regional tropospheric ozone budgets. *Atmos. Chem.. Phys.*, **9**, 8235-8246.

Voulgarakis, A., N.H. Savage, O. Wild, G.D. Carver, K.C. Clemitshaw, J.A. Pyle. 2009b. Upgrading photolysis in the p-TOMCAT CTM: model evaluation and assessment of the role of clouds. *Geoscientific Model Development*, **2**, 59-72.

APPENDIX A

Spatial Plots of Maximum Daily Average 8-hour Ozone Concentrations

Appendix A. Spatial Plots of Maximum Daily Average 8-Hour Ozone Concentrations

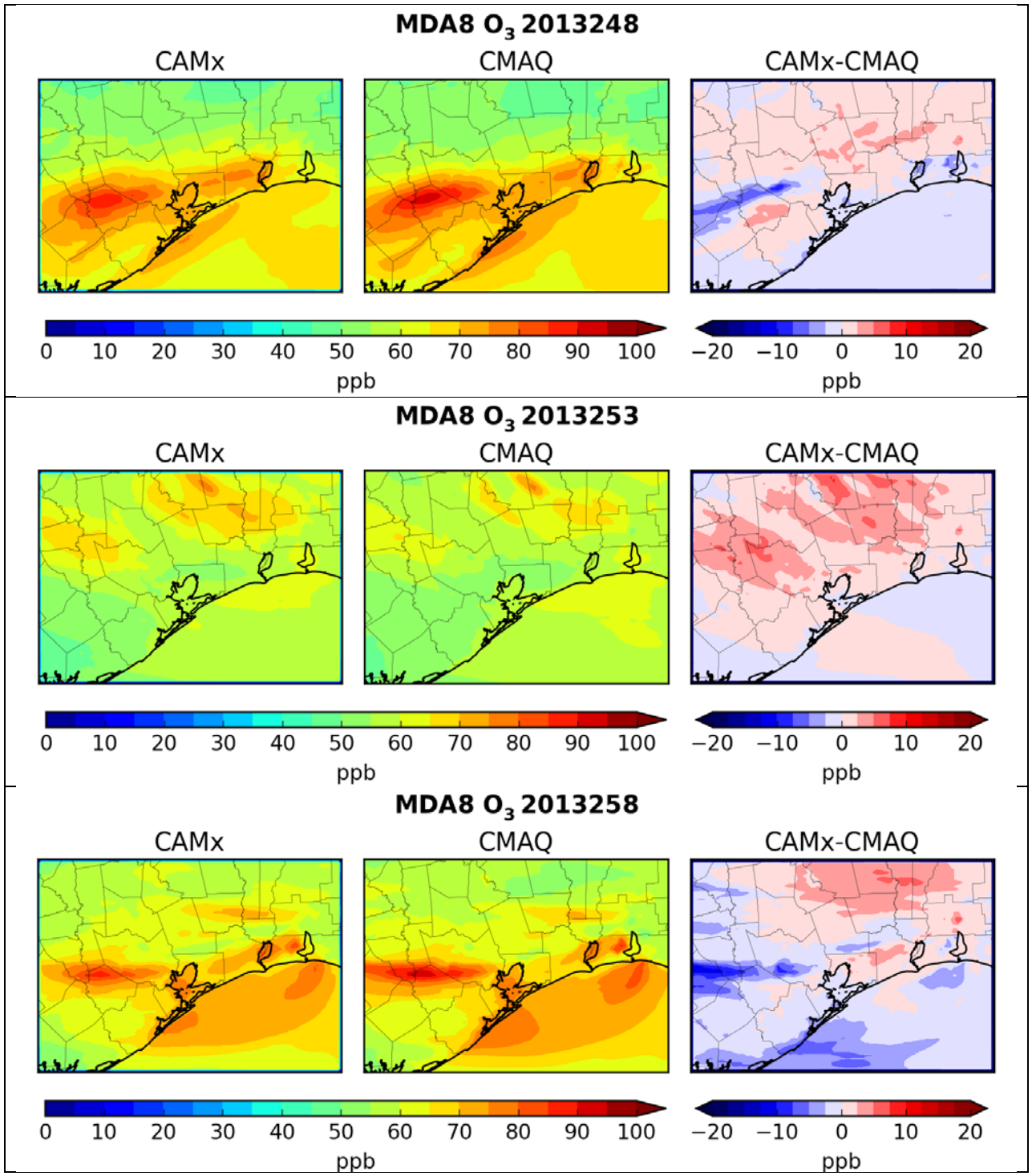

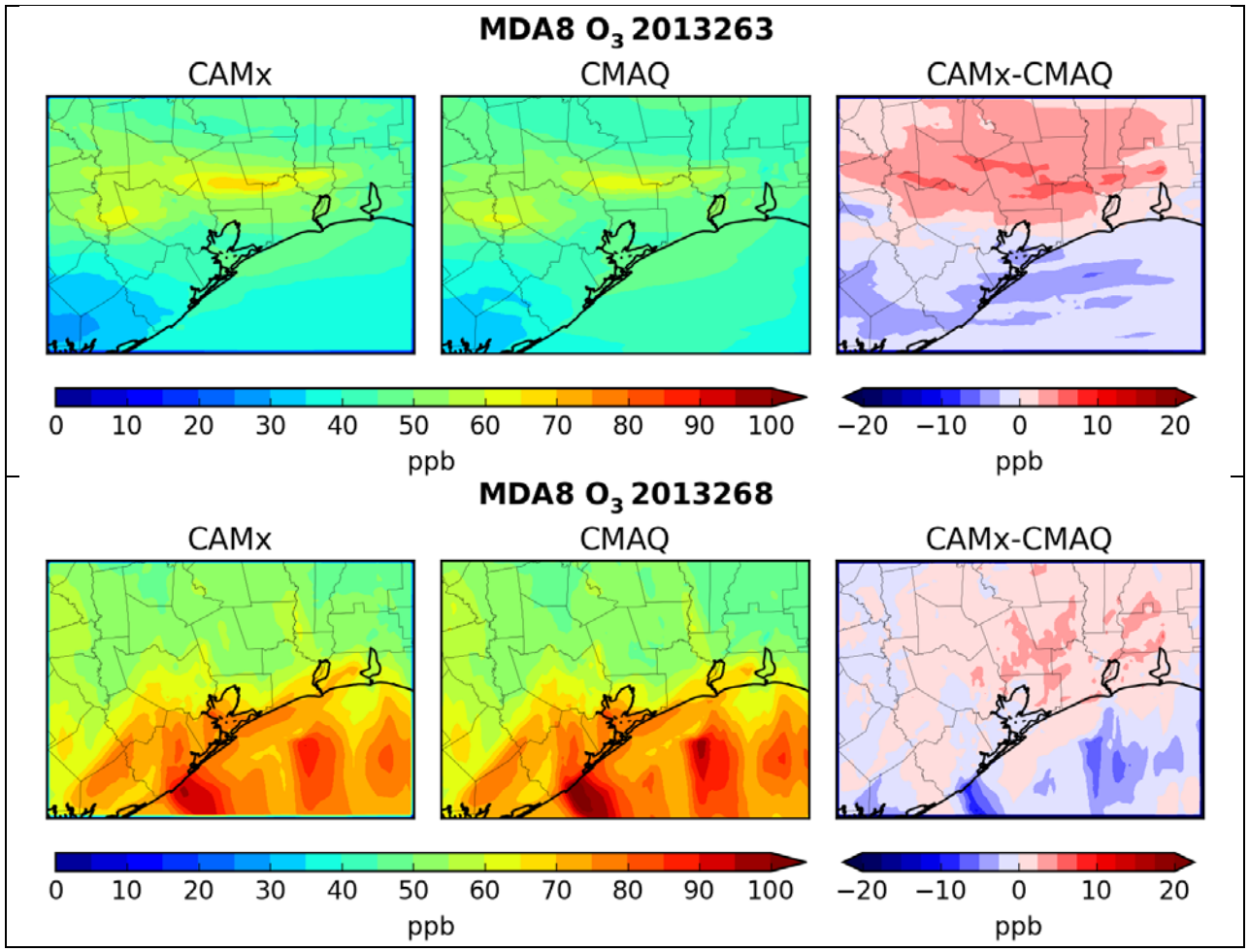

Figure A-1. Maps of daily maximum 8-hour ozone in the 4 km domain from CAMx (left), CMAQ (middle) and the differences between CAMx and CMAQ results (right) on Sep 5, 10, 15, 20, and 25.

APPENDIX B

Performance Evaluation of the 36/12 km CAMx Simulation

Appendix B. Model Performance Evaluation of the 36/12 km CAMx Simulation

An initial CAMx 36/12 km simulation and subsequent sensitivity simulations were compared against surface measurements at the Clean Air Status and Trends Network (CASTNet) sites (Figure B-1). The model evaluation conducted focuses primarily on the operational model evaluation of the CAMx model performance with respect to ozone.

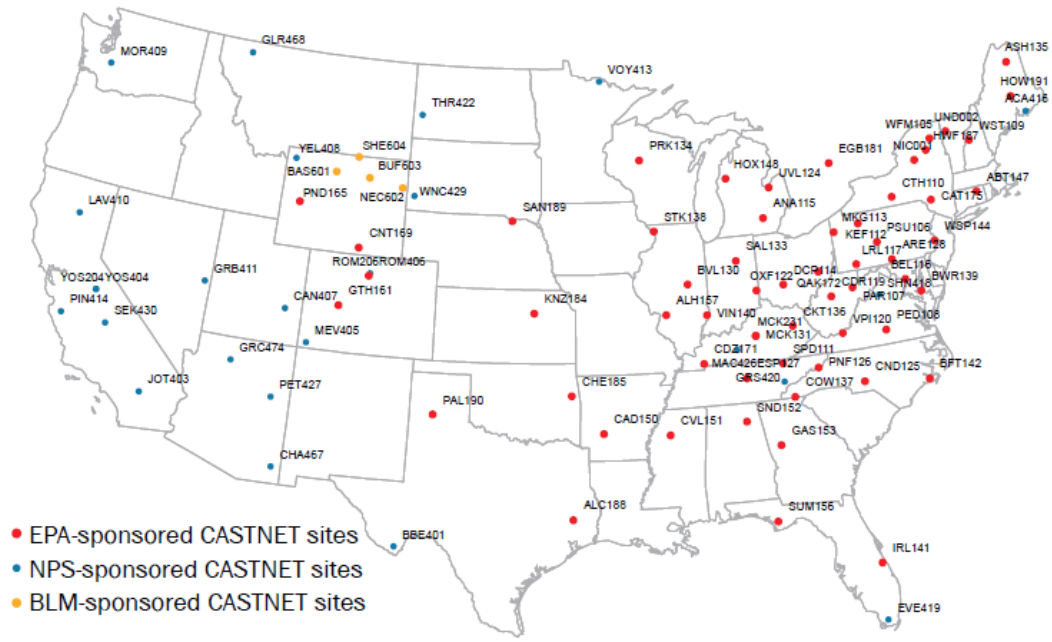

Figure B-1. Location of CASTNet monitoring sites. EPA figure [1].

Model Performance Evaluation (MPE)

The 36 km results for the September 2013 period were examined first. The performance evaluation used an observed ozone concentration cutoff threshold of 40 ppb. Spatial plots of the normalized mean bias and error for individual monitors are shown in Figures B-2. Overall, the model predictions for ozone are biased high but NMB is still within 20% and NME is generally lower than 25%. Without a threshold applied, NMB and NME are more than 50% for multiple sites in the Eastern US, especially those near the coast (Figure B-3). Ozone time series at Sumatra (SUM156) in Florida shows that the observed ozone is commonly lower than 40 ppb (Figure B-4). Using a threshold would screen out most of the data points and result in less meaningful statistics. Discussions below describe our performance evaluation without any threshold applied.

Among the three CASTNET sites in Texas- namely, Alabama-Coushatta (ALC188), Big Bend NP (BBE401), Palo Duro (PAL190)- ALC188 has the poorest ozone performance. Except for the September 24-26 period, the model over predicted both day-time and night-time ozone as

[1] http://epa.gov/castnet/javaweb/docs/CASTNET_Factsheet_2013.pdf

large as 50 ppb (Figure B-5). Better performance is seen at BBE401, but the peaks are still over estimated up to 30 ppb in the first half of September. In contrary, CAMx under predicted ozone at PAL190 (NMB = -3%) which is located further inland compared to the other two sites. Ozone over prediction close to the coast may suggest over estimated ozone from boundary conditions. Finer model grid resolution (i.e., 12 km) only improves model performance slightly.

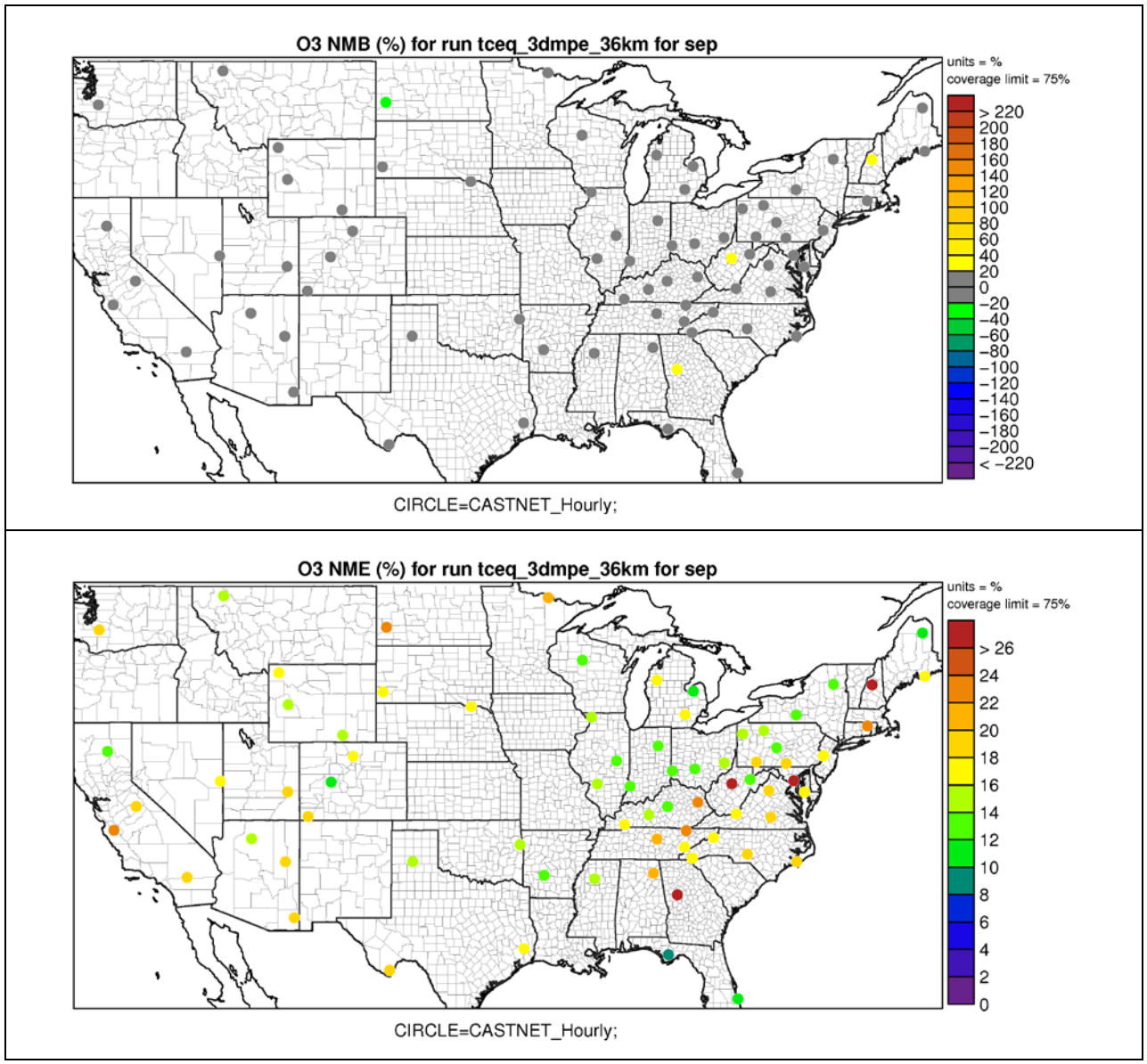

Figure B-2. Normalized Mean Bias (%; top) and Error (%;bottom) of ozone above 40 ppb threshold during September 2013 at CASTNET monitoring sites in the 36 km domain.

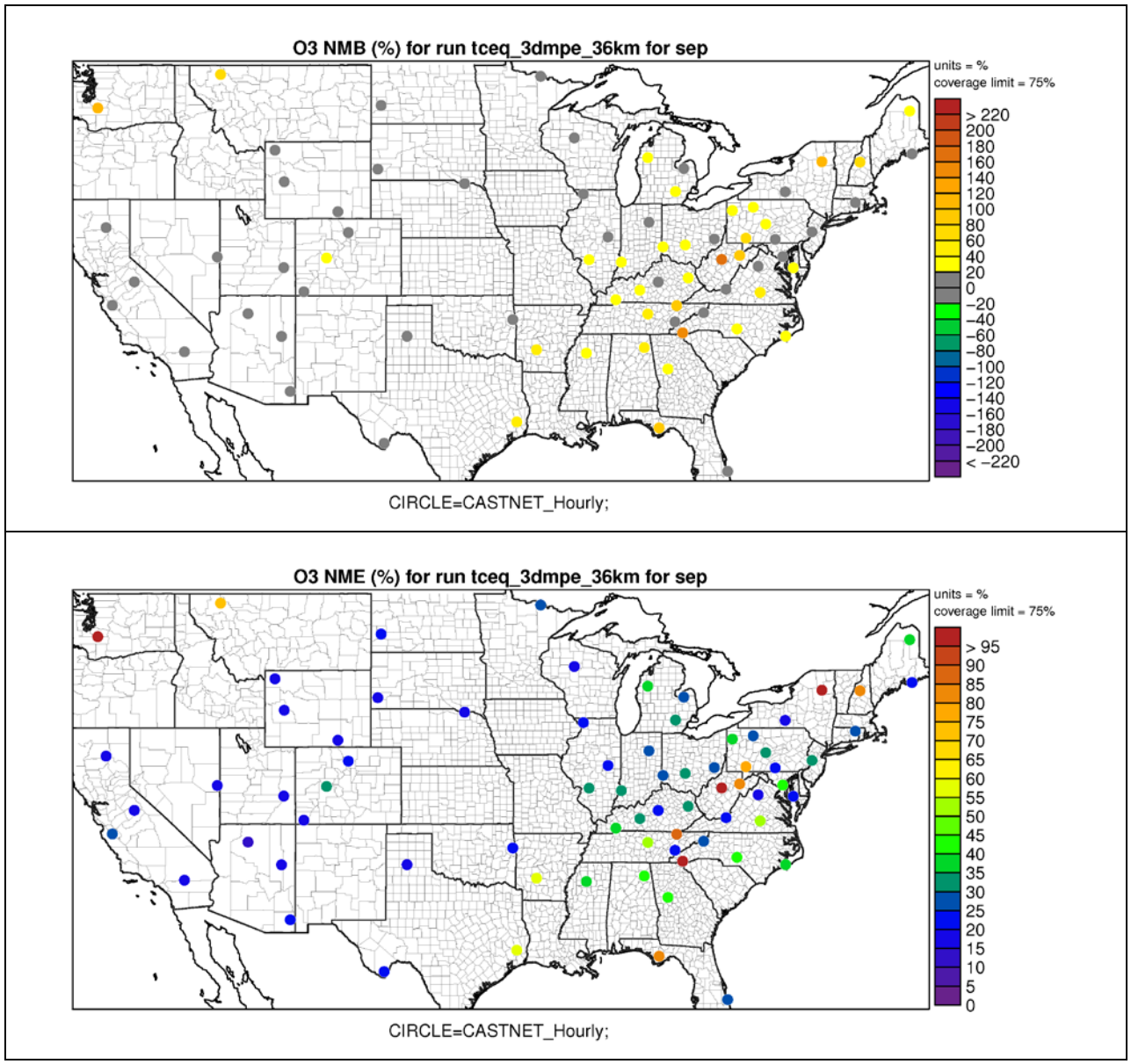

Figure B-3. Normalized Mean Bias (%; top) and Error (%;bottom) of ozone with no threshold applied during September 2013 at CASTNET monitoring sites in the 36 km domain.

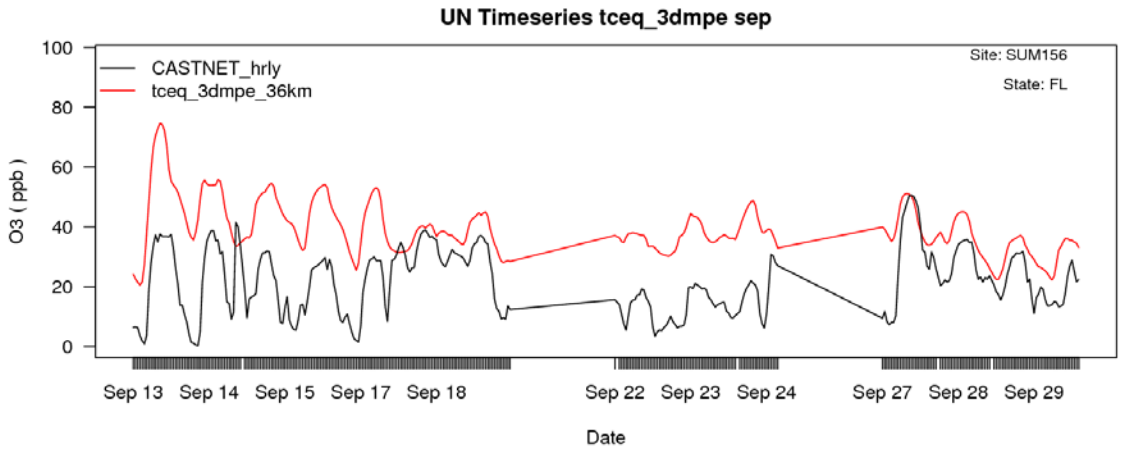

Figure B-4. Time series of observed (black) and predicted (red) ozone at Sumatra site (FL) in September 2013.

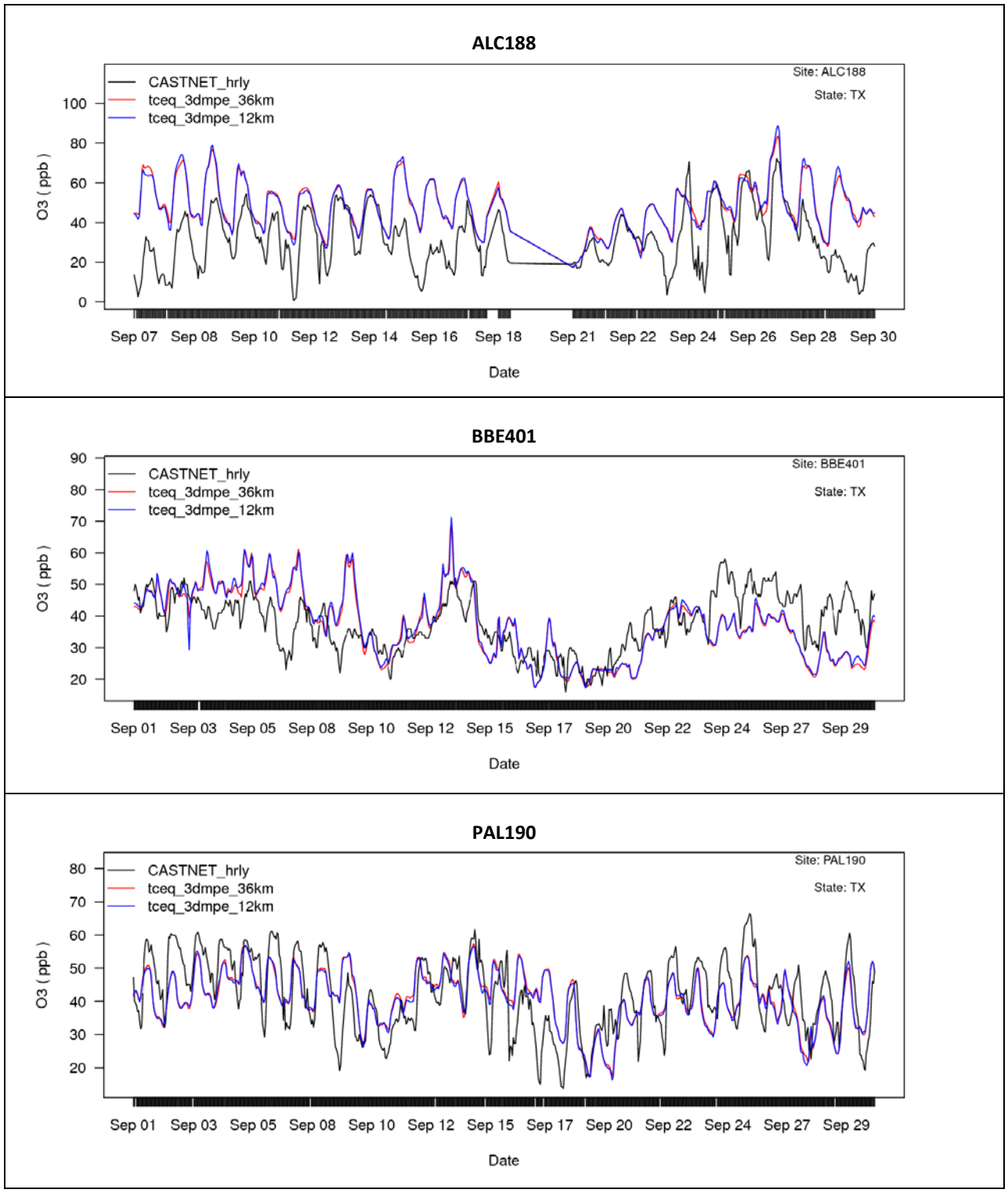

Figure B-5. Time series of observed (black) and predicted (36 km/12 km; red/blue) ozone at Alabama-Coushatta (top), Big Bend NP (middle), and Palo Duro (bottom) in September 2013.

Sensitivity Tests

Ramboll ENVIRON selected three sensitivity tests to investigate potential improvements and measure impacts of different model configurations and inputs, by comparing the results of the sensitivity tests with the initial CAMx simulation. All of the sensitivity tests conducted at the 36 and 12 km resolution are designed with the goal of finding potential sources of persistent ozone over-predictions in the south eastern US. The first CAMx sensitivity test reduced isoprene emissions from the MEGAN biogenic emissions model by a factor of two following an improvement introduced in the Near Real-Time ozone modelling (Johnson et al., 2013). This sensitivity shows relatively small ozone improvements (Figure B-6 compared to Figure B-2).

The next CAMx sensitivity simulation capped ozone from boundary conditions over the Gulf of Mexico at 20 ppb. The cap is applied from layer 1 through layer 23 (i.e., below ~5000 m). Our initial CAMx simulation already applied a flat 15 ppb ozone reduction over the Gulf of Mexico and Atlantic Ocean in order to deplete the ozone coming onshore. We wanted to determine if a further reduction in ozone from boundary conditions would reduce ozone over-predictions. This sensitivity shows negligible changes to surface ozone and model performance (Figure B-7).

The last CAMx sensitivity simulation reduced maximum transmission threshold in CAMx from 1.0 to 0.5. The value of 1.0 reflects no cloud condition which permits 100% transmission of solar radiation. In the case that WRFCAMx suggests a transmission factor higher than 0.5, the factor is reset to 0.5. There is no change if the transmission factor is lower than 0.5. This sensitivity shows significant improvement of ozone performance in the south eastern US. Ozone during peak hours are reduced by 10-20 ppb at many sites near the coast, such as at ALC188 (Figure B-9 top). However, the sensitivity degraded ozone performance at many sites further inland (Figure B-9 bottom) which may imply over-simplification of our methodology. Perhaps the sensitivity test merely emphasizes a challenge in accurately replicating clouds near the coast. Poor representation of cloud in the model can introduce over prediction of ozone. Since the focus of this study is in the Houston area, we implemented this change in the 36/12km Base Case simulation.

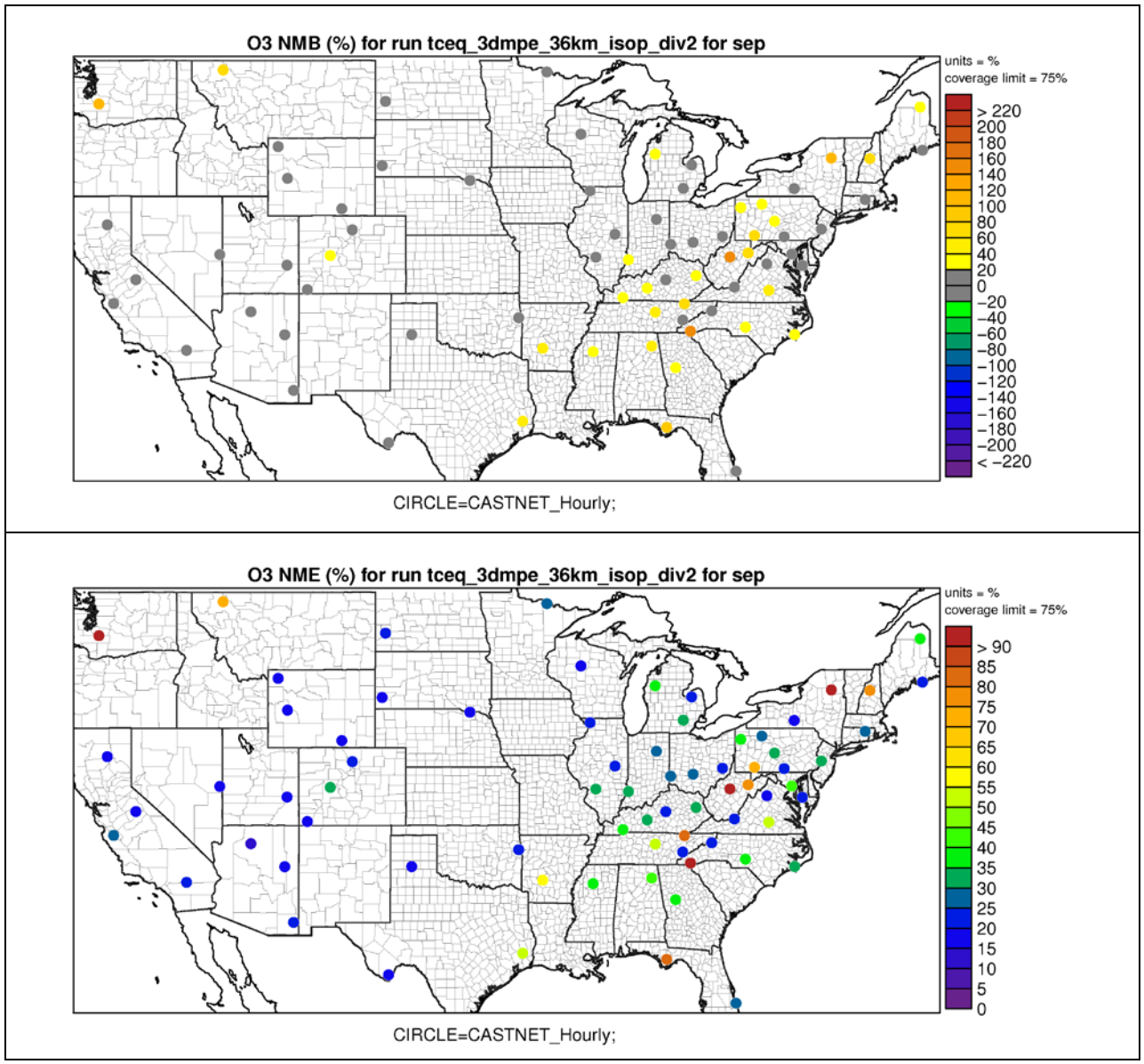

Figure B-6. Normalized Mean Bias (%; top) and Error (%;bottom) of ozone during September 2013 from the isoprene sensitivity test at CASTNET monitoring sites in the 36 km domain .

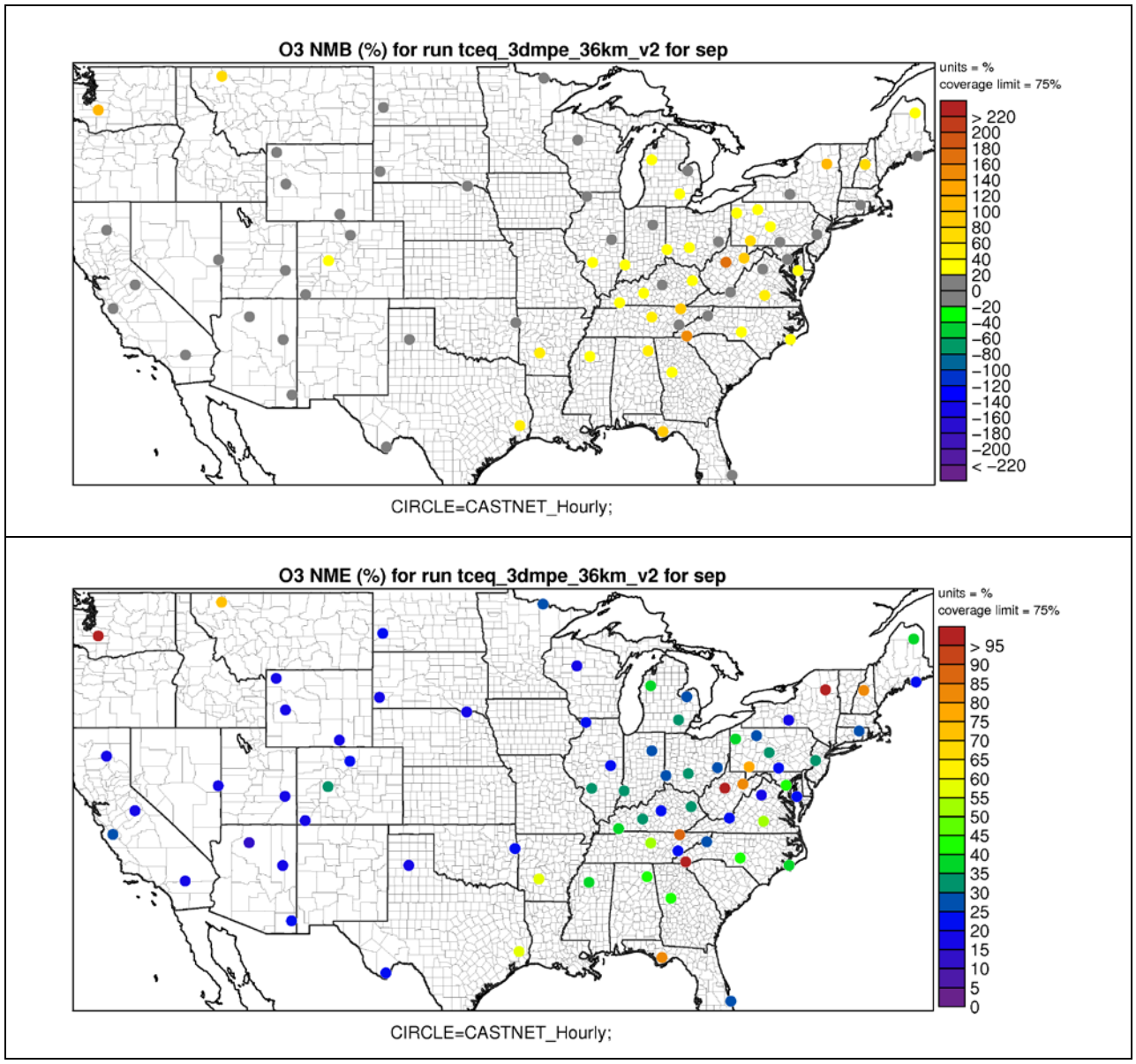

Figure B-7. Normalized Mean Bias (%; top) and Error (%;bottom) of ozone during September 2013 from the BCs sensitivity test at CASTNET monitoring sites in the 36 km domain.

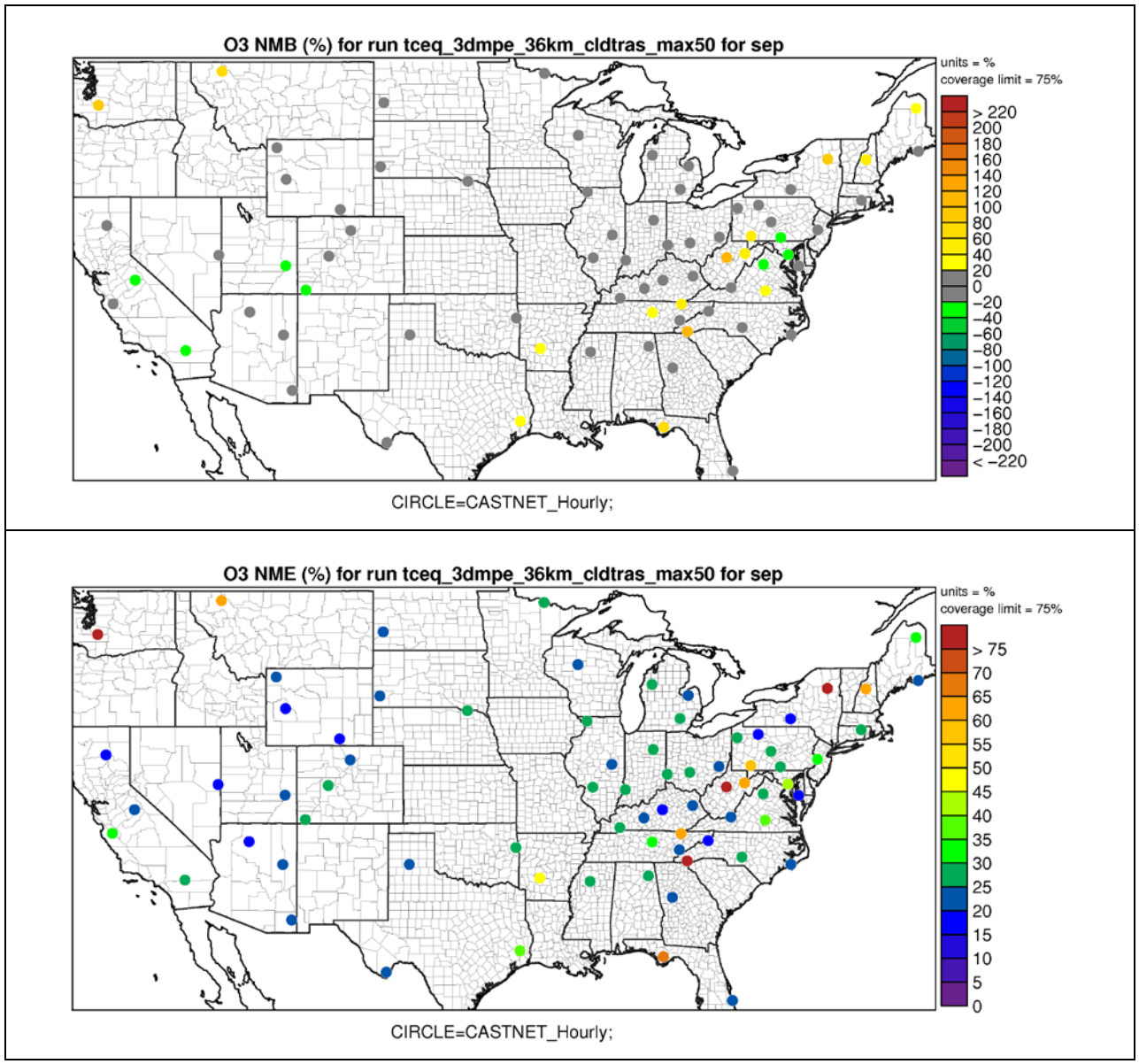

Figure B-8. Normalized Mean Bias (%; top) and Error (%;bottom) of ozone during September 2013 from the transmission sensitivity test at CASTNET monitoring sites in the 36 km domain.

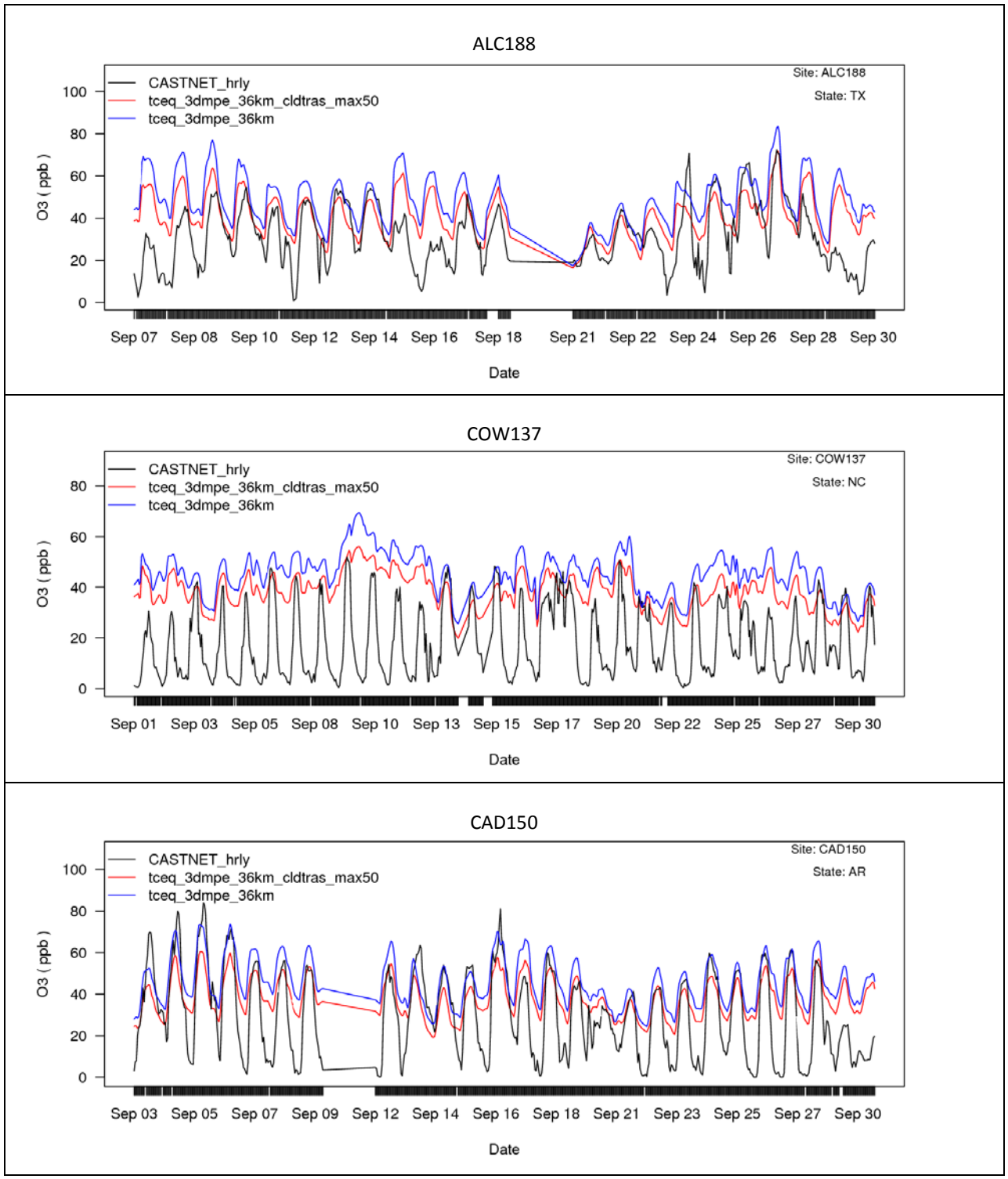

Figure B-9. Time series of observed (black) and predicted (initial run/transmission sensitiviy; blue/red) ozone at Alabama-Coushatta (top), Coweeta, (*middle*), and Caddo Valley (bottom) in September 2013.

Summary

The initial CAMx 36/12 km simulation shows consistent high ozone bias at CASTNET sites, especially in the south eastern US. Sensitivity tests suggest that reducing biogenic isoprene emissions by a factor of two or capping ozone from boundary conditions only slightly impact ozone performance. Reducing the transmission threshold helps reduce the over estimation of ozone during peak hours by 10-20 ppb near the coastal site, but worsens ozone performance further inland. Given the focused area of this study, we implemented the change to biogenic isoprene and transmission threshold for the final 36/12 km Base Case.

References

Johnson, J., E. Tai, P. Karamchandani, G. Wilson, and G. Yarwood, 2013. TCEQ Ozone Forecasting System. Prepared for Mark Estes, TCEQ. November.

APPENDIX C

Time Series of Observed and Predicted Ozone at TCEQ CAMS Sites in September 2013

Appendix C. Time Series of Observed and Predicted Ozone at TCEQ CAMS Sites in September 2013

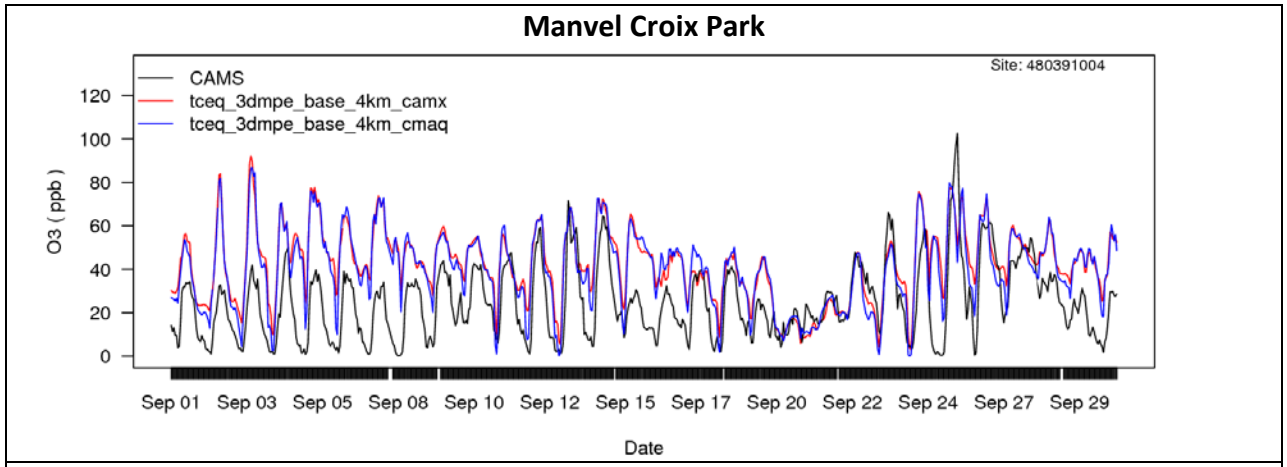

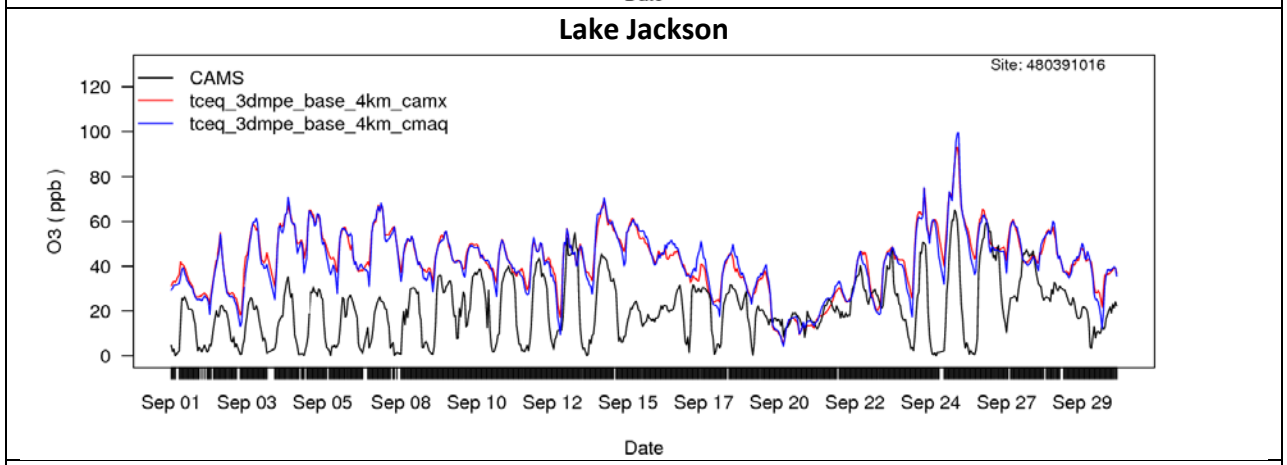

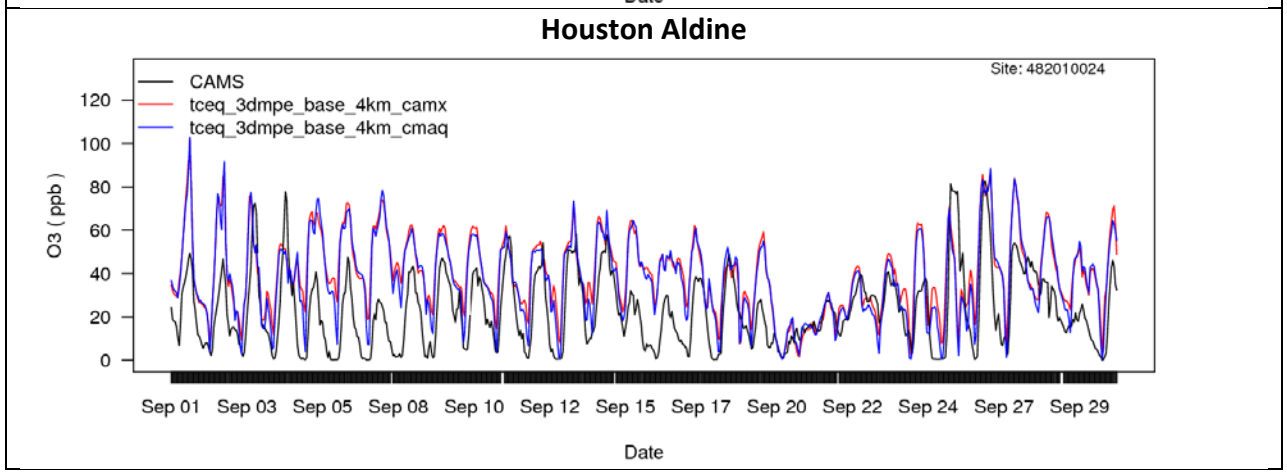

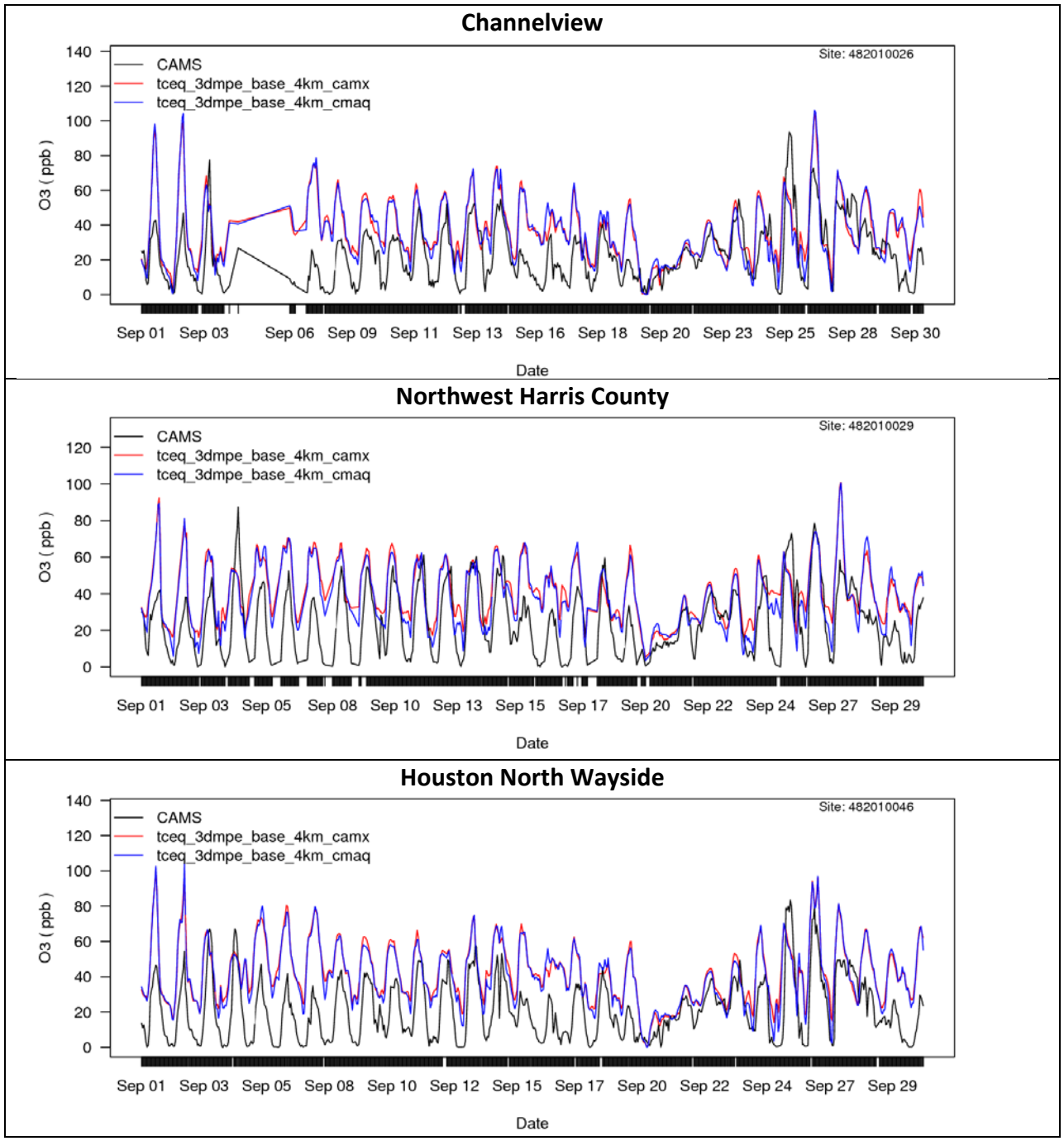
Channelview
Site: 482010026
CAMS
tceq_3dmpe_base_4km_camx
tceq_3dmpe_base_4km_cmaq
O3 (ppb)
Date
Northwest Harris County
Site: 482010029
CAMS
tceq_3dmpe_base_4km_camx
tceq_3dmpe_base_4km_cmaq
O3 (ppb)
Date
Houston North Wayside
Site: 482010046
CAMS
tceq_3dmpe_base_4km_camx
tceq_3dmpe_base_4km_cmaq
O3 (ppb)
Date

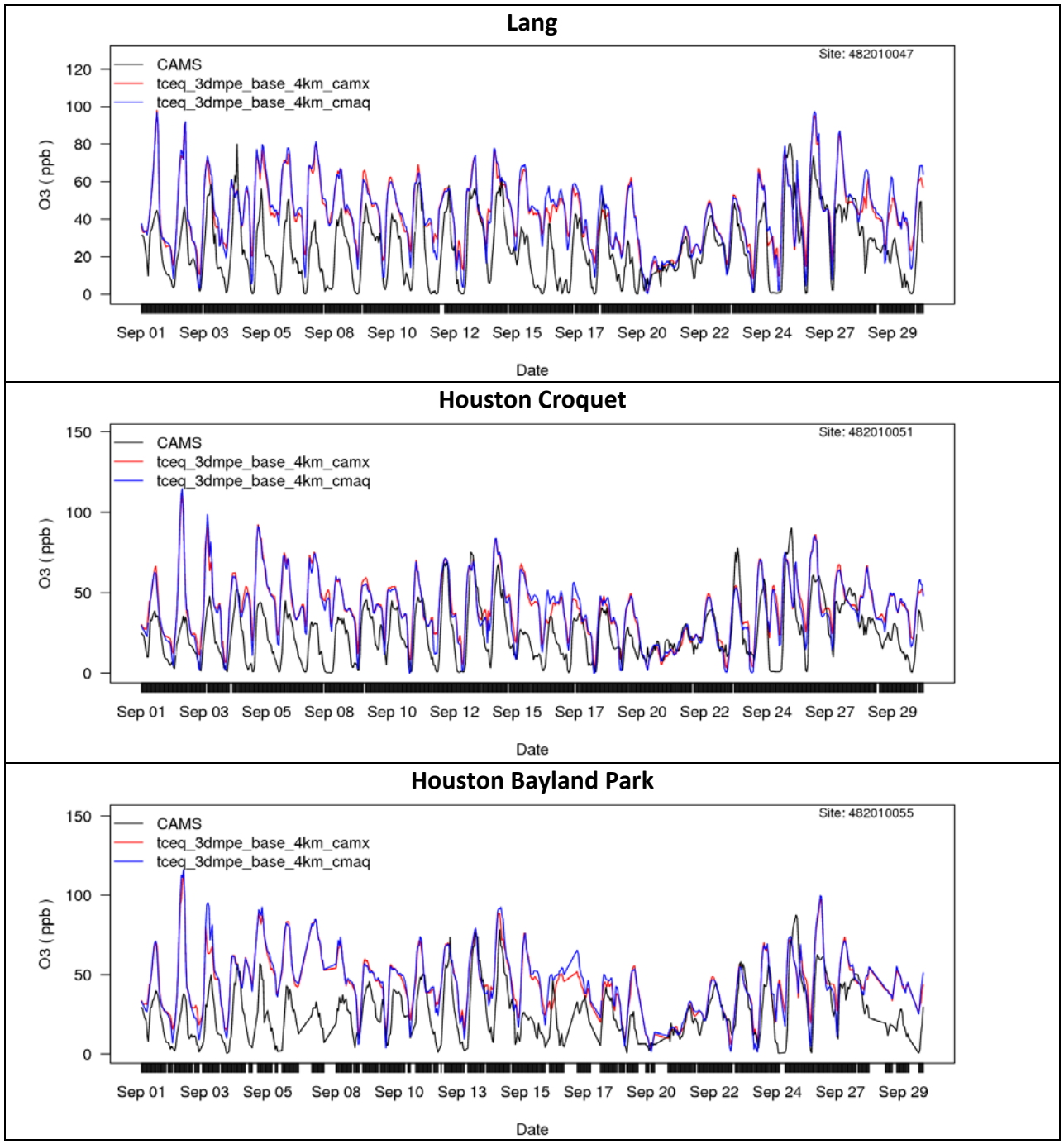
Lang
Site: 482010047
CAMS
tceq_3dmpe_base_4km_camx
tceq_3dmpe_base_4km_cmaq
O3 (ppb)
0
20
40
60
80
100
120
Sep 01
Sep 03
Sep 05
Sep 08
Sep 10
Sep 12
Sep 15
Sep 17
Sep 20
Sep 22
Sep 24
Sep 27
Sep 29
Date
Houston Croquet
Site: 482010051
CAMS
tceq_3dmpe_base_4km_camx
tceq_3dmpe_base_4km_cmaq
O3 (ppb)
0
50
100
150
Sep 01
Sep 03
Sep 05
Sep 08
Sep 10
Sep 12
Sep 15
Sep 17
Sep 20
Sep 22
Sep 24
Sep 27
Sep 29
Date
Houston Bayland Park
Site: 482010055
CAMS
tceq_3dmpe_base_4km_camx
tceq_3dmpe_base_4km_cmaq
O3 (ppb)
0
50
100
150
Sep 01
Sep 03
Sep 05
Sep 08
Sep 10
Sep 13
Sep 15
Sep 17
Sep 20
Sep 22
Sep 24
Sep 27
Sep 29
Date

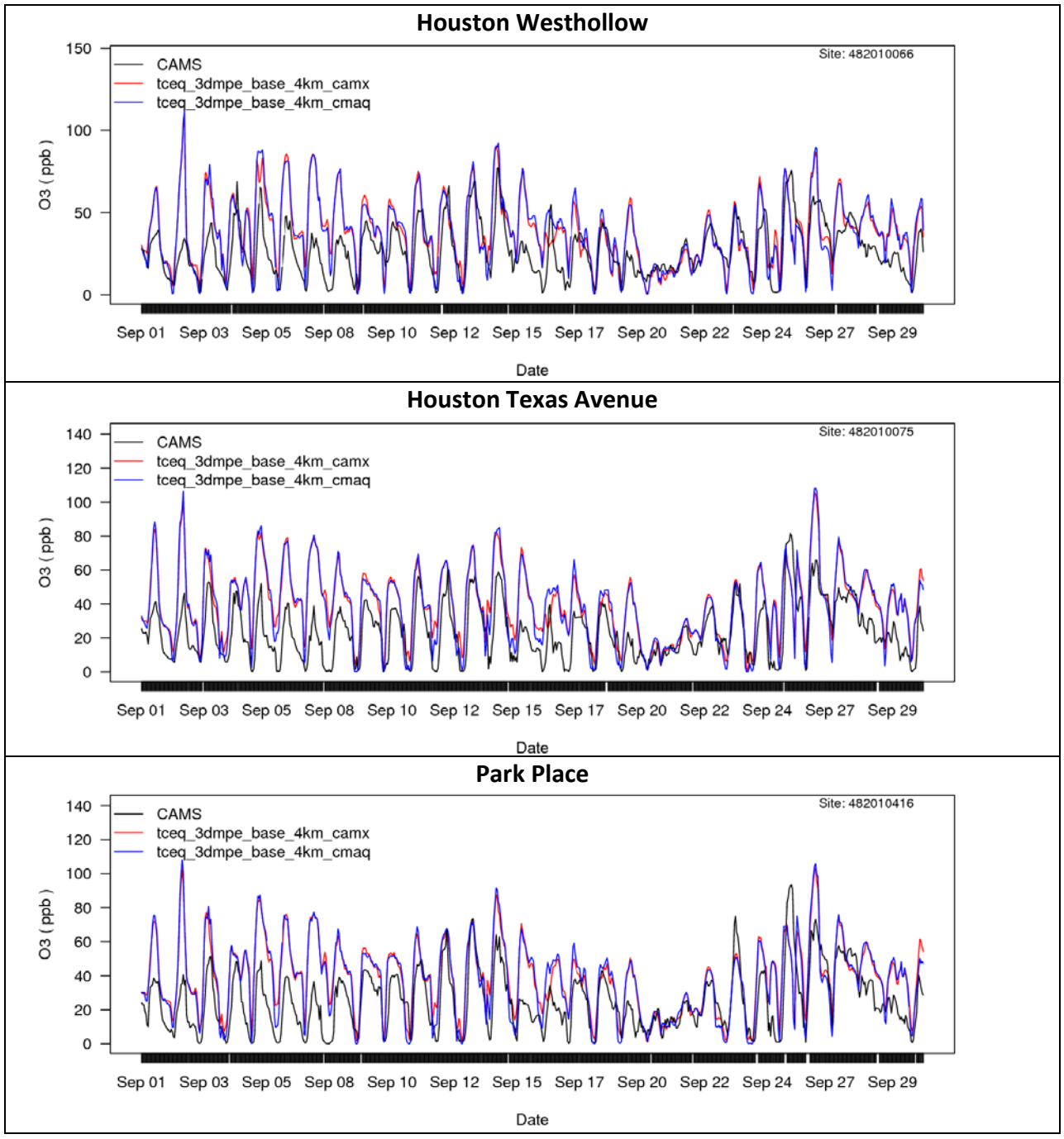
Houston Westhollow
Site: 482010066
CAMS
tceq_3dmpe_base_4km_camx
tceq_3dmpe_base_4km_cmaq
O3 (ppb)
Date
Houston Texas Avenue
Site: 482010075
CAMS
tceq_3dmpe_base_4km_camx
tceq_3dmpe_base_4km_cmaq
O3 (ppb)
Date
Park Place
Site: 482010416
CAMS
tceq_3dmpe_base_4km_camx
tceq_3dmpe_base_4km_cmaq
O3 (ppb)
Date
Sep 01 Sep 03 Sep 05 Sep 08 Sep 10 Sep 12 Sep 15 Sep 17 Sep 20 Sep 22 Sep 24 Sep 27 Sep 29

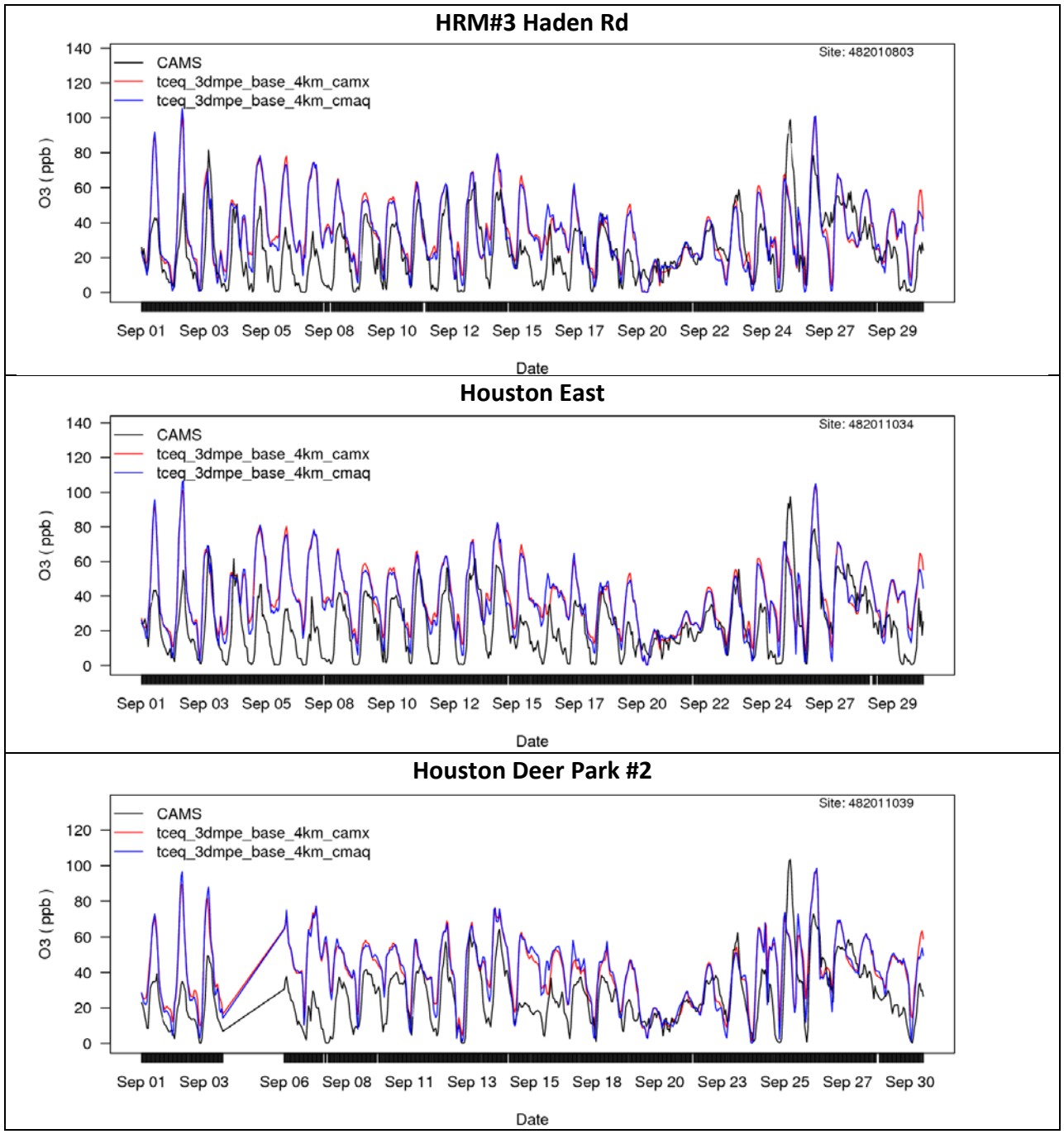
HRM#3 Haden Rd
Site: 482010803
CAMS
tceq_3dmpe_base_4km_camx
tceq_3dmpe_base_4km_cmaq
O3 (ppb)
Date
Houston East
Site: 482011034
CAMS
tceq_3dmpe_base_4km_camx
tceq_3dmpe_base_4km_cmaq
O3 (ppb)
Date
Houston Deer Park #2
Site: 482011039
CAMS
tceq_3dmpe_base_4km_camx
tceq_3dmpe_base_4km_cmaq
O3 (ppb)
Date

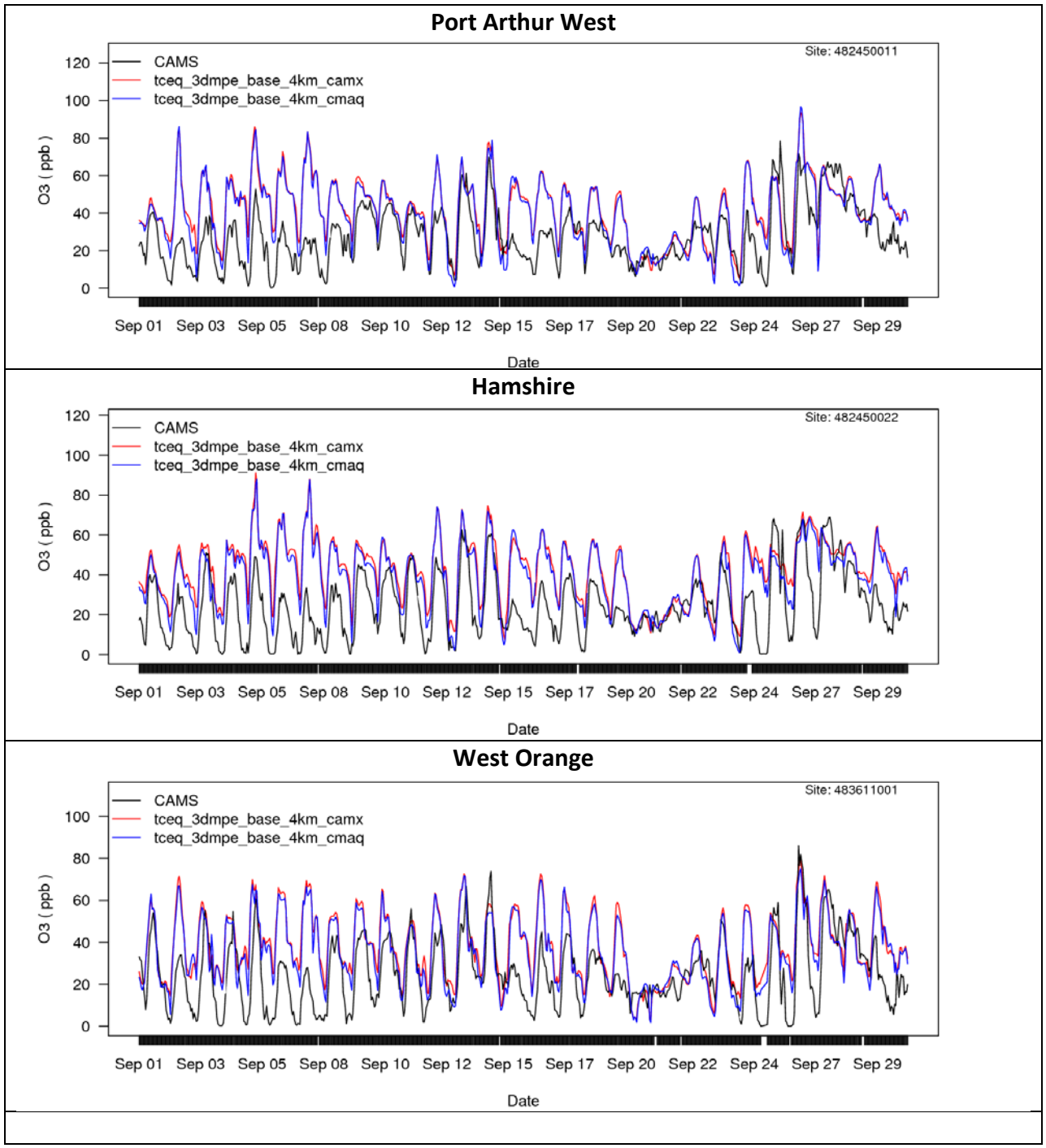

Figure C-1. Time series of observed (black) and predicted (CAMx/CMAQ; red/blue) ozone at TCEQ CAMS sites in September 2013.

APPENDIX D

CAMx and CMAQ-estimated Average $PM_{2.5}$ Concentrations ($\mu g/m^3$) and their Components for Base Case

Appendix D. C CAMx and CMAQ-estimated Average $PM_{2.5}$ Concentrations ($\mu g/m^3$) and their Components for Base Case

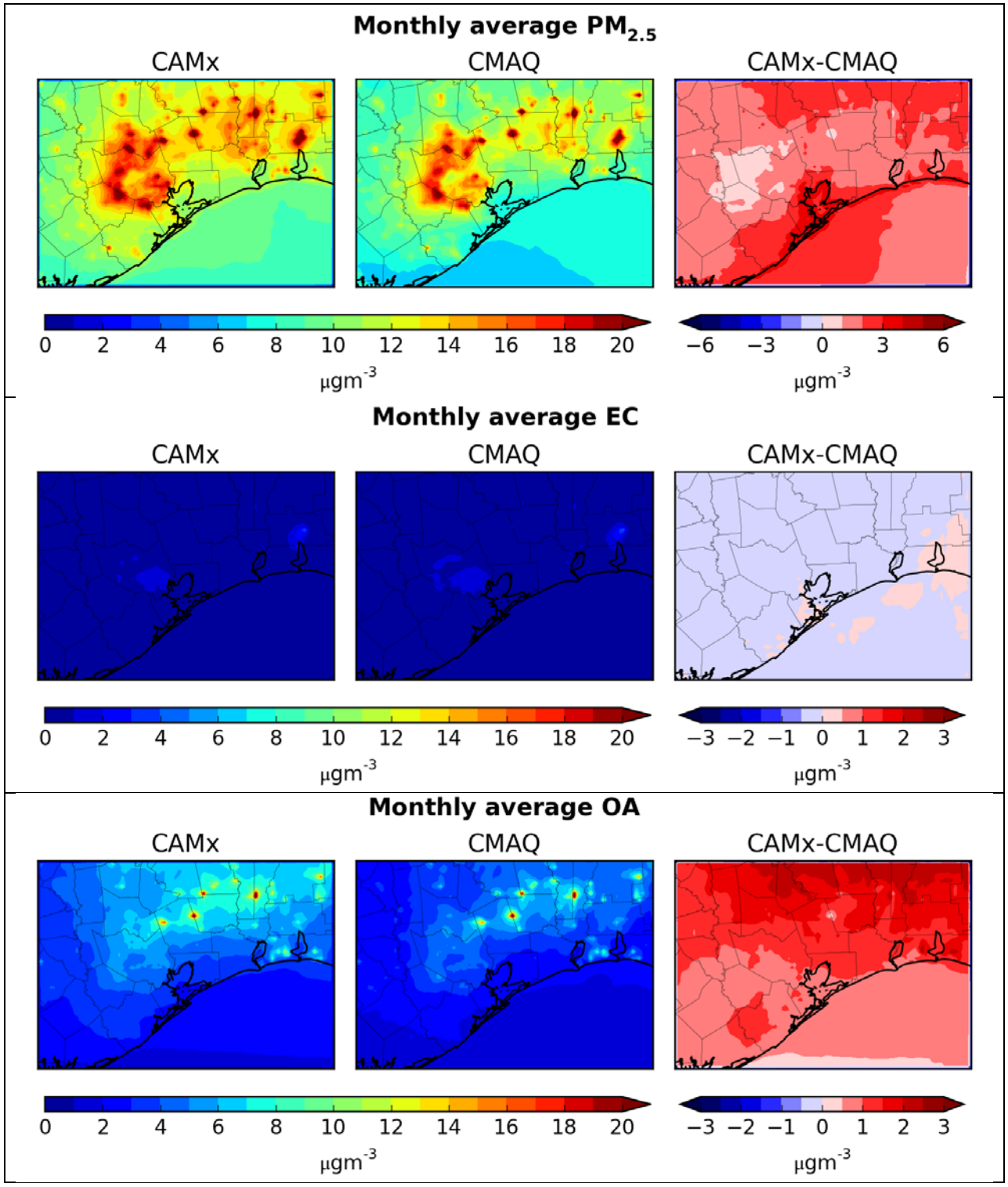

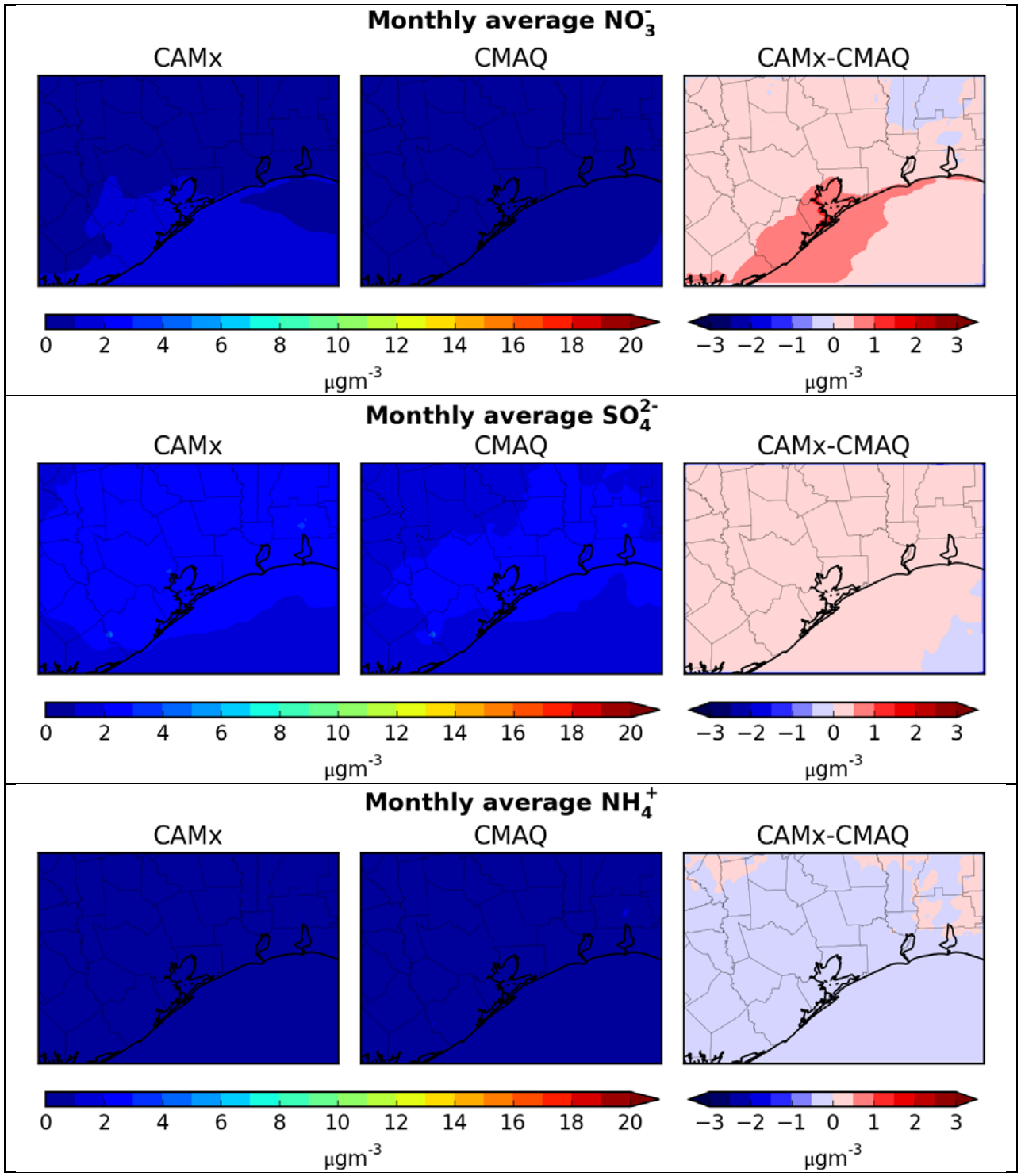
Monthly average NO_3^-
CAMx
CMAQ
CAMx-CMAQ
0 2 4 6 8 10 12 14 16 18 20
μgm-3
−3 −2 −1 0 1 2 3
μgm-3
Monthly average SO_4^{2-}
CAMx
CMAQ
CAMx-CMAQ
0 2 4 6 8 10 12 14 16 18 20
μgm-3
−3 −2 −1 0 1 2 3
μgm-3
Monthly average NH_4^+
CAMx
CMAQ
CAMx-CMAQ
0 2 4 6 8 10 12 14 16 18 20
μgm-3
−3 −2 −1 0 1 2 3
μgm-3

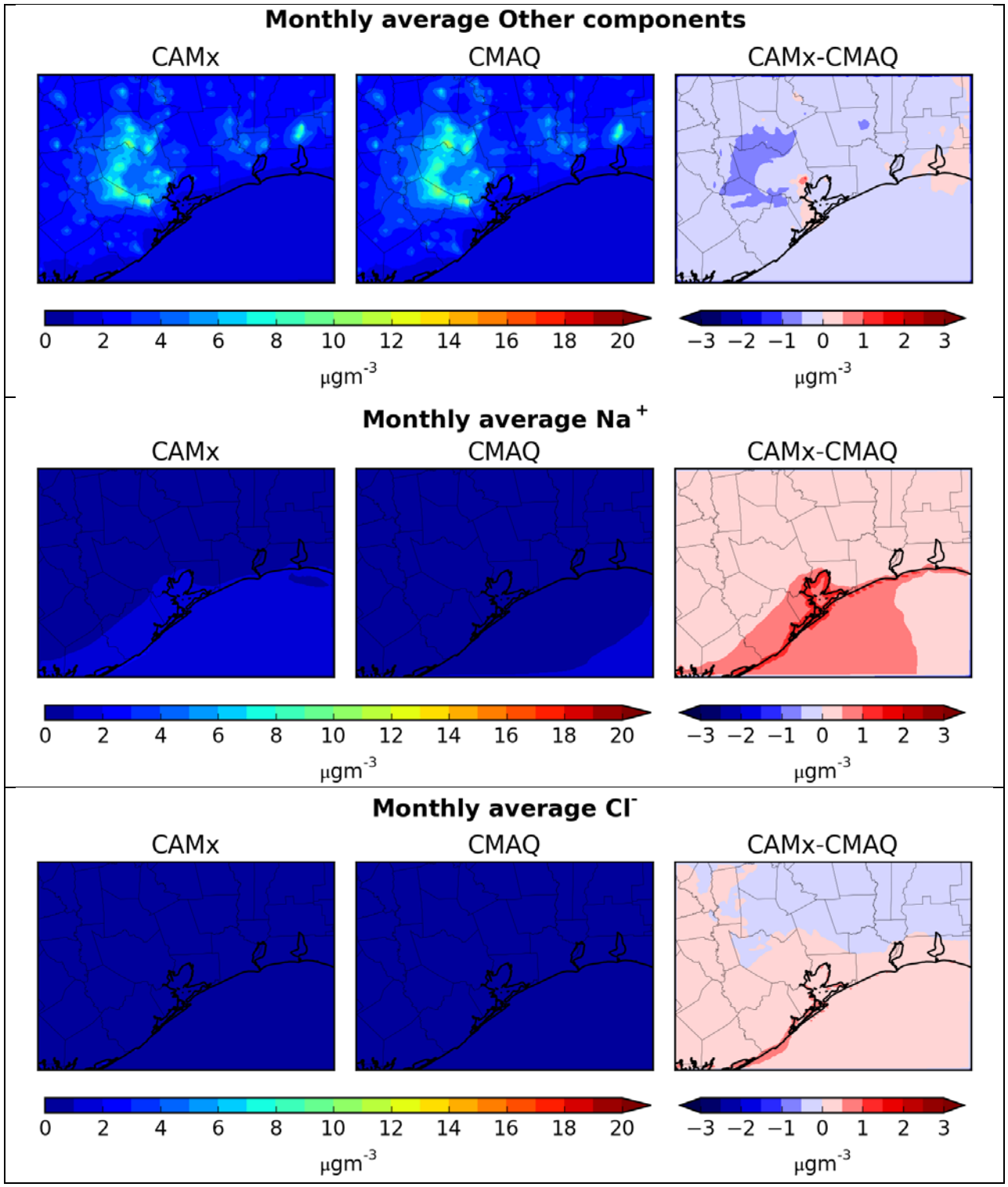
Monthly average Other components
CAMx
CMAQ
CAMx-CMAQ
0 2 4 6 8 10 12 14 16 18 20
μgm-3
−3 −2 −1 0 1 2 3
μgm-3
Monthly average Na+
CAMx
CMAQ
CAMx-CMAQ
0 2 4 6 8 10 12 14 16 18 20
μgm-3
−3 −2 −1 0 1 2 3
μgm-3
Monthly average Cl-
CAMx
CMAQ
CAMx-CMAQ
0 2 4 6 8 10 12 14 16 18 20
μgm-3
−3 −2 −1 0 1 2 3
μgm-3

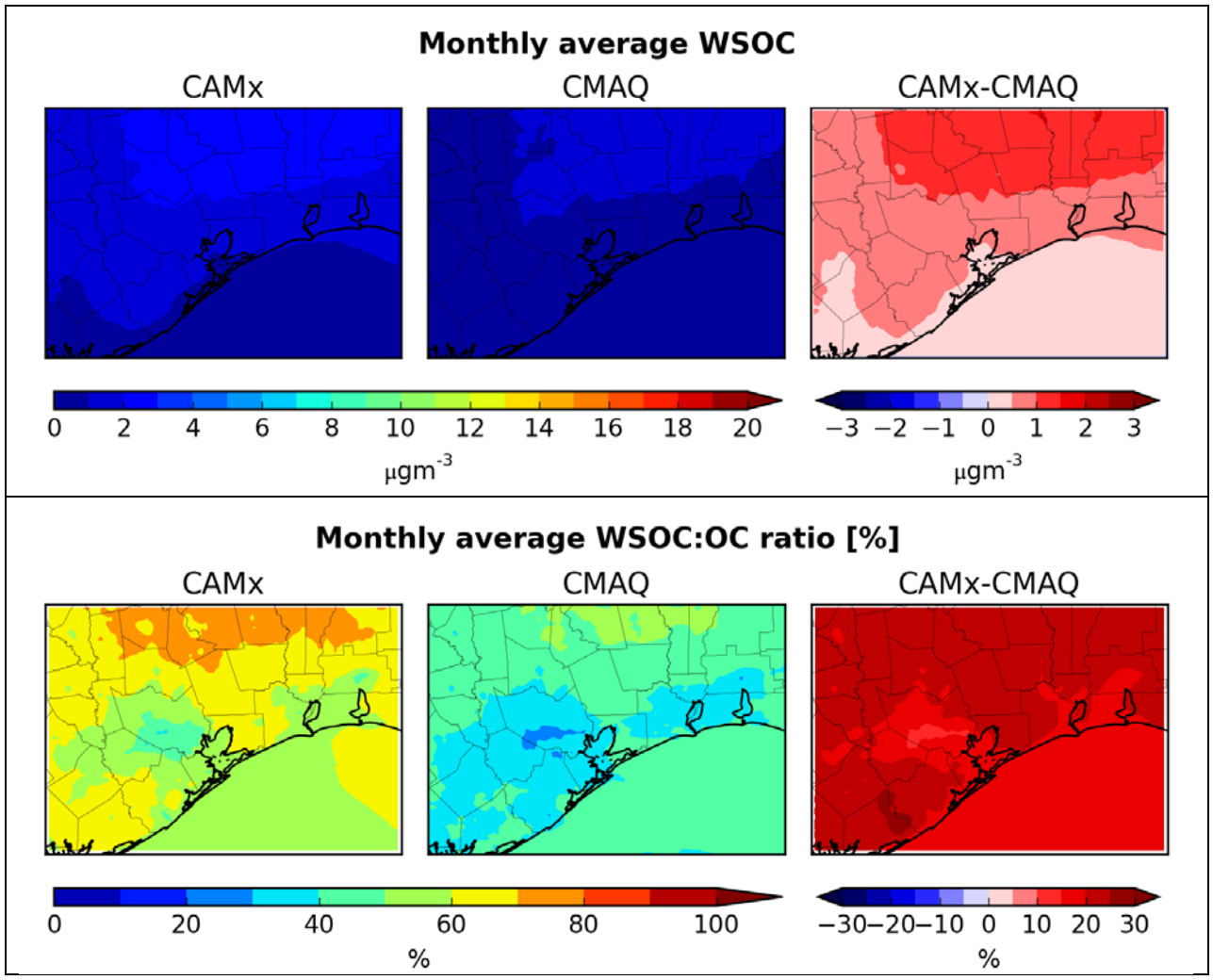

Figure D-1. CAMx and CMAQ predicted monthly average PM2.5 components in September 2013.

APPENDIX E

HYSPLIT Backward Trajectories

Appendix E. HYSPLIT Backward Trajectories

We used a trajectory model analysis to distinguish elevated ozone aloft among that initially generated locally in the Houston region, that transported regionally, and that re-circulated over the bays and back into the city. The Hybrid Single-Particle Lagrangian Integrated Trajectory (HYSPLIT) model back trajectories were used with three different meteorology data: 1) Eta Data Assimilation System (EDAS, 40 km), 2) North American Meso (NAM, 12 km) and 3) WRFCAMx (12 km) generated for this study. The 24-hour back trajectories start from UH Moody Tower (CAMS 695) at noon for 500 m, 1500 m, and 3000 m in altitude.

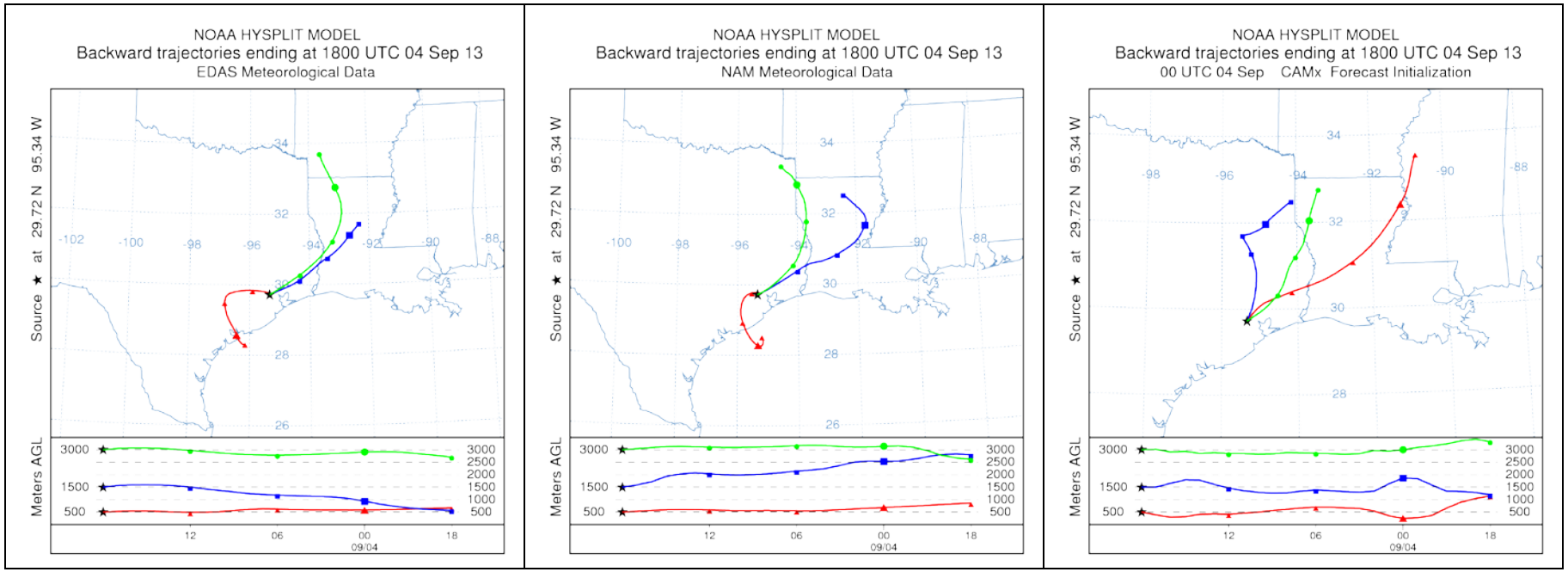

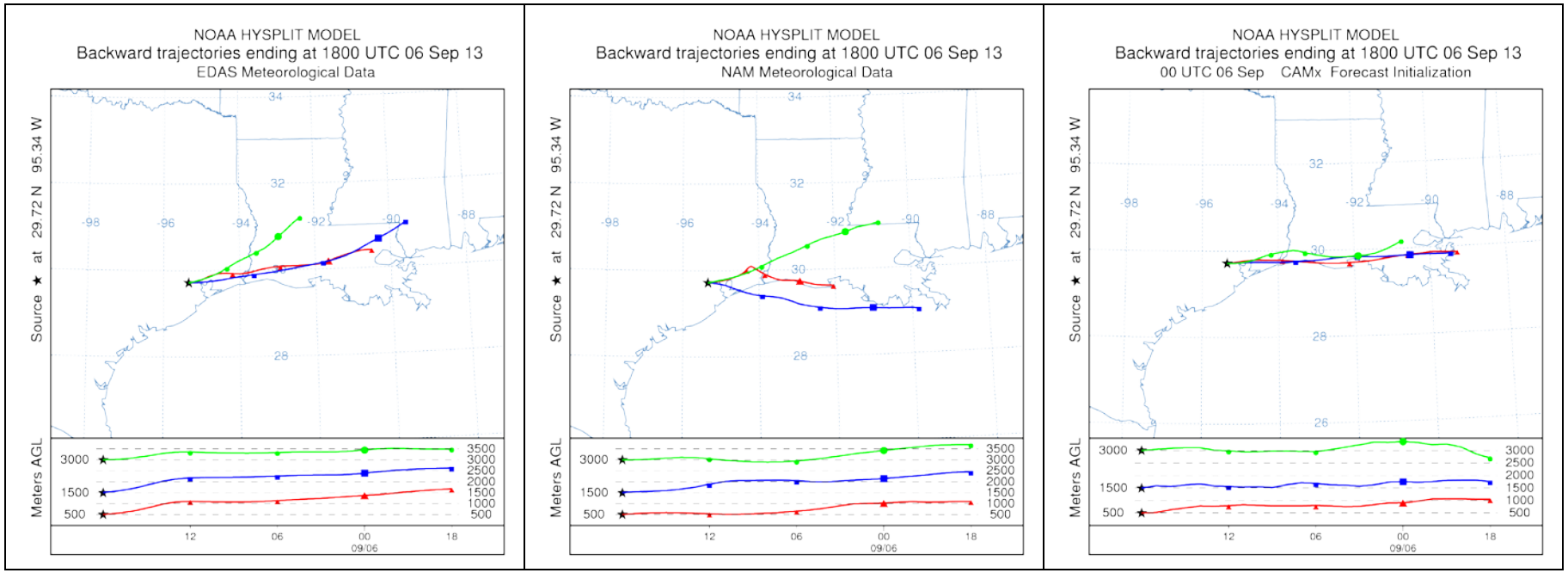
NOAA HYSPLIT MODEL
Backward trajectories ending at 1800 UTC 06 Sep 13
EDAS Meteorological Data
NOAA HYSPLIT MODEL
Backward trajectories ending at 1800 UTC 06 Sep 13
NAM Meteorological Data
NOAA HYSPLIT MODEL
Backward trajectories ending at 1800 UTC 06 Sep 13
00 UTC 06 Sep CAMx Forecast Initialization
Source ★ at 29.72 N 95.34 W
Meters AGL
3000
1500
500
12
06
00
09/06
18

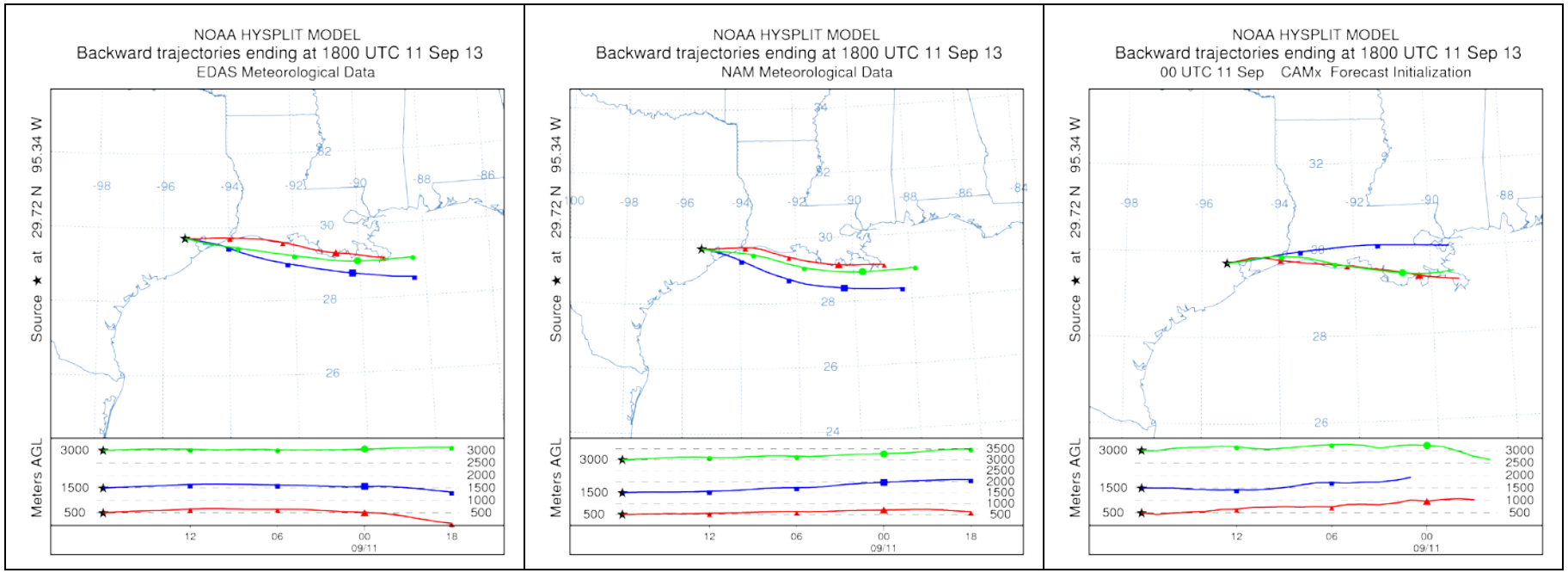
NOAA HYSPLIT MODEL
Backward trajectories ending at 1800 UTC 11 Sep 13
EDAS Meteorological Data
NOAA HYSPLIT MODEL
Backward trajectories ending at 1800 UTC 11 Sep 13
NAM Meteorological Data
NOAA HYSPLIT MODEL
Backward trajectories ending at 1800 UTC 11 Sep 13
00 UTC 11 Sep CAMx Forecast Initialization
Source ★ at 29.72 N 95.34 W
Meters AGL
09/11

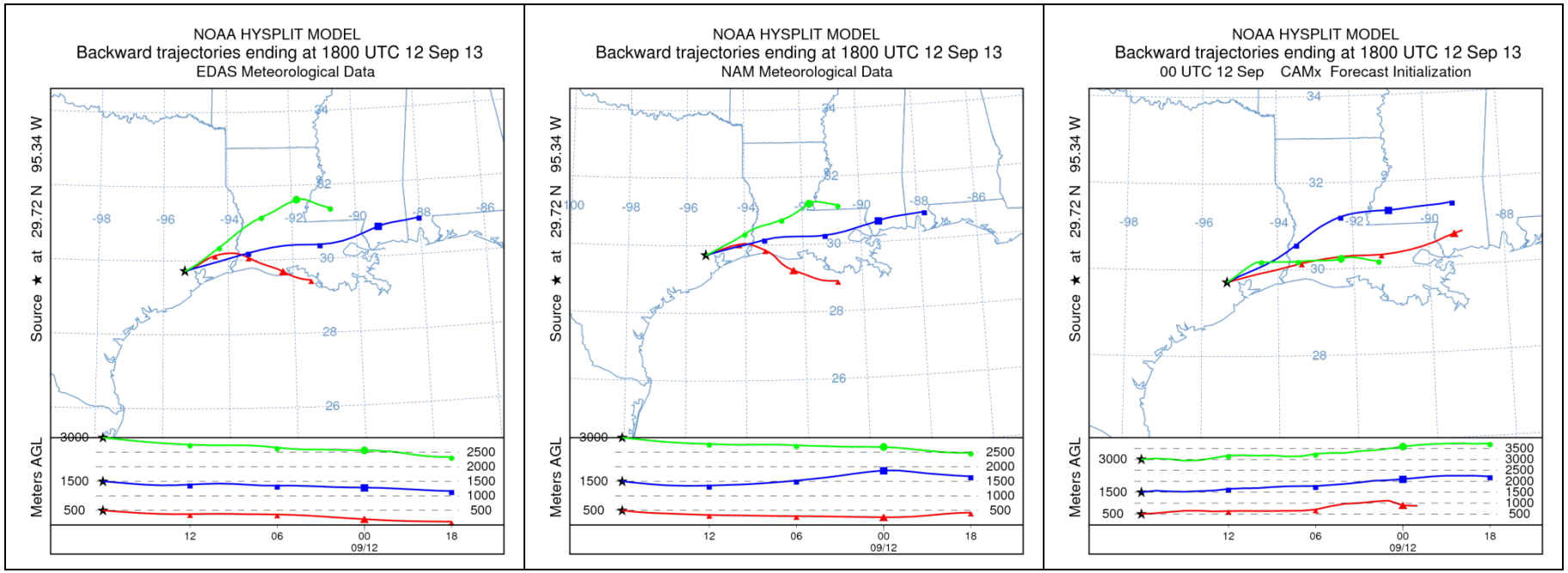
NOAA HYSPLIT MODEL
Backward trajectories ending at 1800 UTC 12 Sep 13
EDAS Meteorological Data
NOAA HYSPLIT MODEL
Backward trajectories ending at 1800 UTC 12 Sep 13
NAM Meteorological Data
NOAA HYSPLIT MODEL
Backward trajectories ending at 1800 UTC 12 Sep 13
00 UTC 12 Sep CAMx Forecast Initialization
Source ★ at 29.72 N 95.34 W
Meters AGL
09/12

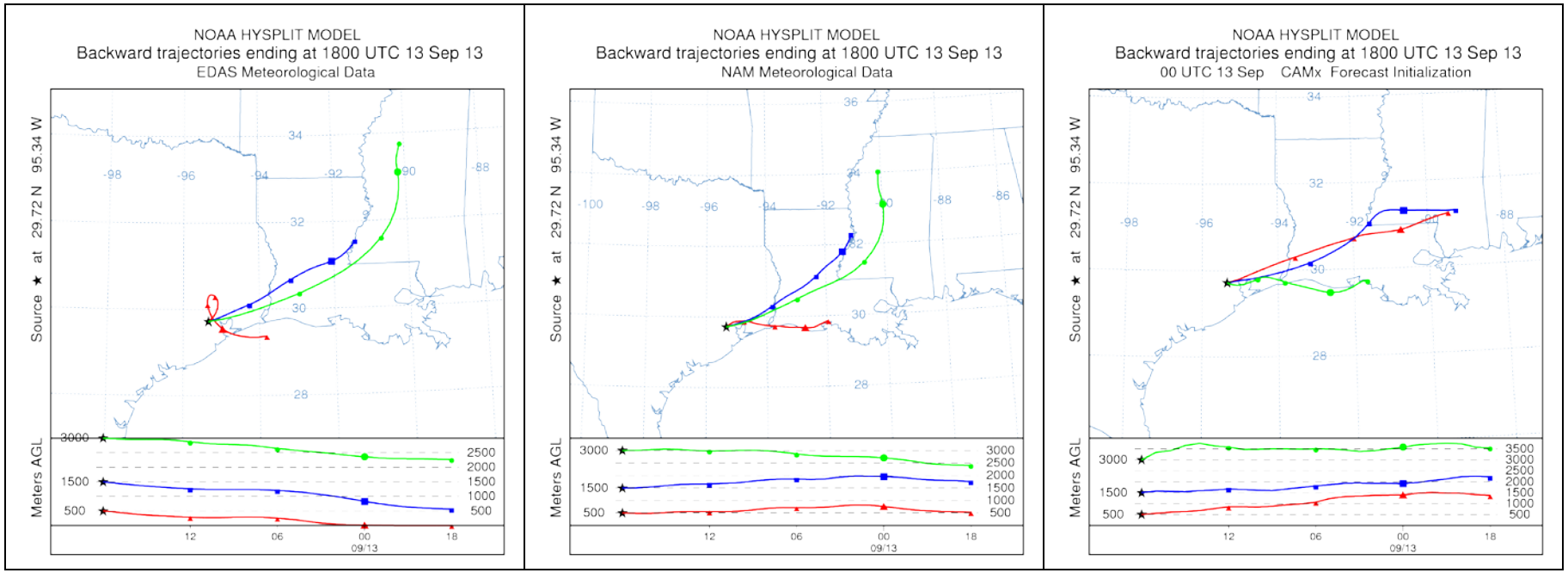
NOAA HYSPLIT MODEL
Backward trajectories ending at 1800 UTC 13 Sep 13
EDAS Meteorological Data
Source ★ at 29.72 N 95.34 W
Meters AGL
NOAA HYSPLIT MODEL
Backward trajectories ending at 1800 UTC 13 Sep 13
NAM Meteorological Data
Source ★ at 29.72 N 95.34 W
Meters AGL
NOAA HYSPLIT MODEL
Backward trajectories ending at 1800 UTC 13 Sep 13
00 UTC 13 Sep CAMx Forecast Initialization
Source ★ at 29.72 N 95.34 W
Meters AGL

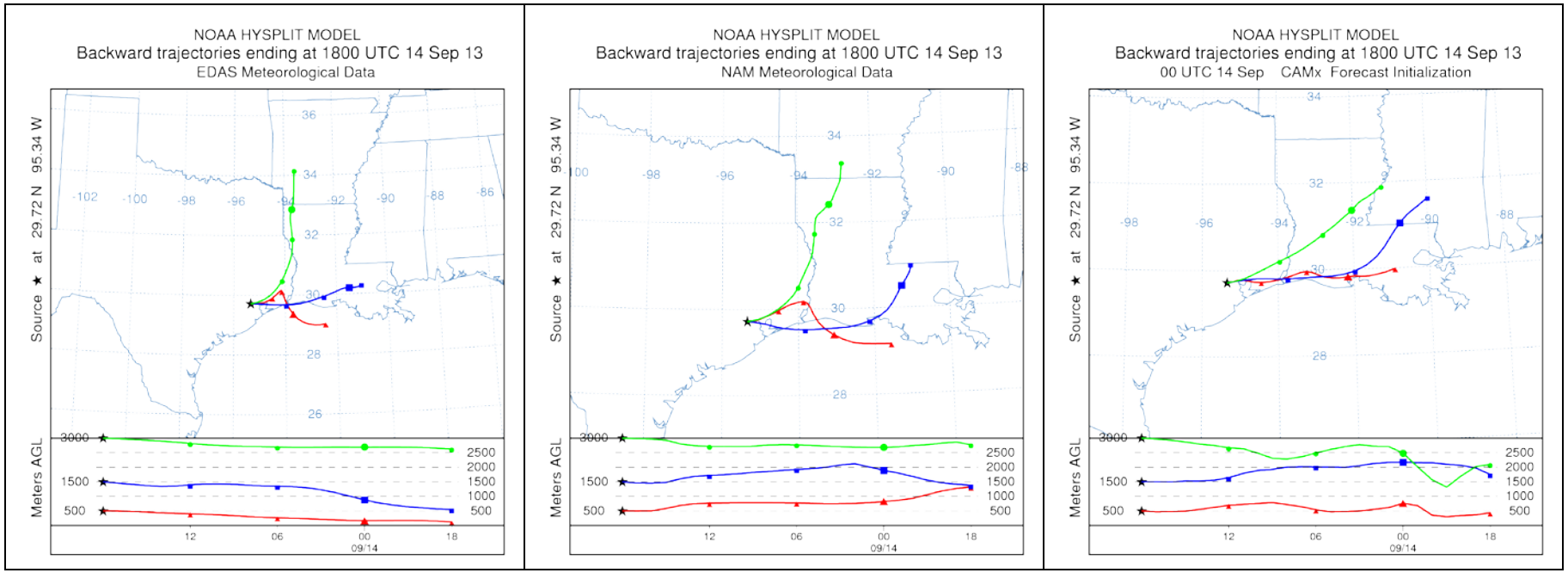
NOAA HYSPLIT MODEL
Backward trajectories ending at 1800 UTC 14 Sep 13
EDAS Meteorological Data
NOAA HYSPLIT MODEL
Backward trajectories ending at 1800 UTC 14 Sep 13
NAM Meteorological Data
NOAA HYSPLIT MODEL
Backward trajectories ending at 1800 UTC 14 Sep 13
00 UTC 14 Sep CAMx Forecast Initialization
Source ★ at 29.72 N 95.34 W
Meters AGL
3000
1500
500
2500
2000
1500
1000
500
12
06
00
09/14
18

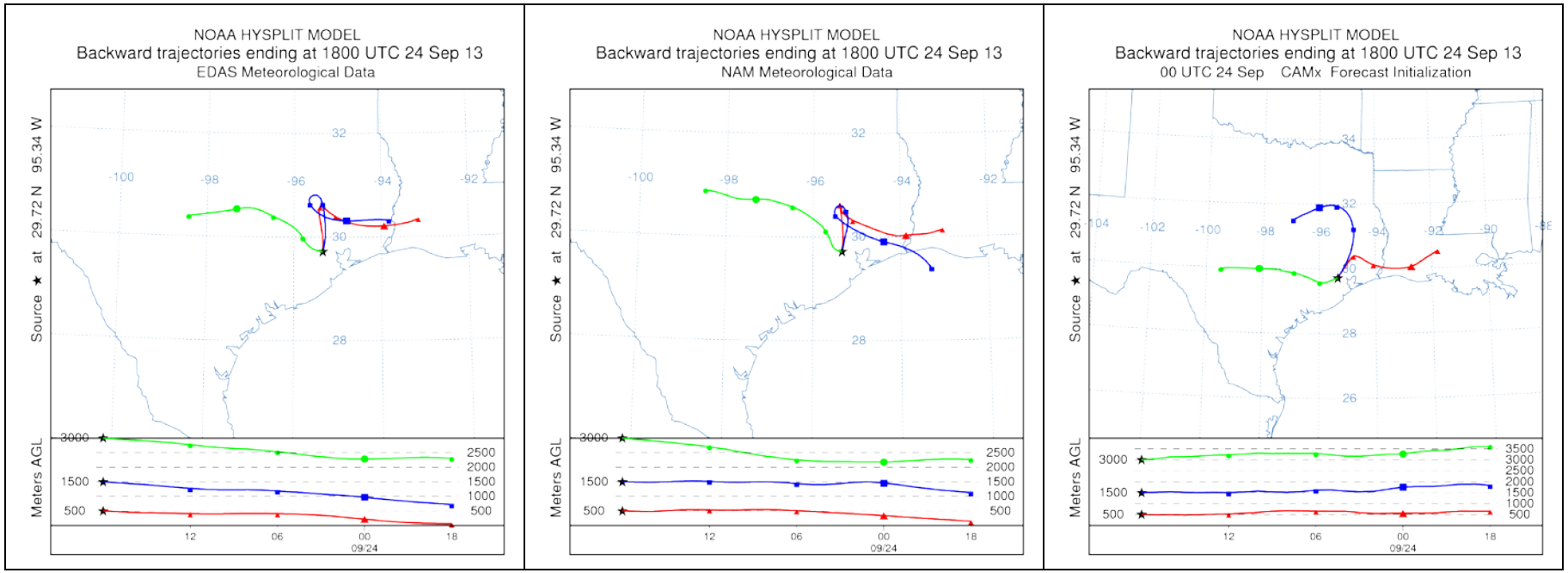
NOAA HYSPLIT MODEL
Backward trajectories ending at 1800 UTC 24 Sep 13
EDAS Meteorological Data
NOAA HYSPLIT MODEL
Backward trajectories ending at 1800 UTC 24 Sep 13
NAM Meteorological Data
NOAA HYSPLIT MODEL
Backward trajectories ending at 1800 UTC 24 Sep 13
00 UTC 24 Sep CAMx Forecast Initialization
Source ★ at 29.72 N 95.34 W
Meters AGL
09/24

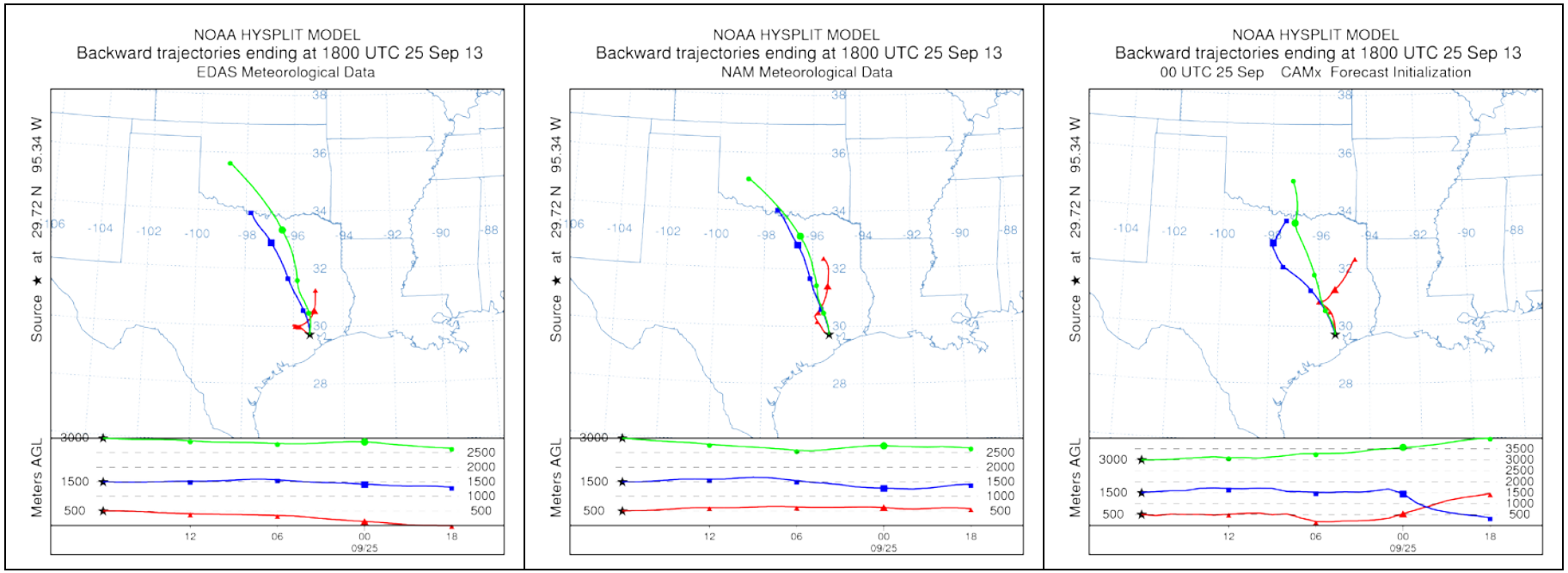
NOAA HYSPLIT MODEL
Backward trajectories ending at 1800 UTC 25 Sep 13
EDAS Meteorological Data
NOAA HYSPLIT MODEL
Backward trajectories ending at 1800 UTC 25 Sep 13
NAM Meteorological Data
NOAA HYSPLIT MODEL
Backward trajectories ending at 1800 UTC 25 Sep 13
00 UTC 25 Sep CAMx Forecast Initialization
Source ★ at 29.72 N 95.34 W
Meters AGL
09/25

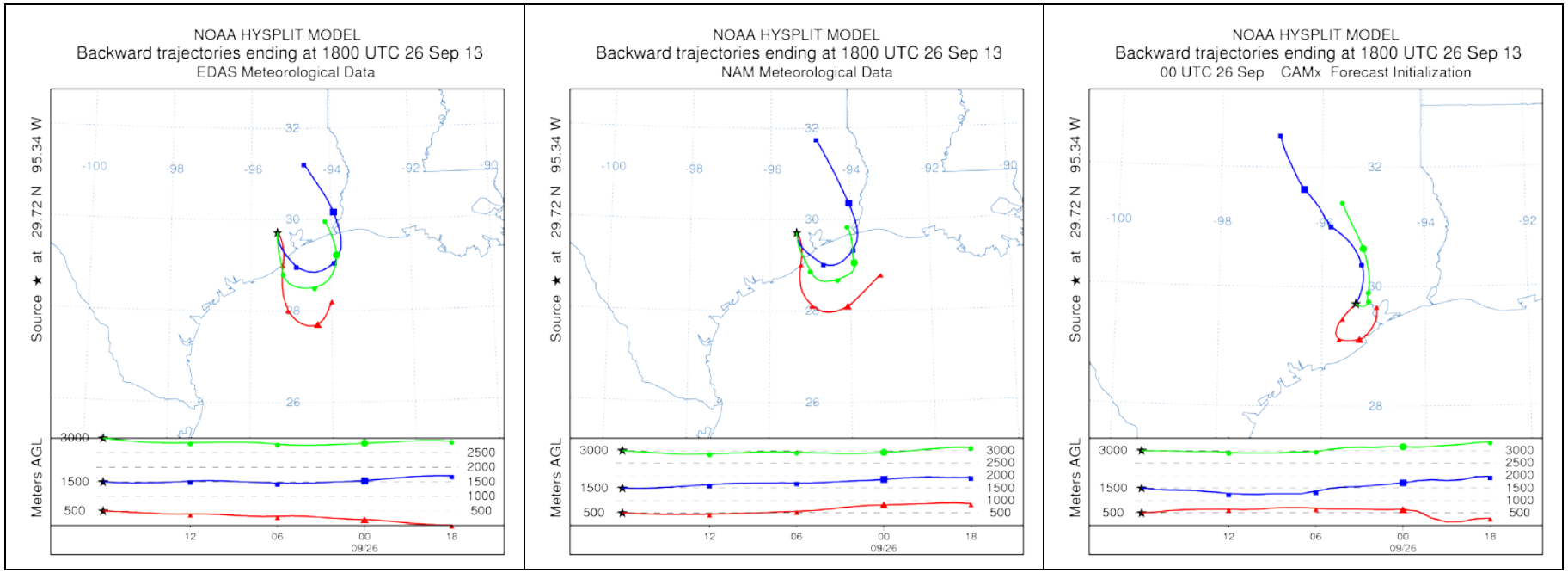

Figure E-1. 24 hour back trajectory at Univ. of Houston Moody Tower 500 m (red), 1500 m (blue), and 300 m (green) above ground by using EDAS40 (1st column), NAM12 (2nd column), and WRFCAMx 12km (3rd column), respectively.